Matrix Isolation Study of Molecular Iridium Oxyfluorides, Fluorides, Fluoride Anions and their Alkali Ion Pairs

Inaugural-Dissertation
to obtain the academic degree
Doctor rerum naturalium (Dr. rer. nat.)

submitted to the
Department of Biology, Chemistry, Pharmacy
of Freie Universität Berlin

by

YAN LU

from Jiangxi, China

2024

The work for this dissertation was done in the time period from October 2019 to April 2024 under the supervision of Prof. Dr. Sebastian Hasenstab-Riedel at the Institute of Chemistry and Biochemistry of Freie Universität Berlin.

Declaration of authorship:
I hereby declare that I alone am responsible for the content of my doctoral dissertation and that I have only used the sources or references cited in the dissertation. This work has not been submitted for any other degree or professional qualification except as specified.

Yan Lu

1st reviewer: Prof. Dr. Sebastian Hasenstab-Riedel

2nd reviewer: Prof. Dr. Martin Kaupp

Date of defense: 1 July 2024

Acknowledgements

First, I would like to thank my supervisor Prof. Dr. Sebastian Hasenstab-Riedel, for giving me the opportunity to work in his group, for his continuous patience, contagious enthusiasm, motivation and support.

I would like to thank Prof. Dr. Martin Kaupp for his time and effort to assess my work as a second reviewer.

I am especially grateful to Dr. Lin Li for her patient support in the experimental and practical part. Thanks to Dr. Robert Medel and Dr. Yetsedaw Tsegaw, who proofread my manuscripts and gave me valuable feedback. I also would like to thank Prof. Dr. Bin Xu, Dr. Hongmin Li, Dr. Tony Stüker, Dr. Pavel Zasimov, Dr. Guohai Deng and Dr. Gene Senges for many nice scientific discussions. I would give thanks to Mei Wen, Xiya Xia, and Deniz Meyer for their kind care and nice friendship.

I am very grateful to Prof. Dr. Martin Kaupp, Dr. Artur Wodyński and Dr. Marc Reimann who provided me with strong support and many helpful discussions in theoretical calculation.

Many thanks to all lovely colleagues of the Hasenstab-Riedel group for providing a happy and friendly working atmosphere, many productive discussions, and everyone's kind help in the day-to-day business. I had a great time working and will have fond memories of you all.

I would like to thank ZEDAT (Zentraleinrichtung für Datenverarbeitung) for computing resources and support. The same thanks I also would like to give the staff of the workshops, our institute, and the BCP office (Promotionsbüro 2).

I am grateful for the financial support afforded by China Scholarship Council (CSC).

Finally, I would like to express my gratitude to my dear parents and little sister Suyi Lu for their encouragement and unfailing support throughout my years of study.

List of Abbreviations

B3LYP	Becke, 3-parameter, Lee-Yang-Parr
BDE	bond dissociation energy
CASSCF	complete active space self-consistent field
CASPT2	complete active space 2nd order perturbation theory
CC	coupled cluster
CCSD(T)	coupled cluster singles, doubles and perturbational triples
CI	configuration interaction
CSS	closed-shell singlet
DFT	density functional theory
DKH	Douglas-Kroll-Hess
EA	electron affinity
ECP	effective core potentials
EPR	electron paramagnetic resonance
FCI	full configuration interaction
FIA	fluoride ion affinity
HOMO	highest occupied molecular orbital
IR	infrared
JT	Jahn-Teller
LED	light-emitting diode
LUMO	lowest unoccupied molecular orbital
MCT	mercury cadmium telluride
MP2	Møller-Plesset perturbation theory second order
NMR	nuclear magnetic resonance

NR	non-relativistic
PFA	perfluoroalkoxy alkanes
PP	pseudopotential
PXRD	powder X-ray diffraction
SOC	spin-orbit coupling
SPDD	synchrotron X-ray powder diffraction
SNSO	scaled nuclear spin–orbit
X2C	exact two-component
XRD	X-ray diffraction
UV	ultraviolet
UV-Vis	ultraviolet and visible
ZORA	zeroth order regular approximation
ZPE	zero point energy

Table of Contents

1. Summary

This thesis is devoted to the investigation of previously unknown molecular iridium compounds with the iridium center in high oxidation states. The species were stabilized using matrix isolation technique and characterized by IR spectroscopy combined with state-of-the-art quantum-chemical calculations to analyze their electronic structures.

It is well-known that the reaction of laser-ablated transition metal atoms with F_2 or OF_2 is particularly useful for the generation of interesting species containing metal atoms in high oxidation states. Iridium oxyfluorides (OIrF, $OIrF_2$, and FOIrF) were prepared for the first time by the reaction of laser-ablated iridium atoms with OF_2. Their assignment was based on the metal–oxygen and metal–fluorine stretching vibrations with characteristic $^{16/18}O$ isotopic shifts. Quantum-chemical calculations provide a better understanding of Ir–O bonding in iridium oxyfluorides, and further compare the metal–oxygen bonding characteristics with similar compounds of group 10 and 11 metals to reflect trends in the bonding of the oxo ligand. Additionally, different iridium fluorides were obtained as side-products. These were further investigated in the analogous reaction of Ir with F_2, yielding a series of molecular iridium fluorides IrF_n ($n = 1–6$), while IrF_7 was not detected. Since fluorine is a neat element, the photo-initiated defluorination of IrF_6 was performed to support their assignment of the low-valent fluorides. The Ir–F stretching vibrations of a series of binary iridium fluorides were utilized for gaining an insight into their molecular structures. Among the observed iridium fluorides, IrF_5 is one of the very rare examples whose structure was found to be significantly affected by spin–orbit coupling (SOC) and was confirmed experimentally. To further explore the higher-valent iridium fluorides, the reaction of IrF_6 with laser-ablated alkali metal fluorides MF (M = Na, K, Rb, Cs) was investigated. This reaction led to the first observation of molecular iridium fluoride anions IrF_5^-, IrF_6^-, and a sequence of molecular alkali ion pairs $M[IrF_6]$ with M = Na, K, Rb, and Cs. Such IrF_5^- and IrF_6^- anions were also obtained by exposing IrF_6 to laser ablation of metals (Ir or Pt) as electron sources. The IrF_6^- anion adopts an O_h structure in a closed-shell ground state stabilized by the SOC effect, rather than a distorted D_{4h} structure in a triplet ground state as predicted by scalar-relativistic calculations. The closed-shell $M[IrF_6]$ ion pairs in C_{3v} symmetry are stabilized by an alkali metal coordination to three F atoms on one face of the anion and their structural change from M = Na to Cs was spectroscopically confirmed.

Zusammenfassung

Diese Arbeit ist der Untersuchung bisher unbekannter molekularer Iridiumverbindungen mit dem Iridiumzentrum in hohen Oxidationsstufen gewidmet. Die Spezies wurden mithilfe der Matrixisolationstechnik stabilisiert und mittels IR-Spektroskopie in Kombination mit modernsten quantenchemischen Berechnungen charakterisiert, um ihre elektronischen Strukturen zu analysieren.

Es ist bekannt, dass die Reaktion laserablatierter Übergangsmetallatome mit F_2 oder OF_2 besonders nützlich für die Erzeugung interessanter Spezies ist, die Metallatome in hohen Oxidationsstufen enthalten. Iridiumoxyfluoride (OIrF, $OIrF_2$ und FOIrF) wurden erstmals durch die Reaktion von laserablatierten Iridiumatomen mit OF_2 hergestellt. Ihre Zuordnung basierte auf den Metall-Sauerstoff- und Metall-Fluor-Streckschwingungen mit charakteristischen $^{16/18}$O-Isotopenverschiebungen. Quantenchemische Berechnungen ermöglichen ein besseres Verständnis der Ir-O-Bindung in Iridiumoxyfluoriden und vergleichen die Metall-Sauerstoff-Bindungseigenschaften mit ähnlichen Verbindungen von Metallen der Gruppen 10 und 11, um Trends in der Bindung des Oxoliganden widerzuspiegeln. Darüber hinaus wurden als Nebenprodukte verschiedene Iridiumfluoride erhalten. Diese wurden in der analogen Reaktion von Ir mit F_2 weiter untersucht und ergaben eine Reihe molekularer Iridiumfluoride IrF_n (n = 1–6), während IrF_7 nicht nachgewiesen wurde. Da Fluor ein Reinelement ist, wurde die photoinitiierte Defluorierung von IrF_6 durchgeführt, um die Zuordnung der niedervalenten Fluoride zu unterstützen. Die Ir–F-Streckschwingungen einer Reihe binärer Iridiumfluoride wurden genutzt, um einen Einblick in ihre molekularen Strukturen zu gewinnen. Unter den beobachteten Iridiumfluoriden ist IrF_5 eines der sehr seltenen Beispiele, dessen Struktur durch Spin-Bahn-Kopplung (spin–orbit coupling, SOC) erheblich beeinflusst und experimentell bestätigt wurde. Um die höheren Iridiumfluoride weiter zu erforschen, wurde die Reaktion von IrF_6 mit laser-ablatierten Alkalimetallfluoriden MF (M = Na, K, Rb, Cs) untersucht. Diese Reaktion führte zur erstmaligen Beobachtung der molekularen Iridiumfluorid-Anionen IrF_5^-, IrF_6^- und einer Sequenz molekularer Alkaliionenpaare $M[IrF_6]$ mit M = Na, K, Rb und Cs. Solche IrF_5^-- und IrF_6^--Anionen wurden auch erhalten, als IrF_6 der Laserablation von Metallen (Ir oder Pt) als Elektronenquellen ausgesetzt wurde. Das IrF_6^--Anion nimmt eine O_h-Struktur in einem geschlossenschaligen Grundzustand an, der durch den SOC-Effekt stabilisiert wird, und nicht eine verzerrte D_{4h}-Struktur in einem Triplett-Grundzustand, wie durch skalar-relativistische Berechnungen vorhergesagt. Die geschlossenschaligen $M[IrF_6]$-Ionenpaare in C_{3v}-Symmetrie werden durch eine Alkalimetallkoordination an drei F-Atome auf einer Seite des Anions stabilisiert und ihre Strukturänderung von M = Na zu Cs wurde spektroskopisch bestätigt.

2. Introduction

The concept of formal oxidation states is of fundamental importance in chemistry, because it is directly related to the redox, acid-base, and physical properties of the species.[1,2] The compounds with unusual oxidation states, in particular transition metal compounds, tend to capture the interest of chemists because their investigation noticeably deepens our understanding of the chemical behavior of these elements and their compounds. Interestingly, the complexes containing transition metal elements in unusually high oxidation states often possess very exciting properties which often determine their usage in synthetic chemistry as fluorinating agents,[3,4] strong oxidizers,[5,6,7] and catalysts.[8,9] A striking example is that in 1962 the third-row transition metal hexafluoride PtF_6 was successfully used by N. Bartlett for the oxidation of xenon leading to the discovery of the first true xenon compounds, namely $[XeF]^+[PtF_6]^-$ and $[XeF]^+[Pt_2F_{11}]^-$, marking the official beginning of the noble gas chemistry.[7,10]

Fluorine is known to be very suitable for the stabilization of extreme oxidation states because of its high electronegativity and the weak covalent F–F bond resulting from the significant electronic repulsions between the fluorine lone pairs.[11] It makes many elements to reach their highest oxidation state in their fluorides, e.g. ReF_7,[12] NiF_4,[13] and HgF_4.[14] On the other hand, the highest oxidation number can also be achieved by oxidation of the elements with oxygen which presents lower electronegativity, e.g. OsO_4[15] and $[RhO_3]^+$.[16] Thus, in general, the family of metal compounds with the highest oxidation state includes oxides, oxyfluorides, and fluorides.[2] It is worth noticing that the number of anionic species is by far larger than that of the known high-oxidation state neutral and cationic species due to the anionic notable stabilization and relatively easier availability. Furthermore, the anionic precursor in the same oxidation state can be used for synthesis of the corresponding neutral complexes.[2,17]

Great effort from both aspects of theoretical predictions and experimental observations has been made to explore the higher oxidation states of the transition metal elements because of the diverse d electron configuration of these elements. It is worth noticing that the key problem of the synthesis of the compounds containing transition metal elements in high oxidation states is their extremely high reactivity and instability under normal ambient conditions which requires the special approaches to their synthesis and stabilization.[4,13,14,18,19] In particular, high pressure is believed to be able to stabilize the compounds of this type. For instance, the highest oxidation state of Au experimentally known so far is +V[17,20] while it was predicted that the reaction of Au and F_2 under the high pressure could yield $Au^{+VI}F_6$.[4] The technetium and osmium fluorides (TcF_7 and OsF_8) are further examples of the theoretical prediction of the extraordinary high oxidation state stabilization under high pressure.[18] An

alternative approach to stabilize these compounds is to put them into solid inert media under cryogenic temperatures, the matrix isolation technique. The combination of this method with IR spectroscopy was proven to be a very powerful approach on the preparation and characterization of highly oxidized transition metal compounds.[13,14]

Iridium, a 5d transition metal element, has so far the highest experimentally attained formal oxidation state (+IX) across all chemical elements and thus has the widest range of oxidation states of any element, from −III to +IX.[21,22] Iridium complexes have been efficiently utilized in catalytic water oxidation,[23] C−H oxidation,[24] biological probes[25] and emitting materials.[26] The oxidation state of +VI for iridium was known for a long time and is represented by IrF_6 and a number of perovskites containing the $[IrO_6]^{6-}$ ion.[2,27–29] Furthermore, a matrix-isolation IR spectroscopic study on the reaction products from co-deposition of laser-ablated iridium atoms and NF_3 demonstrated the existence of $NIr^{+VI}F_3$[30] and that with oxygen provided evidence for the formation of the side-on coordinated peroxide complex $(O_2)Ir^{+VI}O_2$.[31] However, the matrix isolation investigation performed several years later demonstrated the higher oxidation state of Ir, namely that the analogous reaction of Ir with O_2 can produce IrO_4 with iridium in its +VIII oxidation state.[32] In principle, iridium could reach the oxidation state beyond +VIII when its valence shell was completely oxidized. Thus, the removal of the last d electron from the IrO_4 valence electron shell would lead to the $[IrO_4]^+$ cation which represents the +IX oxidation state. Indeed, it was reported in 1969 that a short-lived $[IrO_4]^+$ can be generated as a result of the β-decay of radioactive osmium in OsO_4.[33] The electronic structure calculations performed in 2010 predicted this cation to be stable.[34] Four years later, $[IrO_4]^+$ has been generated in the gas phase and identified by means of IR photodissociation spectroscopy.[22] Furthermore, the plausible existence of an iridium nitride trioxide ($IrNO_3$), a related neutral genuine Ir^{+IX} compound, was predicted based on quantum-chemical calculations.[35] However, its existence has not yet been confirmed experimentally. Additionally, the formal +IX iridium oxidation state may be expected in the $Ir(N)_3$ molecule which, however, has not been experimentally observed so far. Nevertheless, the theoretical research suggests that this species should have a D_{3h} structure in the lowest energy state and not contain Ir^{+IX} but rather Ir^{+VII} with a metal localized (d_{z^2}) configuration.[36]

In spite of the high Ir oxidation states +VIII and +IX achieved in IrO_4 and $[IrO_4]^+$, respectively, experimental confirmation for the existence of iridium compounds with +VII oxidation state has been lacking to date, while $OIrF_5$ and IrF_7 were proposed to be promising Ir^{+VII} candidates.[37] To sum up, one may suggest that the iridium oxyfluorides and fluorides represent very perspective candidates for the stabilization of the less stable iridium oxidation states. The following sections will focus on previous investigations of iridium oxyfluorides (O_xIrF_y), binary fluorides (IrF_n), fluoride monoanions (IrF_n^-) and their alkali metal ion pair.

2.1 Iridium Oxyfluorides

The generation of iridium oxyfluoride $OIrF_4$ was proposed by Ruff and Fischer in 1929 as a result when iridium hexafluoride was left in contact with glass.[27] However, the assignment was questioned by Robinson and Westland in 1956 who further corrected the species to complex salts of quinquevalent iridium of the type $M^{+I}Ir^{+V}F_6$.[38,39] The repeated fluorination of iridium dioxide was also attempted for the preparation of iridium oxyfluorides, but it failed to give any evidence of the oxyfluoride formation.[38] Burns *et al*. later afforded a specific and useful method of oxygen-fluorine exchange for the preparation of transition metal oxide tetrafluorides by using the corresponding hexafluorides with boric oxide B_2O_3.[40] While they successfully obtained some other transition metal oxide tetrafluorides ($MoOF_4$, WOF_4, $ReOF_4$, $OsOF_4$, and UOF_4) in high yield following this method, the reaction of IrF_6 with B_2O_3 only led to the formation of IrF_5, BF_3, O_2 and an involatile iridium-containing solid instead of the expected products $IrOF_4$ and BF_3. Moreover, they were not able to provide clear evidence for confirming that the involatile solid is a lower iridium oxyfluoride. On the other hand, $OsOF_4$ was obtained successfully via the hydrolysis of osmium hexafluoride in liquid hydrogen fluoride. However, this method does not seem to be applicable for the iridium oxide tetrafluoride synthesis because IrF_6 gave the oxonium salt $H_3O^+IrF_6^-$ instead of $OIrF_4$ under this experimental conditions.[41]

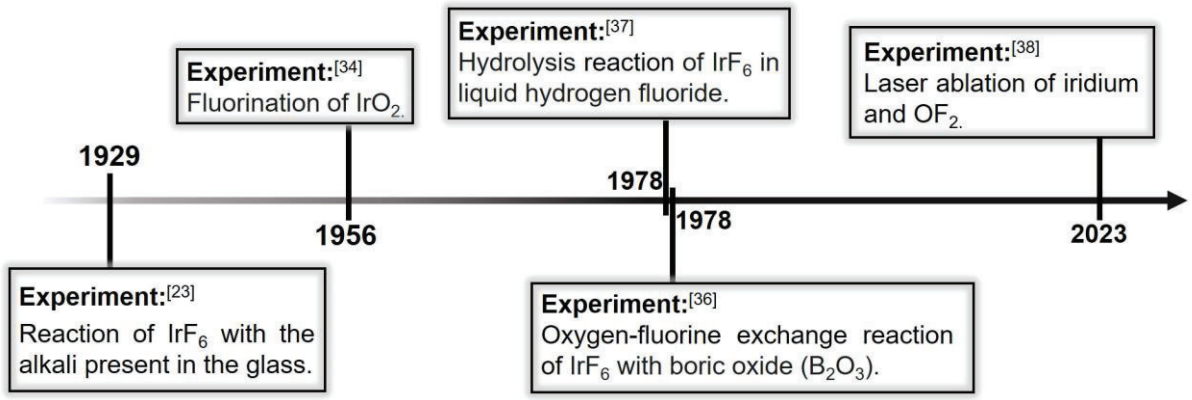

Figure 2.1.1 A timeline of preparation of iridium oxyfluorides.

As mentioned above, various methods and approaches have been proposed to produce iridium oxyfluorides over the years and they were typically based on the hexafluoride as reactant. Unfortunately, there were no iridium oxyfluorides observed in the experiments. To the best of our knowledge, there was no experimental data on iridium oxyfluorides in literature until 2023 when a recent study (Lu, Medel, Deng, Riedel; see Section 5.1) reported for the first time the successful synthesis of iridium oxyfluorides (OIrF, $OIrF_2$, and FOIrF) by the reaction of IR-laser ablated iridium atoms with OF_2.[42]

2.2 Iridium Fluorides

The synthesis of iridium fluorides dates back to 1929 when Ruff and Fisch reported the synthesis of iridium hexafluoride (IrF_6) by heating a fluor spar tube containing Ir powder under a stream of elemental fluorine at ca. 260 °C.[27] In the past decades, IrF_6, a volatile yellow solid, is the most investigated binary iridium fluoride both in the gas phase and solid-state.[9,27,28,38,43–50] The solid-state studies revealed that it has very similar crystallographic properties as the other molecular transition metal hexafluorides.[9,49] IrF_5, a yellow-green powder, was obtained by heating iridium metal and the stoichiometrically required quantity of fluorine[51] or by one-electron silicon or hydrogen redox reaction with IrF_6.[52] IrF_5 has been studied by mass spectrometry in the gas phase as well as by XRD, IR and Raman spectroscopy, diffuse reflectance UV-Vis spectroscopy, and magnetic susceptibility measurements in the solid state.[51–53] In addition to the experimental data mentioned above, another property of IrF_5 was determined, namely fluoride ion affinity (FIA), whose relatively high value indicates that IrF_5 is a strong Lewis acid.[54] The optimum synthetic approach for IrF_4 production was proposed to be the reaction of a large excess of IrF_5 or IrF_6 with iridium metal sponge[38,55] but hydrogen reduction of the hexafluoride also can be used for its preparation.[52] IrF_4 unit cell properties were determined from X-ray powder data. Magnetic susceptibility, thermal stability, electronic diffuse reflectance, mass, and IR spectra were also investigated.[52,55–57] IrF_3 can be produced by heating iridium metal powder in a mixed stream of nitrogen and iridium hexafluoride vapor at 500 °C or by thermal decomposition of iridium tetrafluoride at 400–450 °C.[58] Its unit-cell dimensions were obtained by using the powder X-ray reflexion, and the diffuse reflectance UV-Vis spectrum and thermal stability were reported as well.[38,58,59] In contrast, there is not any experimental data on IrF_2 reported to the best of our knowledge. At the same time, the iridium monofluoride (IrF) was detected and analyzed solely in the $A^3\Phi_i$-$X^3\Phi_i$ and $B^3\Phi_i$-$X^3\Phi_i$ band systems using laser-induced fluorescence and dispersed fluorescence spectroscopy. It was given the fundamental gas-phase frequency at 650 cm^{-1} which was deduced from the electronic band spacings.[60,61]

As mentioned above, the reports for the known iridium fluorides are all based on the solid-state data except for IrF, IrF_5, IrF_4, and IrF_6. It is well-known that IrF_6 has an octahedral molecular structure.[9,28] While IrF_5 and IrF_4 were studied by the gas-phase mass spectrometry,[52] there is still no detailed structural information in literature. The molecular low-valent iridium fluorides IrF_n (n = 1–5) have virtually not been studied spectroscopically yet although their thermochemical studies and structural predictions have been reported.[37,54,62,63] In this way, the bond length of diatomic IrF is 192.8 pm according to the calculations made by Kalamse and co-workers at the MP2 level while the vibrational frequency was predicted to be 575 cm^{-1}.[62] According to the B3LYP calculations involving unspecified basis sets with scalar-

relativistic PP performed by Siddiqui and Rasheed two years later, the Ir–F bond distance in IrF is 194.5 pm.[63] They also calculated the molecular structures for other binary iridium fluorides IrF_2, IrF_3, IrF_4, IrF_5 and IrF_6.[63] Based on the quantum-chemical calculations, IrF_2 has a bent structure with Ir–F bond lengths of 189.7 pm. IrF_3 shows a pyramidal structure with two short Ir–F bond lengths of 186.2 pm and one slightly longer Ir–F bond length of 186.5 pm, while it is hard to recognize the IrF_4, IrF_5 and IrF_6 structure symmetries based on the data provided in Ref. 57.[63] The IrF_5 molecule was also theoretically investigated by Riedel *et al.* and it was predicted to show a C_{2v} structure in the triplet ground state.[37] However, another work reported that the scalar-relativistic B3LYP/aT-PP calculations favor IrF_5 to be in the quintet ground state ($^5B_1$) with C_{4v} symmetry while the $^3A_1/C_{4v}$ state was computed to be slightly higher in energy by 19.7 kJ mol^{-1}.[54] It was also reported that the SOC stabilization increases from IrF_6 to IrF_5, which may be explained by the fact that the $^4A_{1g}$ state of IrF_6 has half-filled degenerate t_{2g} orbitals.[37,54]

Higher oxidation states in binary iridium fluorides than +VI have not yet been confirmed experimentally but some theoretical investigations were reported.[19,37] IrF_7 was predicted to have a pentagonal-bipyramidal (D_{5h} symmetry) structure in the triplet ground state. Furthermore, it was shown that IrF_7 is a kinetically stabilized molecule and potentially might be detected in gas-phase or matrix-isolation experiments.[37] IrF_8 was predicted by quantum-chemical calculations to show a square antiprismatic (D_{4d} symmetry) structure in the doublet ground state.[37] IrF_9 shows a minimum on the potential energy surface with D_{3h} symmetry in its singlet ground state.[37] Moreover, quantum-chemical calculations predicted both IrF_8 and IrF_9 to be metastable towards the decomposition into IrF_6 and F_2 at ambient conditions.[37] However, according to the more recent calculations, high pressure conditions (above 39 GPa) may promote the formation of IrF_8 out of IrF_6 and F_2 molecules.[19]

Based on the data mentioned above, one may conclude that the experimental data on the molecular properties of the binary iridium fluorides are rather scarce, and novel studies are needed to fill this gap. Recently, we managed to synthesize molecular iridium fluorides IrF_n (n = 1–6) and stabilize them under matrix isolation conditions (Lu, Tsegaw, Wodyński, Li, Beckers, Kaupp, Riedel; see Section 5.2). The synthesis of these compounds was performed by two methods: laser ablation of iridium with fluorine and, in the case of IrF_n (n = 1–5), photo-initiated defluorination of iridium hexafluoride. These products were characterized by matrix-isolation IR spectroscopy in conjunction with quantum-chemical calculations.[64]

Table 2.2.1 Experimental and theoretical results for binary iridium fluorides IrF_n ($n = 1–9$).

Species	Experiments		Quantum-chemical calculations	
	State	Method	Method	Symm., State
IrF_9	–	–	B3LYP[37]	D_{3h}, singlet
IrF_8	–	–	B3LYP[37]	D_{4d}, doublet
IrF_7	–	–	B3LYP[37]	D_{5h}, triplet
			B3LYP/SDD[63]	singlet
IrF_6	gas phase	1) IR spectroscopy[46]	B3LYP/SDD[63]	doublet
		2) electron diffraction spectroscopy[28]	DV-Xα[65]	O_h
		3) Raman spectroscopy[44]	CCSD(T)/aT-PP[54]	O_h, $^4A_{1g}$
		4) UV-vis spectroscopy[43]	BLYP-ZORA[54]	O_h, $^4A_{1g}$
	solid (yellow)[50]	1) single crystal X-ray diffraction spectroscopy[49]	BLYP-ZORA-SO[54]	O_h, $^4A_{1g}$
IrF_5	gas phase	1) mass spectrometry[52]	B3LYP[37]	C_{2v}, triplet
	solid (yellow-green)[52]	2) IR spectroscopy[52]	B3LYP/aT-PP[54]	C_{4v}, $^5B_1$
		3) diffuse reflectance UV-Vis spectroscopy[53]	B3LYP/SDD[63]	singlet
		4) X-ray diffraction powder patterns[51]	BLYP/TZ2P[54]	C_{4v}, $^5B_1$
		5) Raman spectroscopy[52]	BLYP-ZORA[54]	C_{4v}, $^5B_1$
		6) magnetic susceptibility measurements[51]	BLYP-ZORA-SO[54]	C_{4v}, $^5B_1$
IrF_4	gas phase	1) mass spectrometry[52]	B3LYP/SDD[63]	doublet
	solid (red-brown)[52]	2) electronic diffuse reflectance spectroscopy[57]		
		3) IR spectroscopy[52]		
		4) X-ray powder reflexion spectroscopy[55]		
		5) magnetic susceptibility measurements[55]		
		6) thermal stability (stable to 400°)[55]		
IrF_3	solid (brownish-black)[38]	1) X-ray powder reflexion[58]	B3LYP/SDD[63]	C_{2v}, singlet
		2) diffuse reflectance UV-Vis spectroscopy[59]		
		3) thermal stability (stable to 250°)[38]		
IrF_2	–	–	B3LYP/SDD[63]	C_s, doublet
IrF	Gas phase	1) laser-induced fluorescence spectroscopy[60]	MP2/SDD[62]	$C_{\infty v}$, $^3\Delta$
		2) dispersed fluorescence spectroscopy[60]	B3LYP/SDD[63]	$C_{\infty v}$, singlet

2.3 Iridium Fluoride Monoanions and their Alkali Ion Pairs

Siddiqui and Rasheed revealed a number of interesting properties of a series of fluoroiridate monoanions IrF_n^- (n = 1–7) by performing DFT calculations based on structural studies: the HOMO–LUMO gap and two fragmentation channels ($IrF_n \rightarrow IrF_{n-1} + F$ and $IrF_n \rightarrow IrF_{n-2} + F_2$).[63] Among the series of monoanions, the maximum HOMO–LUMO gap was found to be at IrF_5^-, and the dissociation energies decrease successively as the number of F atoms increases. However, the only experimentally known binary iridium fluoride monoanion is IrF_6^- which is stabilized in the form of its solid salts with various counterions. Westland and co-authors originally reported the successful synthesis of solid M[IrF_6] (M = Li, Na, K, Rb, Cs) salts containing the IrF_6^- anion. These species were obtained by the reaction of bromine trifluoride with mixtures of alkali metal and iridium bromides.[66] To the best of our knowledge, only solid-state data were reported for such alkali metal salts M[IrF_6], namely single crystal data,[67–69] synchrotron X-ray powder diffraction (SPDD) measurements,[70,71] electronic diffuse reflectance spectra,[72] high-resolution ^{19}F NMR[73] and Raman spectra [68,74] as well as magnetic susceptibility[68,75] measurements. Additionally, it was found that the M[IrF_6] (M = K, or Cs) salts display the temperature-independent paramagnetism which is consistent with the absence of EPR signal of [H_2F][IrF_6].[73,75,76] In a crystalline environment with the counterions $[XeF_5]^+$,[77] $[Br_3]^+$,[78] $[ClF_2]^+$,[79] $[ClO_2]^+$,[80] $[Cl_4]^+$,[76] IrF_6^- has the shape of a slightly distorted octahedron with almost equal Ir–F bonds ranging from 184–187 pm for the shorter and 189–191 pm for the longer bond due to the interactions with the surrounding counter cations. The corresponding Raman bands of IrF_6^- of the known crystals are between 667–679 cm^{-1}.[68,74,76,81] However, experimental spectroscopic and theoretical investigations on the molecular M[IrF_6] ion pairs have been lacking to date.

IrF_6^-, is an isoelectronic molecule to the well-known PtF_6 molecule which is a rare case where relativistic effects in conjunction with SOC effect have an important role for accurate diamagnetic octahedral molecular structure descriptions,[9,82–84] and has therefore drawn considerable attention in theoretical investigations.[54,73,85] The D_{2h} structure of the IrF_6^- anion as predicted by NR *ab initio* Hartree–Fock calculations of Gabuda and co-workers in 2001 is caused by the JT orthorhombic distortion. However, the experimental evidence from the solid-state high-resolution ^{19}F NMR data based on the large SOC constant λ_{so} supports an octahedral IrF_6^- anion in K[IrF_6].[73] The structure of molecular IrF_6^- calculated by Dixon and co-workers in 2010 at the CCSD(T) level and two-component ZORA including SOC levels was predicted to have $^3A_{1g}/D_{4h}$ ground state at both levels while the energies of D_{3d} and D_{4h} structures are extremely close at ZORA-SO level.[54] The theoretical finding reported by Restrepo and co-workers revealed that the structural distortion of D_{4h} symmetry in its singlet

state configuration is presented in non-relativistic calculated IrF_6^- structure while an octahedral molecular structure with the closed-shell singlet (CSS) ground state is stabilized by the SOC effects in relativistic four-component Dirac-DFT calculations.[85]

The high-valent monoanion IrF_7^- was investigated computationally but has never been observed experimentally.[54,63] IrF_7^- was predicted to be a $^2B_1/C_{2v}$ structure which is in contrast to the predicted energetically favored "non-classical" PtF_7^- anion with a very weak external F–F bond between a PtF_6^- fragment and a fluorine atom.[9,54,86] It was also predicted at the B3LYP level that IR-active bands of this species are located at 631, 616, and 595 cm^{-1} while the calculated IrF_6^-–F BDE is about 41.8 kJ mol^{-1}.[54] The possible existence of $[NO]^+[IrF_7]^-$ as a reaction intermediate in the reaction of ONF with IrF_6 was proposed by N. Bartlett and co-workers in 1966 and only one decomposition product $[NO]^+[IrF_6]^-$ was detected.[6,7] Recently, Z. Mazej and co-authors reported experimental attempt to prepare $Cs[IrF_7]$ salt by the photochemical reaction of CsF, iridium metal, and UV-irradiated F_2 in anhydrous HF, but the only obtained main product was $Cs[IrF_6]$ salt.[68]

Table 2.3.1 Predicted structures of molecular IrF_6^- and IrF_7^-.

Species	Method	Symm.; State	*d*(Ir–F) in pm, degree in °
IrF_6^-	CCSD(T)/aug-cc-pVTZ-PP[54]	D_{4h}; $^3A_{1g}$	184.9 (×2), 189.7 (×4)
	CCSD(T)/aug-cc-pVTZ-PP[54]	D_{3d}; $^3A_{1g}$	188.1, 91.3°
	BLYP-ZORA/TZ2P[54]	D_{3d}; $^3A_{1g}$	194.1, 91.1°
	BLYP-ZORA-SO/TZ2P[54]	D_{3d}; triplet	194.0, 90.4°
	BLYP-ZORA-SO/TZ2P[54]	D_{4h}; triplet	195.2 (×2), 193.8 (×4)
	Hartree–Fock[73]	D_{2h}	191.2 (×2), 182.6 (×4)
	four-component relativistic Dirac-LDA/6-311+G*[85]	O_h; singlet	188.8
	four-component relativistic Dirac-LDA/6-311G*[85]	O_h; singlet	188.6
	four-component Dirac-B3LYP[85]	O_h; singlet	190.7
	non-relativistic B3LYP[85]	D_{4h}; singlet	200.9 (×2), 191.4 (×4)
IrF_7^-	B3LYP/aug-cc-pVDZ-PP[54]	C_{2v}; $^2B_1$	191.4 (×2), 193.7 (×2), 191.2 (×2), 189.6 (×1)
	B3LYP/aug-cc-pVTZ-PP[54]	C_{2v}; $^2B_1$	190.7 (×2), 193.1 (×2), 190.2 (×2), 185.5 (×1)
	BP86/aug-cc-pVDZ-PP[54]	C_{2v}; $^2B_1$	193.1 (×2), 195.2 (×2), 192.8 (×2), 191.4 (×1)
	BP86/aug-cc-pVTZ-PP[54]	C_{2v}; $^2B_1$	192.5 (×2), 194.6 (×2), 191.9 (×2), 190.3 (×1)

Our recent work (Lu, Wodyński, Reimann, Medel, Kaupp, Riedel; see Section 5.3) is aimed to fill this blank spot in the experimental identification and characterization of molecular IrF_n^- anions and their ion pairs. The molecular IrF_5^- and IrF_6^- anions and $M[IrF_6]$ (M = Na, K, Rb, Cs) ion pairs were prepared by the co-deposition of the laser-ablated alkali metal fluorides MF with IrF_6 and were stabilized under the matrix isolation conditions.

2.4 Matrix Isolation Spectroscopy

The matrix-isolation method was pioneered and developed by George C. Pimentel and George Porter in the middle of 1950s.[87] This approach was conceived as a tool to be used for trapping isolated guest molecules of interest such as highly reactive or unstable species or their precursors, rapidly co-condensed together with a large excess of an inert host gas under cryogenic temperatures (3–20 K) in an evacuated chamber ($< 10^{-5}$ mbar). At a sufficiently low temperature, each guest molecule is immobilized in a solid cage surrounded by inert host gas thus inhibiting intermolecular interaction.

In order to minimize the perturbation of the electronic structure of a studied molecule, it is best to create an environment which has a minimal interaction with the isolated guest molecules. To this end, the noble gases seem to be the best choice, because they have a completely filled valence shell and thus called as chemically inert atoms. The lower atomic number of a noble gas (Xe > Kr > Ar > Ne) the lower polarizability is observed, which implies the smaller perturbation of guest molecules by this matrix material. It is the reason why Ne and Ar (He cannot be solidified under the conditions used in the matrix isolation) are widely used in the matrix isolation spectroscopy.[88] Thus, neon is one of the most suitable inert host gasses due to the least interaction with guest molecules and its availability to produce a highly transparent matrices. On the other hand, very low temperatures are needed as neon does not form any stable matrix above 12 K. However, argon matrices despite being less inert towards the guest molecules has the higher sublimation temperature (up to 35 K) providing the possibility to investigate chemical reactions in a wider range of temperatures. The heavier noble gases (Kr and Xe) are also utilized for specific tasks in matrix isolation experiments (for example, molecular reactions in a wide range of temperatures), but they are much less suitable for molecular spectroscopy due to the relatively high host-guest interaction. Especially with fluorine it can react and form the corresponding rare gas fluorides.[89] In addition to the noble gas matrices in certain cases, other molecules may be used as a matrix material, for example, N_2, CH_4, SF_6, and other relatively inert molecular hosts.[90] Some reactive matrix hosts (F_2, CO, and O_2) are also used to react with substances of interest to form the demanding compounds. For instance, F_2 as matrix host is known to produce the fluorides in higher oxidation state[91,92] while CO or O_2 can be used for trapping carbenes or nitrenes.[93] Furthermore, in some cases an additive can be doped to inert host material to achieve a certain function, e.g. CCl_4 can be added as an electron acceptor in order to study various radical cations.[94,95]

The trapped species can be probed by a variety of spectroscopic techniques. IR spectroscopy is the most widely used tool because of its versatility and structural informativity,[42,47,84,92,94,95] but other techniques, such as Raman,[96,97] UV-Vis,[97,98] and EPR

spectroscopies[99] are also applied to identify the different highly reactive species trapped in a matrix.

The cryogenic temperatures used in the matrix isolation can reduce the excited state population and keep the trapped molecules in the ground state, apart from the very extreme and thus very rare cases, for example, uranium dioxide (UO_2) molecule. The ground state reversal of UO_2 occurs when replacing the neon matrices by the more polarizable argon matrices.[100] Additionally, the trapped molecules in solid matrices are held tightly within the crystal lattice as compared to gas phase IR study. Therefore, rotations are largely suppressed, reducing the complexity of IR spectra and making the observed bands easier to assign. Vibrational frequencies of molecules are relatively independent from interactions with other molecules in the gas phase, but the interaction between the isolated species and any rigid inert host gas at very low temperature leads to the matrix shifts and matrix splittings. The matrix shift can be described as the difference between the corresponding vibrational frequencies in the gas phase and in a matrix ($\Delta\nu = \nu_{gas} - \nu_{matrix}$) and its magnitude host-guest interaction. In general, the shift due to the weak interaction is rather small in Ne and Ar and is often “red” shifted (downshift), but the case of “blue” shift (upshift) is also known.[101] However, in some cases, in particular the formation of noble-gas complex with a guest molecule and the change of a guest molecule symmetry due to the strong interaction with the host in which the noble gas atoms acting as electron donors into localized low-lying empty or partially filled orbitals of the guest, make a sufficient matrix shift.[102,103] Matrix splitting is another effect which can be observed in the matrix IR spectra. It mainly originates from the different orientations of the trapped molecules inside the slightly different matrix cavities and often disappears after the matrix sample annealing to sufficiently high temperature.[104]

As mentioned above, the process of a matrix deposition implies the co-deposition of the guest molecules or their precursor together with the excess of a host gas onto the cooled cryostat substrate. The easiest case for obtaining certain samples is the simple deposition of a mixture of guest species which are gases at room temperature and pressure (e.g. F_2 or OF_2 used in the present thesis) under access of noble gases. Following this method, the thermally stable species with sufficient volatility without decomposition at room temperature can also be easily prepared (e.g. CCl_4).[94,95] Control of the vapor pressure is important for thermally less stable or highly reactive guest species generation. It is carried out by setting the bath temperature for a U-tube containing the guest species installed in the host-gas line in front of the matrix chamber (e.g. during deposition of 4-acetylbenzoyl azide the temperature of U-tube was about 20 °C).[105] If the guest precursor reacts with the glass, the U-tube can be replaced by PFA tube which is chemically inert and resistant to nearly all chemicals (in this thesis, the PFA tube was used to preserve pure IrF_6). A stream of host gas passing through the tube will carry the guest species together into the matrix chamber and onto the cryogenic matrix support.

More sophisticated approaches are required in such cases if the guest species are nonvolatile materials: the evaporation can be controlled by a Knudsen cell consisting of a quartz tube and a heating element.[106] The flowing host gas allows its efficient mixing with the guest molecules emanating from the heated tube and then co-condensed to the matrix support. Another powerful method which is widely applied for evaporating the species with extremely low vapor pressure is the laser-ablation technique.[88] It seems to be the only appropriate approach in the case of the alkali metal fluorides and the metals like those considered in the present work. Apart from aforementioned introduction for direct deposition of precursor molecules, reaction products can be generated from the corresponding precursor depending on the demands. It can be carried out before or during deposition of host/precursor-mixtures by flash vacuum pyrolysis through a very hot ceramic tube, exposure to far-UV light, or passing through a microwave discharge.[107]

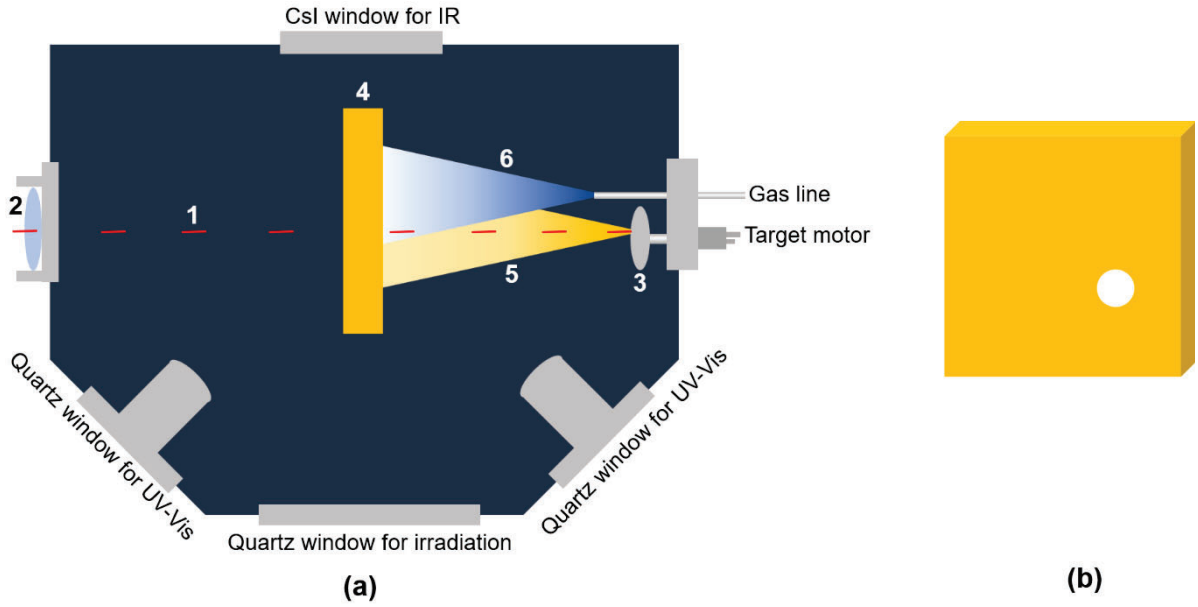

Figure 2.4.1 (a) An illustration of a matrix chamber combined with IR and UV-Vis windows for co-depositing laser-ablated material with a host gas during the laser-ablation process at cryogenic conditions. (b) Side view of a gold-plated copper matrix support with a hole. For IR spectroscopic measurement, the matrix support is rotated 90° counterclockwise, for irradiation experiments or UV-Vis spectroscopic measurement 90° clockwise. 1 pulsed laser beam, 2 focusing quartz lens, 3 a rotating laser ablation target, 4 a gold-plated copper matrix support with a hole, 5 plasma plume, 6 precursor gas.

The basically experimental setup used in this work is shown in Figure 2.4.1. A closed-cycle helium cryostat (Sumitomo Heavy Industries, RDK-205D) was employed to keep the very low-temperature conditions (5–20 K) inside the matrix chamber. Additionally, the high vacuum ($< 10^{-5}$ mbar) system provided by using the combination of an oil diffusion pump (Leybold vacuum DIP 3000) and a rotary pump was maintained at all times within the cryostat. The laser

beam (1) at λ = 1064 nm of a neodymium-doped yttrium aluminum garnet (Nd:YAG) laser (Continuum, Minilite II, 10 Hz repetition rate, 50–60 mJ pulse^{-1}) guided by a focusing quartz lens (2) was focused onto a rotating target (3) through a hole in the gold-plated copper support (4). The vaporized target material forms a plasma plume (5) and reacts with all gaseous precursors (6) and will be rapidly co-deposited on the sufficiently cold gold-plated copper matrix support (4).

After a sufficient amount of material deposition, the matrix support (4) can be rotated 90° counterclockwise or clockwise for IR or UV-Vis spectroscopic measurements, respectively. The CsI window used for IR absorption spectroscopy was attached at the back of the matrix chamber. The IR spectra in this work were recorded on a Bruker Vertex 80v with 0.5 cm^{-1} resolution in the region 4000–450 cm^{-1} by using a liquid-nitrogen-cooled MCT detector. When the matrix support (4) is rotated 90° clockwise after the sample deposition, the radiation of the UV-Vis spectrometer was directed into a quartz optical fiber, through a quartz lens inside the cryostat and passed two times over the matrix deposited on the surface of cold gold-plated mirror. A second quartz lens and fiber collected the reflected radiation, and then directed it into the spectrometer. The UV-Vis spectra in this work were recorded with a Perkin-Elmer Lambda 850+ UV spectrometer with a spectral resolution of 1.0 nm in the range of 200–850 nm.

The matrix reactions can also be induced after a sample formation via the matrix annealing or irradiation. One may irradiate a matrix via a quartz window by using different light sources depending on the needs of the specific experiment, such as LEDs, a UV lamp, or a mercury-vapor lamp and by keeping the matrix support at the UV-Vis measuring position during the sample irradiation. The annealing to higher temperature allows the initially trapped small atoms (and sometimes molecules) to move through the softened matrix which may eventually result in the bimolecular chemical reactions. The exact annealing temperature value depends on the nature of a matrix material and the purpose of an experiment. It is advisable to set up the highest annealing temperature of the used matrix material no more than a half of its melting point. In this work, the Ne matrices were annealed to the temperatures up to 11 K while Ar matrices were annealed up to 35 K.

Furthermore, annealing or photolysis with a specific wavelength can effectively help with the identification of the individual species in a complicated spectrum. Thus, a set of bands which belongs to the same species should show the similar physico-chemical behavior. In this context, the difference spectra are really useful for the discerning the changes of the bands especially the very weak ones. Another powerful approach of the absorption band assignment is the isotopic substitution. The idea of this approach based on the fact that the vibrational frequencies depend on the mass of the atoms involved in these vibrations. Hence, one can expect the shifts of the corresponding absorption bands when changing the atomic mass of

specific atoms, i.e. dealing with the isotopically-labelled compounds. For example, the shift $^{18/16}OF_2$ can be determined as $\Delta\nu = \nu(^{18}OF_2) - \nu(^{16}OF_2)$, while fluorine is a neat element.[42,108]

The other powerful approach is computational chemistry. It can give a lot of useful information about species in question and, in particular, its spectroscopic parameters thus proving or disproving the attribution of the experimentally observed absorption features. Its role will be discussed in the next Section.

2.5 The Role of Computational Chemistry

Quantum-chemical calculations have significantly advanced in the last several decades and now they play a crucial role in physics and chemistry and, in particular, in molecular spectroscopy. Many different theoretical methods have been developed for the calculations of structures and properties of molecules in the last decades.[109–112] DFT, one of the most widely used methods, often gives good predictions for the molecular electronic structure, spectroscopic, and thermochemical data at reasonable computational costs.[113] It is worth noticing that the calculation of systems containing transition metals is still complicated due to a plethora of low-lying nearly degenerate states and near-degeneracy correlation effects on the ground-state structure.[114] However, DFT is suitable in many cases for calculating transition metal compounds.[114]

In the present work, the quantum-chemical calculations were used to support the IR spectra interpretation and structural analysis of the novel iridium compounds. The DFT calculations were performed by using the Gaussian16 Revision A.03[115] and TURBOMOLE Revision V7.4.1 program packages.[116] Commonly, the B3LYP[110,117] functional was chosen for the structure optimizations of the molecules because it was found that this functional provides reliable predictions of the bands observed in IR spectra at relatively low computational cost. Moreover, in order to accurately calculate their properties, more reliable results can be obtained by the use of higher-level ab-initio methods like the CC method, typically CCSD(T),[109,118] also known as “the gold standard of quantum-chemistry” in the field of single reference methods. The CCSD(T) computations were performed by Molpro version 2021.3 software package.[119]

However, none of these methods are satisfactory for systems that display strong static correlation which arises due to presence of low-lying excited states. The computed energies and spectroscopic properties of these systems using single reference methods may subject to large errors and disagree with the experimental results. For the CC theory, T_1, D_1, and %TAE diagnostics can be used as diagnostic values to evaluate the “amount” of multi-reference character in the wavefunction.[120,121] The single-reference treatment was proposed in the literature to yield reliable results for values of $T_1 \leq 0.05$, $D_1 \leq 0.15$ and $|\%TAE| \leq 10$ for 3d transition metal compounds ($T_1 < 0.045$, $D_1 < 0.12$ and $|\%TAE| < 10$ for 4d transition metal compounds).[120,121] However, when low-lying excited states must explicitly be considered, the non-dynamical correlation (static correlation) cannot be neglected and multi-reference calculations are mandatory for the adequate description of the molecules. The most common method for multi-reference calculation is CASSCF(n,m),[111,122] where the FCI problem is solved exactly in an active space of n electrons in m orbitals. While the CASSCF reference deals with strong correlation within the active space, the dynamical correlation is always necessary for

an accurate quantum-chemical description. It can be included by an additional perturbation theory such as CASPT2[123] or CI[124] corrections.

Moreover, it is well-known that relativistic effects have a significant influence on chemical and physical properties of the heavy elements and their compounds: the role of these effects increases with the fourth power of the full nuclear charge (Z^4).[125] Thus, when electrons move really fast and even closer to the speed of light, the non-relativistic quantum mechanics is far from adequate due to the relativistic increase of their kinematic mass. The kinematic effect (mass-velocity effect), also known as scalar-relativistic effect (spin-independent), lead to the contraction and energetic stabilization of atomic s- and p-valence subshells and the expansion and destabilization of d-valence subshells. On the other hand, there is a spin-dependent effect (SOC effect) which arises from the coupling between electron spin and electron orbital momentum. This interaction between the orbital magnetic moments of angular momentum orbitals p, d, or f types with magnetic momentum generated by its spin induces a splitting of energy levels. For example, the p orbital splits into two types: $p_{1/2}$ and $p_{3/2}$. The magnitude of SOC effect also increases as the atomic number increases roughly with the second power of the nuclear charge in the valence shell of molecules.[125] It is often believed that the consideration of SOC is mandatory for the description of the 6d elements and there is only minor importance for 5d elements but it does not mean that the effect can be completely neglected for 5d elements. For instance, in a classic case of PtF_6 molecule, the D_{4h} symmetrical minimum structure with the triplet ground state was predicted in scalar-relativistic calculations, but the consideration of the SOC effect favored an octahedral structure with the closed-shell ground state which in fact was observed in the experiments.[82] In our case, the consideration of relativistic effects including the scalar-relativistic and SOC effects is particularly important for a correct structural description of the observed compounds containing iridium heavy 5d element.[64,125] For example, the symmetry changes were found computationally for the IrF_5 molecule: the C_{2v} symmetry was predicted without the SOC effect while the higher-symmetry C_{4v} structure was expected according to the calculations including the SOC effect (in fact, the latter structure was observed experimentally (see Section 5.2 for details). The most economic and common way to account for relativistic effects is believed to be the use of ECPs.[126] This approach was applied in this work as well. Although the most accurate relativistic method is four-component Dirac Hamiltonian, it is very costly and requires significant computational resources.[127] Thus, in order to consider the relativistic effect, we used the 2c-X2C approach for the calculations containing SOC effect in the present work.[128] Additionally, the consideration of the effects can also be achieved by the DKH,[112] and the ZORA Hamiltonians.[129]

3. Objectives

This work is aimed to explore hitherto unknown molecular iridium compounds in high oxidation states. These compounds are represented by oxyfluorides, neutral iridium fluorides as well as monoanionic fluorides and their alkali metal ion pairs. This research is focused on the formation, IR spectroscopic characterization, and analysis of the electronic structures, bonding, and chemical properties. This work can be divided into three parts.

First, the experimental observation of molecular iridium oxyfluorides is still missing, and the generation and characterization of molecular iridium oxyfluorides is one of the purposes of this research. These species were generated by the reaction of laser-ablated iridium atoms with OF_2. Electronic structure calculations were performed in order to study the nature of Ir–O bond in OIrF and $OIrF_2$, and further compare the M–O bonding characteristics in OMF and OMF_2 (M = Ir, Pt, and Au) to reflect trends in the bonding of the oxo ligand.

The second purpose of this study is to obtain information about molecular iridium fluorides. It is well-known that the IR-laser deposition of transition metal atoms and fluorine is a particularly useful way for the generation of highly fluorinated species.[13,91] This method was applied in this work to synthesize the low-valent molecular iridium fluorides and study the possibility of the formation of unknown species IrF_7. Additionally, in order to support the assignment of the low-valent iridium fluorides and investigate their molecular structures in the electronic ground state, the photo-initiated defluorination of iridium hexafluoride (IrF_6) was used to produce these compounds. A comparison of experimentally observed and computed Ir–F stretching vibrations of a series of binary iridium fluorides IrF_n was utilized in order to gain an insight into their molecular structures.

The third aim of the present study is to investigate the molecular binary iridium fluoride anions and their alkali metal ion pairs. The reaction of alkali metal fluorides (MF, M = Na, K, Rb, Cs) and iridium hexafluoride (IrF_6) was studied by using laser ablation deposition and matrix isolation in order to analyze the formation and structure of molecular IrF_6^- and its alkali ion pairs M[IrF_6], and examine the possibility of the formation of free high-valent IrF_7^- anion and the corresponding alkali ion pairs M[IrF_7]. Since free IrF_6^- is isoelectronic molecule to PtF_6 which is a canonical example of the strong influence of the SOC effect on the molecular structure, electronic structure calculations including the relativistic effects with SOC were performed in order to obtain a deeper understanding of IrF_6^- molecular structure as well as its coordination structure with the alkali metal cations.

The results of this work are briefly outlined in the following chapter. For more details about these three topics, the corresponding peer reviewed articles are presented in Chapter 5.

4. Outline

4.1 The Molecular Iridium Oxyfluorides OIrF, $OIrF_2$ and FOIrF

In this work, it is shown that excited Ir atoms react with OF_2 to yield the novel iridium oxyfluorides OIrF, $OIrF_2$ and FOIrF which were characterized by the matrix isolation IR spectroscopy and electronic structure calculations. The IR spectra (Figure 4.1.1) show all assigned product bands and their isotopic shifts caused by substituting the $^{16}OF_2$ reactant with $^{18}OF_2$. The identification of these compounds was based on the observation of the metal–oxygen and metal–fluorine stretching vibrational modes and was supported by the characteristic $^{16/18}O$ isotopic shifts as well as the electronic structure calculations.

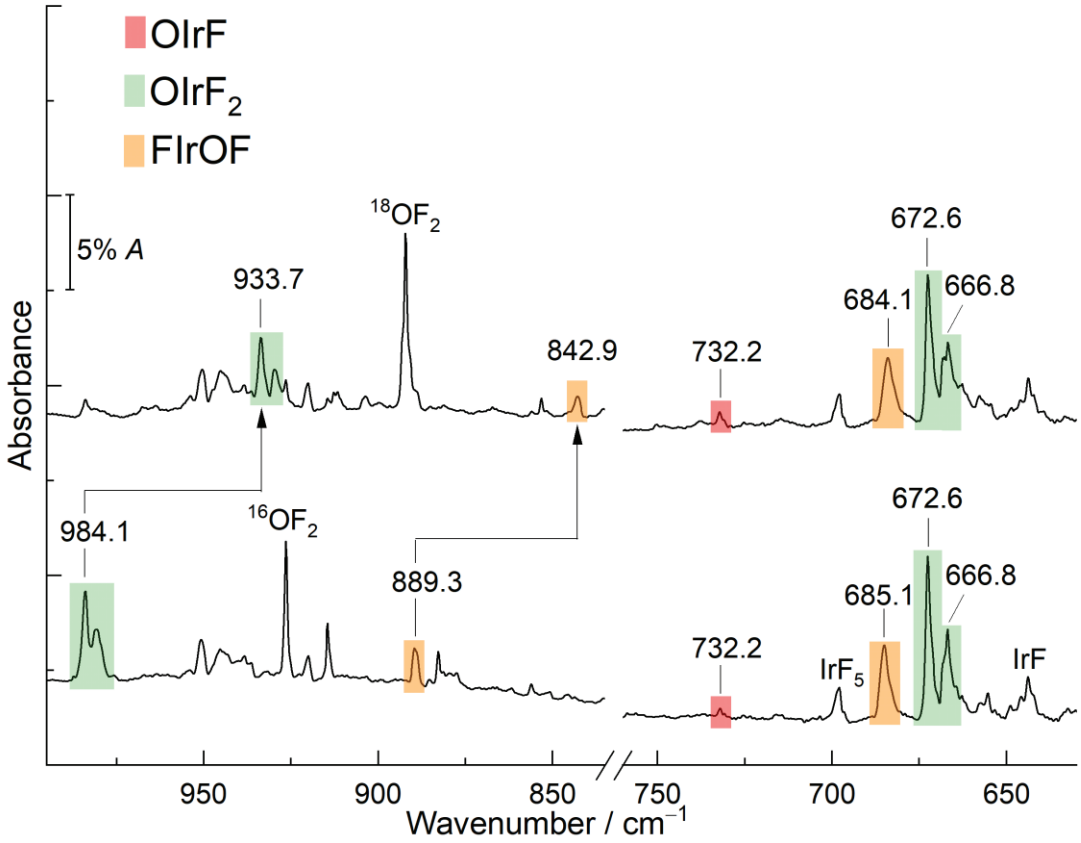

Figure 4.1.1 IR absorption spectra obtained from co-deposition of laser-ablated iridium atoms with $^{18}OF_2$ (top) and $^{16}OF_2$ (bottom) in solid neon at 5 K (see Section 5.1 for details).

The Ir–F vibrational stretch in OIrF was assigned to a weak band at 732.2 cm^{-1} with almost no $^{16/18}$O-isotopic shift in solid neon, but the much weaker O–Ir fundamental of this species which was expected to be located at 1053.4 cm^{-1} from CCSD(T) calculation was not detected. The linear molecule OIrF was found to have the closed–shell singlet ground state with a triple bond character in the terminal Ir–O bond which can be described formally as a triple bond consisting of a σ bond, a π bond, and a dative bond where the oxygen 2p lone pair donates electrons into an empty Ir 5d orbital. Moreover, the Ir–O bond distance (165.4 pm) in this molecule is close to the sum of proposed triple bond radii for iridium and oxygen ([IrO^+], 161.5 pm).[130] The CCSD(T) M–O bond distances take large jumps from 165.4 pm for OIrF to 175.1 pm for OPtF, and further to 181.0 pm for OAuF while the corresponding O–M stretching wavenumbers in OMF decrease continuously in the row Ir (1053.4 cm^{-1}) > Pt (848.3 cm^{-1}) > Au (767.9 cm^{-1}),[108,131] which can be explained by the multiple bond character for OIrF, terminal oxyl radical bond character for OPtF, and biradical bond character for OAuF.[108,131]

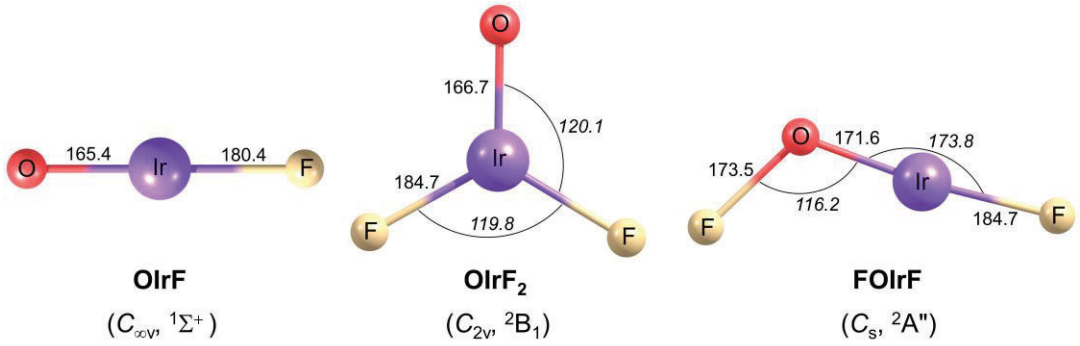

Figure 4.1.2 Optimized structures of OIrF, $OIrF_2$, and FOIrF in their ground states obtained at the CCSD(T)/aug-cc-pVTZ-PP level. Selected bond lengths in pm and angles in degrees (in *italics*) are shown.

The wavenumber band at 984.1 cm^{-1} is shifted to 933.7 cm^{-1} with an $^{16}O/^{18}O$ frequency ratio of 1.0540 which is close to the value of diatomic IrO (1.0530),[32] indicating a terminal Ir–O stretch. The bands at 666.8 and 672.6 cm^{-1} are located in the region of Ir–F stretching mode absorptions and show almost no $^{16/18}$O-isotopic shifts which are assigned to the symmetric and antisymmetric F–Ir–F stretches of $OIrF_2$. The $OIrF_2$ molecule was predicted to have the $^2B_1$ ground state with the C_{2v} symmetry which has the unpaired electron to reside in the Ir–O π*-antibonding molecular orbital. The M–O bond distance in $OIrF_2$ (166.7 pm) is notably shorter than those in $OPtF_2$ (172.8 A) and $OAuF_2$ (186.1 pm), since the M–O bond changes from a double bond in $OIrF_2$ to a single bond with radical character on the O atom in $OAuF_2$. Furthermore, a much lower spin density at the oxygen atom was found in $OIrF_2$ (even slightly lower than that at the iridium center) as compared to the $OPtF_2$ and $OAuF_2$ carrying large spin densities at the oxygen atom.[108,131]

Similar to the case of FOPdF molecule showing small $^{16/18}$O-isotope shift of 3.3 cm^{-1} of the Pd–F stretching,[108] the band at 685.1 cm^{-1} associated with the Ir–F stretching of FOIrF exhibits a small $^{16/18}$O-isotopic shift of 1.0 cm^{-1}. The predicted $^{16/18}$O shift of 47.9 cm^{-1} for Ir–O stretching in FIrOF is in good agreement with the experimental value of 46.4 cm^{-1}. The O–F vibrational stretch in FIrOF which is computed at 464.4 cm^{-1} at the CCSD(T) level was not detected due to limitations of detection range of our FTIR spectrometer (MCT-B detector, 4000–450 cm^{-1}). This molecule in the ^{2}A"/C_s state has a planar structure in which the FO and IrF moieties adopt a *trans* conformation with respect to the O–Ir bond at the CCSD(T) level.

IR-laser ablation generates excited iridium atoms which are expected to insert into the O–F bonds of OF_2 yielding the hypofluorite FOIrF during the matrix deposition. Three reaction mechanisms were considered for the formation of molecular $OIrF_2$. The first one is that $OIrF_2$ is produced spontaneously from the reaction of iridium atoms with OF_2. It was proposed based on the sample annealing results: this reaction was calculated to be highly exothermic and require virtually no activation energy. Another way of $OIrF_2$ formation is that initially formed FOIrF undergoes an exothermic rearrangement to $OIrF_2$ molecule. The third pathway is the intermediate formation of OIrF as a result of the reaction of iridium atoms and OF radicals, and OIrF reacts rapidly with F atoms to produce $OIrF_2$. It may explain the reason why the OIrF bands are very weak in the experimental observations (see Section 5.1 for details).

4.2 The Molecular Iridium Fluorides

The investigation of iridium fluorides started at 1929 beginning with the first reports on IrF_6 which is so far the highest valent binary iridium fluoride observed.[9,27,28,38,43–48] However, IrF_7 was predicted to be a kinetically stable molecule.[37] A series of binary low-valent iridium fluorides in solid state have been extensively investigated, but their molecular structures have not been yet characterized. In this work, the molecular iridium fluorides IrF_n ($n = 1–6$) were prepared by two different routes. The former one is reaction of excited laser-ablated iridium atoms with fluorine. The latter one which was used to synthesize low-valent iridium fluorides IrF_n ($n = 1–5$) is photo-initiated fluorine elimination from IrF_6. Photolysis ($\lambda = 278$ nm) of IrF_6 enabled a highly efficient and almost quantitative formation of IrF_4, whereas subsequent UV irradiation ($\lambda = 266$ nm) of IrF_4 results in the formation of IrF_6, IrF_5, IrF_3 and IrF_2 by addition and elimination of fluorine radicals and/or molecular fluorine. The products are further characterized by the matrix isolation IR and UV-Vis spectroscopies. The combination of these spectroscopic techniques allows one to correlate changes in the band intensities in the IR and UV-Vis regions during the IrF_6 photodecomposition strengthening the band assignments of the newly formed binary iridium fluorides. The quantum-chemical calculations support the attribution and allow thorough investigations of the electronic and geometric structure of the products.

The bands assigned to the IrF_6, IrF_4, IrF_3, IrF_2, and IrF are consistent with those for the structures predicted at both one- (1c-X2C) and two-component (2c-X2C) all electron DFT computations which accounts for scalar-relativistic and SOC effects, respectively. At the same time, iridium pentafluoride (IrF_5) is an intriguing molecule, since its structure has been subject to controversial discussions. The DFT computations performed by Riedel and co-workers predicted a $^3B_1$ electronic ground state with C_{2v} symmetry.[37] These predictions are in line with the results of our computations performed at the scalar-relativistic 1c-X2C and CCSD(T) levels. On the other hand, Dixon *et al*. reported that the square-pyramidal $^5B_1$ ground state with the C_{4v} symmetry is more favorable than a $^3A_1/C_{4v}$ state of an IrF_5 molecule at the scalar-relativistic B3LYP/aT-PP level.[54] However, the predicted positions and intensities of the bands for both $^5B_1/C_{4v}$ and $^3B_1/C_{2v}$ states do not agree well with our experimental values. Inclusion of SOC for IrF_5 2c-X2C-B3LYP computations results in a C_{4v} structure in the triplet ground state, and its predicted frequencies are in good agreement with the experimentally observed absorption band positions. Hence, IrF_5 is one of the very rare examples of a dominant SOC influence on the molecular structure, where a high-symmetry (C_{4v}) triplet structure is favored energetically at 2c-X2C level over the JT distorted $^3B_1/C_{2v}$ structure obtained at the scalar-relativistic levels.

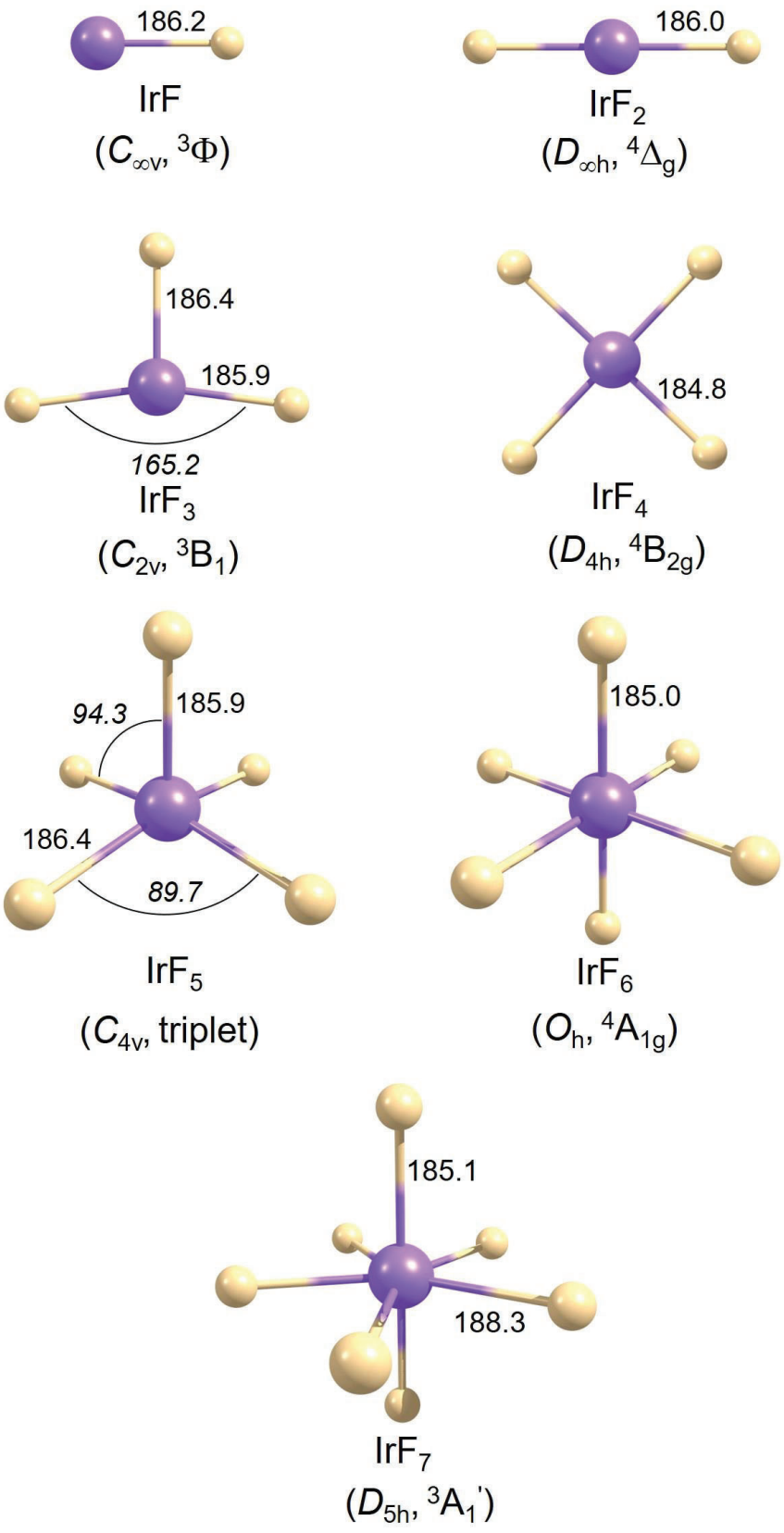

Figure 4.2.2 Structures of molecular iridium fluorides IrF_n (n = 1–7) computed at 2c-X2C-B3LYP/x2c-TZVPall-2c level. Selected bond lengths (pm) and angles (degrees, in *italics*) are highlighted.

The quantum-chemical prediction of IrF_7 makes it a target for matrix isolation[37] and opens up the possibility of detecting this molecule in our experiments. Unfortunately, all attempts to detect the absorption bands of IrF_7 were not successful, probably because they are either too weak or overlap with the absorption features of the other species. The possible formation of the $IrF_4 \cdot F_2$ complex was also examined. IrF_4 and F_2 fragments can be formed by the initial photolysis of IrF_6 and should be trapped together within the same matrix cage. However, the difference in predicted wavenumbers between the absorption band maximum positions of the isolated IrF_4 molecules and the $IrF_4 \cdot F_2$ complexes is very small (ca. 1.5 cm^{-1}). Therefore, the formation of this complex in our experiments could be suggested based on the observed photochemical reactions but could not be reliably confirmed spectroscopically as the absorption bands of this complex could overlap with the stronger features of isolated IrF_4 molecules (for details see Section 5.2).

4.3 The Molecular IrF_5^- and IrF_6^- anions and M[IrF_6] Alkali Ion Pairs

The molecular structure of free IrF_6^- has attracted a lot of interest in recent years because of the relativistic effects that have a dramatic impact on its electronic structures similar to the case of the isoelectronic molecule PtF_6. It was found that the calculations for IrF_6^- based on the non-relativistic and scalar relativistic methods result in a slightly distorted molecular structure D_{2h} or D_{4h} in the triplet ground state.[54,73] However, the four-component Dirac molecular DFT calculations result in a octahedral structure with an closed-shell ground state for this anion.[85]

The free IrF_6^- anion has not yet been experimentally detected as well as the lower-valent iridium fluoride monoanions although numerous experimental data on IrF_6^- as monoanionic ligand were associated with solid salts.[67,68,70–73,76–80,132] It should be noted that the IrF_6^- as ligand is not a regular octahedral in solid state due to the interactions with the surrounding counter cations.

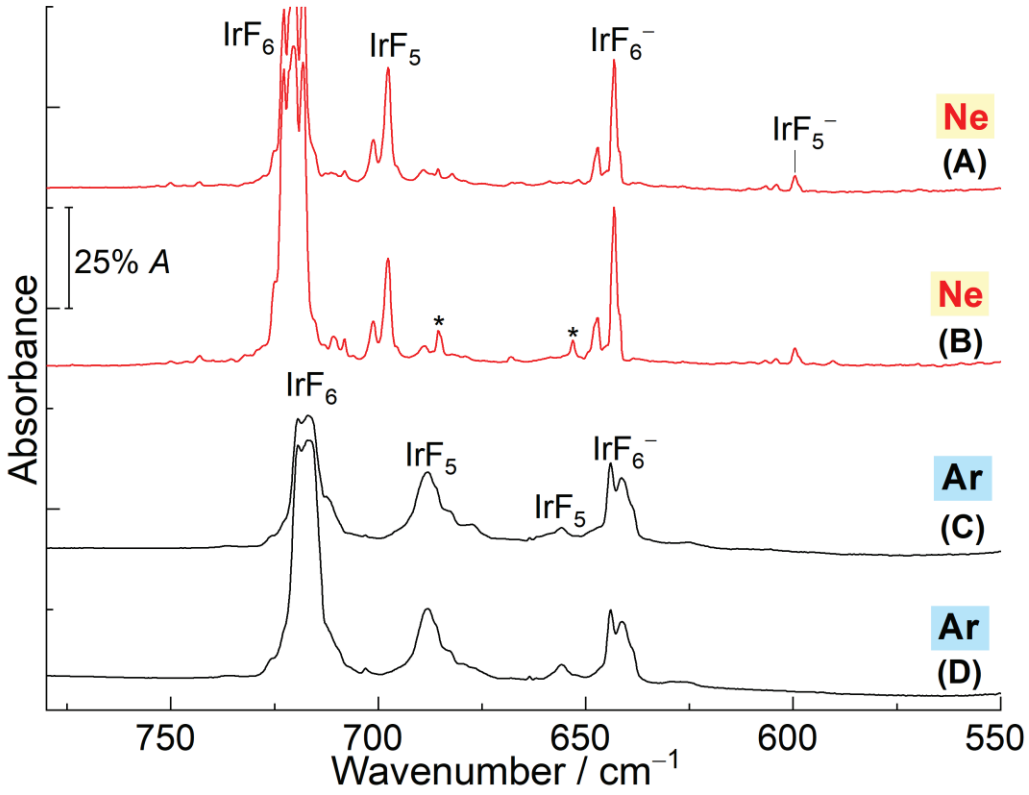

Figure 4.3.1 Infrared matrix-isolation spectra obtained in neon ((A) and (B)) and argon ((C) and (D)) matrices at 5 K. (A) and (C) represent the spectra of the reaction products of laser ablation of Pt with IrF_6; (B) and (D) represent the spectra of the reaction products of laser ablation of Ir with IrF_6. The bands marked with asterisks were not assigned.

We report the first spectroscopic characterization of isolated IrF_5^- and IrF_6^- anions. The infrared spectra recorded after co-deposition of laser-ablated metal atoms (Ir or Pt) with IrF_6 in

excess neon or argon at 5 K are shown in Figure 4.3.1. Apart from the unreacted precursor IrF_6 and the assigned IrF_5, metal-independent IR absorptions of both molecular IrF_6^- and IrF_5^- were detected in the neon matrix. However, there is no indication of the formation of the IrF_5^- anion in argon matrices. Their identification of both species is based on the results of the joint matrix-isolation IR and quantum-chemical investigations. Furthermore, the vibrational band positions provide detailed insights into their molecular structures.

The laser ablation process is associated with a hot plasma plume and a bright broad-band radiation where the IrF_5 is most likely formed by photodissociation of IrF_6 while the formation of IrF_5^- and IrF_6^- anions involves the electron capture process. It is worth noting that the high EAs of 5.81 and 6.73 eV of IrF_5 and IrF_6 sufficiently exceed those of the halogens (3.0–3.6 eV) suggesting that both molecules belong to the "superhalogens" category.[133] It implies that the IrF_5 and IrF_6 should be able to capture free electrons and form the trapped IrF_5^- and IrF_6^- anions in our experiments.

The scalar-relativistic (1c-X2C) calculations of IrF_6^- in a triplet ground state predict a D_{4h} structure with two vibrational Ir–F bands at 650 and 615 cm^{-1} having an intensity distribution of about 1:2, which clearly does not agree with the observed absorptions. The 2c-X2C calculations with SOC support a closed-shell ground state for IrF_6^- with O_h symmetry. This is consistent with the single observed IR band, no EPR signal for $[H_2F]^+[IrF_6]^-$,[76] and the temperature-independent paramagnetism for $M[IrF_6]$ (M = K and Cs).[73,75]

Another interesting result of this work is the formation and characterization of molecular $M[IrF_6]$ (M = Na, K, Rb, Cs) ion pairs which were only investigated in a solid state so far. These ion pairs were produced by the reaction of laser-ablated alkali metal fluorides MF with IrF_6 and isolated under cryogenic conditions in solid neon or argon matrices. It is worth noticing that the wavenumbers of the strongest alkali metal-dependent bands located at 661.9, 658.4, 657.4, and 656.7 cm^{-1} in neon matrices (656.5, 654.1, 653.0, and 652.1 cm^{-1}, argon matrices) in the separate experiments from NaF to CsF are higher than the Ir–F vibrational stretching frequency of isolated IrF_6^- anion at 643.2 cm^{-1} in neon and 641.2 cm^{-1} in argon matrices. This is the typical relationship for ion pairs similar to the cases of the free AuF_4^- anion (611.3 cm^{-1} in a neon matrix)[103] and $M[AuF_4]$ (M = K, Rb, Cs) ion pairs (ca. 632 cm^{-1} in a neon matrix).[134]

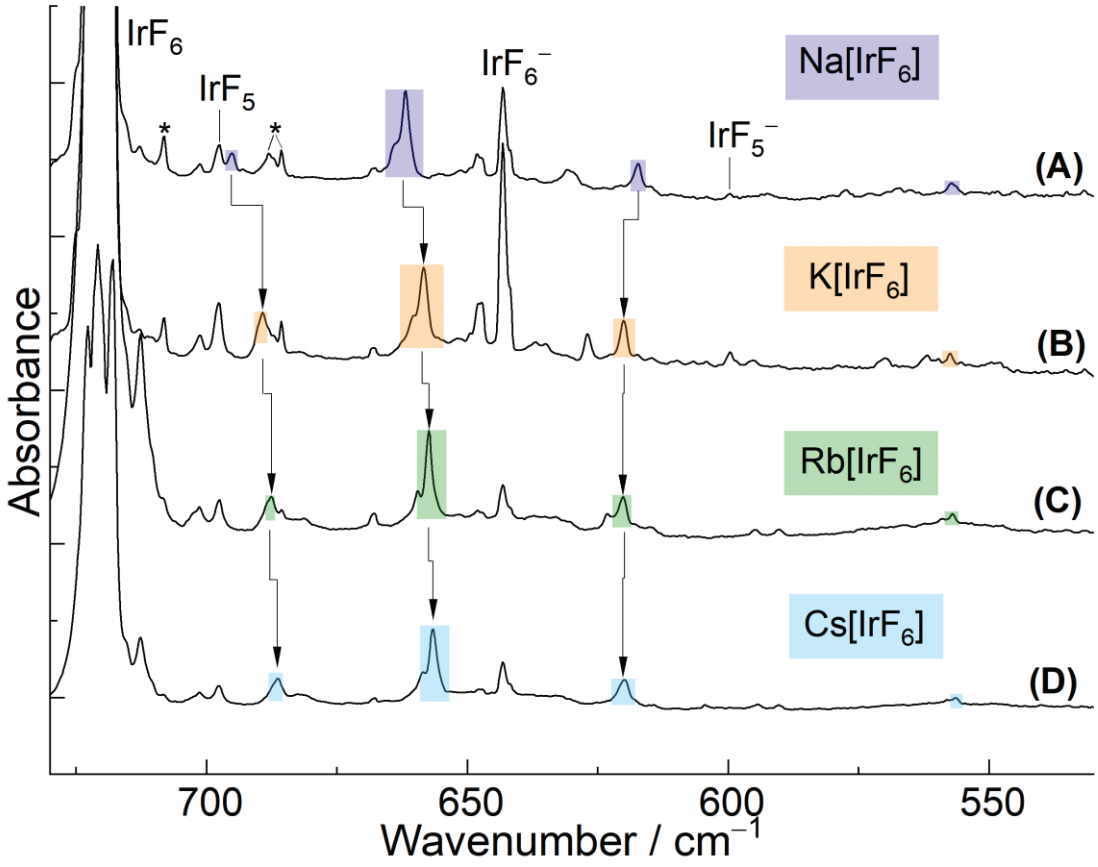

Figure 4.3.2 IR spectra of reaction products of laser-ablated MF (M = Na, K, Rb, Cs) with IrF_6 trapped in neon matrix at 5 K: (A) NaF, (B) KF, (C) RbF, and (D) CsF. The bands marked with asterisks were not assigned.

Based on the stretching fundamentals of molecular $M[IrF_6]$ (M = Na, K, Rb, Cs) ion pairs, it was concluded that all ion pairs adopt C_{3v} structures which is stabilized by alkali metal coordination to three F atoms. Similar to the case of molecular IrF_6^-, the predicted frequencies of a closed-shell ground state at 2c-X2C level with SOC show best agreement with the observed values. The observed red-shifts and blue-shifts of Ir–F vibrational stretches in the series from NaF to CsF spectra in neon matrices are excellently matched by the trend of the calculated harmonic frequencies. This is consistent with an increase of M-uncoordinated Ir–F bond length and a decrease of M-coordinated Ir–F bond length in $M[IrF_6]$ from Na to Cs, respectively.

The assignment of these bands to $M[IrF_7]$ ion pairs can be safely ruled out, because the alkali metal-dependent bands assigned to $M[IrF_6]$ were also observed and show similar photochemical behavior in the experiments of laser-ablated alkali metal chlorides MCl with IrF_6. It is worth noticing that the laser ablation of MF together with TMF_n (TM = transition metal) allows the formation of the $M[TMF_{n+1}]$: it was proven by the production of molecular alkali tetrafluorido aurate $M[AuF_4]$ (M = K, Rb, or Cs) ion pairs as a result of the reaction of laser-

ablated MF and AuF_3 in solid neon.[134] Moreover, IR bands of both IrF_7 and IrF_7^-, which are alkali metal-independent, were not observed although the high fluoride ion affinity was reported for IrF_6,[54] and the neutral molecule IrF_7 was regarded as a potential species to be observed in the gas-phase or matrix-isolation studies[37,64] (for details see Section 5.3).

5. Publications

5.1 Infrared Spectroscopic and Theoretical Investigations of Novel Iridium Oxyfluorides

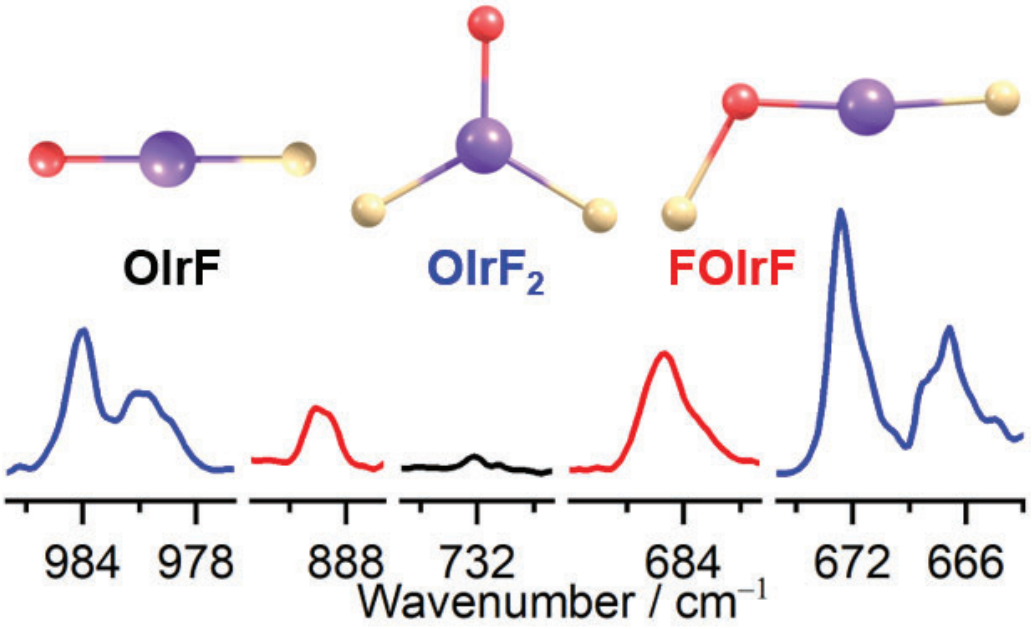

Yan Lu, Robert Medel, Guohai Deng, and Sebastian Riedel

Chemical Communication **2023**, *59*, 8532–8535. (HOT Article)

https://doi.org/10.1039/D3CC02216A

Author contribution

Yan Lu designed the project, carried out all experiments, and performed all quantum-chemical calculations, and wrote the first draft of the manuscript. Guohai Deng provided scientific guidance. Robert Medel revised the manuscript. Sebastian Riedel managed the project and revised the manuscript.

ChemComm

ROYAL SOCIETY OF CHEMISTRY

COMMUNICATION

View Article Online
View Journal | View Issue

Cite this: *Chem. Commun.*, 2023, **59**, 8532

Received 6th May 2023,
Accepted 8th June 2023

DOI: 10.1039/d3cc02216a

rsc.li/chemcomm

Infrared spectroscopic and theoretical investigations of novel iridium oxyfluorides†

Yan Lu, Robert Medel, Guohai Deng and Sebastian Riedel *

The iridium oxyfluorides (OIrF, $OIrF_2$ and FOIrF) were prepared for the first time by the reaction of IR-laser ablated iridium atoms and OF_2, isolated in solid neon and argon matrices. The assignments of the main vibrational absorptions of these products were supported by a combined analysis of IR-matrix-isolation spectroscopy with $^{18}OF_2$ substitution and quantum-chemical calculations. The OIrF molecule exhibits triple bond character. In contrast to terminal oxyl radical species $OPtF_2$ and $OAuF_2$, a much lower spin-density contribution at the oxygen atom was found in $OIrF_2$.

Iridium, one of the rarest transition metal elements in the earth's crust, is the only confirmed chemical element capable of attaining the highest oxidation state +IX in the iridium tetroxide cation $[IrO_4]^+$.[1] In general, apart from oxides, the family of such compounds with transition metals in their highest oxidation states includes fluoride and oxyfluoride molecules.[1,2] The +I to +VI oxidation states of Ir have been experimentally observed in binary iridium fluorides, with most studies focusing on the characterization of the IrF_6 molecule.[3–6] However, less is known about iridium oxyfluorides from both theoretical and experimental perspectives.[5–10] The $IrOF_5$ molecule was predicted by us as an alternative target for oxidation state +VII.[7] To the best of our knowledge, iridium oxyfluorides have not yet been experimentally verified, although various methods and approaches have been proposed to produce them over the years, typically based on hexafluorides as reactants.[5,6,8–10]

The generation of iridium oxyfluorides was first proposed by Ruff and Fischer in 1929 in the reaction of iridium hexafluoride with the alkali present in the glass.[5] However, the produced iridium oxyfluoride in this reaction was later identified to the complex salts of quinquevalent iridium in 1956.[6,9] In the following decades, some other methods were also tried out to prepare iridium oxyfluorides, such as fluorination of iridium dioxide,[6] oxygen–fluorine exchange[10] and hydrolysis reactions.[8] Unfortunately, there were no iridium oxyfluorides observed, which were proposed to be extremely unstable intermediate products, while the methods have been used successfully in the preparation of other transition metal oxyfluorides ($ReOF_4$, $OsOF_4$, UOF_4, *etc.*).[8,10] Therefore, due to their highly reactive nature, it is still a challenge to develop a useful procedure to prepare the so far experimentally unknown class of iridium oxyfluorides.

An established quite efficient and facile route to produce oxyfluoride molecules under cryogenic conditions in rare gas matrices is the reaction of laser-ablated metal atoms with OF_2.[11–17] The successful preparation and identification of such compounds indicate that synthesizing iridium oxyfluorides might be possible as well. In this work, we describe for the first-time the preparation of molecular iridium oxyfluorides (OIrF, $OIrF_2$ and FOIrF) *via* the reaction of laser-ablated iridium atoms with OF_2 in excess neon and argon at cryogenic temperatures. The matrix-isolation infrared spectroscopic identification of these new oxyfluorides is supported by isotope labelling of $^{18}OF_2$ and quantum-chemical calculations.

The infrared spectra from the reactions of laser-ablated iridium atoms with either $^{16}OF_2$ or $^{18}OF_2$ in solid neon (5 K) followed by annealing and irradiation are shown in Fig. 1. The spectra from analogous experiments in solid argon (12 K) are shown in Fig. S1 in the ESI.† The observed and calculated vibrational frequencies are summarized in Table 1 and Tables S1–S6 (ESI†).

The diatomic OF radical is the most common species in the spectra from the reactions of OF_2 and laser-ablated metal atoms and its absorption was observed at 1031.3/1028.6 cm^{-1} (^{16}OF in solid Ne/Ar) and at 1000.2/997.7 cm^{-1} (^{18}OF in solid Ne/Ar).[12,18] The bands at 643.6 and 697.8 cm^{-1} were obtained in the reaction of Ir with F_2 in excess neon, which have previously been assigned to IrF and IrF_5, respectively.[3] In addition to these known fluoride molecules, in the present work, newly formed product absorptions were observed clearly at 666.8, 672.6, 685.1, 889.3 and 984.1 cm^{-1} (Fig. 1(a)). The less intense absorption 685.1 cm^{-1} and a weak absorption at 889.3 cm^{-1}

Freie Universität Berlin, Department for Chemistry and Biochemistry, Fabeckstr. 34/36, Berlin, Germany. E-mail: s.riedel@fu-berlin.de

† Electronic supplementary information (ESI) available. See DOI: https://doi.org/10.1039/d3cc02216a

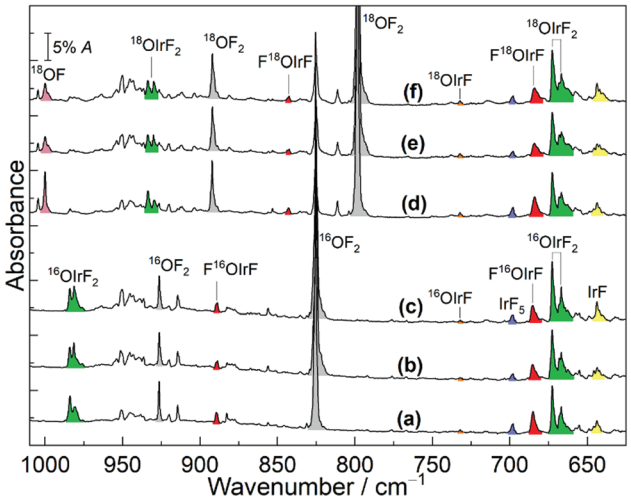

Fig. 1 IR spectra in the neon matrix at 5 K. (a) IR spectrum of the reaction products of laser-ablated Ir atoms with 0.02% $^{16}OF_2$; (b) after annealing to 9 K; (c) after full arc (>220 nm) irradiation for 15 min; (d) IR spectrum of reaction products of laser-ablated Ir atoms with 0.1% $^{18}OF_2$; (e) after annealing to 9 K; (f) after full arc (>220 nm) irradiation for 15 min.

decreased substantially after annealing to 9 K, but both absorptions increased slightly when the sample was further exposed to $\lambda > 220$ nm irradiation. However, both sample annealing and irradiation resulted in an increase of the above mentioned bands at 666.8, 672.6 and 984.1 cm^{-1}. The spectra were also recorded after sample deposition in solid argon (Fig. S1, ESI†). Apart from the known species IrF, IrF_2 and IrF_4,[3] the newly observed bands at 657.5, 663.6 and 976.0 cm^{-1} in solid argon on deposition show continued growth during annealing and irradiation of the sample.

To aid in the assignment of the new bands, all the experiments in neon and argon matrices were repeated by employing the isotopically enriched reagent $^{18}OF_2$ under similar conditions (Fig. 1 and Fig. S1, ESI†). According to the almost same behaviour of the absorptions during annealing and subsequent broadband irradiation, a large red-shift of 46.4 cm^{-1} was observed for the 889.3 cm^{-1} band in the neon matrix, while the more intense band 685.1 cm^{-1} displayed a small $^{16/18}$O-isotopic shift of 1.0 cm^{-1}. Moreover, the band at 984.1 cm^{-1} showed a distinct red-shift of 50.4 cm^{-1}, whereas no shifts were observed for the two strong bands at 666.8 and 672.6 cm^{-1} upon ^{18}O substitution. In the argon matrix, there were almost no $^{16/18}$O shifts for bands at 657.5 and 663.6 cm^{-1}. However, the higher wavenumber signal at 976.0 cm^{-1} displayed a noticeable isotopic shift of 50.2 cm^{-1}.

The bands at 666.8, 672.6 and 984.1 cm^{-1} in the neon matrix (657.5, 663.6 and 976.0 cm^{-1}, Ar-matrix) produced in the Ir and OF_2 reactions were not observed when Ir was reacted with F_2 or O_2 in previous matrix-isolation investigations.[3,19,20] This group of bands should be due to the different vibrational modes of iridium oxyfluoride molecules based on their identical behaviours throughout the experiments. Since the bands at 666.8 and 672.6 cm^{-1} in the neon matrix (657.5 and 663.6 cm^{-1}, Ar-matrix) are located in the region of Ir–F stretching mode absorptions and show almost no $^{16/18}$O-isotopic shifts, they are assigned to the symmetric and antisymmetric F–Ir–F stretches of this new molecule, respectively. The higher wavenumber band at 984.1 cm^{-1} is shifted to 933.7 cm^{-1} with an $^{16}O/^{18}O$ frequency ratio of 1.0540, which is close to the value of diatomic IrO (1.0530),[19] indicating a terminal Ir–O stretch. Hence, based on the observation of two F–Ir–F stretches and one terminal Ir–O, the new molecule is identified as $OIrF_2$.

The assignment of $OIrF_2$ is also further supported by quantum-chemical calculations. The $OIrF_2$ molecule is predicted to have three infrared-active absorptions above 600 cm^{-1} at CCSD(T) and B3LYP levels (Table 1 and Tables S1, S2, ESI†). The observed band positions at 666.8 and 672.6 cm^{-1} in the neon matrix (657.5 and 663.6 cm^{-1}, Ar-matrix) are consistent with the calculated symmetric and antisymmetric F–Ir–F stretches at 682.8 and 684.1 cm^{-1} and no $^{16/18}$O shifts were observed at the CCSD(T) level (670.5 and 671.7 cm^{-1}, B3LYP level). Similar to most of the other metal oxydifluorides OMF_2,[11,12,15–17] the predicted harmonic vibrational wavenumbers of M–O are larger than the experimental fundamentals due to neglected anharmonicity.[17] However, the calculated $^{16/18}$O-isotopic shifts due to Ir–O stretching at the CCSD(T) ($\Delta\nu(^{16/18}O)$ = 54.5 cm^{-1}) and B3LYP levels ($\Delta\nu(^{16/18}O)$ = 55.2 cm^{-1}) are in good agreement with the observed ones of ($\Delta\nu(^{16/18}O)$ = 50.4 cm^{-1}) Ne-matrix and ($\Delta\nu(^{16/18}O)$ = 50.2 cm^{-1}) Ar-matrix, further supporting the assignments for $OIrF_2$.

The set of absorptions at 685.1 and 889.3 cm^{-1} in the spectra belongs to another new product molecule. Both bands

Table 1 Calculated and experimentally observed IR wavenumbers (in cm^{-1}) of iridium oxyfluorides[a]

	Exp.						Calc.			
	Ne			Ar			CCSD(T)[b]			
Species	$\nu(^{16}O)$	$\nu(^{18}O)$	$\Delta\nu$	$\nu(^{16}O)$	$\nu(^{18}O)$	$\Delta\nu$	$\nu(^{16}O)$	$\nu(^{18}O)$	$\Delta\nu$	Modes
OIrF	—[c]	—[c]	—[c]	—[c]	—[c]	—[c]	1053.4	998.0	55.4	ν(Ir–O)
($^1\Sigma^+$, $C_{\infty v}$)	732.2	732.2	0.0	—[c]	—[c]	—[c]	741.7	741.4	0.3	ν(Ir–F)
$OIrF_2$	984.1/980.7	933.7/929.6	50.4/51.1	976.0/973.6	925.8/922.6	50.2/51.0	1033.1	978.6	54.5	ν(Ir–O)
($^2B_1$, C_{2v})	672.6	672.6	0.0	663.6	663.6	0.0	684.1	684.1	0.0	$\nu_{as}(IrF_2)$
	666.8	666.8	0.0	657.5	657.5	0.0	682.8	682.8	0.0	$\nu_s(IrF_2)$
FOIrF	889.3	842.9	46.4	—[c]	—[c]	—[c]	938.5	890.6	47.9	ν(Ir–O)
($^2A''$, C_s)	685.1	684.1	1.0	—[c]	—[c]	—[c]	698.1	697.9	0.2	ν(Ir–F)
	—[c]	—[c]	—[c]	—[c]	—[c]	—[c]	464.4	446.1	18.3	ν(O–F)

[a] The complete set of calculated frequencies is provided in the ESI (Tables S1–S6). For the CCSD(T) calculations no intensities are available. [b] Harmonic frequencies calculated at the CCSD(T)/aug-cc-pVTZ-PP level. [c] Bands were not observed, or too weak.

were detected in the neon matrix after sample deposition and decreased dramatically on sample annealing, which can be assigned to the molecule FOIrF. Surprisingly, the corresponding bands of this product were not detected in solid argon. Similar to the small $^{16/18}$O-isotope shift of 3.3 cm^{-1} of the Pd–F stretching in molecule FOPdF,[12] the band at 685.1 cm^{-1} exhibits a small but significant $^{16/18}$O-isotopic shift of 1.0 cm^{-1} and is associated with the Ir–F stretching band of this hypofluorite. Both the band positions and $^{16/18}$O-isotopic shifts show good agreement with the predicted wavenumbers at 698.1 cm^{-1} and the $^{16/18}$O-isotope shift of 0.2 cm^{-1} at the CCSD(T) level (Table 1 and Table S4, ESI†). Moreover, while the calculated wavenumber (938.5 cm^{-1}) for Ir–O stretching in FIrOF is higher than the experimental value (889.3 cm^{-1}), the predicted $^{16/18}$O shift of 47.9 cm^{-1} is in good agreement with the experimental value (46.4 cm^{-1}), similar to $OIrF_2$. The ^{16}O–F and ^{18}O–F vibrational stretches in FIr$^{16/18}$OF are computed at 464.4 and 446.1 cm^{-1} at the CCSD(T) level, respectively, but our search for both bands was unsuccessful in the detection range of our FTIR spectrometer (MCT-B detector, 4000–450 cm^{-1}).

Since OMF was the major product from the reaction of hot metal atoms with OF_2,[11–17] the formation of the elusive OIrF in the experiments should also be considered. In contrast to the very strongly IR-active Au–F stretch and the extremely weakly IR-active Au–O stretch in OAuF,[11] the B3LYP calculation predicts two absorbances for OIrF at 735.4 and 1106.0 cm^{-1} with an approximate intensity ratio of 4 : 3 (Table 1 and Tables S5, S6, ESI†). The Ir–F band in OIrF is tentatively assigned to a weak band at 732.2 cm^{-1} with almost no $^{16/18}$O-isotopic shift in solid neon, which has a large blue-shift of 88.6 cm^{-1} relative to the stretching vibration in IrF (643.6 cm^{-1}, Ne-matrix).[3] However, the O–Ir fundamental of this species was expected to be located at 1106.0 ($\Delta\nu(^{16/18}O)$ = 58.5 cm^{-1}) or 1053.4 cm^{-1} ($\Delta\nu(^{16/18}O)$ = 55.4 cm^{-1}) from B3LYP and CCSD(T) calculations, respectively. It is reasonable that this mode was not observed in this work because it is even weaker than the 732.2 cm^{-1} band. Similar to the cases of OPtF and OAuF,[11,12] attempts to detect the species OIrF in argon matrices failed, which is most likely due to the stronger Ar interactions with the formed intermediate species. In argon experiments, only the $OIrF_2$ product was produced and identified by IR spectroscopy (Fig. S1, ESI†).

To get further insights into the structures and electronic configurations of the new species, the iridium oxyfluorides OIrF, FOIrF and $OIrF_2$ were calculated at the DFT and CCSD(T) levels in conjunction with scalar relativistic pseudopotentials. All possible spin states have been considered for each molecule, which further support the experimental spectral assignments for the new species. The optimized structures are presented in Fig. 2.

A linear structure with a closed–shell singlet ground state for OIrF was obtained at both CCSD(T) and B3LYP levels (Table S5, ESI†). The calculated bond length of Ir–F in OIrF is 180.4 pm at the CCSD(T) level, shorter than that in free IrF (186.1 pm) and IrF_2 (184.9 pm).[3] Additionally, this metal–fluorine bond is much shorter than those in OPtF (189.7 pm) and OAuF (188.2 pm) (Fig. S2, ESI†).[11,12] The M–F stretching frequencies

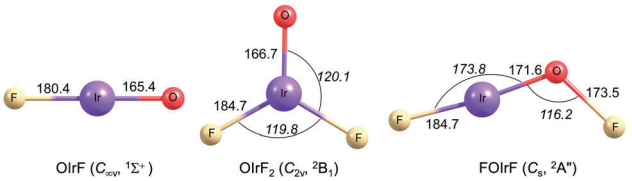

Fig. 2 Optimized structures of OIrF, $OIrF_2$ and FOIrF in their ground states at the CCSD(T)/aug-cc-pVTZ-PP level. Selected bond lengths in pm and angles in deg (in italics) are shown.

in OMF follow the same trend and are confirmed by the experiments (ν(Ir–F) > ν(Au–F) > ν(Pt–F)). Moreover, the CCSD(T) M–O bond distances take large jumps from 165.4 pm for OIrF to 175.1 pm for OPtF to 181.0 pm for OAuF, and the corresponding O–M stretching wavenumbers in OMF decrease continuously from Ir (1053.4 cm^{-1}), Pt (848.3 cm^{-1}) to Au (767.9 cm^{-1}).[11,12] Neither of the O–M vibrational stretches in OMF (M = Ir, Pt and Au) were observed in the experiments (Table S7, ESI†).[11,12] The large differences in M–O bond distances and stretching wavenumbers in OMF (M = Ir, Pt and Au) can be explained by multiple bond character for OIrF, terminal oxyl radical character for OPtF, and biradical character for OAuF.[11,12] The OIrF orbital plots show (Fig. S3, ESI†) one σ bond and two π bonds formed by the O 2p and Ir 5d atomic orbitals, although oxygen has only two unpaired electrons. Similar to the case of the closed–shell OScF molecule,[15] the terminal Ir–O bond in OIrF can be described formally as a triple bond consisting of a σ bond, a π bond and a dative bond where the oxygen 2p lone pair donates electrons into an empty Ir 5d orbital. Consistent with this character, the Ir–O bond distance (165.4 pm) in the OIrF molecule is close to the sum of proposed triple bond radii for iridium and oxygen ([IrO$^+$], 161.5 pm).[21]

At the CCSD(T) level, the hypofluorite FOIrF in C_s symmetry is predicted to have a quartet ground state (^{4}A″), closely followed by 1.2 and 16.5 kJ mol^{-1} less stable ^{4}A′/C_s and ^{2}A″/C_s structures, respectively. However, attempts to optimize a doublet structure for FOIrF failed at the B3LYP level, and the ^{2}A″/C_s state yields one imaginary frequency and the ^{2}A′/C_s state undergoes isomerization to $OIrF_2$ during optimization. While the energy difference favours the ^{4}A″/C_s structure, the vibrational wavenumbers and their $^{16/18}$O isotope shifts for the ^{2}A″/C_s state are in better agreement with our experimental values (Table S4, ESI†). The FIrOF molecule in the ^{2}A″/C_s state has a planar structure in which the FO and IrF moieties adopt a *trans* conformation with respect to the O–Ir bond (∠(Ir–O–F) = 116.2°; ∠(F–Ir–O) = 173.8°) at the CCSD(T) level (Fig. 2), similar to the structure of FOPdF.[12]

$OIrF_2$ is optimized to have a $^2B_1$ ground state with C_{2v} symmetry. The $^4B_2/C_{2v}$ state is 97.4 kJ mol^{-1} higher in energy than the ground state at the CCSD(T) level (Table S1, ESI†). The ∠(F–M–O) angles in OMF_2 (M = Ir, Pt and Au) substantially decrease from Ir to Pt to Au at the CCSD(T) level (Fig. S4, ESI†). The M–O bond distance in $OIrF_2$ (166.7 pm) is slightly longer than that in OIrF (165.4 pm), but is notably shorter than those in $OPtF_2$ (172.8 pm) and $OAuF_2$ (186.1 pm). The significant decrease in the M–O stretching wavenumber from $OIrF_2$ and $OPtF_2$ to $OAuF_2$ is consistent with a significant increase in the M–O bond distance as the M–O bond transitions from a double

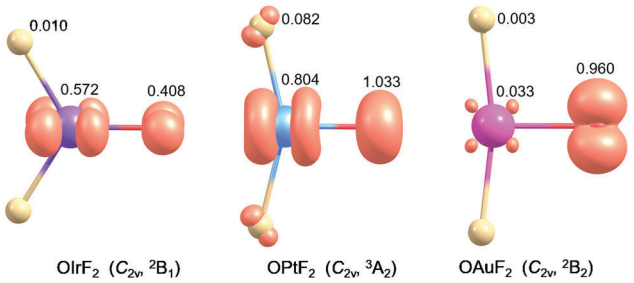

Fig. 3 The spin density (iso-surface = 0.03 electron a.u.$^{-3}$) of $OIrF_2$, $OPtF_2$ and $OAuF_2$ obtained at the B3LYP/aug-cc-pVTZ-PP level.

bond for $OIrF_2$ to a single bond with radical character on the O atom for $OAuF_2$ (Fig. S4 and Table S8, ESI†).[11,12] An analysis of the electronic structures for $OIrF_2$ showed that the unpaired electron of the $^2B_1$ state is found to reside in the Ir–O π^*-antibonding molecular orbital (Fig. S5, ESI†). In contrast to $OPtF_2$ and $OAuF_2$ carrying large spin densities ($\geq$0.96) at the oxygen atom,[11,12] a much lower spin density at the oxygen atom was found in $OIrF_2$, even slightly lower than that at the iridium center (Fig. 3). Comparing the M–F bond distances shows that there is a great increase from $OIrF_2$ (184.6 pm) to $OPtF_2$ (189.2 pm) and $OAuF_2$ (190.0 pm) (Fig. S4, ESI†).

The thermochemical stability of the observed compounds was investigated (Table S9, ESI†). IR-laser ablation generates excited iridium atoms, which are expected to be inserted into the O–F bonds of OF_2 to yield the hypofluorite FOIrF during deposition. The observed main product $OIrF_2$ is likely to have formed from three channels. One is that $OIrF_2$ is produced spontaneously from the reaction of iridium atoms with OF_2, based on sample annealing, during which negligible activation energy is required and the reaction is calculated to be highly exothermic of -929.7 kJ mol^{-1}. Another way of formation is that $OIrF_2$ is formed by an exothermic rearrangement (FOIrF $\rightarrow$ $OIrF_2$ $\Delta E = -389.0$ kJ mol^{-1}) of the initially formed FOIrF. The third way is that OIrF is initially formed from the reaction of iridium atoms and OF radicals, but it reacts rapidly further with F atoms to become $OIrF_2$, which might explain why the OIrF bands are very weak in the experimental observations.

In conclusion, excited Ir atoms were made to react with OF_2 to form the iridium oxyfluoride molecules OIrF, $OIrF_2$ and FOIrF, which have been characterized using matrix-isolation IR spectroscopy and electronic structure calculations. The identification of these compounds was based on the metal–oxygen and metal–fluorine stretches with characteristic $^{16/18}O$ isotopic shifts and support from electronic structure calculations at B3LYP and CCSD(T) levels. The B3LYP calculated molecular orbitals reveal that the linear OIrF molecule in the closed-shell singlet ground state exhibits triple Ir–O bond character. This is in accordance with the shorter bond distance and higher metal–oxygen stretching wavenumber compared with those of OPtF and OAuF. The molecule $OIrF_2$ possesses a planar geometry with C_{2v} symmetry in the $^2B_1$ ground state, for which the unpaired electron is located mainly in the Ir–O π^*-antibonding molecular orbital. A much lower spin-density contribution at the oxygen atom was found in $OIrF_2$, which is in contrast to that in terminal oxyl radical species $OPtF_2$ and $OAuF_2$ with high spin densities at the oxygen atom, along with the sharply increasing M–O bond distance as well as the decreasing FMO bond angles from $OIrF_2$ and $OPtF_2$ to $OAuF_2$.

The authors gratefully thank the Zentraleinrichtung für Datenverarbeitung (ZEDAT) of the Freie Universität Berlin for the allocation of computing resources. The authors thank for the continuous support provided by the ERC Project HighPotOx as well as the CRC 1349 (SFB 1349) Fluorine-Specific Interactions-Project-ID 387284271. Y. L. thanks the China Scholarship Council (PhD Program) for financial support.

Conflicts of interest

There are no conflicts to declare.

Notes and references

1 G. Wang, M. Zhou, J. T. Goettel, G. J. Schrobilgen, J. Su, J. Li, T. Schlöder and S. Riedel, *Nature*, 2014, **514**, 475.
2 (*a*) M. Da Silva Santos, T. Stüker, M. Flach, O. S. Ablyasova, M. Timm, B. von Issendorff, K. Hirsch, V. Zamudio-Bayer, S. Riedel and J. T. Lau, *Angew. Chem., Int. Ed.*, 2022, **61**, e202207688; (*b*) S. Riedel and M. Kaupp, *Coord. Chem. Rev.*, 2009, **253**, 606; (*c*) T. Vogt, A. N. Fitch and J. K. Cockcroft, *Science*, 1994, **263**, 1265; (*d*) E. G. Hope, W. Levason and J. S. Ogden, *J. Chem. Soc., Dalton Trans.*, 1988, 61.
3 Y. Lu, Y. A. Tsegaw, A. Wodyński, L. Li, H. Beckers, M. Kaupp and S. Riedel, *Chem. – Eur. J.*, 2022, **28**, e202104005.
4 (*a*) T. Drews, J. Supel, A. Hagenbach and K. Seppelt, *Inorg. Chem.*, 2006, **45**, 3782; (*b*) A. D. Richardson, K. Hedberg and G. M. Lucier, *Inorg. Chem.*, 2000, **39**, 2787; (*c*) R. T. Paine and L. B. Asprey, *Inorg. Chem.*, 1975, **14**, 1111.
5 O. Ruff and J. Fischer, *Z. Anorg. Allg. Chem.*, 1929, **179**, 161.
6 P. L. Robinson and G. J. Westland, *J. Chem. Soc.*, 1956, 4481.
7 S. Riedel and M. Kaupp, *Angew. Chem., Int. Ed.*, 2006, **45**, 3708.
8 H. Selig, W. A. Sunder, F. A. Disalvo and W. E. Falconer, *J. Fluorine Chem.*, 1978, **11**, 39.
9 M. A. Hepworth and P. L. Robinson, *J. Inorg. Nucl. Chem.*, 1957, **4**, 24.
10 R. C. Burns, T. A. O'Donnell and A. B. Waugh, *J. Fluorine Chem.*, 1978, **12**, 505.
11 L. Li, T. Stüker, S. Kieninger, D. Andrae, T. Schlöder, Y. Gong, L. Andrews, H. Beckers and S. Riedel, *Nat. Commun.*, 2018, **9**, 1267.
12 L. Li, H. Beckers, T. Stüker, T. Lindič, T. Schlöder, D. Andrae and S. Riedel, *Inorg. Chem. Front.*, 2021, **8**, 1215.
13 R. Wei, Z. T. Fang, M. Vasiliu, D. A. Dixon, L. Andrews and Y. Gong, *Inorg. Chem.*, 2019, **58**, 9796.
14 L. Andrews, X. Wang, Y. Gong, T. Schlöder, S. Riedel and M. J. Franger, *Angew. Chem., Int. Ed.*, 2012, **51**, 8235.
15 Y. Gong, L. Andrews and C. W. Bauschlicher, *Chem. – Eur. J.*, 2012, **18**, 12446.
16 Y. Gong, L. Andrews and C. W. Bauschlicher, Jr., *J. Phys. Chem. A*, 2012, **116**, 10115.
17 R. Wei, Q. N. Li, Y. Gong, L. Andrews, Z. Fang, K. S. Thanthiriwatte, M. Vasiliu and D. A. Dixon, *J. Phys. Chem. A*, 2017, **121**, 7603.
18 A. Arkell, R. R. Reinhard and L. P. Larson, *J. Am. Chem. Soc.*, 1965, **87**, 1016.
19 Y. Gong, M. Zhou, M. Kaupp and S. Riedel, *Angew. Chem., Int. Ed.*, 2009, **121**, 8019.
20 A. Citra and L. Andrews, *J. Phys. Chem. A*, 1999, **103**, 4182.
21 P. Pyykkö, S. Riedel and M. Patzschke, *Chem. – Eur. J.*, 2005, **11**, 3511.

5.2 Investigation of Molecular Iridium Fluorides IrF_n (n = 1–6): A Combined Matrix-Isolation and Quantum-Chemical Study

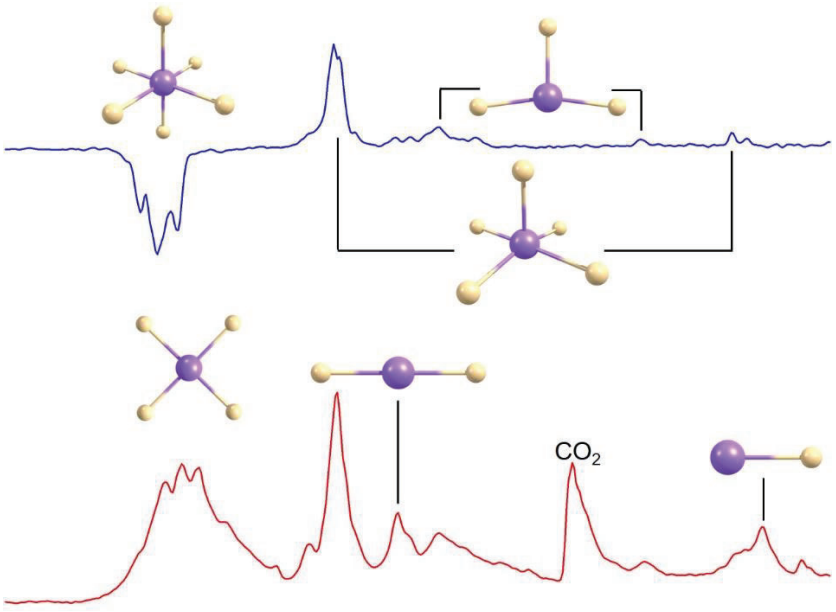

Yan Lu, Yetsedaw A. Tsegaw, Artur Wodyński, Lin Li, Helmut Beckers, Martin Kaupp, and Sebastian Riedel

Chemistry — A European Journal **2022**, *28*, e202104005.

https://doi.org/10.1002/chem.202104005

Author contribution

Yan Lu designed the project, carried out all experiments, performed quantum-chemical calculations, and wrote the first draft of the manuscript. Artur Wodyński performed quantum-chemical calculations with the SOC effect and discussed the results. Lin Li and Helmut Beckers provided scientific guidance. Yetsedaw A. Tsegaw and Martin Kaupp revised the manuscript. Sebastian Riedel managed the project and revised the manuscript.

Chemistry–A European Journal
Research Article
doi.org/10.1002/chem.202104005
Chemistry Europe
European Chemical Societies Publishing

www.chemeurj.org

Investigation of Molecular Iridium Fluorides IrF_n ($n = 1$–6): A Combined Matrix-Isolation and Quantum-Chemical Study

Yan Lu,[a] Yetsedaw A. Tsegaw,[a] Artur Wodyński,[b] Lin Li,[a] Helmut Beckers,[a] Martin Kaupp,[b] and Sebastian Riedel*[a]

Abstract: The photo-initiated defluorination of iridium hexafluoride (IrF_6) was investigated in neon and argon matrices at 6 K, and their photoproducts are characterized by IR and UV-vis spectroscopies as well as quantum-chemical calculations. The primary photoproducts obtained after irradiation with $\lambda = 365$ nm are iridium pentafluoride (IrF_5) and iridium trifluoride (IrF_3), while longer irradiation of the same matrix with $\lambda = 278$ nm produced iridium tetrafluoride (IrF_4) and iridium difluoride (IrF_2) by Ir–F bond cleavage or F_2 elimination. In addition, IrF_5 can be reversed to IrF_6 by adding a F atom when exposed to blue-light ($\lambda = 470$ nm) irradiation. Laser irradiation ($\lambda = 266$ nm) of IrF_4 also generated IrF_6, IrF_5, IrF_3 and IrF_2. Alternatively, molecular binary iridium fluorides IrF_n ($n = 1$–6) were produced by co-deposition of laser-ablated iridium atoms with elemental fluorine in excess neon and argon matrices under cryogenic conditions. Computational studies up to scalar relativistic CCSD(T)/triple-ζ level and two-component quasirelativistic DFT computations including spin-orbit coupling effects supported the formation of these products and provided detailed insights into their molecular structures by their characteristic Ir–F stretching bands. Compared to the Jahn-Teller effect, the influence of spin-orbit coupling dominates in IrF_5, leading to a triplet ground state with C_{4v} symmetry, which was spectroscopically detected in solid argon and neon matrices.

Introduction

Iridium is one of the rarest transition metal elements in the earth's crust and its complexes have been efficiently utilized in catalytic water oxidation,[1] C–H oxidation,[2] biological probes[3] and emitting materials.[4] The most common oxidation states encountered for iridium-complexes are +I and +III,[5] but IrF_6 is the most investigated and so far highest observed oxidation state of binary iridium fluoride species, and its synthesis dates back to 1929.[6] Higher oxidation states +VIII in IrO_4[7] and +IX in $[IrO_4^+]$[8] have recently been detected by infrared spectroscopy in the gas-phase, and thus iridium has the widest range of oxidation states of any element, from -III to +IX.[9] The higher oxidation states of binary iridium fluorides beyond +VI had not yet been confirmed experimentally. Computational studies predicted that IrF_7 is a kinetically stabilized molecule and a good candiadate to be detected in the gas-phase or matrix-isolation studies, whereas IrF_8 and IrF_9 were shown to be metastable due to decomposition by strongly exothermic F_2 elimination.[10] Moreover, recent theoretical studies suggested that IrF_8 can be stablized and obtained by the reaction of IrF_6 and F_2 under high pressure conditions.[11]

Numerous spectroscopic investigations of IrF_6 in the gas-phase and solid-state are well documented.[12] It was also shown that IrF_6 has very similar crystallographic properties as the other molecular transition metal hexafluorides.[13] However, experimental data on the molecular structure and spectroscopic studies of low-valent iridium fluorides are missing, while some experimental and thermochemical studies have been reported.[10,14] A systematic investigation that considers all possible iridium fluoride species is still lacking in the literature. IrF_5 was studied in the gas-phase by mass spectrometry as well as in the solid state by X-ray diffraction, infrared and Raman spectroscopy, diffuse reflectance UV-vis spectroscopy and magnetic susceptibility measurements.[14b–d] On the other hand, only the solid-state data were reported for IrF_4[14c,f,g,h] and IrF_3.[14i,j] To the best of our knowledge, molecular IrF_2 has not yet been studied spectroscopically, nor is its solid-state structure known. Molecular IrF was observed and analyzed in $A^3\Phi_i$-$X^3\Phi_i$ and $B^3\Phi_i$-$X^3\Phi_i$ band systems only, using laser induced fluorescence and dispersed fluorescence spectroscopy.[14k,l]

Herein, we report a combined experimental and quantum-chemical investigation of a series of molecular iridium fluorides IrF_n ($n = 1$–6). Different methods were applied to produce these species under matrix-isolation conditions at 6–12 K. First, it is well-known that the matrix-isolation infrared spectroscopic studies on the reaction products by co-deposition of laser-ablated transition metal atoms and fluorine is particularly useful

[a] Y. Lu, Dr. Y. A. Tsegaw, Dr. L. Li, Dr. H. Beckers, Prof. Dr. S. Riedel
Freie Universität Berlin
Institut für Chemie und Biochemie-Anorganische Chemie
Fabeckstrasse 34/36, 14195 Berlin (Germany)
E-mail: s.riedel@fu-berlin.de

[b] Dr. A. Wodyński, Prof. Dr. M. Kaupp
Technische Universität Berlin
Institut für Chemie Theoretische Chemie/Quantenchemie
Sekr. C7, Strasse des 17. Juni 135, 10623 Berlin (Germany)

Supporting information for this article is available on the WWW under https://doi.org/10.1002/chem.202104005

for the generation of highly fluorinated species.[15] Thus, the reaction between laser-ablated iridium atoms and fluorine (0.5 and 1%) in an excess of nobel gases (neon or argon) were carried out. Alternatively, binary iridium fluorides were generated by a photo-initiated defluorination of IrF_6 in solid neon and argon matrices under cryogenic conditions, allowing a systematic comparison of the results of both methods. The assignments of the obtained binary iridium fluoride species are further supported by quantum-chemical calculations up to scalar relativistic coupled cluster CCSD(T)[16] calculations and up to two-component quasirelativistic DFT calculations including spin-orbit coupling (SOC) effects.[17]

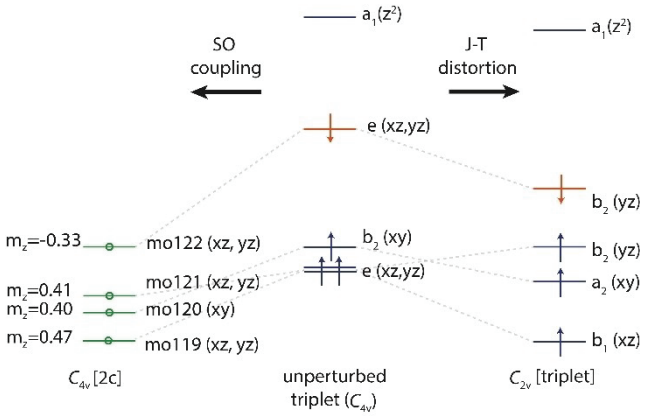

Figure 1. Simplified scheme of Jahn-Teller (JT) distortion and spin-orbit coupling (SOC) on the iridium 5d orbital splitting of triplet pyramidal IrF_5. The energy levels for the unperturbed C_{4v} triplet state were modeled from an unrestricted calculation by spatial averaging of the b_1 and b_2 levels of a C_{2v}-symmetrical wave function to the e-level that is shown. See Figure S1 for the difference energy values.

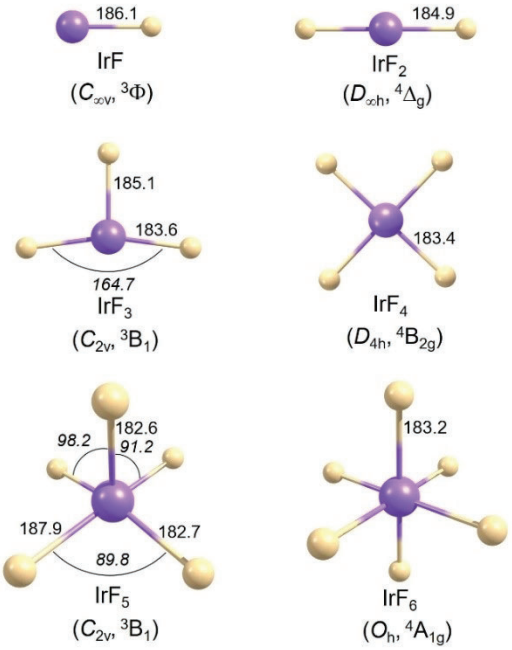

Figure 2. Computed structures of molecular iridium fluorides IrF_n ($n=1$–6) at the scalar-relativistic pseudopotential CCSD(T) level. Selected bond lengths (pm) and angles (°, in *italics*) are shown. A complete list of the computed structures is given in Tables S1-S5.

Results and Discussion

Computational results

The electronic structure of the binary iridium fluorides IrF_n ($n=$ 1–7) and of the $IrF_4 \cdot F_2$ complex were initially calculated at the DFT and CCSD(T) levels (using scalar relativistic pseudopotentials), considering all reasonable spin multiplicities. Subsequently, one- (1c-X2C) and two-component (2c-X2C) all electron DFT calculations with the exact two-component (X2C) Hamiltonian were carried out on IrF_n to evaluate the importance of SOC effects (see Figure 1). Optimized structures are shown in Figures 2, 3 and S3, and vibrational frequencies are compiled in Table 1 and Tables S5–S10 in Supporting Information. The bond length of diatomic IrF calculated by Kalamse and co-workers at the MP2 level was 192.8 pm,[14m] while our value of 186.1 pm at the CCSD(T) level is closer to the 185.1 pm obtained experimentally by laser induced fluorescence and dispersed fluorescence spectroscopy.[14k] Siddiqui reported that IrF_2 has a bent structure with Ir–F bond lengths of 189.7 pm at B3LYP DFT level with a scalar relativistic PP using unspecified basis sets.[14n] However, according to our calculations, IrF_2 is linear with a CCSD(T) bond length of 184.9 pm. Similar to the structure of AuF_3 described in the literature,[18] the triplet ground state of IrF_3 also exhibits a planar T-shaped structure with one long (185.1 pm) and two short (183.6 pm) Ir–F bond lengths. Of all possible structures for IrF_4, a square-planar structure ($^4B_{2g}/D_{4h}$ symmetry) is the most stable with a bond length of 183.4 pm. The $^2B_{3g}/D_{2h}$ and $^2B_2/D_{2d}$ states for IrF_4 are less stable than the $^4B_{2g}/D_{4h}$ ground state by up to 109.3 kJ mol^{-1} and 154.6 kJ mol^{-1}, respectively (Table S1).

Previously, it was reported that a square-pyramidal quintet ground state of IrF_5, with $^5B_1/C_{4v}$ symmetry is more favorable at scalar relativistic B3LYP/aT-PP level than a $^3A_1/C_{4v}$ state which was computed to be slightly higher in energy by 19.7 kJ mol^{-1}.[14e] The e-type orbital in the undistorted triplet C_{4v} state of IrF_5 (Figure 1) breaks spin-symmetry and orbital degeneracy has to be lifted either by J-T distortion or by SOC (the $^5B_1/C_{4v}$ state is a result of C_{4v} symmetry being imposed at scalar-relativistic level). This assumption agrees with our computations. In scalar relativistic calculations at the CCSD(T)/aug-cc-pVTZ-PP (or 1c-X2C-B3LYP all-electron) level, IrF_5 distorts to a $^3B_1/C_{2v}$ ground-state structure with an axial Ir–F bond of 182.6 (183.5) pm and two equatorial long bonds of 187.9 (189.2) pm and two shorter bonds of 182.7 (184.1) pm (Figure 2 and Table S2), consistent with previously reported optimized structures.[10] On the other hand, the inclusion of SOC effects at 2c-X2C-B3LYP level (Figure 3) leads to a square-pyramidal structure (triplet state, C_{4v} symmetry) for which a geometric parameter $\tau=0$ was determined.[19] Following the procedures described by Addison et al. with $\tau=(\beta-\alpha)/60°$ ($\tau=0$, square pyramidal geometry; $\tau=1$, trigonal bipyramidal geometry),

Table 1. Calculated and experimentally observed IR frequencies of Ir–F stretching modes of molecular iridium fluorides.[a]

Molecule	Mode	Calc. (Int.) CCSD(T)[c]	1c-X2C-B3LYP	2c-X2C-B3LYP	Exp. Ne	Ar
IrF[b] ($C_{\infty v}$, $^3\Phi$)	Σ^+	632.6	639 (100)	652 (100)	643.6	629.5
IrF_2 ($D_{\infty h}$, $^4\Delta_g$)	Σ_u^+	709.8	709 (176)	701 (158)	690.1	676.8
IrF_3 (C_{2v}, $^3B_1$)	A_1	710.6	700 (0)	680 (9)	_[d]	_[d]
	B_2	708.3	699 (200)	689 (181)	684.9	_[d]
	A_1	663.9	655 (62)	651 (42)	658.8	_[d]
IrF_4 (D_{4h}, $^4B_{2g}$)	E_u	727.9	716 (183)×2	715(161), 713 (168)	719.6/717.5/715.5	712.1
IrF_5[g] (C_{4v}, triplet)				696 (1)	_[d]	_[d]
				690 (186)×2	701.3/697.8	689.0[e], 685.9, 682.6[e]
				638 (37)	647.5/645.5	655.7
IrF_6 (O_h, $^4A_{1g}$)	T_{1u}		715 (100)×3	716 (100)×3	722.8/720.6/718.1	719.3/716.0[f]
IrF_7 (D_{5h}, $^3A_1'$)	A_2''		718 (100)	718 (100)		
	E_1'		662 (74)×2	663 (73)		
				661 (80)		

[a] The complete set of calculated frequencies is provided in Supporting Information (Tables S5-S10). Frequencies in cm^{-1} and intensities are shown in %. For the CCSD(T) calculations no intensities are available. [b] The frequency of IrF in the gas-phase was reported at 650 cm^{-1}.[14k] [c] aug-cc-pVTZ-PP basis sets. [d] Bands not observed, or too weak. [e] Matrix site. [f] Ref.[12f]. [g] Computed frequencies (in cm^{-1}) of IrF_5 (C_{2v}, $^3B_1$) obtained at the CCSD(T)/aug-cc-pVTZ-PP level: 725.8, 724.4, 710.4, 682.5, 652.5 and at the 1c-X2C-B3LYP (relative intensities in parentheses): 720 (16), 706 (177), 695 (15), 667 (190), 637 (0).

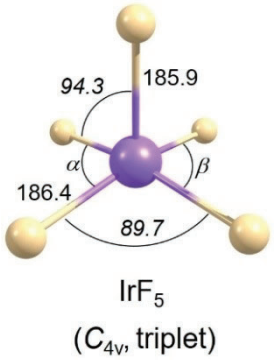

Figure 3. Computed structure of molecular IrF_5 at the 2c-X2C-B3LYP/x2c-TZVPall-2c level. Selected bond lengths (pm) and angles (°, in *italics*) are shown. The computed structures of other iridium fluorides at this level are shown in Figure S3.

where β and α (Figure 3) are the largest angles in the coordination sphere, $\tau = 0$ ($\beta = \alpha = 89.7°$) stands for perfectly square pyramidal geometries (C_{4v}). For more angle details, see Table S2 in the Supporting Information. The 2c-X2C-B3LYP structure of IrF_5 has a short axial Ir–F bond length of 185.9 pm and four longer bonds of 186.4 pm (Figure 3). That is, the computations suggest that SOC quenches the J-T distortion observed for the triplet state at scalar relativistic levels. Upon introduction of SOC, a clear assignment of a molecular term symbol becomes more difficult, as spin ceases to be a good quantum number. We nevertheless assign the ground state to be a C_{4v} triplet state based on the length of its spin magnetization vector indicating two unpaired electrons (see values of m_z in Figure 1).

The calculated bond length of 183.2 pm for the quartet IrF_6 ground state with its well-known O_h structure shows good agreement with the gas-phase electron diffraction value of 183.9 pm[12a] as well as with the EXAFS value of 182.2 pm measured in the solid-state.[13] Furthermore, a pentagonal-bipyramidal triplet ground-state (D_{5h}) for IrF_7 has been reported previously[10] at the B3LYP level of theory, which is consistent with our calculations (Figure S2).

Experimental Results

A. Photodecomposition of IrF_6

Figure 4 reveals the IR and UV-vis spectra of iridium hexafluoride before and after irradiation ($\lambda = 365$ and 278 nm) in neon matrix at 6 K. Similar experiments in argon matrix are also shown in Figure 5 and additional results are provided in Supporting Information (Figures S5–S10). A comparison between the experimentally observed and calculated frequencies is shown in Table 1.

UV-vis experiments

To understand the photochemical decomposition behavior of IrF_6 in detail, the IR and UV-vis spectra of IrF_6 in the same neon matrix under cryogenic conditions at 6 K are shown in Figure 4. These experiments allow to correlate changes in band intensities in the IR and UV-vis regions and confirm the band assignments of the newly formed binary iridium fluoride species. We will first discuss the UV-vis results, and the IR results will be described in the next sections.

The UV-vis spectrum of IrF_6 in neon matrix at 6 K shows continuous absorption in this region (200–500 nm). The absorbance contains mainly the intense broad bands at 283.6 and 241.8 nm and a distinct, relatively intense shoulder at 336.8 nm, which is in good agreement with the reported values in nitrogen matrix.[12f] Detailed UV studies of IrF_6 including vibrational progression and transitions have been discussed in the literature.[12f] After 40 min of UV light photolysis ($\lambda =$ 365 nm), the intensity of the absorption bands at 241.8, 283.6, and 336.8 nm decreased by half, indicating the photo-initiated

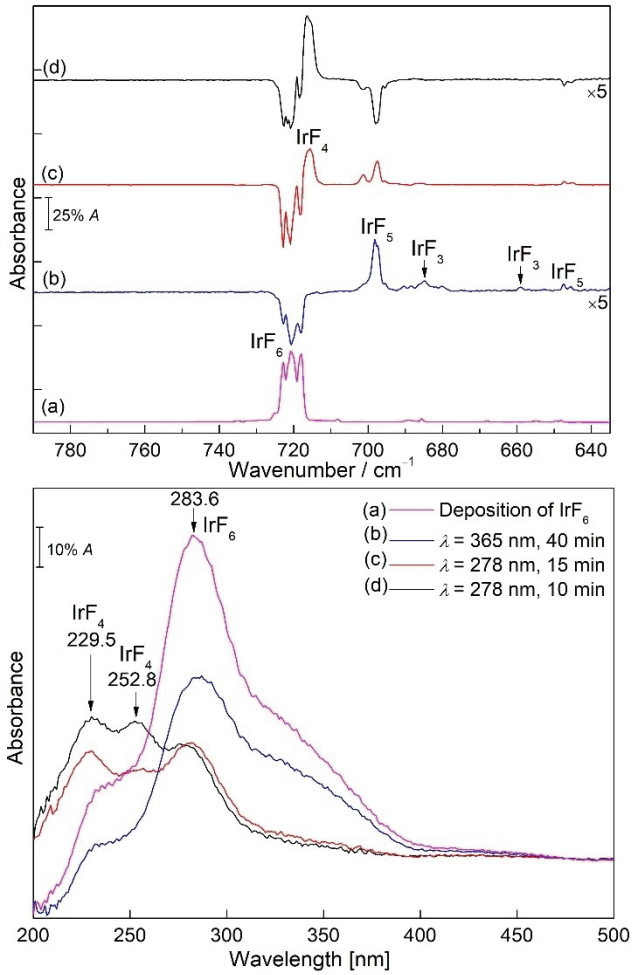

Figure 4. IR (top) and UV-vis (bottom) spectra recorded from the same neon matrix at 6 K showing the photochemistry of IrF_6. (a) Spectra of IrF_6 obtained after deposition for 30 min (pink lines), (b) UV-vis and difference IR spectra obtained after $\lambda = 365$ nm irradiation for 40 min (blue lines), (c) subsequent irradiation of the same matrix at $\lambda = 278$ nm for 15 min (red lines), and (d) subsequent irradiation of the same matrix at $\lambda = 278$ nm for 10 min (black lines). Upward bands in the difference spectra are formed at the expense of downward bands.

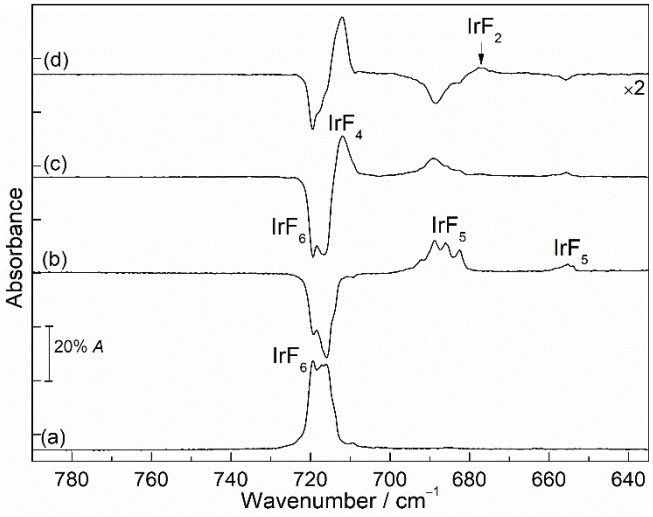

Figure 5. IR spectra in argon matrix at 6 K showing the photochemistry of IrF_6. (a) Spectrum of IrF_6 obtained after deposition for 40 min, (b) difference IR spectrum obtained after $\lambda = 365$ nm irradiation for 60 min, (c) subsequent irradiation of the same matrix at $\lambda = 278$ nm for 15 min, and (d) subsequent irradiation of the same matrix at $\lambda = 278$ nm for 30 min. Upward bands in the difference spectra are formed at the expense of downward bands.

defluorination of IrF_6 to the lower-valent iridium fluorides. However, no obvious new absorption UV bands have been identified to allow a further assignment of possible decomposition products. Robinson and Westland described earlier that IrF_4 is formed by irradiation of IrF_6 with UV light.[14a] But later Bartlett and Rao corrected the previous assignment to IrF_5,[14b] suggesting the photodecomposition of IrF_6 to the lower-valent iridium fluorides.

Previously the visible spectra of IrF_5 in HF solution were reported with two absorption bands at 683 and 840 nm.[14c] Later, the diffuse reflectance UV-vis spectrum for solid IrF_5 with strong absorption bands in a broad range from about 200 to 500 nm, 840, and 1524 nm and similarly for IrF_3 at 256, 300, and 500 nm were published.[14d,j] Additionally, the electronic diffuse reflectance spectrum of solid IrF_4 was characterized at 263, 320, 405 and 510 nm.[14h] To the best of our knowledge no UV-vis studies for IrF_2 and IrF have been reported so far. However, our attempts to obtain a clear UV absorption band for molecular IrF_5 were so far unsuccessful, probably because of the overlapping absorption of IrF_6 and the very low abundance of the molecule and the detection range of our UV-vis spectrometer (200–850 nm).

In addition, subsequent irradiation of the same matrix at $\lambda =$ 278 nm for 15 min produced two distinct new bands at 229.5 and 252.8 nm in the UV-vis spectrum, while the absorption band at 283.6 nm of IrF_6 was slightly reduced (Figure 4c, bottom trace). Further irradiation at the same wavelength increased the newly formed bands at 229.5 and 252.8 nm, which could be tentatively assigned to IrF_4 based on IR data (Figure 4d). However, the difference in the rate of rise of the two bands upon further 10 min irradiation at $\lambda = 278$ nm suggests that the assigned absorption band of IrF_4 at 229.5 nm may have overlapped with the band of other binary iridium fluorides.

IR experiments

In analogy to the UV-vis experiments, several IR experiments were performed to understand the photochemistry of IrF_6, and the species produced by irradiation. The IR band positions of iridium hexafluoride in argon and nitrogen matrices were previously reported by Holloway[12f] and agree very well with our experimental results obtained in neon and argon matrices (Figures 4, 5 and S5–S10). In the neon matrix, the bands of IrF_6 split into three components with almost equal intensity at 722.8, 720.6 and 718.1 cm^{-1} whereas in argon only two bands at 719.3 and 716.0 cm^{-1} are observed, explained by the weak interactions with the atoms in the matrix host.

Irradiation with UV light ($\lambda = 365$ nm) of IrF_6 isolated in a neon matrix resulted in the decline of all IR absorptions of IrF_6 and formation of a complex spectrum, with the strongest IR bands at 697.8 cm^{-1} and other weaker bands at 684.9, 658.8, 647.5 and 645.5 cm^{-1} (Figure 4b, top trace). In order to distinguish these IR bands, the matrix was further irradiated at 278 nm for 15 min. The corresponding IR difference spectrum (Figure 4c, top trace) demonstrates an increase of the aforementioned three IR bands at 697.8, 647.5 and 645.5 cm^{-1} as well as a new IR band at 717.5 cm^{-1} and concurrently a decrease of bands of IrF_6 at 722.8, 720.6 and 718.1 cm^{-1}. Interestingly, attempts to increase the abundance of the newly produced species by prolonged irradiation with 278 nm resulted in an intensity decrease of the bands at 697.8, 647.5 and 645.5 cm^{-1}, while the intensity of the IR band at 717.5 cm^{-1} increased significantly (Figure 4d, top trace). The prololonged irradiation ($\lambda = 278$ nm) completely destroyed the IR bands of IrF_6 and clearly indicated that the band at 717.5 cm^{-1} belongs to a new species whose absorption is close to that of the precursor IrF_6 (Figures S5 and S6).

In a separate analogy experiment, the neon matrix containing the 365 nm photolysis product of IrF_6 was irradiated with a blue-light source ($\lambda = 470$ nm) for 15 minutes (Figure S7). This resulted in a decrease of the IR bands at 697.8, 647.5, and 645.5 cm^{-1} and an increase of the IR bands of IrF_6. Concomitantly, a new band at 717.5 cm^{-1} and two weak bands at 684.9 and 658.8 cm^{-1} are formed (Figure S7).

Similarly, the UV-light ($\lambda = 365$ nm) irradiation of IrF_6 was also performed in solid argon matrix (Figure 5). This irradiation produced a broad band centered at 685.9 cm^{-1} and a weak band at 655.7 cm^{-1}, which are comparable to the observation of a sharp band at 697.8 cm^{-1} and other weak bands in the neon matrix experiments discussed above. Furthermore, both sets of bands show similar photochemical behavior in the subsequent 278 nm or 470 nm irradiations (Figures 5c, 5d and S8). A strong band at 712.1 cm^{-1} that is very close to the band of IrF_6 was also observed, and a weak band at 676.8 cm^{-1} becomes apparent upon prolonged irradiation at 278 nm (Figure S6).

Based on the changes in the IR spectra, obtained at different photolysis wavelengths and times, and annealing behavior, in comparison with UV-vis data obtained in the same matrix experiments, and using further support by quantum-chemical calculations, we were able to assign the newly formed species to the low-valent iridium fluorides IrF_n ($n = 1$–5). The IR bands at 697.8, 647.5 and 645.5 cm^{-1} in solid neon (685.9 cm^{-1} and 655.7 cm^{-1} in solid argon) produced in the photolysis of IrF_6 can be grouped and belong to different vibrational modes of the same new molecule. For the photolysis products of IrF_6, the most likely candidates are IrF_5 and IrF_4, which could be produced by homolytic Ir–F bond cleavage and by elimination of F_2. Quantum-chemical calculations were performed to support the assignments, and the calculated IR spectra of the binary iridium fluorides are summarized in Table 1 as well as in Tables S1–S11. Craciun and co-workers reported that the calculated frequencies of IrF_5 in the $^5B_1/C_{4v}$ ground state are 702 and 526 cm^{-1} with an intensity distribution of about 7:1.[14e] In addition, IrF_5 with a C_{2v} triplet ground state was also mentioned,[10] for which two different Ir–F stretching bands with almost identical intensities would be expected (Table S7). However, these predicted positions and intensities of the bands do not agree well with our experimental values. This may be explained by the influence of SOC for the IrF_5 system. Inclusion of SOC for the triplet state of IrF_5 with C_{4v} structure at the 2c-X2C-B3LYP level gave harmonic IR frequencies at 690 and 638 cm^{-1}, which are in good agreement with the observed band positions at 697.8, 647.5 and 645.5 cm^{-1} in neon and at 685.9 and 655.7 cm^{-1} in argon matrices, respectively (Tables 1 and S7). The bands at 689.0 and 682.6 cm^{-1} in argon were assigned to the matrix site bands of IrF_5 based on the behavior during annealing, where these bands quickly disappeared (Figure S9).

Moreover, the two very weak bands at 684.9 and 658.8 cm^{-1} observed after 365 nm irradiation of IrF_6 were assigned to IrF_3, in agreement with the calculations for the T-shaped planar structure of IrF_3 at B3LYP and CCSD(T) levels (Table 1). This species is likely formed upon further photolysis of IrF_5 generated in the matrix experiments. However, the absorption of IrF_3 identified in neon could not be detected in the argon matrix, probably due to its low abundance or overlap with the broad IR bands of IrF_5. According to the calculated vibrational displacement vectors, the bands at 684.9 cm^{-1} and 658.8 cm^{-1} correspond to the asymmetric stretching vibrations of F–Ir–F and the stretching vibrations of Ir–F, which both have large blue-shifts of 33.3 cm^{-1} and 96.7 cm^{-1}, respectively, compared to the stretching vibrations in $NIrF_3$ (651.6 and 562.1 cm^{-1}, Ne-matrix).[20] This is in agreement with the absence of a frequency for the remaining F–Ir–F symmetric stretching frequency of IrF_3 in the recorded spectra, for which a very low intensity was predicted (Table 1).

Next, bands for the new IrF_4 molecule are observed at 717.5 cm^{-1} in Ne and 712.1 cm^{-1} in Ar matrices under cryogenic conditions at 6 K. As shown in Figures S5 and S6, the formation of IrF_4 by 278 nm irradiation of IrF_6 is almost quantitative in both solid neon and argon matrices. The assignment to this molecule is based on the basis of our experimental observations. For a tetrahedral structure, only a single infrared active absorption would be expected in the Ir–F stretching vibration region, as recently discussed in detail for the analogous PtF_4 molecule.[21] Formation of IrF_5 and IrF_4 is evident after short irradiation of IrF_6 with 278 nm. However, the efficient formation of IrF_4 and the depletion of the initially generated IrF_5 under prolonged 278 nm irradiation indicate the formation of IrF_4 as photolysis product of IrF_5 instead of as a product of F_2-elimination from IrF_6. The CCSD(T) calculations predict a square-planar structure for molecular IrF_4, and the observed frequencies are consistent with the calculated fundamental IR frequencies at 727.9 cm^{-1} (Table 1). It is noteworthy that solid-state IR data of IrF_4 showed a strong iridium-fluorine bridging stretching vibration located at around 550 cm^{-1}.[14c] As expected, no corresponding IR band for IrF_4 has been detected in the range of 500–600 cm^{-1} in our experiments (Figures S5 and S6). Furthermore, laser irradiation ($\lambda = 266$ nm) of IrF_4 produced IR

bands of IrF_6, IrF_5, IrF_3 and an unknown new band at 690.1 cm^{-1} in the neon matrix (Figure S10).

Similarly, the argon matrix containing the 365 nm photolysis products of IrF_6 was further subjected to 278 nm irradiation (Figure 5d). In addition to the dominant formation of the IR band of IrF_4 at 712.1 cm^{-1}, a new carrier also appeared after photolysis (278 nm) with a weak but distinguishable IR band at 676.8 cm^{-1}, which continued to grow slightly with longer photolysis. This carrier could be a photolysis product from decomposition of IrF_4. Recall that the new band at 690.1 cm^{-1} was produced upon laser irradiation ($\lambda = 266$ nm) of IrF_4 in neon matrix. Similar to the observed shifts of neon to argon matrix of PtF_2 ($\Delta\nu = -14.5$ cm^{-1}),[21] the assignment of the new band at 690.1 cm^{-1} in neon (and 676.8 cm^{-1} in argon) to IrF_2 in the current experiment is plausible when assuming a reasonable blue shift in the neon matrix (shift to argon: $\Delta\nu = -13.2$ cm^{-1}). Also, the observed band positions are consistent with the strongest fundamental IR vibration at 709.8 cm^{-1} calculated at the CCSD(T) level for the linear IrF_2 molecule (Table 1) and associated with the asymmetric F–Ir–F stretching vibration.

B. Reaction of laser-ablated iridium atoms with fluorine

Alternatively, the binary iridium fluorides were synthesized by the reaction of laser-ablated iridium atoms with fluorine diluted in excess neon and argon under cryo-conditions at 6 K. This method has also been used successfully for the synthesis of other metal fluorides in our group.[15,21] Figure 6 shows spectra obtained after deposition of laser-ablated iridium atoms with 1% fluorine in solid neon followed by irradiation at different wavelengths. This experiment supported our assignments obtained from the photolysis of IrF_6: five groups of absorptions were observed, four of which above have been assigned to IrF_5, IrF_4, IrF_3 and IrF_2, whereas an additional band observed at 643.6 cm^{-1} was unknown before. Irradiation of the same neon matrix by the blue-light (470 nm) leads to a decrease in the IrF_5 bands and an increase in the corresponding IrF_6, IrF_4, and IrF_3 bands, while the band at 643.6 cm^{-1} increases slightly, but there is no noticeable change in the IrF_2 band (Figure 6b). This means that the new band at 643.6 cm^{-1} belongs to a new species not observed in our experiments before. Subsequent irradiation at 278 nm further destroyed the bands of IrF_3 and increased the intensity of IrF_4 as well as the unassigned band at 643.6 cm^{-1}.

Analogous spectra were recorded after sample deposition in argon (Figure 7). There are two remarkable differences between the neon and argon experiments. One is that a strong, sharp band of IrF_2 in argon corresponds to a weaker absorption in the neon matrix. The other is that IrF_5 is the major product after sample deposition when neon was used as the matrix host, whereas the corresponding bands in the argon matrix only appeared after annealing to 35 K. Surprisingly, the spectra show no evidence for the formation of a trifluoride in argon. New bands at 690.8 and 629.5 cm^{-1} that were also observed in argon on deposition, decreased substantially during annealing of the sample. The higher band at 690.8 cm^{-1} is nearly unaffected by photolysis. It could not be assigned properly, although we considered the formation of dimers and charged species.

The lower observed bands mentioned above at 643.6 cm^{-1} in neon and at 629.5 cm^{-1} in argon after deposition could be assigned as the Ir–F stretching vibrational mode of the diatomic IrF molecule (Figures 6 and 7). This assignment is in accordance with the fundamental gas-phase frequency of IrF at 650 cm^{-1} deduced from electronic band spacings.[14k] Our CCSD(T) calculations predict a strong stretching frequency for this species at 632.6 cm^{-1}, slightly lower than the above values obtained in neon matrix (Table 1), but significantly blue-shifted in comparison to the reported value (575.0 cm^{-1}) obtained

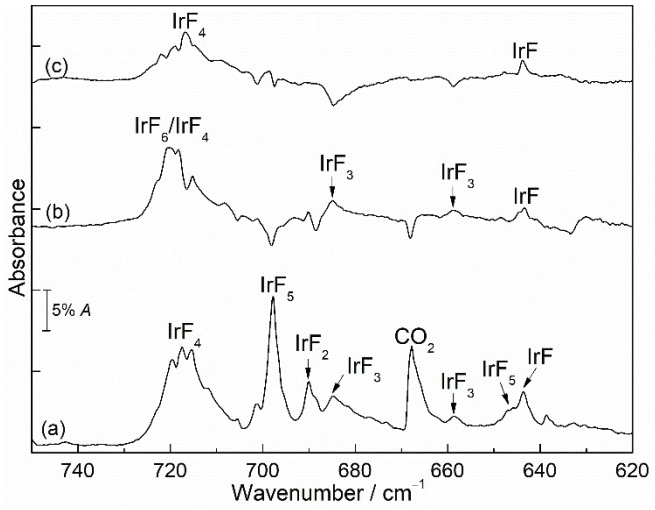

Figure 6. IR spectra in neon matrix at 6 K. (a) IR spectrum of reaction products of laser-ablated Ir atoms with 1% F_2. Difference IR spectrum obtained after (b) $\lambda = 470$ nm irradiation for 20 min and (c) subsequent $\lambda = 278$ nm irradiation for 25 min.

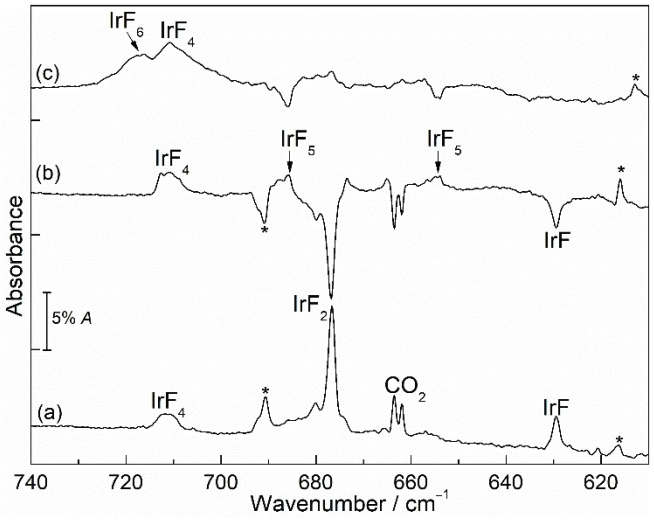

Figure 7. IR spectra in argon matrix at 12 K. (a) IR spectrum of reaction products of laser-ablated Ir atoms with 0.5% F_2. (b) Difference IR spectrum obtained after annealing to 35 K and (c) subsequent $\lambda = 470$ nm irradiation for 30 min. The bands marked with asterisks are assigned to unknown impurities.

previously at second-order Moller-Plesset (MP2) perturbation theory level.[14m]

The theoretically predicted structure of D_{5h} symmetry of IrF_7 would have two bands at 718 and 662 cm^{-1} with an intensity distribution of about 3:4 (Table 1). Unfortunately, all attempts to detect IR bands of a higher iridium fluoride such as IrF_7, that has been regarded as a candidate species in matrix-isolation studies,[10] by additional photolysis of the deposits were not successful. In addition, similar to our findings on the interaction between PtF_4 and F_2 in the matrix,[21] the possible formation of difluorine complexes $IrF_4 \cdot F_2$ and $IrF_5 \cdot F_2$ based on fluorine-specific interactions between the metal fluoride and elemental F_2 was investigated. The optimized structures of $IrF_4 \cdot F_2$ complex were obtained with both side-on and end-on coordination of fluorine to iridium at the B3LYP-D3/aug-cc-pVTZ-PP level (Figure S4), and the energy difference between these two structures is relatively small (1.7 kJ mol^{-1}). The optimization of the $IrF_5 \cdot F_2$ complex failed due to initiation of F–F bond cleavage at the B3LYP-D3/aug-cc-pVTZ-PP level, indicating the already strong Lewis character of the IrF_5 species that leads to the formation of IrF_6 and a F atom. Furthermore, the predicted Ir–F stretching frequency of the $IrF_4 \cdot F_2$ complex is only 1.5 cm^{-1} higher than that for isolated IrF_4 (B3LYP-D3/aug-cc-pVTZ-PP level; Table S11). Therefore, the presence of the $IrF_4 \cdot F_2$ complex in our spectra could not be completely excluded, as it could overlap with the strong band of isolated IrF_4.

Computed thermochemical data

Having already assigned the experimentally obtained iridium fluorides, we now propose the possible decomposition channels and computationally analyze the thermochemical stability of the observed compounds (Table 2). This technique has also been used previously in the literature to examine the stability of molecular fluorides under cryogenic conditions.[15a,22] Based on our experimental observations in argon and neon matrices, concerted elimination of F_2 and homolytic cleavage of one iridium-fluorine bond were considered for IrF_n ($n = 1$–6). These decomposition channels of IrF_6 are strongly endothermic at the 2c-X2C-B3LYP and CCSD(T) levels (Table 2) as well as at B3LYP/aT-PP and 1c-X2C-B3LYP levels (Table S12). Therefore, it should be possible to obtain the IrF_5 and IrF_4 molecules under appropriate conditions, for example using the matrix isolation techniques shown in this work. Similarly, the value of 204.0 kJ mol^{-1} at 2c-X2C-B3LYP level obtained for the $IrF_5 \rightarrow IrF_4 + F$ reaction indicates a low thermal stability of molecular IrF_5, which is consistent with our experimental results that the initially generated IrF_5 can be transformed into other binary fluorides upon 470 or 278 nm irradiations. The calculated thermochemistry predicts the low-valent fluorides IrF and IrF_2 to be stable against fluorine elimination and homolytic bond cleavage.

Table 2. Computed thermochemical stability of iridium fluorides (298.15 K, kJ mol^{-1}) at different levels of theory.

Reaction	2c-X2C-B3LYP[a] $\Delta E + \Delta ZPE$	$\Delta_r H$	CCSD(T)[b] $\Delta E + \Delta ZPE$(B3LYP)[c]	$\Delta_r H$[d]
$IrF_6 \rightarrow IrF_4 + F_2$	312.7	316.6	308.9	312.5
$IrF_6 \rightarrow IrF_5 + F$	256.0	260.5	310.1	315.4
$IrF_5 \rightarrow IrF_3 + F_2$	421.3	424.6	374.4	376.5
$IrF_5 \rightarrow IrF_4 + F$	204.0	207.0	145.0	146.9
$IrF_4 \rightarrow IrF_2 + F_2$	507.2	510.6	526.2	529.4
$IrF_4 \rightarrow IrF_3 + F$	364.6	368.5	375.7	379.4
$IrF_3 \rightarrow IrF + F_2$	607.2	609.5	654.1	656.2
$IrF_3 \rightarrow IrF_2 + F$	289.9	293.1	296.8	299.8
$IrF_2 \rightarrow Ir + F_2$	681.7	684.3	716.9	719.2
$IrF_2 \rightarrow IrF + F$	464.5	467.3	503.6	506.2
$IrF \rightarrow Ir + F$	364.5	367.9	359.6	362.9

[a] x2c-TZVPall-2c basis sets. [b] aug-cc-pVTZ-PP basis sets. [c] Using B3LYP zero point energy corrections for the electronic energies at CCSD(T) level. [d] The enthalpies at CCSD(T) level were calculated by adding the enthalpy corrections (B3LYP) to electronic energy changes.

Conclusions

A series of molecular iridium fluorides IrF_n ($n = 1$–6) were prepared by the reaction of laser-ablated iridium atoms with elemental fluorine and by the photo-initiated defluorination of IrF_6, isolated in solid noble-gas matrices. These fluorides were spectroscopically identified and supported by quantum-chemical calculations. The species IrF_n ($n = 1$–5) were produced for the first time under the cryogenic conditions, and their formation in the laser ablation experiments depends on the noble gas host, similar to the chemistry of platinum fluorides.[21] However, efficient formation of IrF_5 together with minor IrF_3 products was achieved by irradiation into the absorption maxima of IrF_6 in the UV region ($\lambda = 365$ nm), while subsequent irradiation ($\lambda = 278$ nm) leads to almost quantitative formation of IrF_4 in both neon and argon matrices. Further irradiation into the absorption maxima of IrF_4 ($\lambda = 266$ nm) leads to the formation of IrF_6, IrF_5, IrF_3 and IrF_2 in neon matrices by addition and elimination of fluorine radicals and/or molecular fluorine. The assignment of these species was computationally supported by one- and two-component quasirelativistic DFT methods and scalar-relativistic CCSD(T) calculations. IrF_5 is one of the very rare examples in which a significant influence of SO coupling on the structure is found, where a high-symmetry (C_{4v}) triplet structure is favored energetically at 2c-X2C level over the Jahn-Teller distorted $^3B_1/C_{2v}$ structure obtained at scalar relativistic levels. The presence of SOC effects leading to a triplet ground state with C_{4v} symmetry of IrF_5 in solid neon and argon matrices was confirmed by the observed IR frequencies. Attempts to detect IR bands of higher iridium fluorides such as IrF_7 and/or difluorine complexes of IrF_5 or IrF_4 were unsuccessful which is perhaps due to low yield or overlap of the bands.

Experimental and Computational Details

The technique of matrix-isolation infrared (IR) spectroscopy and laser-ablation apparatus have been described in detail in previous works.[15,21] Matrix samples were prepared by co-deposition of laser-ablated iridium atoms with 0.5% and 1% elemental fluorine diluted in neon (99.999%, Air Liquide) or argon (99.999%, Sauerstoffwerk

Friedrichshafen). The stainless-steel F_2 storage cylinder was cooled in liquid nitrogen to freeze out impurities before the released F_2 was premixed with neon or argon in a custom-made stainless-steel mixing chamber. The mixing chamber was connected to a self-made matrix chamber by a stainless-steel capillary. The gas mixture was condensed with laser-ablated iridium atoms onto a gold-plated mirror cooled to 6 K for neon and 12 K for argon using a closed-cycle helium cryostat (Sumitomo Heavy Industries, RDK-205D) inside the matrix chamber. For the laser-ablation, the 1064 nm fundamental of a Nd:YAG laser (Continuum, Minilite II, 10 Hz repetition rate, 50–60 mJ pulse^{-1}) was focused onto a rotating iridium metal target through a hole in the cold window. The infrared spectra were recorded on a Bruker Vertex 80v with 0.5 cm^{-1} resolution in the region 4000–450 cm^{-1} by using a liquid-nitrogen-cooled mercury cadmium telluride (MCT) detector. Matrix samples were annealed to different temperatures and irradiated by selected light-emitting diode (LED) sources (OSLON 80 4+ PowerStar Circular 4 LED Arrays: $\lambda = 470 \pm 20$ nm (blue), $\lambda = 365 \pm 10$ nm (Qioptiq ML3 UV LED) and $\lambda = 278$ nm (100 mW, AMPYR LE-D33UV278-6060-100), as well as a pulsed 266 nm Q-switched solid-state laser (CryLas 6FQSS266-Q2-OEM, 266/532 nm, 0.8 μJ @10 kHz).

UV-vis spectra were recorded with a Perkin-Elmer Lambda 850+ UV spectrometer in the range of 200–850 nm with a spectral resolution of 1.0 nm. The radiation of the spectrometer was directed into a quartz optical fiber of 2 m length, through a quartz lens inside the cryostat and passed two times over the matrix deposited on the cold gold mirror. A second quartz fiber collected the reflected radiation, and then directed it into the spectrometer.

Preparation of iridium hexafluoride followed procedures described in the literature.[12a] It was prepared by heating iridium metal powder in a stainless-steel autoclave with an excess of fluorine at 300 °C for about 8 h. Similar to our previous work on PtF_6,[21] the product IrF_6 was stored in fluoroplastic (PFA) tube and trapped by liquid nitrogen. It was further purified by long pumping and its initial purity was monitored by IR spectroscopy. After purification, the gas sample was mixed by passing a stream of neon or argon gas through a cold PFA tube (−96 °C) containing the IrF_6 sample and deposited on the matrix support for further measurements.

Initial quantum-chemical structure optimizations of the molecules at density functional theory (DFT) level used the B3LYP[23] hybrid functional in conjunction with the augmented triple-ζ basis sets aug-cc-pVTZ for fluorine and the aug-cc-pVTZ-PP[24] valence basis and associated scalar-relativistic pseudopotential (PP) for iridium. These calculations were performed using the Gaussian16 program package.[25] All reasonable spin multiplicities have been considered. Subsequent structure optimizations as well as harmonic vibrational frequency analyses at the CCSD(T)[16] (coupled-cluster singles-doubles with perturbational triples) level with aug-cc-pVTZ-PP basis sets were carried out for the ground states of IrF_n ($n = 1$–6) in the spin unrestricted ROHF-UCCSD(T) open-shell coupled cluster formalism using default frozen core settings as implemented in the Molpro 2019 software package.[26] Due to the previously suggested significant SOC stabilization of IrF_5,[10] additional quasirelativistic all-electron calculations using the exact two-component (X2C) Hamiltonian at one- and two-component (1c-X2C and 2c-X2C[17,27]) DFT levels[28] have been performed for all systems using Turbomole 7.5.0[29] with x2c-TZVPall-2c all-electron basis sets.[30] Two-electron SOC terms were approximated using the scaled-nuclear-spin-orbit (SNSO)[31] approach in its original parameterization by Böttcher.[32] To optimize the $IrF_4 \cdot F_2$ complex, dispersion corrections were included using Grimme's DFT-D3[33] scheme with Becke-Johnson (BJ) damping[34] for the B3LYP functional using aug-cc-pVTZ-PP valence basis and the associated scalar-relativistic pseudopotential (PP) for iridium.

Acknowledgements

We gratefully acknowledge the Zentraleinrichtung für Datenverarbeitung (ZEDAT) of the Freie Universität Berlin for the allocation of computing resources.[35] We thank the ERC Project HighPotOx as well as the CRC 1349 (SFB 1349) Fluorine-Specific Interactions-Project-ID 387284271 for continuous support. Y. L. thanks the China Scholarship Council (PhD Program) for financial support. Open Access funding enabled and organized by Projekt DEAL.

Conflict of Interest

The authors declare no conflict of interest.

Data Availability Statement

The data that support the findings of this study are available from the corresponding author upon reasonable request.

Keywords: IR spectroscopy · iridium fluorides · Jahn-Teller effect · laser-ablation · matrix-isolation · photochemistry · quantum-chemical calculations · spin-orbit effect · UV-vis spectroscopy

[1] a) N. D. McDaniel, F. J. Coughlin, L. L. Tinker, S. Bernhard, *J. Am. Chem. Soc.* **2008**, *130*, 210–217; b) R. Lalrempuia, N. D. McDaniel, H. Müller-Bunz, S. Bernhard, M. Albrecht, *Angew. Chem. Int. Ed.* **2010**, *49*, 9765–9768; *Angew. Chem.* **2010**, *122*, 9959–9962; c) D. G. H. Hetterscheid, J. N. H. Reek, *Chem. Commun.* **2011**, *47*, 2712–2714; d) J. M. Thomsen, S. W. Sheehan, S. M. Hashmi, J. Campos, U. Hintermair, R. H. Crabtree, G. W. Brudvig, *J. Am. Chem. Soc.* **2014**, *136*, 13826–13834; e) S. W. Sheehan, J. M. Thomsen, U. Hintermair, R. H. Crabtree, G. W. Brudvig, C. A. Schmuttenmaer, *Nat. Commun.* **2015**, *6*, 294.

[2] a) M. Zhou, N. D. Schley, R. H. Crabtree, *J. Am. Chem. Soc.* **2010**, *132*, 12550–12551; b) D. L. Huang, D. J. Vinyard, J. D. Blakemore, S. M. Hashmi, R. H. Crabtree, *Organometallics* **2017**, *36*, 199–206.

[3] a) K. K.-W. Lo, K. Y. Zhang, S.-K. Leung, M.-C. Tang, *Angew. Chem. Int. Ed.* **2008**, *47*, 2213–2216; *Angew. Chem.* **2008**, *120*, 2245–2248; b) K. K.-W. Lo, S. P.-Y. Li, K. Y. Zhang, *New J. Chem.* **2011**, *35*, 265–287; c) K. K.-W. Lo, *Acc. Chem. Res.* **2015**, *48*, 2985–2995.

[4] a) M. A. Baldo, M. E. Thompson, S. R. Forrest, *Nature* **2000**, *403*, 750–753; b) P.-N. Lai, C. H. Brysacz, M. K. Alam, N. A. Ayoub, T. G. Gray, J. Bao, T. S. Teets, *J. Am. Chem. Soc.* **2018**, *140*, 10198–10207; c) Q. Li, C. Shi, M. Huang, X. Wei, H. Yan, C. Yang, A. Yuan, *Chem. Sci.* **2019**, *10*, 3257–3263; d) C. Shi, H. Huang, Q. Li, J. Yao, C. Wu, Y. Cao, F. Sun, D. Ma, H. Yan, C. Yang, A. Yuan, *Adv. Opt. Mater.* **2021**, *9*, 2002060.

[5] a) C. E. Housecroft in *Encyclopedia of Inorganic and Bioinorganic Chemistry*; (Ed. R. A. Scott), John Wiley & Sons, Ltd, Chichester, UK, **2011**, p .1; b) S. B. Sinha, D. Y. Shopov, L. S. Sharninghausen, C. J. Stein, B. Q. Mercado, D. Balcells, T. B. Pedersen, M. Reiher, G. W. Brudvig, R. H. Crabtree, *J. Am. Chem. Soc.* **2017**, *139*, 9672–9683.

[6] O. Ruff, J. Fischer, *Z. Anorg. Allg. Chem.* **1929**, *179*, 161–185.

[7] Y. Gong, M. Zhou, M. Kaupp, S. Riedel, *Angew. Chem.* **2009**, *121*, 8019–8023; *Angew. Chem. Int. Ed.* **2009**, *48*, 7879–7883.

[8] G. Wang, M. Zhou, J. T. Goettel, G. J. Schrobilgen, J. Su, J. Li, T. Schlöder, S. Riedel, *Nature* **2014**, *514*, 475–477.

[9] P. Pyykkö, W.-H. Xu, *Angew. Chem. Int. Ed.* **2015**, *54*, 1080–1081; *Angew. Chem.* **2015**, *127*, 1094–1095.

[10] S. Riedel, M. Kaupp, *Angew. Chem. Int. Ed.* **2006**, *45*, 3708–3711; *Angew. Chem.* **2006**, *118*, 3791–3794.

[11] J. Lin, Z. Zhao, C. Liu, J. Zhang, X. Du, G. Yang, Y. Ma, *J. Am. Chem. Soc.* **2019**, *141*, 5409–5414.

[12] a) A. D. Richardson, K. Hedberg, G. M. Lucier, *Inorg. Chem.* **2000**, *39*, 2787–2793; b) V. Boudon, M. Rotger, D. Avignant, *Spectrochim. Acta Part A* **1996**, *52*, 1175–1182; c) H. H. Claassen, H. Selig, *Isr. J. Chem.* **1969**, *7*, 499–504; d) M. Kimura, V. Schomaker, D. W. Smith, *J. Chem. Phys.* **1968**, *48*, 4001–4012; e) H. C. Mattraw, N. J. Hawkins, D. R. Carpenter, W. W. Sabol, *J. Chem. Phys.* **1955**, *23*, 985–986; f) J. H. Holloway, G. Stanger, E. G. Hope, W. Levason, J. S. Ogden, *J. Chem. Soc. Dalton Trans.* **1988**, 1341–1345.

[13] A. K. Brisdon, J. H. Holloway, E. G. Hope, W. Levason, J. S. Ogden, A. K. Saad, *J. Chem. Soc. Dalton Trans.* **1992**, 139–143.

[14] a) P. L. Robinson, G. J. Westland, *J. Chem. Soc.* **1956**, 4481–4487; b) N. Bartlett, P. R. Rao, *Chem. Commun.* **1965**, 252–253; c) R. T. Paine, L. B. Asprey, *Inorg. Chem.* **1975**, *14*, 1111–1113; d) E. G. Hope, *Polyhedron* **1993**, *12*, 2977–2980; e) R. Craciun, D. Picone, R. T. Long, S. Li, D. A. Dixon, K. A. Peterson, K. O. Christe, *Inorg. Chem.* **2010**, *49*, 1056–1070; f) W. A. Sunder, W. E. Falconer, *Inorg. Nucl. Chem. Lett.* **1972**, *8*, 537–540; g) P. R. Rao, A. Tressaud, N. Bartlett, *J. Inorg. Nucl. Chem.* **1976**, *28*, 23–28; h) R. C. Burns, T. A. O'Donnell, *J. Inorg. Nucl. Chem.* **1980**, *42*, 1285–1291; i) M. A. Hepworth, K. H. Jack, R. D. Peacock, G. J. Westland, *Acta Crystallogr. Sect. A* **1957**, *10*, 63–69; j) A. L. Hector, W. Levason, M. T. Weller, E. G. Hope, *J. Fluorine Chem.* **1997**, *84*, 161–165; k) A. G. Adam, A. D. Granger, L. E. Downie, D. W. Tokaryk, C. Linton, *Can. J. Phys.* **2009**, *87*, 557–565; l) X. Zhuang, T. C. Steimle, C. Linton, *J. Chem. Phys.* **2010**, *133*, 164310; m) V. Kalamse, N. Wadnerkar, A. Chaudhari, *Int. J. Quantum Chem.* **2011**, *111*, 2014–2020; n) S. A. Siddiqui, T. Rasheed, *Int. J. Quantum Chem.* **2013**, *113*, 959–965.

[15] a) T. Schlöder, T. Vent-Schmidt, S. Riedel, *Angew. Chem. Int. Ed.* **2012**, *51*, 12063–12067; *Angew. Chem.* **2012**, *124*, 12229–12233; b) L. Li, A. K. Sakr, T. Schlöder, S. Klein, H. Beckers, M.-P. Kitsaras, H. V. Snelling, N. A. Young, D. Andrae, S. Riedel, *Angew. Chem. Int. Ed.* **2021**, *60*, 6391–6394.

[16] a) G. D. Purvis, R. J. Bartlett, *J. Chem. Phys.* **1982**, *76*, 1910–1918; b) K. Raghavachari, G. W. Trucks, J. A. Pople, M. Head-Gordon, *Chem. Phys. Lett.* **1989**, *157*, 479–483.

[17] A. Baldes, F. Weigend, *Mol. Phys.* **2013**, *111*, 2617–2624.

[18] X. Wang, L. Andrews, K. Willmann, F. Brosi, S. Riedel, *Angew. Chem. Int. Ed.* **2012**, *51*, 10628–10632; *Angew. Chem.* **2012**, *124*, 10780–10784.

[19] a) A. W. Addison, T. N. Rao, J. Reedijk, J. van Rijn, G. C. Verschoor, *J. Chem. Soc. Dalton Trans.* **1984**, 1349–1356; b) H. Haller, J. Schröder, S. Riedel, *Angew. Chem. Int. Ed.* **2013**, *52*, 4937–4940; *Angew. Chem.* **2013**, *125*, 5037–5040; c) R. Mukherjee, *Coord. Chem. Rev.* **2000**, *203*, 151–218.

[20] T. Stüker, T. Hohmann, H. Beckers, S. Riedel, *Angew. Chem. Int. Ed.* **2020**, *59*, 23174–23179; *Angew. Chem.* **2020**, *132*, 23374–23379.

[21] G. Senges, L. Li, A. Wodyński, H. Beckers, R. Müller, M. Kaupp, S. Riedel, *Chem. Eur. J.* **2021**, *27*, 13642–13650.

[22] a) T. Vent-Schmidt, S. Riedel, *Inorg. Chem.* **2015**, *54*, 11114–11120; b) F. Brosi, T. Schlöder, A. Schmidt, H. Beckers, S. Riedel, *Dalton Trans.* **2016**, *45*, 5038–5044; c) A. V. Wilson, T. Nguyen, F. Brosi, X. Wang, L. Andrews, S. Riedel, A. J. Bridgeman, N. A. Young, *Inorg. Chem.* **2016**, *55*, 1108–1123.

[23] a) S. H. Vosko, L. Wilk, M. Nusair, *Can. J. Phys.* **1980**, *58*, 1200–1211; b) C. Lee, W. Yang, R. G. Parr, *Phys. Rev. B* **1988**, *37*, 785–789; c) A. D. Becke, *J. Chem. Phys.* **1993**, *98*, 5648–5652; d) P. J. Stephens, F. J. Devlin, C. F. Chabalowski, M. J. Frisch, *J. Phys. Chem.* **1994**, *98*, 11623–11627.

[24] a) R. A. Kendall, T. H. Dunning, R. J. Harrison, *J. Chem. Phys.* **1992**, *96*, 6796–6806; b) K. A. Peterson, D. Figgen, M. Dolg, H. Stoll, *J. Chem. Phys.* **2007**, *126*, 124101; c) D. Figgen, K. A. Peterson, M. Dolg, H. Stoll, *J. Chem. Phys.* **2009**, *130*, 164108.

[25] M. J. Frisch, G. W. Trucks, H. B. Schlegel, G. E. Scuseria, M. A. Robb, J. R. Cheeseman, G. Scalmani, V. Barone, G. A. Petersson, H. Nakatsuji, X. Li, M. Caricato, A. V. Marenich, J. Bloino, B. G. Janesko, R. Gomperts, B. Mennucci, H. P. Hratchian, J. V. Ortiz, A. F. Izmaylov, J. L. Sonnenberg, D. Williams-Young, F. Ding, F. Lipparini, F. Egidi, J. Goings, B. Peng, A. Petrone, T. Henderson, D. Ranasinghe, V. G. Zakrzewski, J. Gao, N. Rega, G. Zheng, W. Liang, M. Hada, M. Ehara, K. Toyota, R. Fukuda, J. Hasegawa, M. Ishida, T. Nakajima, Y. Honda, O. Kitao, H. Nakai, T. Vreven, K. Throssell, J. A. Montgomery, Jr, J. E. Peralta, F. Ogliaro, M. J. Bearpark, J. J. Heyd, E. N. Brothers, K. N. Kudin, V. N. Staroverov, T. A. Keith, R. Kobayashi, J. Normand, K. Raghavachari, A. P. Rendell, J. C. Burant, S. S. Iyengar, J. Tomasi, M. Cossi, J. M. Millam, M. Klene, C. Adamo, R. Cammi, J. W. Ochterski, R. L. Martin, K. Morokuma, O. Farkas, J. B. Foresman, and D. J. Fox, *Gaussian 16;* Gaussian, Inc, Wallingford CT, **2016**.

[26] H.-J. Werner, P. J. Knowles, G. Knizia, F. R. Manby, M. Schütz, P. Celani, W. Györffy, D. Kats, T. Korona, R. Lindh, A. Mitrushenkov, G. Rauhut, K. R. Shamasundar, T. B. Adler, R. D. Amos, S. J. Bennie, A. Bernhardsson, A. Berning, D. L. Cooper, M. J. O. Deegan, A. J. Dobbyn, F. Eckert, E. Goll, C. Hampel, A. Hesselmann, G. Hetzer, T. Hrenar, G. Jansen, C. Köppl, S. J. R. Lee, Y. Liu, A. W. Lloyd, Q. Ma, R. A. Mata, A. J. May, S. J. McNicholas, W. Meyer, T. F. Miller III, M. E. Mura, A. Nicklass, D. P. O'Neill, P. Palmieri, D. Peng, K. Pflüger, R. Pitzer, M. Reiher, T. Shiozaki, H. Stoll, A. J. Stone, R. Tarroni, T. Thorsteinsson, M. Wang, M. Welborn, *MOLPRO, version 2019.2, a package of ab initio programs.*

[27] M. K. Armbruster, F. Weigend, C. van Wüllen, W. Klopper, *Phys. Chem. Chem. Phys.* **2008**, *10*, 1748–1756.

[28] D. Peng, N. Middendorf, F. Weigend, M. Reiher, *J. Phys. Chem.* **2013**, *138*, 184105.

[29] S. G. Balasubramani, G. P. Chen, S. Coriani, M. Diedenhofen, M. S. Frank, Y. J. Franzke, F. Furche, R. Grotjahn, M. E. Harding, C. Hättig, A. Hellweg, B. Helmich-Paris, C. Holzer, U. Huniar, M. Kaupp, A. Marefat Khah, S. Karbalaei Khani, T. Müller, F. Mack, B. D. Nguyen, S. M. Parker, E. Perlt, D. Rappoport, K. Reiter, S. Roy, M. Rückert, G. Schmitz, M. Sierka, E. Tapavicza, D. P. Tew, C. van Wüllen, V. K. Voora, F. Weigend, A. Wodyński, J. M. Yu, *J. Phys. Chem.* **2020**, *152*, 184107.

[30] P. Pollak, F. Weigend, *J. Chem. Theory Comput.* **2017**, *13*, 3696–3705.

[31] Y. J. Franzke, N. Middendorf, F. Weigend, *J. Chem. Phys.* **2018**, *148*, 104110.

[32] J. C. Boettger, *Phys. Rev. B* **2000**, *62*, 7809–7815.

[33] S. Grimme, J. Antony, S. Ehrlich, H. Krieg, *J. Chem. Phys.* **2010**, *132*, 154104.

[34] S. Grimme, S. Ehrlich, L. Goerigk, *J. Comput. Chem.* **2011**, *32*, 1456–1465.

[35] L. Bennett, B. Melchers, B. Proppe, *Freie Universität Berlin*, **2020**, DOI: 10.17169/refubium-26754.

Manuscript received: November 6, 2021
Accepted manuscript online: February 19, 2022
Version of record online: March 18, 2022

5.3 Investigation of Isolated IrF_5^-, IrF_6^- Anions and $M[IrF_6]$ (M = Na, K, Rb, Cs) Ion Pairs by Matrix-Isolation Spectroscopy and Relativistic Quantum-Chemical Calculations

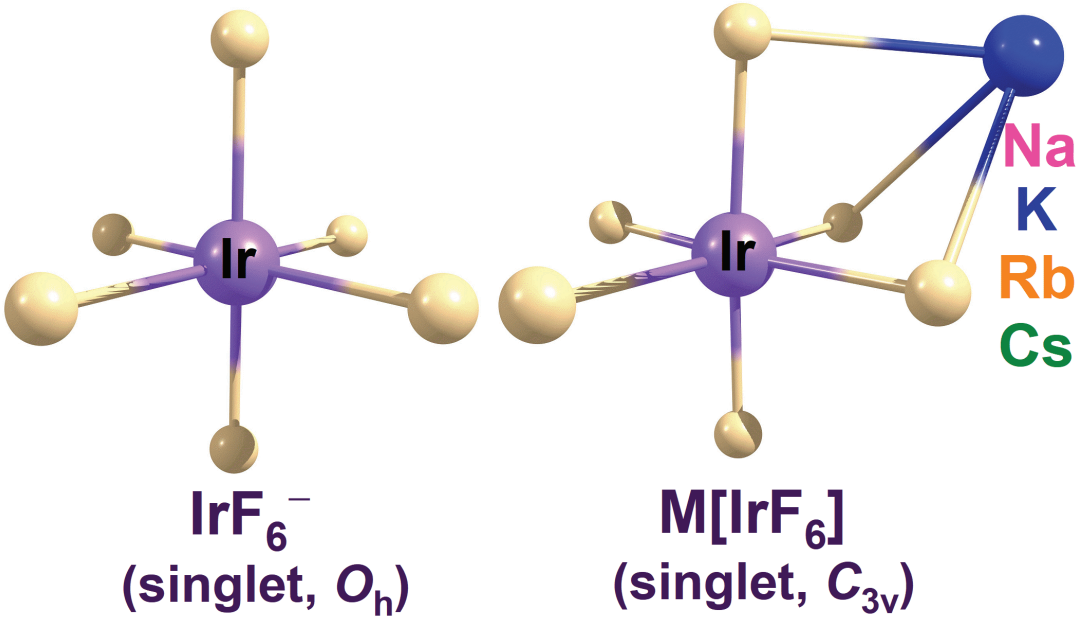

Yan Lu, Artur Wodyński, Marc Reimann, Robert Medel, Martin Kaupp, and Sebastian Riedel

Chemistry — A European Journal **2024**, e202401015.

https://doi.org/10.1002/chem.202401015

Author contribution

Yan Lu carried out all experiments, performed quantum-chemical calculations, and wrote the first draft of the manuscript. Artur Wodyński and Marc Reimann performed the further calculations with the SOC effect and wrote part of the manuscript. Robert Medel revised the manuscript. Sebastian Riedel and Martin Kaupp managed the project and revised the manuscript.

Chemistry
A European
Journal

Chemistry Europe
European Chemical Societies Publishing

Accepted Article

Title: Investigation of Isolated IrF5−, IrF6− Anions and M[IrF6] (M = Na, K, Rb, Cs) Ion Pairs by Matrix-Isolation Spectroscopy and Relativistic Quantum-Chemical Calculations

Authors: Yan Lu, Artur Wodyński, Marc Reimann, Robert Medel, Martin Kaupp, and Sebastian Hasenstab-Riedel

To be cited as: *Chem. Eur. J.* **2024**, e202401015

Link to VoR: https://doi.org/10.1002/chem.202401015

WILEY VCH

10.1002/chem.202401015

WILEY VCH

RESEARCH ARTICLE

Investigation of Isolated IrF_5^-, IrF_6^- Anions and M[IrF_6] (M = Na, K, Rb, Cs) Ion Pairs by Matrix-Isolation Spectroscopy and Relativistic Quantum-Chemical Calculations

Yan Lu,[a] Artur Wodyński,[b] Marc Reimann,[b] Robert Medel,[a] Martin Kaupp,*[b] Sebastian Riedel*[a]

Dedication ((optional))

[a] M. Sc. Yan Lu, Dr. Robert Medel, Prof. Dr. Sebastian Riedel
Institut für Chemie und Biochemie-Anorganische Chemie
Freie Universität Berlin
Fabeckstrasse 34/36, 14195 Berlin, Germany
E-mail: s.riedel@fu-berlin.de

[b] Dr. Artur Wodyński, Dr. Marc Reimann, Prof. Dr. Martin Kaupp
Institut für Chemie Theoretische Chemie/Quantenchemie
Technische Universität Berlin
Sekr. C7, Strasse des 17. Juni 135, 10623 Berlin, Germany
E-mail: martin.kaupp@tu-berlin.de

Supporting information for this article is given via a link at the end of the document.

Abstract: The molecular IrF_5^-, IrF_6^- anions and M[IrF_6] (M = Na, K, Rb, Cs) ion pairs were prepared by co-deposition of laser-ablated alkali metal fluorides MF with IrF_6 and isolated in solid neon or argon matrices under cryogenic conditions. The free anions were obtained as well by co-deposition of IrF_6 with laser-ablated metals (Ir or Pt) as electron sources. The products were characterized in a combined analysis of matrix IR spectroscopy and electronic structure calculations using two-component quasi-relativistic DFT methods accounting for scalar-relativistic and spin-orbit coupling (SOC) effects as well as multi-reference configuration-interaction (MRCI) approaches with SOC. Inclusion of SOC is crucial in the prediction of spectra and properties of IrF_6^- and its alkali-metal ion pairs. The observed IR bands and the computations show that the IrF_6^- anion adopts an O_h structure in a nondegenerate ground state stabilized by SOC effects, and not a distorted D_{4h} structure in a triplet ground state as suggested by scalar-relativistic calculations. The corresponding "closed-shell" M[IrF_6] ion pairs with C_{3v} symmetry are stabilized by coordination of an alkali metal ion to three F atoms, and their structural change in the series from M = Na to Cs was proven spectroscopically. There is no evidence for the formation of IrF_7, IrF_7^- or M[IrF_7] (M = Na, K, Rb, Cs) ion pairs in our experiments.

Introduction

The electronic molecular structure of heavy group 10 hexafluorides, which exhibit $(t_{2g})^4$ non-bonding molecular orbitals, has attracted substantial interest in the past few years due to the competition between Jahn-Teller (JT) distortion and spin-orbit coupling (SOC) effects.[1,2,3,4–8] A JT-distorted $^3A_{1g}/D_{4h}$ structure has been predicted as the ground state for the hitherto hypothetical PdF_6 in scalar-relativistic calculations without SOC contribution.[1,7] However, when SOC is taken into account, a D_{3d} structure also becomes energetically competitive with the D_{4h} and O_h structures. It was therefore suggested that PdF_6 would be highly fluxional and most likely would exhibits an average O_h structure under most experimental conditions.[7] This would be in line with four-component relativistic Dirac–Hartree–Fock (DHF) calculations where the JT distortion of PdF_6 is quenched by SOC and a diamagnetic, octahedral singlet structure is predicted.[4] However, the exact prediction of the structure as well as the electronic configuration is still challenging, especially if there is no convincing experimental evidence for the existence of PdF_6.[1,9] For the heavier PtF_6, relativistic effects like SOC become more pronounced, and its inclusion in computations changes the ground state from a D_{4h} triplet[10] to a nondegenerate state with O_h symmetry consistent with various spectroscopic observations.[11,12] This holds at two-component X2C and four-component relativistic DHF and DIRAC-DFT levels.[2,4–6,13] David *et al.* reported that the Dirac-LDA calculations afford SOC splittings of 1326.4 and 4376.4 cm^{-1} for PdF_6 and PtF_6, respectively.[4]

Based on these interesting results for the palladium and platinum hexafluorides, it is interesting to investigate the isoelectronic $5d^4$ anion IrF_6^-. This anion was predicted by scalar-relativistic coupled-cluster calculations to show a distorted triplet ground state[10] while two-component ZORA-DFT calculations suggested D_{3d} and D_{4h} structures which are very similar in energy.[10] Experimental evidence from solid-state high-resolution ^{19}F NMR data favors a nondegenerate octahedral "diamagnetic" complex IrF_6^- in K[IrF_6].[8] Indeed, relativistic Dirac-DFT computations including SOC suggested an octahedral "singlet".[14] Experimental SO splittings of IrF_6^- (3400 cm^{-1}) are found to be lower than for PtF_6 (5200 cm^{-1}), in keeping with the trend of calculated λ^{so} values of K[IrF_6] (10256 cm^{-1}) and PtF_6 (12082

10.1002/chem.202401015

cm^{-1}) at Dirac-Fock level.[8,11,12,15] Moreover, solid-state $[H_2F]^+[IrF_6]^-$ is EPR-silent, and K[IrF_6] and Cs[IrF_6] display temperature-independent paramagnetism. All of these data favor a nondegenerate ground state for IrF_6^-.[8,16,17]

To the best of our knowledge, the free IrF_6^- anion has not yet been experimentally detected and known experimental data are all based on solid salts.[8,15,16,18,19–21] Although its alkali metal salts M[IrF_6] have been characterized by single-crystal[20–22] and synchrotron X-ray powder diffraction (SPDD),[19] there is a lack of experimental spectroscopic or theoretical investigations on the molecular M[IrF_6] (M = Na, K, Rb, Cs) ion pairs. Additionally, the lower-valent pentafluoroiridate(IV) anion IrF_5^- has not yet been studied spectroscopically, nor is its solid-state structure known in salts, in contrast to many investigations on iridium(IV) complexes containing $[IrF_6]^{2-}$ units involving various counterions.[20,23] Finally, the high-valent anion IrF_7^- was only investigated computationally,[10] while the possible existence of $[NO]^+[IrF_7]^-$ as a reaction intermediate has been postulated.[24] A recent study reported an unsuccessful attempt for the preparation of Cs[IrF_7] salt.[21]

The combination of laser ablation and matrix-isolation spectroscopy has proven to be a powerful method for producing novel unstable anionic species.[25–29] In our previous reports, non-metal F_3^- and F_5^- anions were formed after condensation of F_2 with laser-ablated metal atoms as electron sources.[25,26,30] Therefore, the molecular IrF_6^- anion might be expected to be formed by electron capture by neutral IrF_6 molecules during the laser ablation process. Additionally, the successful preparation and identification of the alkali metal ion pairs M[F_3][25,26,31] and M[AuF_4][32] formed by the reaction of MF with F_2, and MF with AuF_3, respectively, in solid noble gases may suggest the possible identification of molecular M[IrF_7] (M = Na, K, Rb, Cs) ion pairs via the laser ablation of the corresponding alkali metal fluorides MF with IrF_6.

Herein, we report for the first time on the preparation and matrix-isolation IR spectroscopic characterization as well as accompanying relativistic quantum-chemical studies of the electronic structures of molecular IrF_5^-, IrF_6^- anions and MIrF_6 (M = Na, K, Rb, Cs) alkali ion pairs. These products were generated by the laser ablation of alkali metal fluorides MF with IrF_6 in cryogenic solid neon or argon matrices. Both of the free anions were also detected in separate matrix-isolation experiments based on laser ablation of metals (Ir or Pt) as electron sources in the presence of IrF_6. Their identification is based on the experimental Ir−F stretching vibrational frequencies and further supported by two-component quasi-relativistic DFT computations[33] as well as MRCI computations[34–36] including SOC effects. Electron affinities and fluoride ion affinities of IrF_6 and IrF_5 have also been calculated.

Results and Discussion

Computational Results

The structures of IrF_5^-, IrF_6^- and the M[IrF_6] (M = Na, K, Rb, Cs) ion pairs in their ground states were optimized using two-component (2c-X2C) all-electron density functional theory (DFT) calculations, as depicted in Figure 1. These optimizations utilized 1c-X2C calculations with selected multiplicities as starting points (optimized 1c-X2C structures are presented in Figures S1 and S2 in Supporting Information). Optimization at 2c-X2C level was performed in C_1 symmetry, allowing for slight deviations from the initial higher-symmetric structures. We note that after incorporation of the substantial SOC in the 2c calculations, spin is not a good quantum number anymore. When discussing spin multiplicities for the 2c calculations, we refer exclusively to the multiplicity of the Kohn-Sham orbital guess employed. We denote the electronic configuration states as pseudo multiplicities, indicating that these refer solely to the 1c configurations used as initial guesses.

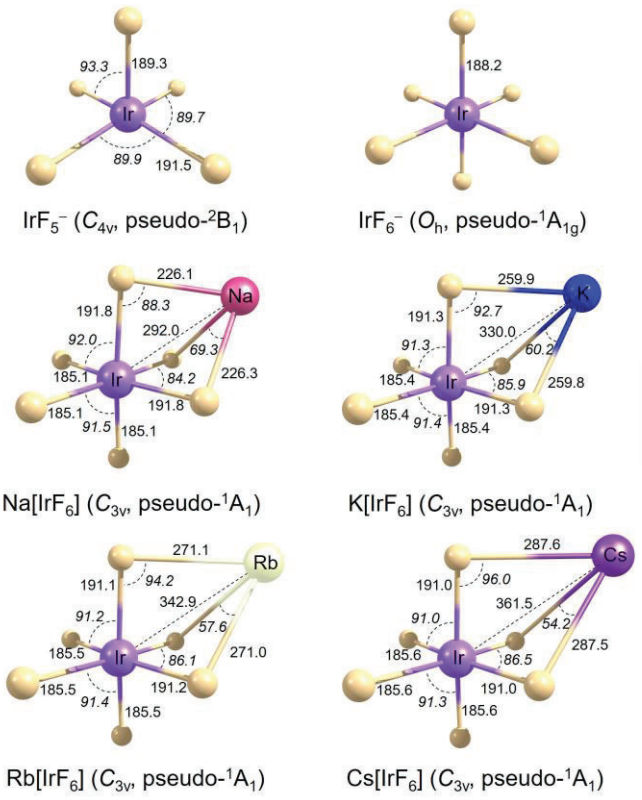

Figure 1. Molecular structures of M[IrF_6] (M = Na, K, Rb, Cs) ion pairs and IrF_5^- and IrF_6^- anions in their ground states obtained at the 2c-X2C-PBE0-D3(BJ)/x2c-TZVPall-2c (M[IrF_6]) and 2c-X2C-PBE0/x2c-TZVPall-2c (anions) levels. Selected bond lengths (pm) and angles (°, in *italics*) are shown. Optimization at 2c-X2C level was performed in C_1 symmetry.

The IrF_5^- anion, in its pseudo-doublet ground state, shows a C_{4v}-symmetric (square-pyramidal) structure characterized by an axial and four longer equatorial Ir−F bonds. This agrees with previous predictions for the IrF_5 and PtF_5 molecules.[5,37] Due to numerical reasons, our DFT-optimized structures show slight distortions from perfect C_{4v}. For the IrF_6^- anion, 2c-X2C DFT calculations incorporating SOC revealed that, in contrast to scalar-relativistic predictions indicating a $^3A_{1g}/D_{4h}$ ground state (as shown in Figure S1), the ground state is a Kramers-restricted pseudo-closed-shell one with O_h symmetry. The pseudo-triplet configuration was found to be energetically less favourable, lying 22–27 kJ/mol above the ground state. It is worth mentioning that 2c-X2C calculations may converge to two distinct pseudo-open-shell electronic configurations depending on the initial 1c-X2C guess used. One of these configurations, despite being slightly lower in energy than the Kramers-restricted pseudo-closed-shell

10.1002/chem.202401015

configuration, was identified as exhibiting broken symmetry and is thus excluded from further analysis (detailed information can be found in Comment S1 in Supporting Information). We observed similar behavior for the isoelectronic PtF_6.[5]

We note that the octahedral symmetry of the ground state of IrF_6^- (or of PdF_6 and PtF_6) can be justified without the use of explicit spin-multiplicities: in an O_h-symmetric configuration, IrF_6^- exhibits (in the non-relativistic limit) a $^3T_{1g}$ ground state (see Figure. 2). As this is an orbital-degenerate state, it will experience Jahn-Teller (JT) distortion towards D_{4h} symmetry in such a manner that the ground state becomes nondegenerate. This $^3A_{2g}$ state, however, is still triply degenerate in the spin-domain, leading to, for example, an EPR signal. Under strong spin-orbit coupling (SOC), the $^3T_{1g}$ state splits into several different states upon coupling of the orbital and the spin functions,[38] leading to four states, $T_{1g} \otimes T_{1g} = A_{1g} \oplus E_g \oplus T_{1g} \oplus T_{2g}$, for which spin is no longer a good quantum number. Using configurational energies obtained at the 1c-X2C-MRCI+Q level (see Computational Details) to diagonalize the SOC matrix, we arrive at the diagram shown on the right-hand site of Figure 2. The ground state is totally symmetric and will therefore not exhibit JT distortion. We also do not expect an EPR signal or temperature-dependent paramagnetism, as the first excited T_{1g} state is too high in energy (ca. 4500 cm^{-1}) to be accessible thermally or via typical microwave frequencies used for EPR. This result can be directly transferred to PdF_6 and PtF_6 and potentially other d^4 systems with strong spin-orbit coupling. It provides a more precise description of the electronic states of IrF_6^- than the 2c-DFT calculations shown above.

2c-X2C DFT structure optimizations of $M[IrF_6]$ ion pairs (M = Na, K, Rb, Cs) provide C_{3v}-symmetrical structures, characterized by an alkali metal atom being coordinated by three fluorine atoms from the IrF_6 moiety, as illustrated in Figure 1. The optimizations were performed for the Kramers-restricted pseudo-closed-shell ground state to be consistent with the results obtained for the isolated anion (see above).

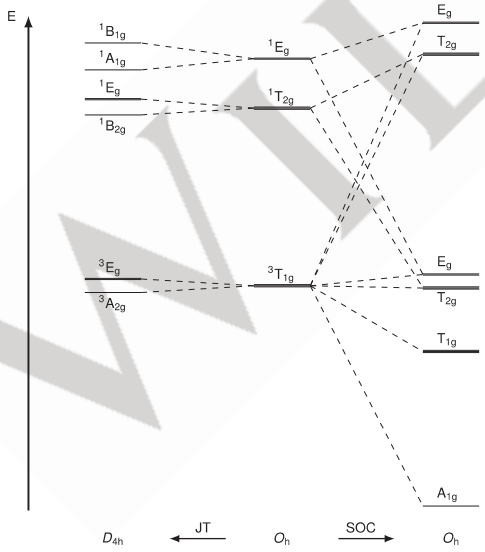

Figure 2. Semi-quantitative state diagram of IrF_6^- in the scalar-relativistic limit and perfect O_h symmetry (middle) and under JT distortion to D_{4h} (left) or when considering SOC (right). State energies were calculated at the MRCI+Q level (see Computational Details) using symmetrized structures obtained at the 2c-X2C-PBE0 level.

Experimental Results

Laser Ablation of Metals with IrF_6

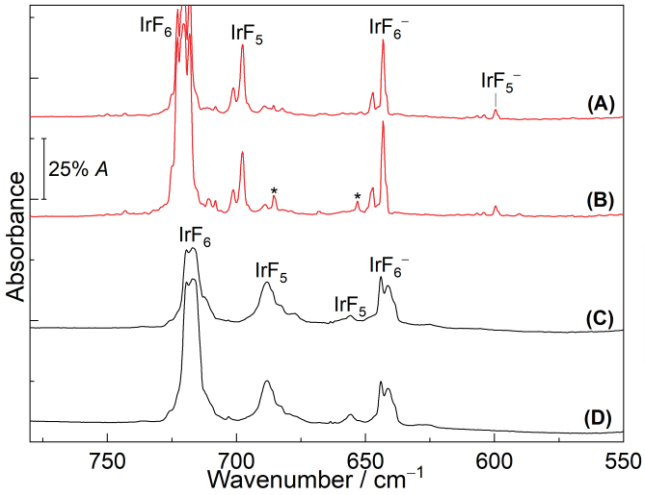

Figure 3. Infrared matrix-isolation spectra of neon (**A** and **B**) and argon (**C** and **D**) matrices at 5 K. (**A**) and (**C**) are spectra of the reaction products from laser ablation of Pt with IrF_6. (**B**) and (**D**) are spectra of the reaction products from laser ablation of Ir with IrF_6. The bands marked with asterisks were not assigned.

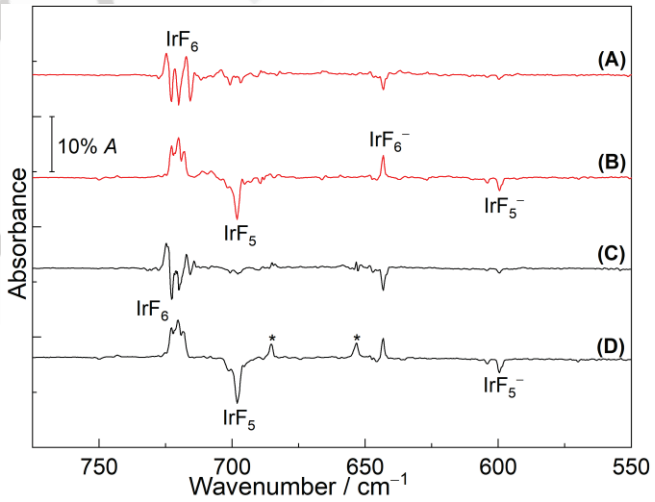

Figure 4. Infrared matrix-isolation spectra of neon matrices at 5 K. (**A**) IR difference spectrum reflecting the changes of the reaction products from laser ablation of Pt with IrF_6 upon annealing to 9 K; (**B**) IR difference spectrum reflecting the changes of the reaction products upon subsequent 656 nm LED irradiation for 20 min; (**C**) IR difference spectrum reflecting the changes of the reaction products from laser ablation of Ir with IrF_6 upon annealing to 9 K; (**D**) IR difference spectrum reflecting the changes of the reaction products upon subsequent 656 nm LED irradiation for 20 min. The bands marked with asterisks were not assigned.

The infrared spectra recorded after co-deposition of laser-ablated metal atoms (Ir or Pt) with IrF_6 in excess neon or argon at 5 K are shown in Figures 3 and 4. The binary fluoride molecules IrF_5 and IrF_6 as common products were observed after sample deposition. Clearly, IrF_5 is present in the matrix as a result of the homolytic cleavage of one Ir–F bond in IrF_6 by the UV radiation

10.1002/chem.202401015

RESEARCH ARTICLE

Table 1. Calculated and experimentally observed IR vibrational frequencies (in cm^{-1}) of the IrF_5^- and IrF_6^- anions.[a]

Species	Sym.	Calc. (Int.)[b] 2c-X2C DFT B3LYP	PBE0	Exp. Ne	Ar
IrF_5^- (C_{4v}, pseudo-$^2B_1$)	a_1	619.2 (6)	644.8 (8)	–[c]	–[c]
	e	585.3 (239) × 2	603.7 (251) × 2	599.8	–[c]
	a_1	560.9 (47)	589.1 (46)	–[c]	–[c]
	b_2	544.6 (0)	565.0 (1)	–[c]	–[c]
IrF_6^- (O_h, pseudo-$^1A_{1g}$)	T_{1u}	631.3 (219) × 3	652.4 (231) × 3	647.2/643.2	644.1/641.1

[a] The complete set of calculated frequencies is provided in Supporting Information (Tables S1 and S6). Intensities are shown in parentheses in km mol^{-1}. [b] x2c-TZVPall-2c basis set. [c] Bands not observed, or too weak.

accompanying the laser ablation of metals.[37] Apart from the known species IrF_6 and IrF_5, new IR absorptions at 647.2/643.2 and 599.8 cm^{-1} appeared simultaneously in the neon spectra from the laser-ablation experiments using different metal (Ir or Pt) targets in the presence of IrF_6 (Figures 3(A) and 3(B)). In order to distinguish the newly formed metal-independent IR bands, further annealing and irradiation of the sample was performed (Figures 4, S5 and S6). Both absorptions in the separate Ir and Pt experiments decreased during annealing of the sample to 9 K. However, further irradiation with red light (λ = 656 nm, 20 min) increased the more intense band at 643.2 cm^{-1}, while the weaker band at 599.8 cm^{-1} decreased slightly, indicating that two new species were formed in neon matrices. Analogous spectra from separate Ir and Pt experiments were also recorded after sample deposition in solid argon (Figures 3(C) and 3(D)). However, in this case only one new metal-independent broad band at 644.4/641.1 cm^{-1} appeared in addition to the identified IrF_6 and IrF_5 absorptions.[37]

Based on the observed metal-independent absorptions with similar photochemical and annealing behaviors in neon matrices in the Ir and Pt experiments, most likely, the two new products are IrF_6^- and IrF_5^- anions, which could be formed via electron capture by the precursor IrF_6 and the photodissociation product IrF_5. The weak metal-independent band at 599.8 cm^{-1} observed in the neon spectra is attributed to a strong equatorial asymmetric IrF_4 stretching mode of the hitherto unknown molecular IrF_5^- anion. It shows a large red-shift of 98.0 cm^{-1}, relative to the same stretching vibration in neutral IrF_5 located at 697.8 cm^{-1} in neon matrix.[37] The observed band agrees well with the predicted most intense absorption, but the computed much weaker IR-active absorption for axial Ir–F vibrational stretching of the IrF_5^- anion was not detected in our experiments (Table 1). Unfortunately, no counterpart of the 599.8 cm^{-1} band was detected in the argon matrix, which is most likely due to its low abundance.

The strong metal-independent absorptions at 643.2 cm^{-1} in neon and 641.1 cm^{-1} in argon matrices were assigned to the free IrF_6^- anion. Similar to the cases of IrF_6 (720.6 cm^{-1} in neon matrix; 719.3 cm^{-1} in argon matrix)[37] and PtF_6 (705.6 cm^{-1} in neon matrix; 705.5 cm^{-1} in argon matrix),[5] the band of IrF_6^- also shows a small matrix shift (2.1 cm^{-1}) going from argon to neon. Moreover, such a matrix shift was also observed in the AuF_4^- anion (611.3 cm^{-1} in neon matrix; 610.6 cm^{-1} in argon matrix).[39] Similar to our own 1c-X2C calculations (Table S5), previous scalar-relativistic calculations of IrF_6^- in a triplet ground state predicted a D_{4h} structure with two vibrational Ir–F bands at 650 and 615 cm^{-1} having an intensity distribution of about 1:2.[10] This clearly does not match the observed absorptions. As discussed above, our 2c-X2C calculations including SOC afford a diamagnetic octahedral structure in a Kramers-restricted pseudo-closed-shell ground state for IrF_6^-, supported by high-level MRCI+Q energy calculations with SOC. This is consistent with the single observed IR band (Table 1), the absence of an EPR signal for $[H_2F]^+[IrF_6]^-$, and the temperature-independent paramagnetism for $M[IrF_6]$ (M = K and Cs).[8,16,17]

Laser Ablation of Alkali Metal Fluorides with IrF_6

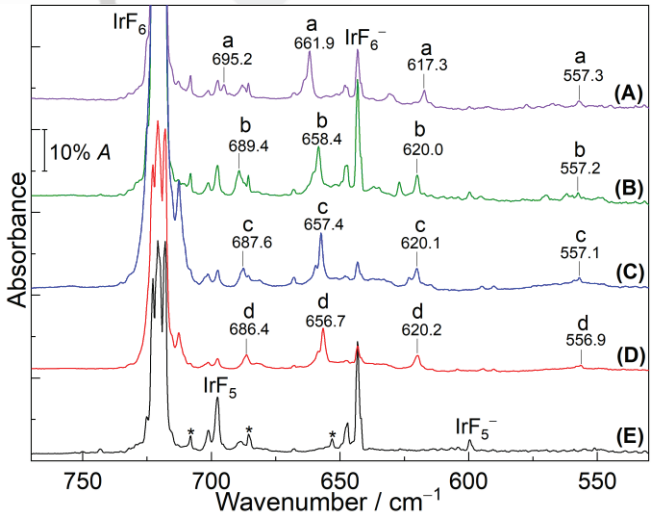

Figure 5. Infrared matrix-isolation spectra of neon matrices at 5 K. (**A–D**) Spectra of reaction products of laser-ablated MF (M = Na, K, Rb, Cs) with IrF_6. (**A**) NaF, (**B**) KF, (**C**) RbF and (**D**) CsF. (**E**) Spectrum of the reaction products from laser ablation of Ir with IrF_6. The IR bands of $Na[IrF_6]$, $K[IrF_6]$, $Rb[IrF_6]$, $Cs[IrF_6]$ were labeled with **a**, **b**, **c**, and **d**, respectively. The bands marked with asterisks were not assigned.

IR spectra were recorded after co-deposition of laser-ablated alkali metal fluorides MF (M = Na, K, Rb, Cs) with IrF_6 in excess neon or argon at 5 K (Figures 5 and 6). The common absorptions assigned to the IrF_6^- and IrF_5^- anions as electron capture products (see above) were also observed in the experiments when the alkali metal fluorides were used, which further confirms the assignment of these anions. In addition to the identified species, the present experiments also led to the formation of some new bands which were found to be alkali-metal dependent and were

10.1002/chem.202401015

RESEARCH ARTICLE

not observed in the experiment using laser-ablated Ir with IrF_6 (Figures 5(E) and 6(E)). These bands can be grouped and belong to different vibrational modes of the same new molecule upon subsequent irradiation with light of a wavelength λ = 656 nm (Figures S7–S10).

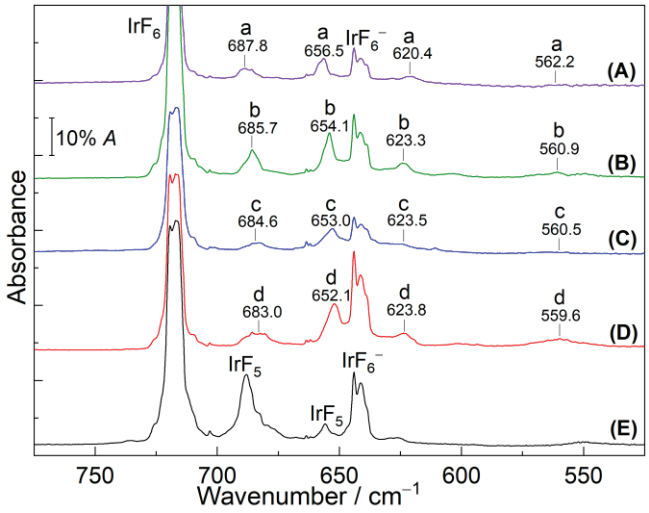

Figure 6. Infrared matrix-isolation spectra of argon matrices at 5 K. (**A–D**) Spectra of reaction products of laser-ablated MF (M = Na, K, Rb, Cs) with IrF_6. (**A**) NaF, (**B**) KF, (**C**) RbF and (**D**) CsF. (**E**) Spectrum of the reaction products from laser ablation of Ir with IrF_6. The IR bands of Na[IrF_6], K[IrF_6], Rb[IrF_6], Cs[IrF_6] were labeled with **a**, **b**, **c**, and **d**, respectively.

The wavenumber of the most intense Ir–F stretching band depending on the alkali metal ion of 661.9, 658.4, 657.4, and 656.7 cm^{-1} for NaF through CsF in neon matrix (656.5, 654.1, 653.0, and 652.1 cm^{-1} in argon matrix) are higher than for the isolated IrF_6^- anion at 643.2 cm^{-1} in neon and 641.2 cm^{-1} in argon matrices. This is the typical relationship for ion pairs, similar to the cases of the free AuF_4^- anion (611.3 cm^{-1} in a neon matrix)[39] and its M[AuF_4] (M = K, Rb, Cs) ion pairs (ca. 632 cm^{-1} in a neon matrix).[32] Therefore, the IrF_6^- anion trapped in solid neon or argon is most likely coordinated by an alkali metal atom, and the observed alkali-metal dependent bands can be assigned to the M[IrF_6] (M = Na, K, Rb, Cs) ion pairs. Unfortunately, the highest-frequency Ir–F stretching band in the series of the M[IrF_6] ion pairs located at 695.2, 689.4, 687.6, and 686.4 cm^{-1}, respectively, in neon matrix (687.8, 685.7, 684.6, 683.0 cm^{-1} in argon matrix) overlaps with either absorptions of IrF_5 or of unknown impurities.

The assignment of the stretching bands of M[IrF_6] (M = Na, K, Rb, Cs) ion pairs in C_{3v} symmetry was further supported by 2c-X2C DFT calculations including SOC (Tables 2 and S9–S12). Analogous to the case of isolated IrF_6^-, use of a Kramers-restricted pseudo-closed-shell ground state at 2c-X2C level provides best agreement with the observed values. Additionally, in the series of spectra from NaF to CsF, the observed red-shifts of Ir–F vibrational stretching bands in neon matrices at 695.2–686.4 cm^{-1} (687.8–683.0 cm^{-1} in argon), at 661.9–656.7 cm^{-1} (656.5–652.1 cm^{-1} in argon) and at 557.3–556.9 cm^{-1} (562.2–559.6 cm^{-1} in argon), and the blue-shift of the bands at 617.3–620.2 cm^{-1} (620.4–623.8 cm^{-1} in argon) are excellently matched by the trend of the calculated harmonic frequencies, consistent with an increase of the uncoordinated Ir–F bond lengths and a decrease of M-coordinated Ir–F bond lengths in M[IrF_6] from Na to Cs (Table 2 and Figure 1), following the decrease of the Lewis acidity of the alkali cations in the order $Na^+ > K^+ > Rb^+ > Cs^+$.[40]

Table 2. Calculated and experimentally observed IR wavenumbers (in cm^{-1}) of M[IrF_6] (M = Na, K, Rb, Cs) ion pairs.[a]

Species	Sym.	Calc. (Int.)[b] 2c-X2C-PBE0 (pseudo-$^1A_1$, C_{3v})	Exp. Ne	Ar
Na[IrF_6]	a_1	713.4 (76)	695.2	687.8
	e	682.7 (155) × 2	661.9	656.5
	a_1	619.9 (148)	617.3	620.4
	e	567.0 (54) × 2	557.3	562.2
K[IrF_6]	a_1	707.4 (78)	689.4	685.7
	e	674.5 (169) × 2	658.4	654.1
	a_1	622.5 (167)	620.0	623.3
	e	563.0 (40) × 2	557.2	560.9
Rb[IrF_6]	a_1	706.4 (81)	687.6	684.6
	e	673.5 (167) × 2	657.4	653.0
	a_1	623.2 (175)	620.1	623.5
	e	563.2 (37) × 2	557.1	560.5
Cs[IrF_6]	a_1	704.8 (84)	686.4	683.0
	e	672.0 (164) × 2	656.7	652.1
	a_1	624.1 (186)	620.2	623.8
	e	563.0 (32) × 2	556.9	559.6

[a] The complete set of calculated frequencies is provided in Supporting Information (Tables S9–S12). Intensities are shown in parentheses in km mol^{-1}. [b] Values calculated at 2c-X2C-PBE0-D3(BJ) level with x2c-TZVPall-2c basis set.

Since the molecular alkali tetrafluorido aurate M[AuF_4] (M = K, Rb, Cs) ion pairs could be previously generated by the reaction of laser-ablation MF and AuF_3 in solid neon,[32] we have also considered the M[IrF_7] ion pairs for the alkali-metal dependent bands mentioned above. However, M[IrF_7] ion pairs can be ruled out safely, because the alkali-metal dependent bands assigned to M[IrF_6] were also observed in experiments of laser-ablated alkali metal chlorides MCl with IrF_6 (Figure S7). This also prompted us to consider the possible product IrF_7 and its anion IrF_7^- by adding an F atom or a F^- anion to IrF_6, so far only investigated in computational studies.[10] The pentagonal-bipyramidal (D_{5h} symmetry) structure of IrF_7 in a pseudo-triplet ground state has been reported previously in one- and two-component all electron DFT calculations. Its predicted vibrational frequencies would be located at 718 and 662 cm^{-1} with an intensity ratio of 2:3.[37,41] It was also reported that addition of F^- to IrF_6 leads to a $^2B_1/C_{2v}$ structure for the anion IrF_7^- computed at scalar-relativistic B3LYP/aug-cc-pVTZ-PP level,[10] which is consistent with our calculations at 1c-X2C level (Figure S3 and Table S7). Inclusion of SOC in 2c-X2C calculations provides a pentagonal-bipyramidal structure with D_{5h} symmetry for this anion (Figure S4 and Table S8). However, the alkali-metal independent absorptions of either IrF_7 or IrF_7^- were not observed in our experiments.

Since the SOC contribution is essential for predicting the electron affinities for 5d metal hexafluorides,[10] 2c-X2C-DFT calculations including SOC effects were carried out for the electron affinities (EAs) and fluoride ion affinities (FIAs) of IrF_6 and

IrF_5 (Table 3). The corresponding 1c-X2C-DFT values without SOC contribution are given in Supporting Information (Table S13). Various bond dissociation energies (BDEs) of IrF_6^-, IrF_7^- anions and M[IrF_6] (M = Na, K, Rb, Cs) ion pairs are shown in Table 4.

Table 3. Calculated electron affinities (EAs) and fluoride ion affinities (FIAs) at 2c-X2C-B3LYP level.

Species	Calculated[a]		Experiment	Reported values	
	EA [eV]	FIA [kJ mol^{-1}]	EA [eV]	EA [eV]	FIA [kJ mol^{-1}]
IrF_5	5.81	496.0		5.75[c]	563.2[d]
IrF_6	6.73	251.5	6.50 ± 0.38[b]	5.99,[d] 5.34,[e] 7.2[f]	292.9[d]

[a] Calculated value in this work at 2c-X2C-B3LYP/x2c-TZVPall-2c level with additional diffuse basis functions for fluorine. [b] Ref.[42]. [c] Ref.[43]. [d] Ref.[10]. [e] Ref.[44] [f] Ref.[45].

Table 4. Computed bond dissociation energies (BDEs) of IrF_6^-, IrF_7^- and M[IrF_6] ion pairs (298.15 K, kJ mol^{-1}) at 2c-X2C-DFT level.

Process	$\Delta E + \Delta$ZPE	$\Delta_r H$	$\Delta_r G$
$IrF_6^- \rightarrow IrF_5^- + F$[a]	366.4	365.3	365.2
$IrF_7^- \rightarrow IrF_6^- + F$[a]	34.3	31.5	38.2
$Na[IrF_6] \rightarrow IrF_6^- + Na^+$[b]	480.8	476.3	486.3
$K[IrF_6] \rightarrow IrF_6^- + K^+$[b]	425.4	420.1	433.9
$Rb[IrF_6] \rightarrow IrF_6^- + Rb^+$[b]	412.2	406.6	423.6
$Cs[IrF_6] \rightarrow IrF_6^- + Cs^+$[b]	394.6	388.6	408.1

[a] 2c-X2C-B3LYP/x2c-TZVPall-2c level. [b] 2c-X2C-PBE0-D3(BJ)/x2c-TZVPall-2c level.

Our calculated value of 6.73 eV for the EA of IrF_6 is consistent with the values predicted by theoretical calculations,[10,44,45] but also is in excellent agreement with the experimental value of 6.50 ± 0.38 kcal/mol obtained by using high-temperature Knudsen cell mass spectrometry.[42] Compared to the 1c-X2C-B3LYP value (Table S13), the EA of IrF_6 is increased by 33.8 kJ mol^{-1} at 2c-X2C-B3LYP level (Table 3), slightly more than an earlier reported increase by 25.0 kJ mol^{-1}.[10] However, inclusion of SOC effects gives much smaller effects (2.9 kJ mol^{-1}) for the EA of IrF_5 in the present calculations. The high EAs of 5.81 and 6.73 eV for IrF_5 and IrF_6 sufficiently exceed those of the halogens (3.0–3.6 eV), suggesting that both molecules fall in the category of "superhalogens".[46] Moreover, both EAs also are dramatically larger than those of CCl_4 (2.00 ± 0.20 eV),[47] which serves as electron trapping agent in matrix isolation experiments.[27,48] Hence, the neutral precursor IrF_6 and the photodissociation product IrF_5 should each be able to capture an electron and form IrF_6^- and IrF_5^- anions, respectively, trapped in inert noble-gas matrices. Our 2c-X2C-B3LYP calculated value of 496.0 kJ mol^{-1} for the FIA of IrF_5 is lower than those of 563.2 kJ mol^{-1} calculated by Dixon.[10] Based on the high FIA value, IrF_5 was proposed as an strong Lewis acid. The FIA of IrF5 is substantially larger (by 244.5 kJ mol^{-1}) than that of IrF6, but the order of the EA values is reversed.

The Ir–F BDE of IrF_6^- is predicted to be 365.3 kJ mol^{-1}, consistent with the observed stability of these anions. In contrast, the predicted low BDE of 31.5 kJ mol^{-1} for IrF_7^- (slightly lower than a previously computed value of 42.7 kJ mol^{-1}[10]) suggests that IrF_7^- is less stable and difficult to prepare in our experiments. The computational results show that the ion-pair BDEs of M[IrF_6] (M = Na, K, Rb, Cs) decrease from $NaIrF_6$ (476.3 kJ mol^{-1}) to $CsIrF_6$ (388.6 kJ mol^{-1}). These ion pairs should thus be stable with respect to loss of an alkali-metal ion.

Conclusions

We have reported for the first-time matrix IR spectra of the molecular IrF_5^- and IrF_6^- anions and of the M[IrF_6] (M = Na, K, Rb and Cs) ion pairs stabilized under cryogenic conditions in neon and argon matrices. These species were produced during the laser ablation of different alkali-metal fluorides (NaF, KF, RbF, CsF) with excess IrF_6 in neon or argon at 5 K. However, attempts to prepare IrF_7, the IrF_7^- anion, or its ion pairs M[IrF_7] by this method failed. The alkali-metal independent anions IrF_5^- and IrF_6^- were formed either via electron capture during the laser ablation process, or via the laser ablation of different metals (Ir or Pt) and their reaction with IrF_6. Scalar-relativistic computations (1c-X2C) would predict a D_{4h} structure in a triplet ground state for IrF_6^-, but the calculated frequencies do not match the observed absorptions. The observed single band of IrF_6^- agrees with the predicted frequencies of a Kramer-restricted pseudo-closed-shell ground state with O_h symmetry in the presence of SOC effects at 2c-X2C level. This is in perfect agreement with the energy spectrum obtained from MRCI+Q calculations with SOC. The observed alkali-metal dependent IR absorptions of the Ir–F stretching frequencies for the M[IrF_6] (M = Na, K, Rb, Cs) ion pairs in C_{3v} symmetry stabilized by an alkali metal coordination to three F atoms on one face of the anion are consistent with the structural changes of these complexes when varying the alkali-metal ions from Na to Cs in the computations.

Experimental and Computational Details

The techniques of matrix-isolation infrared (IR) spectroscopy and the laser-ablation apparatus have been described in more detail in previous works.[5,28,37]The alkali-metal fluoride powder MF (M = Na, K, Rb, Cs) was pressed into a cylindric pellet using a hydraulic lab press. The pellet was subsequently mounted onto a rotatable target holder with a magnetic bearing motor and was transferred into a self-built matrix chamber. The Nd:YAG laser fundamental (Continuum, Minilite II, 1064 nm, 10 Hz repetition Rate, 45–50 mJ pulse^{-1}) was focused onto the alkali metal fluoride or metal (Ir or Pt) targets, which gave an energetic plasma beam and free electrons reacting with IrF_6 spreading toward a gold-plated mirror cooled to 5 K for neon (99.999%, Air Liquide) and argon (99.999%, Sauerstoffwerk Friedrichshafen) using a closed-cycle helium cryostat (Sumitomo Heavy Industries, RDK-205D) inside the matrix chamber. The infrared spectra were recorded on a Bruker Vertex 80v with 0.5 cm^{-1} resolution in the region 4000–450 cm^{-1} by using a liquid-nitrogen-cooled mercury cadmium telluride (MCT) detector. Matrix samples were annealed to 9 K and irradiated by selected light-emitting diode (LED) sources (λ = 656±10 nm).

Preparation of iridium hexafluoride followed procedures described in the literature.[49] It was prepared by heating iridium metal powder in a stainless-steel autoclave with an excess of fluorine at 300 °C for about 8 h. The

product IrF_6 was stored in a fluoroplastic (PFA) tube, trapped by liquid nitrogen. It was further purified by long pumping, and its initial purity was monitored by IR spectroscopy. After purification, the gas sample was mixed by passing a stream of neon or argon gas through a cold PFA tube (−96 °C) containing the IrF_6 sample and deposited on the matrix support for measurements.

As relativistic effects are known to be crucial for the description of Ir complexes, quasi-relativistic all-electron DFT calculations using the "exact-two-component" (X2C) Hamiltonian were performed at one-component and Kramers-restricted two-component (1c-X2C and 2c-X2C)[33,50] levels, using either the B3LYP[51] or PBE0[52] functionals, x2c-TZVPall-2c all-electron basis sets,[53] and a very fine quadrature grid (TURBOMOLE gridsize m5). For the calculation of fluoride ion affinities, the x2c-TZVPall-2c basis set of fluorine was supplemented by additional diffuse basis functions taken from the def2-TZVPD basis set.[54] These calculations were done with Turbomole 7.4.1.[55] For the M[IrF_6] (M = Na, K, Rb, Cs) ion pairs, additional dispersion corrections were included using Grimme's DFT-D3[56] scheme with Becke-Johnson (BJ) damping[57] and the parameters for either B3LYP or PBE0. Two-electron SOC terms were approximated using the scaled-nuclear-spin-orbit (SNSO)[58] approach in its original parameterization by Boettger.[59] A finite-nucleus model was used in all calculations.[60]

Additional calculations at the MRCI level[34,35] were performed with the MOLPRO program, Version 2022.2[61] All calculations employed the 1c-X2C Hamiltonian, ANO-RCC basis sets,[62] and D_{2h} symmetry. MRCI+Q calculations were performed based on state-averaged CASSCF calculations with an active space of 8 electrons in 7 orbitals, containing the five 5d orbitals of Ir and the two symmetrically adapted ligand orbitals of (formal) e_g symmetry. State-averaging was performed over all components of the lowest crystal field states ($^1T_{2g}$, ^1E_g, $^1A_{1g}$, $^3T_{1g}$ and ^5E_g). Spin-orbit coupling eigenstates were obtained by diagonalization of the sum of the electronic and the Breit-Pauli SOC Hamiltonian in the basis of the MRCI wave functions obtained for all states mentioned above.[36] The energy eigenvalues of the electronic Hamiltonian were adapted to include the Davidson size-consistency correction (+Q)[63] using a relaxed reference.

Supporting Information

The authors have cited additional references within the Supporting Information.[2, 5]

Acknowledgements

We gratefully acknowledge the Zentraleinrichtung für Datenverarbeitung (ZEDAT) of the Freie Universität Berlin for the allocation of computing resources.[64] Computations at Technische Universität Berlin used local resources at the Faculty II computing center. We thank the ERC Project HighPotOx as well as the CRC 1349 (SFB 1349) Fluorine-Specific Interactions-Project-ID 387284271 for continuous support. Y. L. thanks the China Scholarship Council (PhD Program) for financial support.

Keywords: IR spectroscopy • matrix isolation • d^4 transition-metal compounds • spin-orbit coupling • quantum chemistry

[1] A. V. Wilson, T. Nguyen, F. Brosi, X. Wang, L. Andrews, S. Riedel, A. J. Bridgeman, N. A. Young, *Inorg. Chem.* **2016**, *55*, 1108.
[2] L. Alvarez-Thon, J. David, R. Arratia-Pérez, K. Seppelt, *Phys. Rev. A* **2008**, *77*, 34502.
[3] a) S. P. Gabuda, S. G. Kozlova, *Phys. Rev. A* **2009**, *79*, 056501; b) G. Aullon, S. Alvarez, *Inorg. Chem.* **2007**, *46*, 2700; c) F. Wöhler, *Ann. Chim. Phys.* **1828**, *37*, 101.
[4] J. David, P. Fuentealba, A. Restrepo, *Chem. Phys. Lett.* **2008**, *457*, 42.
[5] G. Senges, L. Li, A. Wodyński, H. Beckers, R. Müller, M. Kaupp, S. Riedel, *Chem. Eur. J.* **2021**, *27*, 13642.
[6] K. Seppelt, *Chem. Rev.* **2015**, *115*, 1296.
[7] R. Craciun, R. T. Long, D. A. Dixon, K. O. Christe, *J. Phys. Chem. A* **2010**, *114*, 7571.
[8] S. P. Gabuda, V. N. Ikorskii, S. G. Kozlova, P. S. Nikitin, *JETP Letters* **2001**, *73*, 35.
[9] A. A. Timakov, V. N. Prusakov, Y. V. Drobyshevskii, *Zh. Neorg. Khim.* **1982**, *27*, 3007.
[10] R. Craciun, D. Picone, R. T. Long, S. Li, D. A. Dixon, K. A. Peterson, K. O. Christe, *Inorg. Chem.* **2010**, *49*, 1056.
[11] W. Moffitt, G. L. Goodman, M. Fred, B. Weinstock, *Mol. Phys.* **1959**, *2*, 109.
[12] J. H. Holloway, G. Stanger, E. G. Hope, W. Levason, J. S. Ogden, *J. Chem. Soc., Dalton Trans.* **1988**, 1341.
[13] R. Fernandes De Farias, *Inorg. Chem.* **2016**, *55*, 12126.
[14] J. David, D. Guerra, A. Restrepo, *Inorg. Chem.* **2011**, *50*, 1480.
[15] G. C. Allen, G. A. M. El-Sharkawy, K. D. Warren, *Inorg. Chem.* **1972**, *11*, 51.
[16] S. Seidel, K. Seppelt, *Angew. Chem. Int. Ed.* **2000**, *39*, 3923.
[17] A. Earnshaw, B. N. FIGGIS, J. Lewis, R. D. Peacock, *J. Chem. Soc.* **1961**, 3132.
[18] a) S. I. Ivlev, K. Gaul, M. Chen, A. J. Karttunen, R. Berger, F. Kraus, *Chem. Eur. J.* **2019**, *25*, 5793; b) B. Scheibe, A. J. Karttunen, F. Kraus, *Eur. J. Inorg. Chem.* **2021**, *2021*, 405; c) M. A. Hepworth, K. H. Jack, G. J. Westland, *J. Inorg. Nucl. Chem.* **1956**, *2*, 79; d) R. D. W. Kemmitt, D. R. Russell, D. W. A. Sharp, *J. Chem. Soc.* **1963**, 4408; e) D. H. Brown, D. R. Russell, D. W. A. Sharp, *J. Chem. Soc., A* **1966**, 18.
[19] O. Graudejus, A. P. Wilkinson, L. C. Chacon, N. Bartlett, *Inorg. Chem.* **2000**, *39*, 2794.
[20] H. Fitz, B. G. Muller, O. Graudejus, N. Bartlett, *Z. Anorg. Allg. Chem.* **2002**, *628*, 133.
[21] Z. Mazej, E. Goreshnik, K. O. Christe, *J. Fluorine Chem.* **2023**, *268*, 110128.
[22] Z. Mazej, R. Hagiwara, *J. Fluorine Chem.* **2007**, *128*, 423.
[23] a) K. S. Pedersen, J. Bendix, A. Tressaud, E. Durand, H. Weihe, Z. Salman, T. J. Morsing, D. N. Woodruff, Y. Lan, W. Wernsdorfer, C. Mathonière, S. Piligkos, S. I. Klokishner, S. Ostrovsky, K. Ollefs, F. Wilhelm, A. Rogalev, R. Clérac, *Nat. Commun.* **2016**, *7*, 12195; b) A. I. Gubanov, A. I. Smolentsev, E. Filatov, N. V. Kuratieva, A. M. Danilenko, S. V. Korenev, *ACS omega* **2021**, *6*, 27697; c) M. Rossi, M. Retegan, C. Giacobbe, R. Fumagalli, A. Efimenko, T. Kulka, K. Wohlfeld, A. I. Gubanov, M. Moretti Sala, *Phys. Rev. B* **2017**, *95*.
[24] a) N. Bartlett, S. P. Beaton, N. K. Jha, *Chem. Commun.* **1966**, 168; b) N. Bartlett, *Angew. Chem. Int. Ed.* **1968**, *7*, 433.
[25] T. Vent-Schmidt, F. Brosi, J. Metzger, T. Schlöder, X. Wang, L. Andrews, C. Müller, H. Beckers, S. Riedel, *Angew. Chem. Int. Ed.* **2015**, *54*, 8279.
[26] S. Riedel, T. Köchner, X. Wang, L. Andrews, *Inorg. Chem.* **2010**, *49*, 7156.
[27] L. Zhang, J. Dong, M. Zhou, Q. Qin, *J. Chem. Phys.* **2000**, *113*, 10169.
[28] F. A. Redeker, H. Beckers, S. Riedel, *Chem. Commun.* **2017**, *53*, 12958.
[29] M. Zhou, L. Zhang, Q. Qin, *J. Am. Chem. Soc.* **2000**, *122*, 4483.
[30] F. Brosi, T. Vent-Schmidt, S. Kieninger, T. Schlöder, H. Beckers, S. Riedel, *Chem. Eur. J.* **2015**, *21*, 16455.
[31] F. A. Redeker, H. Beckers, S. Riedel, *RSC Adv.* **2015**, *5*, 106568.
[32] F. A. Redeker, M. A. Ellwanger, H. Beckers, S. Riedel, *Chem. Eur. J.* **2019**, *25*, 15059.
[33] A. Baldes, F. Weigend, *Mol. Phys.* **2013**, *111*, 2617.
[34] H.-J. Werner, P. J. Knowles, *J. Chem. Phys.* **1988**, *89*, 5803.
[35] P. J. Knowles, H.-J. Werner, *Chem. Phys. Lett.* **1988**, *145*, 514.
[36] A. Berning, M. Schweizer, H.-J. Werner, P. J. Knowles, P. Palmieri, *Mol. Phys.* **2000**, *98*, 1823.
[37] Y. Lu, Y. A. Tsegaw, A. Wodyński, L. Li, H. Beckers, M. Kaupp, S. Riedel, *Chem. Eur. J.* **2022**, *28*, e202104005.

[38] G. Herzberg, *Molecular Spectra and Molecular Structure: III. Electronic Spectra and Electronic Structure of Polyatomic Molecules*, Van Nostrand Reinhold, New York, **1966**.
[39] X. Wang, L. Andrews, F. Brosi, S. Riedel, *Chem. Eur. J.* **2013**, *19*, 1397.
[40] R. C. Deka, R. Kinkar Roy, K. Hirao, *Chem. Phys. Lett.* **2004**, *389*, 186.
[41] S. Riedel, M. Kaupp, *Angew. Chem. Int. Ed.* **2006**, *45*, 3708.
[42] M. V. Korobov, S. V. Kuznetsov, L. N. Sidorov, V. A. Shipachev, V. N. Mit'kin, *Int. J. Mass Spectrom. Ion Processes* **1989**, *87*, 13.
[43] S. A. Macgregor, K. H. Moock, *Inorg. Chem.* **1998**, *37*, 3284.
[44] Gutsev, G. L., Boldyrev, A. I., *Chem. Phys. Lett.* **1983**, *101*, 441.
[45] S. A. Siddiqui, T. Rasheed, *Int. J. Quantum Chem.* **2013**, *113*, 959.
[46] G. L. Gutsev, A. I. Boldyrev, *Chem. Phys.* **1981**, *56*, 277.
[47] a) H. Dispert, K. Lacmann, *Int. J. Mass Spectrom. Ion Phys.* **1978**, *28*, 49; b) K. Lacmann, M. J. P. Maneira, A. M. C. Moutinho, U. Weigmann, *J. Chem. Phys.* **1983**, *78*, 1767.
[48] M. Zhou, L. Andrews, *J. Am. Chem. Soc.* **1998**, *120*, 11499.
[49] A. D. Richardson, K. Hedberg, G. M. Lucier, *Inorg. Chem.* **2000**, *39*, 2787.
[50] a) M. K. Armbruster, F. Weigend, C. van Wüllen, W. Klopper, *Phys. Chem. Chem. Phys.* **2008**, *10*, 1748; b) D. Peng, N. Middendorf, F. Weigend, M. Reiher, *J. Phys. Chem.* **2013**, *138*, 184105.
[51] a) P. J. Stephens, F. J. Devlin, C. F. Chabalowski, M. J. Frisch, *J. Phys. Chem.* **1994**, *98*, 11623; b) A. D. Becke, *J. Chem. Phys.* **1993**, *98*, 5648; c) C. Lee, W. Yang, R. G. Parr, *Phys. Rev. B* **1988**, *37*, 785; d) S. H. Vosko, L. Wilk, M. Nusair, *Can. J. Phys.* **1980**, *58*, 1200.
[52] a) C. Adamo, V. Barone, *J. Chem. Phys.* **1999**, *110*, 6158; b) J. P. Perdew, M. Ernzerhof, K. Burke, *J. Chem. Phys.* **1996**, *105*, 9982.
[53] P. Pollak, F. Weigend, *J. Chem. Theory Comput.* **2017**, *13*, 3696.
[54] D. Rappoport, F. Furche, *J. Chem. Phys.* **2010**, *133*, 134105.
[55] a) *TURBOMOLE V7.4.1 2019. a development of University of Karlsruhe and Forschungszentrum Karlsruhe GmbH, 1989–2007, TURBOMOLE GmbH, since 2007. Available from: http://www.turbomole.com.*; b) S. G. Balasubramani, G. P. Chen, S. Coriani, M. Diedenhofen, M. S. Frank, Y. J. Franzke, F. Furche, R. Grotjahn, M. E. Harding, C. Hättig, A. Hellweg, B. Helmich-Paris, C. Holzer, U. Huniar, M. Kaupp, A. Marefat Khah, S. Karbalaei Khani, T. Müller, F. Mack, B. D. Nguyen, S. M. Parker, E. Perlt, D. Rappoport, K. Reiter, S. Roy, M. Rückert, G. Schmitz, M. Sierka, E. Tapavicza, D. P. Tew, C. van Wüllen, V. K. Voora, F. Weigend, A. Wodyński, J. M. Yu, *J. Phys. Chem.* **2020**, *152*, 184107.
[56] S. Grimme, J. Antony, S. Ehrlich, H. Krieg, *J. Chem. Phys.* **2010**, *132*, 154104.
[57] S. Grimme, S. Ehrlich, L. Goerigk, *J. Comput. Chem.* **2011**, *32*, 1456.
[58] Y. J. Franzke, N. Middendorf, F. Weigend, *J. Chem. Phys.* **2018**, *148*, 104110.
[59] J. C. Boettger, *Phy. Rev. B* **2000**, *62*, 7809.
[60] L. Visscher, K. G. Dyall, *At. Data Nucl. Data Tables* **1997**, *67*, 207.
[61] a) H.-J. Werner, P. J. Knowles, F. R. Manby, J. A. Black, K. Doll, A. Heßelmann, D. Kats, A. Köhn, T. Korona, D. A. Kreplin, Q. Ma, T. F. Miller III, A. Mitrushchenkov, K. A. Peterson, I. Polyak, G. Rauhut, M. Sibaev, *J. Chem. Phys.* **2020**, *152*, 144107; b) H.-J. Werner, P. J. Knowles, G. Knizia, F. R. Manby, M. Schütz, P. Celani, W. Györffy, D. Kats, T. Korona, R. Lindh, A. Mitrushenkov, G. Rauhut, K. R. Shamasundar, T. B. Adler, R. D. Amos, S. J. Bennie, A. Bernhardsson, A. Berning, D. L. Cooper, M. J. O. Deegan, A. J. Dobbyn, F. Eckert, E. Goll, C. Hampel, A. Hesselmann, G. Hetzer, T. Hrenar, G. Jansen, C. Köppl, S. J. R. Lee, Y. Liu, A. W. Lloyd, Q. Ma, R. A. Mata, A. J. May, S. J. McNicholas, W. Meyer, T. F. Miller III, M. E. Mura, A. Nicklass, D. P. O'Neill, P. Palmieri, D. Peng, T. Petrenko, K. Pflüger, R. Pitzer, M. Reiher, T. Shiozaki, H. Stoll, A. J. Stone, R. Tarroni, T. Thorsteinsson, M. Wang, and M. Welborn, *Molpro, version 2022.2. a package of ab initio programs, http://www.molpro.net*.
[62] a) B. O. Roos, R. Lindh, P.-A. Malmqvist, V. Veryazov, P.-O. Widmark, *J. Phys. Chem. A* **2005**, *109*, 6575; b) B. O. Roos, R. Lindh, P.-Å. Malmqvist, V. Veryazov, P.-O. Widmark, *J. Phys. Chem. A* **2004**, *108*, 2851.
[63] S. R. Langhoff, E. R. Davidson, *Int J Quantum Chem.* **1974**, *8*, 61.
[64] L. Bennett, B. Melchers, B. Proppe, *Curta: A General-purpose High-Performance Computer at ZEDAT, Freie Universität Berlin*, Freie Universität Berlin, **2020**.

10.1002/chem.202401015

WILEY VCH

RESEARCH ARTICLE

Entry for the Table of Contents

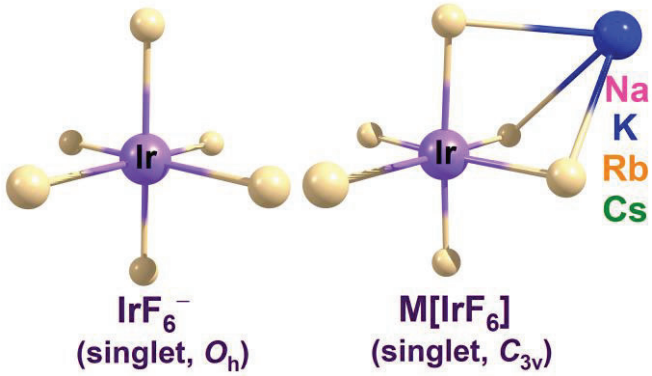

The IR spectra of molecular IrF_5^-, IrF_6^- anions and $M[IrF_6]$ (M = Na, K, Rb, Cs) ion pairs isolated in rare-gas matrices are presented. The closed-shell IrF_6^- anion with O_h symmetry stabilized by SOC effects has been verified spectroscopically in the low-temperature matrices. The $M[IrF_6]$ ion pairs with C_{3v} symmetry feature coordination of an alkali metal ion to three F atoms.

Institute and/or researcher Twitter usernames: @RiedelLab

6. Conclusion and Outlook

6.1 Conclusion

One goal of this thesis was to synthesize compounds with iridium in high oxidation states, including the unobserved +VII, by three avenues: oxyfluorides, fluorides, and fluoride anions. These products trapped in solid neon or argon matrices were characterized by matrix isolation IR spectroscopy and quantum-chemical calculations which provided a detailed insight into their molecular structures.

In the first part of this work, the iridium oxyfluorides (OIrF, $OIrF_2$, and FOIrF) were prepared for the first time by the reaction of laser-ablated iridium atoms with OF_2, while the previously predicted $OIrF_5$ was not detected.[37] The linear OIrF molecule in the closed-shell singlet ground state exhibits triple Ir–O bond character consisting of a σ bond, a π bond and a dative bond where the oxygen 2p lone pair donates electrons into an empty Ir 5d orbital. This triple Ir–O bond character for OIrF is in contrast to the terminal oxyl radical character for OPtF,[108] and biradical character for OAuF.[131] The molecule $OIrF_2$ possesses a planar structure with C_{2v} symmetry in the $^2B_1$ ground state, and the unpaired electron is found to reside in the Ir–O π^*-antibonding molecular orbital. A much lower spin-density contribution at the oxygen atom was found in $OIrF_2$ compared to the terminal oxyl radical species $OPtF_2$ and $OAuF_2$ with high spin densities at the oxygen atom.[108,131] FIrOF was found to be a planar structure in which the FO and IrF moieties adopt a *trans* conformation with respect to the O–Ir bond.

In the second part of this work, the molecular iridium fluorides IrF_n ($n = 1–6$) were obtained by the reaction of laser-ablated iridium atoms with F_2. Alternatively, the low-valent iridium fluorides can be obtained by the photo-initiated defluorination of IrF_6. It was found that the formation of IrF_4 by UV light ($\lambda = 278$ nm) irradiation of IrF_6 is almost quantitative in both solid neon or argon matrices. IR spectra of the reaction products isolated in rare-gas matrices under cryogenic conditions provide, for the first time, experimental vibrational frequencies of molecular IrF_5, IrF_4, IrF_3, and IrF_2. Among the iridium fluorides IrF_n ($n = 1–7$), the influence of the SOC effect was found to be significant for IrF_5, where a high-symmetry (C_{4v}) triplet structure is favored energetically in two-component calculations with SOC contribution and was confirmed experimentally, compared to the Jahn-Teller distorted $^3B_1/C_{2v}$ structure obtained at scalar relativistic levels. Although further calculations predict structures and IR spectra of higher iridium fluoride IrF_7 and difluorine complexes $IrF_4 \cdot F_2$ and $IrF_5 \cdot F_2$, such compounds could not be assigned in the experimental spectra.

In the third part of this work, by reacting IrF_6 with laser-ablated alkali metal fluorides MF (M = Na, K, Rb, Cs), the molecular IrF_5^-, IrF_6^- anions, and $M[IrF_6]$ (M = Na, K, Rb, Cs) ion pairs were obtained, while IrF_7^- and the corresponding $M[IrF_7]$ ion pairs were not observed. The free anions were also obtained by co-deposition of IrF_6 with laser-ablated metals (Ir or Pt) as electron sources. The IrF_5^- anion in the $^2B_1$ ground state shows a square-pyramidal structure with C_{4v} symmetry. A distorted D_{4h} structure in a triplet ground state for IrF_6^- was predicted by scalar-relativistic computations, but the calculated frequencies do not match the observed absorptions. IR spectroscopic evidence and relativistic computations including SOC favor a diamagnetic octahedral molecule with a closed-shell ground state for IrF_6^-. The $M[IrF_6]$ ion pairs in closed-shell ground state were found to be stabilized by alkali metal coordination to three F atoms in C_{3v} symmetry. The structural change of these ion pairs from alkali-metal atom Na to Cs coordination was proven spectroscopically and is in consistent with the theoretical predictions.

Overall, by comparing the M–O bonding characteristics in OMF and OMF_2 (M = Ir, Pt, and Au), some trends in the bonding of the oxo ligand were investigated. In group 9 iridium oxyfluorides closed-shell oxido ligand (O^{2-}) are preferentially formed instead of open-shell oxyl radical ligands ($O^{\bullet-}$), compared to the groups 10 and 11 terminal oxyl radical species,[108,131] which is in line with the trend of gradual increase of degree of oxyl radical character from left to right in the d block series. As the d electron count increases stepwise from Ir to Au in OMF and OMF_2 molecules, the occupation of anti-bonding π* and even further σ* orbitals weaken the M−O bond. As expected, reducing the number of ancillary ligands frees up orbitals for molecular orbital multiple bonding, which means that crossing the “oxo wall” is allowed.[135] Only three terminal iridium oxo complexes, closed-shell $[Ir^{V}O(Mes)_3]$,[136] triplet $[Ir^{III}(O)(PNP)]$,[137] and doublet $[Ir^{IV}(O)(PNP)]^+$ (PNP = $N(CHCHP\textit{t}Bu)_2$)[138] are the well-defined examples. Closed-shell OIrF is an intriguing molecule with a triple Ir–O bond character, while the well-known closed-shell $[Ir^{V}O(mesityl)_3]$ is often cited as an “oxo-wall” violation.[135] Despite the absence of observation of Ir–O stretching frequency of OIrF, CCSD(T) calculations suggest a shorter Ir–O distance (165.4 pm) than in $OIrF_2$ (166.7 pm), indicating a stronger Ir–O bond for OIrF. The observed O–Ir stretching frequency of $OIrF_2$ (ν = 984.1 cm^{-1}), considerably higher than that of reported closed-shell $[Ir^{V}O(mesityl)_3]$ (ν = 802 cm^{-1})[136] and triplet $[Ir^{III}(O)(PNP)]$ (PNP = $N(CHCHP\textit{t}Bu)_2$) (ν = 743 cm^{-1})[137] oxo complexes, suggested that the O–Ir bond in OIrF would be the strongest in the known iridium oxo complexes.

On the other hand, the iridium fluorides IrF_n (n = 1–7), anionic monofluorides IrF_5^-, and IrF_6^- were calculated by one- and two-component calculations which accounts for scalar-relativistic and SOC effects, respectively. It was found that inclusion of SOC is crucial in the prediction of spectra and properties of IrF_5 and IrF_6^- similar to the known case of PtF_6.[9,82–84] The IrF_5, IrF_6^-,

and PtF_6 molecules all feature $5d^4$ electronic configuration. Hence, it is suggested that the SOC effect should be considered in the transition metal fluorides with an electronic configuration of $5d^4$, or possibly with that of $4d^4$ and $6d^4$. Moreover, both electron affinities (EAs) and fluoride ion affinities (FIAs) of IrF_5 and IrF_6 were calculated. The EAs are direct measures for the oxidizer strengths, and FIAs provide an estimate of the Lewis acid strength. The oxidizing power increases from IrF_5 (5.81 eV) to IrF_6 (6.73 eV), and both molecules definitely fall in the category of “superhalogens”. Based on the high FIA value, IrF_5 can be proposed as a strong Lewis acid.

Some novel iridium compounds with interesting structures and properties were obtained successfully in this work, while there was no clear evidence of the formation of $OIrF_5$ and IrF_7 as Ir^{+VII} candidates.[37] The quest for Ir^{+VII} remains an open topic. It can be concluded that the experimental preparation of iridium oxyfluorides and fluorides in high oxidation states remains a challenging task.

6.2 Outlook

The IrF_7 might be obtained via the reaction of laser ablation of iridium with IrF_6 in the presence of F_2, and isolated in the solid neon or argon matrices under cryogenic conditions.

For the lighter elements cobalt and rhodium in group 9, cobalt oxyfluorides OCoF ($C_{\infty v}$, $^5\Sigma$) and $OCoF_2$ ($^4A_1$) were obtained by the reaction of laser-ablated cobalt atoms with OF_2 and isolated in argon matrices.[139] Additionally, the hypofluorite product FOCoF might be stable in neon matrices, as found here for FOIrF.

There are no experimental and computational data for rhodium oxyfluorides. The reaction of rhodium with OF_2 may lead to ORhF, $ORhF_2$ and FORhF.

Analogous to iridium fluorides, experimental spectroscopic investigations on the molecular rhodium fluorides RhF_n ($n = 2–5$) are not yet available.

Based on the interesting results for molecular IrF_6^- with $5d^4$ electronic configuration, it is interesting to investigate the $4d^4$ anion RhF_6^-.

7. References

[1] a) C. K. Jørgensen, *Oxidation numbers and Oxidation States*, Springer, Berlin, **1969**; b) S. X. Hu, W. L. Li, J. B. Lu, J. L. Bao, H. S. Yu, D. G. Truhlar, J. K. Gibson, J. Marçalo, M. Zhou, S. Riedel et al., *Angew. Chem. Int. Ed.* **2018**, *57*, 3242.

[2] S. Riedel, M. Kaupp, *Coord. Chem. Rev.* **2009**, *253*, 606.

[3] a) J. H. Holloway, E. G. Hope, P. J. Townson, R. L. Powell, *J. Fluorine Chem.* **1996**, *76*, 105; b) W. W. Dukat, J. H. Holloway, E. G. Hope, M. R. Rieland, P. J. Townson, R. L. Powell, *J. Chem. Soc., Chem. Commun.* **1993**, 1429.

[4] J. Lin, S. Zhang, W. Guan, G. Yang, Y. Ma, *J. Am. Chem. Soc.* **2018**, *140*, 9545.

[5] a) W. Levason, F. M. Monzittu, G. Reid, W. Zhang, E. G. Hope, *J. Fluorine Chem.* **2017**, *200*, 190; b) B. C. Bales, P. Brown, A. Dehestani, J. M. Mayer, *J. Am. Chem. Soc.* **2005**, *127*, 2832; c) G. Green, W. P. Griffith, D. M. Hollinshead, S. V. Ley, M. Schröder, *J. Chem. Soc., Perkin Trans. 1* **1984**, 681.

[6] N. Bartlett, S. P. Beaton, N. K. Jha, *Chem. Commun.* **1966**, 168.

[7] N. Bartlett, *Angew. Chem. Int. Ed.* **1968**, *7*, 433.

[8] a) W. Levason, F. M. Monzittu, G. Reid, *Coord. Chem. Rev.* **2019**, *391*, 90; b) W. Levason, F. M. Monzittu, G. Reid, W. Zhang, *Chem. Commun.* **2018**, *54*, 11681.

[9] K. Seppelt, *Chem. Rev.* **2015**, *115*, 1296.

[10] a) L. Graham, O. Graudejus, N. K. Jha, N. Bartlett, *Coord. Chem. Rev.* **2000**, *197*, 321; b) N. Bartlett, *Proc. Chem. Soc.* **1962**, 218; c) N. Bartlett, D. H. Lohmann, *Proc. Chem. Soc.* **1962**, 115.

[11] a) L. E. Forslund, N. Kaltsoyannis, *New J. Chem.* **2003**, *27*, 1108; b) C. Esterhuysen, G. Frenking, *Theor. Chem. Acc.* **2004**, *111*, 381.

[12] T. Vogt, A. N. Fitch, J. K. Cockcroft, *Science* **1994**, *263*, 1265.

[13] L. Li, A. K. Sakr, T. Schlöder, S. Klein, H. Beckers, M.-P. Kitsaras, H. V. Snelling, N. A. Young, D. Andrae, S. Riedel, *Angew. Chem. Int. Ed.* **2021**, *60*, 6391.

[14] X. Wang, L. Andrews, S. Riedel, M. Kaupp, *Angew. Chem. Int. Ed.* **2007**, *46*, 8371.

[15] a) B. Krebs, K. D. Hasse, *Acta Cryst. B* **1976**, *B32*, 1334; b) A. Zalkin, D. H. Templeton, *Acta Cryst.* **1953**, *6*, 106.

[16] M. Da Silva Santos, T. Stüker, M. Flach, O. S. Ablyasova, M. Timm, B. von Issendorff, K. Hirsch, V. Zamudio-Bayer, S. Riedel, J. T. Lau, *Angew. Chem. Int. Ed.* **2022**, *61*, e202207688.

[17] I.-C. Hwang, K. Seppelt, *Angew. Chem. Int. Ed.* **2001**, *40*, 3690.

[18] J. Lin, X. Du, M. Rahm, H. Yu, H. Xu, G. Yang, *Angew. Chem. Int. Ed.* **2020**, *59*, 9155.

[19] J. Lin, Z. Zhao, C. Liu, J. Zhang, X. Du, G. Yang, Y. Ma, *J. Am. Chem. Soc.* **2019**, *141*, 5409.

[20] A. J. Edwards, W. E. Falconer, J. E. Griffiths, W. A. Sunder, M. J. Vasile, *J. Chem. Soc., Dalton Trans.* **1974**, 1129.

[21] P. Pyykkö, W.-H. Xu, *Angew. Chem. Int. Ed.* **2015**, *54*, 1080.

[22] G. Wang, M. Zhou, J. T. Goettel, G. J. Schrobilgen, J. Su, J. Li, T. Schlöder, S. Riedel, *Nature* **2014**, *514*, 475.

[23] a) S. W. Sheehan, J. M. Thomsen, U. Hintermair, R. H. Crabtree, G. W. Brudvig, C. A. Schmuttenmaer, *Nat. Commun.* **2015**, *6*, 294; b) J. M. Thomsen, S. W. Sheehan, S. M. Hashmi, J. Campos, U. Hintermair, R. H. Crabtree, G. W. Brudvig, *J. Am. Chem. Soc.* **2014**, *136*, 13826; c) D. G. H. Hetterscheid, J. N. H. Reek, *Chem. Commun.* **2011**, *47*, 2712; d) R. Lalrempuia, N. D. McDaniel, H. Müller-Bunz, S. Bernhard, M. Albrecht, *Angew. Chem. Int. Ed.* **2010**, *49*, 9765; e) N. D. McDaniel, F. J. Coughlin, L. L. Tinker, S. Bernhard, *J. Am. Chem. Soc.* **2008**, *130*, 210.

[24] a) D. L. Huang, D. J. Vinyard, J. D. Blakemore, S. M. Hashmi, R. H. Crabtree, *Organometallics* **2017**, *36*, 199; b) M. Zhou, N. D. Schley, R. H. Crabtree, *J. Am. Chem. Soc.* **2010**, *132*, 12550.

[25] a) K. K.-W. Lo, *Acc. Chem. Res.* **2015**, *48*, 2985; b) K. K.-W. Lo, S. P.-Y. Li, K. Y. Zhang, *New J. Chem.* **2011**, *35*, 265; c) K. K.-W. Lo, K. Y. Zhang, S.-K. Leung, M.-C. Tang, *Angew. Chem. Int. Ed.* **2008**, *47*, 2213.

[26] a) C. Shi, H. Huang, Q. Li, J. Yao, C. Wu, Y. Cao, F. Sun, D. Ma, H. Yan, C. Yang et al., *Adv. Optical Mater.* **2021**, *9*, 2002060; b) Q. Li, C. Shi, M. Huang, X. Wei, H. Yan, C. Yang, A. Yuan, *Chem. Sci.* **2019**, *10*, 3257; c) P.-N. Lai, C. H. Brysacz, M. K. Alam, N. A. Ayoub, T. G. Gray, J. Bao, T. S. Teets, *J. Am. Chem. Soc.* **2018**, *140*, 10198; d) M. A. Baldo, M. E. Thompson, S. R. Forrest, *Nature* **2000**, *403*, 750.

[27] O. Ruff, J. Fischer, *Z. Anorg. Allgem. Chem.* **1929**, *179*, 161.

[28] A. D. Richardson, K. Hedberg, G. M. Lucier, *Inorg. Chem.* **2000**, *39*, 2787.

[29] J.-H. Choy, D.-K. Kim, G. Demazeau, D.-Y. Jung, *J. Phys. Chem.* **1994**, *98*, 6258.

[30] T. Stüker, T. Hohmann, H. Beckers, S. Riedel, *Angew. Chem. Int. Ed.* **2020**, *59*, 23174.

[31] A. Citra, L. Andrews, *J. Phys. Chem. A* **1999**, *103*, 4182.

[32] Y. Gong, M. Zhou, M. Kaupp, S. Riedel, *Angew. Chem. Int. Ed.* **2009**, *48*, 7879.

[33] P. Rother, F. Wagner, U. Zahn, *Radiochim. Acta* **1969**, *11*, 203.

[34] D. Himmel, C. Knapp, M. Patzschke, S. Riedel, *Chem. Phys. Chem.* **2010**, *11*, 865.

[35] Ł. Wolański, M. Domański, W. Grochala, P. Szarek, *Chem. Eur. J.* **2019**, *25*, 10290.

[36] T. Stüker, H. Beckers, S. Riedel, *Chem. Eur. J.* **2020**, *26*, 7384.

[37] S. Riedel, M. Kaupp, *Angew. Chem. Int. Ed.* **2006**, *45*, 3708.

[38] P. L. Robinson, G. J. Westland, *J. Chem. Soc.* **1956**, 4481.

[39] M. A. Hepworth, P. L. Robinson, *J. Inorg. Nucl. Chem.* **1957**, *4*, 24.

[40] R. C. Burns, T. A. O'Donnell, A. B. Waugh, *J. Fluorine Chem.* **1978**, *12*, 505.

[41] H. Selig, W. A. Sunder, F. A. Disalvo, W. E. Falconer, *J. Fluorine Chem.* **1978**, *11*, 39.

[42] Y. Lu, R. Medel, G. Deng, S. Riedel, *Chem. Commun.* **2023**, *59*, 8532.

[43] V. Boudon, M. Rotger, D. Avignant, *Spectrochim. Acta Part A* **1996**, *52*, 1175.

[44] H. H. Claassen, H. Selig, *Isr. J. Chem.* **1969**, *7*, 499.

[45] M. Kimura, V. Schomaker, D. W. Smith, *J. Chem. Phys.* **1968**, *48*, 4001.

[46] H. C. Mattraw, N. J. Hawkins, D. R. Carpenter, W. W. Sabol, *J. Chem. Phys.* **1955**, *23*, 985.

[47] J. H. Holloway, G. Stanger, E. G. Hope, W. Levason, J. S. Ogden, *J. Chem. Soc., Dalton Trans.* **1988**, 1341.

[48] A. K. Brisdon, J. H. Holloway, E. G. Hope, W. Levason, J. S. Ogden, A. K. Saad, *J. Chem. Soc., Dalton Trans.* **1992**, 139.

[49] T. Drews, J. Supel, A. Hagenbach, K. Seppelt, *Inorg. Chem.* **2006**, *45*, 3782.

[50] V. Boudon, M. Rotger, D. Avignant, *J. Mol. Spectrosc.* **1996**, *175*, 327.

[51] N. Bartlett, P. R. Rao, *Chem. Commun.* **1965**, 252.

[52] R. T. Paine, L. B. Asprey, *Inorg. Chem.* **1975**, *14*, 1111.

[53] E. G. Hope, *Polyhedron* **1993**, *12*, 2977.

[54] R. Craciun, D. Picone, R. T. Long, S. Li, D. A. Dixon, K. A. Peterson, K. O. Christe, *Inorg. Chem.* **2010**, *49*, 1056.

[55] P. R. Rao, A. Tressaud, N. Bartlett, *J. Inorg. Nucl. Chem.* **1976**, *28*, 23.

[56] W. A. Sunder, W. E. Falconer, *Inorg. Nucl. Chem. Lett.* **1972**, *8*, 537.

[57] R. C. Burns, T. A. O'Donnell, *J. Inorg. Nucl. Chem.* **1980**, *42*, 1285.

[58] M. A. Hepworth, K. H. Jack, R. D. Peacock, G. J. Westland, *Acta Cryst. A* **1957**, *10*, 63.

[59] A. L. Hector, W. Levason, M. T. Weller, E. G. Hope, *J. Fluorine Chem.* **1997**, *84*, 161.

[60] A. G. Adam, A. D. Granger, L. E. Downie, D. W. Tokaryk, C. Linton, *Can. J. Phys.* **2009**, *87*, 557.

[61] X. Zhuang, T. C. Steimle, C. Linton, *J. Chem. Phys.* **2010**, *133*, 164310.

[62] V. Kalamse, N. Wadnerkar, A. Chaudhari, *Int. J. Quantum Chem.* **2011**, *111*, 2014.

[63] S. A. Siddiqui, T. Rasheed, *Int. J. Quantum Chem.* **2013**, *113*, 959.

[64] Y. Lu, Y. A. Tsegaw, A. Wodyński, L. Li, H. Beckers, M. Kaupp, S. Riedel, *Chem. Eur. J.* **2022**, *28*, e202104005.

[65] Gutsev, G. L., Boldyrev, A. I., *Chem. Phys. Lett.* **1983**, *101*, 441.

[66] M. A. Hepworth, P. L. Robinson, G. J. Westland, *J. Chem. Soc.* **1954**, 4269.

[67] H. Fitz, B. G. Muller, O. Graudejus, N. Bartlett, *Z. Anorg. Allg. Chem.* **2002**, *628*, 133.

[68] Z. Mazej, E. Goreshnik, K. O. Christe, *J. Fluorine Chem.* **2023**, *268*, 110128.

[69] Z. Mazej, R. Hagiwara, *J. Fluorine Chem.* **2007**, *128*, 423.

[70] M. A. Hepworth, K. H. Jack, G. J. Westland, *J. Inorg. Nucl. Chem.* **1956**, *2*, 79.

[71] O. Graudejus, A. P. Wilkinson, L. C. Chacon, N. Bartlett, *Inorg. Chem.* **2000**, *39*, 2794.

[72] G. C. Allen, G. A. M. El-Sharkawy, K. D. Warren, *Inorg. Chem.* **1972**, *11*, 51.

[73] S. P. Gabuda, V. N. Ikorskii, S. G. Kozlova, P. S. Nikitin, *JETP Letters* **2001**, *73*, 35.

[74] G. Tavčar, B. Žemva, *Inorg. Chem.* **2013**, *52*, 4319.

[75] A. Earnshaw, B. N. FIGGIS, J. Lewis, R. D. Peacock, *J. Chem. Soc.* **1961**, 3132.

[76] S. Seidel, K. Seppelt, *Angew. Chem. Int. Ed.* **2000**, *39*, 3923.

[77] Z. Mazej, E. Goreshnik, *Molecules* **2023**, *28*.

[78] S. I. Ivlev, K. Gaul, M. Chen, A. J. Karttunen, R. Berger, F. Kraus, *Chem. Eur. J.* **2019**, *25*, 5793.

[79] B. Scheibe, R. Haiges, S. I. Ivlev, A. J. Karttunen, U. Müller, K. O. Christe, F. Kraus, *Eur. J. Inorg. Chem.* **2020**, *2020*, 4483.

[80] B. Scheibe, A. J. Karttunen, F. Kraus, *Eur. J. Inorg. Chem.* **2021**, *2021*, 405.

[81] F. O. Sladky, P. A. Bulliner, N. Bartlett, *J. Chem. Soc. A* **1969**, *14*, 2179.

[82] L. Alvarez-Thon, J. David, R. Arratia-Pérez, K. Seppelt, *Phys. Rev. A* **2008**, *77*, 34502.

[83] J. David, P. Fuentealba, A. Restrepo, *Chem. Phys. Lett.* **2008**, *457*, 42.

[84] G. Senges, L. Li, A. Wodyński, H. Beckers, R. Müller, M. Kaupp, S. Riedel, *Chem. Eur. J.* **2021**, *27*, 13642.

[85] J. David, D. Guerra, A. Restrepo, *Inorg. Chem.* **2011**, *50*, 1480.

[86] K. O. Christe, *Chem. Commun.* **2013**, *49*, 4588.

[87] a) E. Whittle, D. A. Dows, G. C. Pimentel, *J. Chem. Phys.* **1954**, *22*, 1943; b) I. Norman, G. Porter, *Nature* **1954**, *174*, 508.

[88] V. E. Bondybey, A. M. Smith, J. Agreiter, *Chem. Rev.* **1996**, *96*, 2113.

[89] a) C. L. Chernick, H. H. Claassen, P. R. Fields, H. H. Hyman, J. G. Malm, W. M. Manning, M. S. Matheson, L. A. Quarterman, F. Schreiner, H. H. Selig et al., *Science* **1962**, *138*, 136; b) M. Tramšek, B. Žemva, *Acta Chim. Slov.* **2006**, *53*, 105.

[90] a) S. P. Church, M. Poliakoff, J. A. Timney, J. J. Turner, *Inorg. Chem.* **1983**, *22*, 3259; b) A. J. Tursi, E. R. Nixon, *J. Chem. Phys.* **1970**, *52*, 1521; c) L. Brewer, B. King, *J. Chem. Phys.* **1970**, *53*, 3981.

[91] T. Schlöder, T. Vent-Schmidt, S. Riedel, *Angew. Chem. Int. Ed.* **2012**, *51*, 12063.

[92] F. Brosi, T. Vent-Schmidt, S. Kieninger, T. Schlöder, H. Beckers, S. Riedel, *Chem. Eur. J.* **2015**, *21*, 16455.

[93] a) I. R. Dunkin, P. C. P. Thomson, *J. Chem. Soc., Chem. Commun.* **1982**, 1192; b) J. Mieres-Pérez, E. Mendez-Vega, K. Velappan, W. Sander, *J. Org. Chem.* **2015**, *80*, 11926.

[94] M. Zhou, L. Andrews, *J. Chem. Phys.* **2000**, *112*, 6576.

[95] L. Andrews, M. Zhou, *J. Chem. Phys.* **1999**, *111*, 6036.

[96] a) W. F. Howard, L. Andrews, *J. Am. Chem. Soc.* **1973**, *95*, 3045; b) J. W. Nibler, *J. Chem. Phys.* **1971**, *55*, 5133.

[97] E. S. Prochaska, B. S. Ault, L. Andrews, *Inorg. Chem.* **1977**, *16*, 2021.

[98] M. von Hobe, F. Stroh, H. Beckers, T. Benter, H. Willner, *Phys. Chem. Chem. Phys.* **2009**, *11*, 1571.

[99] a) H. A. Joly, J. A. Howard, *J. Phys. Chem. A* **1997**, *101*, 2817; b) S. V. Chapyshev, D. Grote, C. Finke, W. Sander, *J. Org. Chem.* **2008**, *73*, 7045.

[100] I. Infante, L. Andrews, X. Wang, L. Gagliardi, *Chem. Eur. J.* **2010**, *16*, 12804.

[101] M. E. Jacox, *J. Mol. Spectrosc.* **1985**, *113*, 286.

[102] a) O. M. Wilkin, N. Harris, J. F. Rooms, E. L. Dixon, A. J. Bridgeman, N. A. Young, *J. Phys. Chem. A* **2018**, *122*, 1994; b) Y. Zhao, M. Zhou, *Sci. China Chem.* **2010**, *53*, 327.

[103] X. Wang, L. Andrews, F. Brosi, S. Riedel, *Chem. Eur. J.* **2013**, *19*, 1397.

[104] A. J. Barnes, *J. Mol. Struct.* **1984**, *113*, 161.

[105] E. A. Pritchina, N. P. Gritsan, A. Maltsev, T. Bally, T. Autrey, Y. Liu, Y. Wang, J. P. Toscano, *Phys. Chem. Chem. Phys.* **2003**, *5*, 1010.

[106] M. J. Linevsky, *J. Chem. Phys.* **1961**, *34*, 587.

[107] a) C. Wentrup, *Angew. Chem. Int. Ed.* **2017**, *56*, 14808; b) B. Nelander, A. Engdahl, T. Svensson, *Chem. Phys. Lett.* **2000**, *332*, 403.

[108] L. Li, H. Beckers, T. Stüker, T. Lindič, T. Schlöder, D. Andrae, S. Riedel, *Inorg. Chem. Front.* **2021**, *8*, 1215.

[109] G. D. Purvis, R. J. Bartlett, *J. Chem. Phys.* **1982**, *76*, 1910.

[110] S. H. Vosko, L. Wilk, M. Nusair, *Can. J. Phys.* **1980**, *58*, 1200.

[111] B. O. Roos, P. R. Taylor, P. E. Sigbahn, *Chem. Phys.* **1980**, *48*, 157.

[112] A. Wolf, M. Reiher, B. A. Hess, *J. Chem. Phys.* **2002**, *117*, 9215.

[113] F. Neese, *Coord. Chem. Rev.* **2009**, *253*, 526.

[114] C. J. Cramer, D. G. Truhlar, *Phys. Chem. Chem. Phys.* **2009**, *11*, 10757.

[115] M. J. Frisch, G. W. Trucks, H. B. Schlegel, G. E. Scuseria, M. A. Robb, J. R. Cheeseman, G. Scalmani, V. Barone, G. A. Petersson, H. Nakatsuji, X. Li, M. Caricato, A. V. Marenich, J. Bloino, B. G. Janesko, R. Gomperts, B. Mennucci, H. P. Hratchian, J. V. Ortiz, A. F. Izmaylov, J. L. Sonnenberg, D. Williams-Young, F. Ding, F. Lipparini, F. Egidi, J. Goings, B. Peng, A. Petrone, T. Henderson, D. Ranasinghe, V. G. Zakrzewski, J. Gao, N. Rega, G. Zheng, W. Liang, M. Hada, M. Ehara, K. Toyota, R. Fukuda, J. Hasegawa, M. Ishida, T. Nakajima, Y. Honda, O. Kitao, H. Nakai, T. Vreven, K. Throssell, J. A. Montgomery, Jr., J. E. Peralta, F. Ogliaro, M. J. Bearpark, J. J. Heyd, E. N. Brothers, K. N. Kudin, V. N. Staroverov, T. A. Keith, R. Kobayashi, J. Normand, K. Raghavachari, A. P. Rendell, J. C. Burant, S. S. Iyengar, J. Tomasi, M. Cossi, J. M. Millam, M. Klene, C. Adamo, R. Cammi, J. W. Ochterski, R. L. Martin, K. Morokuma, O. Farkas, J. B. Foresman, and D. J. Fox, *Gaussian 16*, Gaussian, Inc., Wallingford CT, **2016**.

[116] a) S. G. Balasubramani, G. P. Chen, S. Coriani, M. Diedenhofen, M. S. Frank, Y. J. Franzke, F. Furche, R. Grotjahn, M. E. Harding, C. Hättig et al., *J. Phys. Chem.* **2020**, *152*, 184107; b) *TURBOMOLE V7.4.1 2019*. *a development of University of Karlsruhe and Forschungszentrum Karlsruhe GmbH, 1989–2007, TURBOMOLE GmbH, since 2007. Available from: http://www.turbomole.com.*

[117] a) C. Lee, W. Yang, R. G. Parr, *Phys. Rev. B* **1988**, *37*, 785; b) A. D. Becke, *J. Chem. Phys.* **1993**, *98*, 5648; c) P. J. Stephens, F. J. Devlin, C. F. Chabalowski, M. J. Frisch, *J. Phys. Chem.* **1994**, *98*, 11623.

[118] K. Raghavachari, G. W. Trucks, J. A. Pople, M. Head-Gordon, *Chem. Phys. Lett.* **1989**, *157*, 479.

[119] H.-J. Werner, P. J. Knowles, G. Knizia, F. R. Manby, M. Schütz, P. Celani, W. Györffy, D. Kats, T. Korona, R. Lindh, A. Mitrushenkov, G. Rauhut, K. R. Shamasundar, T. B. Adler, R. D. Amos, S. J. Bennie, A. Bernhardsson, A. Berning, D. L. Cooper, M. J. O. Deegan, A. J. Dobbyn, F. Eckert, E. Goll, C. Hampel, A. Hesselmann, G. Hetzer, T. Hrenar, G. Jansen, C. Köppl, S.

J. R. Lee, Y. Liu, A. W. Lloyd, Q. Ma, R. A. Mata, A. J. May, S. J. McNicholas, W. Meyer, T. F. Miller III, M. E. Mura, A. Nicklass, D. P. O'Neill, P. Palmieri, D. Peng, K. Pflüger, R. Pitzer, M. Reiher, T. Shiozaki, H. Stoll, A. J. Stone, R. Tarroni, T. Thorsteinsson, M. Wang, M. Welborn, *MOLPRO, version 2019.2, a package of ab initio programs*.

[120] J. Wang, S. Manivasagam, A. K. Wilson, *J. Chem. Theory Comput.* **2015**, *11*, 5865.

[121] W. Jiang, N. J. DeYonker, A. K. Wilson, *J. Chem. Theory Comput.* **2012**, *8*, 460.

[122] a) P. E. M. Siegbahn, J. Almlöf, A. Heiberg, B. O. Roos, *J. Chem. Phys.* **1981**, *74*, 2384; b) J. Olsen, *Int. J. Quantum Chem.* **2011**, *111*, 3267.

[123] a) K. Andersson, P.-A. Malmqvist, B. O. Roos, *J. Chem. Phys.* **1992**, *96*, 1218; b) K. Andersson, P.-A. Malmqvist, B. O. Roos, A. J. Sadlej, K. Wolinski, *J. Phys. Chem.* **1990**, *14*, 5483.

[124] a) L. B. Harding, S. J. Klippenstein, A. W. Jasper, *Phys. Chem. Chem. Phys.* **2007**, *9*, 4055; b) P. G. Szalay, T. Müller, G. Gidofalvi, H. Lischka, R. Shepard, *Chem. Rev.* **2012**, *112*, 108.

[125] P. Pyykkö, *Ann. Rev. Phys. Chem.* **2012**, *63*, 45.

[126] M. Dolg, *Relativistic Electronic Structure Theory, Part 1: Fundamentals, Theoretical and Computational Chemistry,* edited by P. Schwerdtfeger*,* **2002**, *11*, 793.

[127] a) M. Reiher, *Chimia* **2009**, *63*, 140; b) M. Reiher, A. Wolf, *Relativistic Quantum Chemistry*: *The Fundamental Theory of Molecular Science*, 2nd ed., Weinheim, **2015**.

[128] a) A. Baldes, F. Weigend, *Mol. Phys.* **2013**, *111*, 2617; b) M. K. Armbruster, F. Weigend, C. van Wüllen, W. Klopper, *Phys. Chem. Chem. Phys.* **2008**, *10*, 1748.

[129] a) E. van Lenthe, E. J. Baerends, J. G. Snijders, *J. Chem. Phys.* **1993**, *99*, 4597; b) J. G. Snijders, A. J. Sadlej, *Chem. Phys. Lett.* **1996**, *252*, 51.

[130] P. Pyykkö, S. Riedel, M. Patzschke, *Chem. Eur. J.* **2005**, *11*, 3511.

[131] L. Li, T. Stüker, S. Kieninger, D. Andrae, T. Schlöder, Y. Gong, L. Andrews, H. Beckers, S. Riedel, *Nat. Commun.* **2018**, *9*, 1267.

[132] R. D. W. Kemmitt, D. R. Russell, D. W. A. Sharp, *J. Chem. Soc.* **1963**, 4408.

[133] G. L. Gutsev, A. I. Boldyrev, *Chem. Phys.* **1981**, *56*, 277.

[134] F. A. Redeker, M. A. Ellwanger, H. Beckers, S. Riedel, *Chem. Eur. J.* **2019**, *25*, 15059.

[135] J. R. Winkler, H. B. Gray in *Molecular Electronic Structures of Transition Metal Complexes I* (Eds.: D. M. P. Mingos, P. Day, J. P. Dahl), Springer, Berlin, Germany, **2012**, pp. 17.

[136] R. S. Hay-Motherwell, G. Wilkinson, B. Hussain-Bates, *Polyhedron* **1993**, *12*, 2009.

[137] D. Delony, M. Kinauer, M. Diefenbach, S. Demeshko, C. Würtele, M. C. Holthausen, S. Schneider, *Angew. Chem. Int. Ed.* **2019**, *58*, 10971.

[138] M. A. Tepaske, A. Fitterer, H. Verplancke, D. Delony, M. C. Neben, B. de Bruin, M. C. Holthausen, S. Schneider, *Angew. Chem. Int. Ed.* **2024***, 63,* e202316729.

[139] R. Wei, Z. T. Fang, M. Vasiliu, D. A. Dixon, L. Andrews, Y. Gong, *Inorg. Chem.* **2019**, *58*, 9796.

8. Publications and Conference Contributions

Publications

[1] **Yan Lu**, Yetsedaw A. Tsegaw, Artur Wodyński, Lin Li, Helmut Beckers, Martin Kaupp, and Sebastian Riedel, "Investigation of Molecular Iridium Fluorides IrF_n (n = 1–6): A Combined Matrix-Isolation and Quantum-Chemical Study", *Chem. Eur. J.*, **2022**, *28*, e202104005.
https://doi.org/10.1002/chem.202104005

[2] **Yan Lu**, Robert Medel, Guohai Deng, and Sebastian Riedel, "Infrared Spectroscopic and Theoretical Investigations of Novel Iridium Oxyfluorides", *Chem. Commun.*, **2023**, *59*, 8532–8535.
https://doi.org/10.1039/D3CC02216A

[3] **Yan Lu**, Artur Wodyński, Marc Reimann, Robert Medel, Martin Kaupp, and Sebastian Riedel, "Investigation of Isolated IrF_5^-, IrF_6^- Anions and $M[IrF_6]$ (M = Na, K, Rb, Cs) Ion Pairs by Matrix-Isolation Spectroscopy and Relativistic Quantum-Chemical Calculations", *Chem. Eur. J.*, **2024**, e202401015.
https://doi.org/10.1002/chem.202401015

[4] Guohai Deng, **Yan Lu**, Tony Stüker, and Sebastian Riedel, "Nitrogen Trifluoride Complexes of Group 10 Transition Metals $M(NF_3)$ (M = Pd, Pt)", *Chem. Sci.*, **2023**, *14*, 8592–8597.
https://doi.org/10.1039/d3sc02313c

[5] Guohai Deng, Robert Medel, **Yan Lu**, and Sebastian Riedel, "Photoinduced Dual C–F Bond Activation of Hexafluorobenzene Mediated by Boron Atom", *Chem. Eur. J.*, **2024**, e202303874.
https://doi.org/10.1002/chem.202303874

[6] Mei Wen, Robert Medel, Guohai Deng, Yetsedaw A. Tsegaw, **Yan Lu**, and Sebastian Riedel, "Infrared Spectroscopic and Theoretical Investigations of Group 13 Oxyfluorides OMF_2 and OMF (M = B, Al, Ga, In)", *Chem. Eur. J.*, **2023**, e202301676.
https://doi.org/10.1002/chem.202301676

Conference Contributions–Poster Presentations

[1] **Yan Lu**, Sebastian Riedel, “Iridium Oxyfluorides”, *Chemistry and Physics at Low Temperatures*, **2022**, Visegrád, Hungary.

[2] **Yan Lu**, Yetsedaw A. Tsegaw, Artur Wodyński, Sebastian Riedel, “Investigation of Molecular Transition Metal Fluorides: A Combined Matrix-Isolation and Quantum-Chemical Study”, *20th European Symposium on Fluorine Chemistry*, **2022**, Berlin, Germany.

9. Curriculum Vitae

The curriculum vitae is not included for reasons of data protection

10. Appendix

10.1 Infrared Spectroscopic and Theoretical Investigations of Novel Iridium Oxyfluorides

Electronic Supplementary Material (ESI) for ChemComm.

Supporting Information

Infrared Spectroscopic and Theoretical Investigations of the novel Iridium Oxyfluorides

Yan Lu,[a] Robert Medel,[a] Guohai Deng,[a] Sebastian Riedel*[a]

[a] Y. Lu, Dr. R. Medel, Dr. G. H. Deng, Prof. Dr. S. Riedel
Freie Universität Berlin
Institut für Chemie und Biochemie–Anorganische Chemie
Fabeckstrasse 34/36, 14195 Berlin (Germany)
E-mail: s.riedel@fu-berlin.de

Contents

Experimental and computational details

The technique of matrix-isolation infrared (IR) spectroscopy and laser-ablation apparatus have been described in previous studies.[1,2,3] Matrix samples were prepared by co-deposition of laser-ablated iridium atoms with 0.02 % and 0.5 % OF_2 diluted in neon (99.999 %, Air Liquide) and argon (99.999 %, Sauerstoffwerk Friedrichshafen), respectively. The OF_2 was premixed with neon or argon in a custom-made stainless-steel mixing chamber.

The mixing chamber was connected to a self-made matrix chamber by a stainless-steel capillary. The gas mixture was condensed with laser-ablated iridium atoms onto a gold-plated mirror cooled to 5 K for neon and 12 K for argon using a closed-cycle helium cryostat (Sumitomo Heavy Industries, RDK-205D) inside the matrix chamber. For the laser-ablation, the 1064 nm fundamental of a Nd:YAG laser (Continuum, Minilite II, 10 Hz repetition rate, 55–60 mJ $pulse^{-1}$) was focused onto a rotating iridium metal target (∅ 10 mm) using a plano-convex lens (∅ 25.4 mm, focal length of 125.0 mm) through a hole in the cold mirror.

Preparation of $^{16/18}OF_2$ followed procedures described in the literature.[4] $^{16/18}OF_2$ was synthesized by the reaction of elemental fluorine and $^{16/18}OH_2$ dispersed in solid NaF.[4] Infrared spectra of the reaction products were recorded on a Bruker Vertex 80v spectrometer with a resolution of 0.5 cm^{-1} in the region 4000–450 cm^{-1} using a liquid-nitrogen-cooled mercury cadmium telluride (MCT) detector. Matrix samples were annealed at different temperatures, and the samples were subjected to photolysis using a mercury arc streetlamp (Osram HQL 250) with the outer globe removed ($\lambda > 220$ nm).

Density functional theory (DFT) calculations were performed using the Gaussian16 program package[5] employing the hybrid functional B3LYP[6] with the augmented triple-ζ basis sets aug-cc-pVTZ[7] for fluorine and oxygen and the aug-cc-pVTZ-PP[8] valence basis and associated scalar-relativistic pseudopotential (PP) for iridium. Subsequent structure optimizations as well as harmonic vibrational frequency analyses at the CCSD(T)[9](coupled-cluster singles-doubles with perturbational triples) level with aug-cc-pVTZ-PP basis sets were carried out in the spin unrestricted ROHF-UCCSD(T) open-shell coupled cluster formalism using default frozen core settings as implemented in the Molpro 2019 software package.[10]

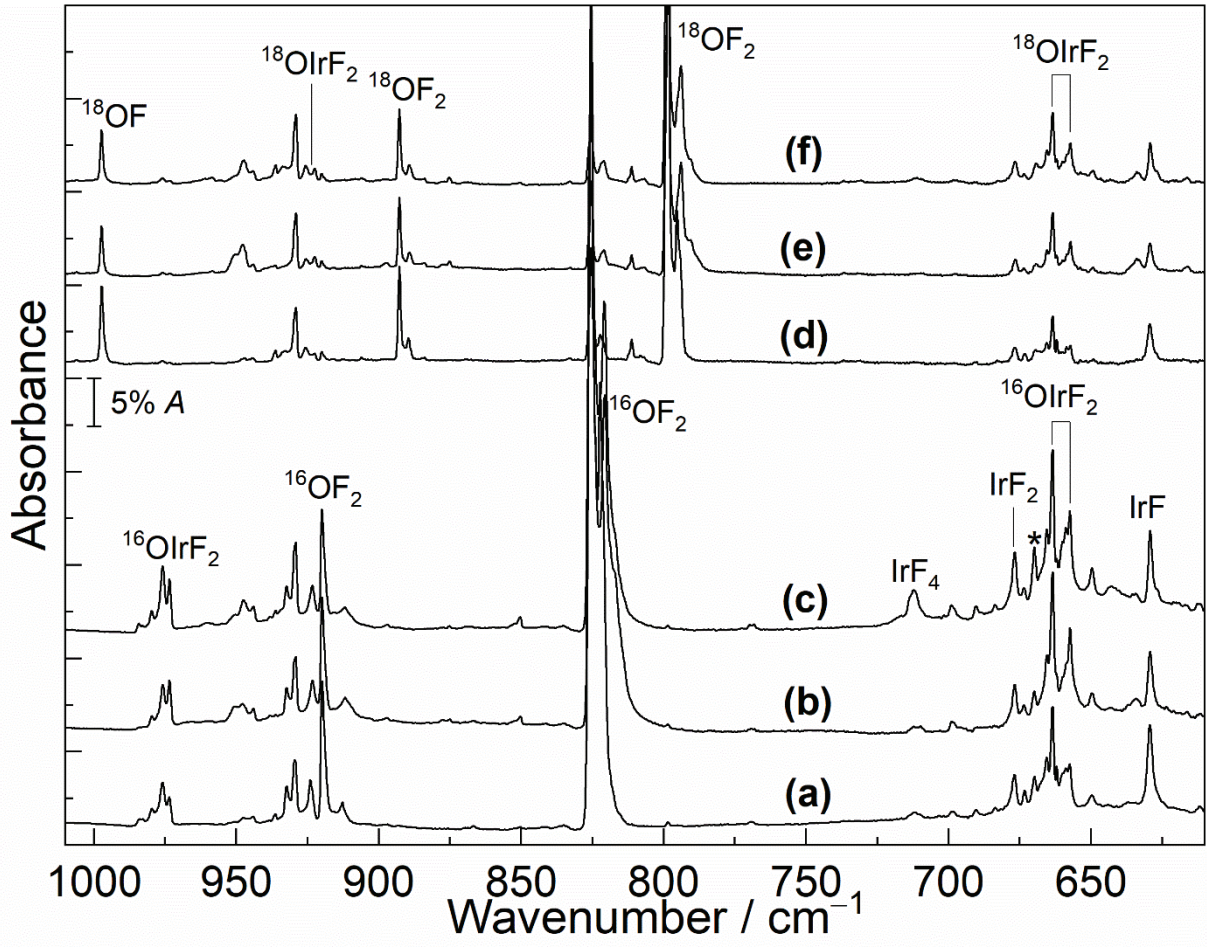

Figure S1. IR spectra in argon matrix at 12 K. (a) IR spectrum of reaction products of laser-ablated Ir atoms with 0.5% $^{16}OF_2$; (b) after annealing to 25 K; (c) after full-arc (> 220 nm) for 20 min. (d) IR spectrum of reaction products of laser-ablated Ir atoms with 0.5% $^{18}OF_2$; (e) after annealing to 25 K; (f) after full-arc (> 220 nm) for 20 min. The bands marked with asterisks are assigned to unknown impurities.

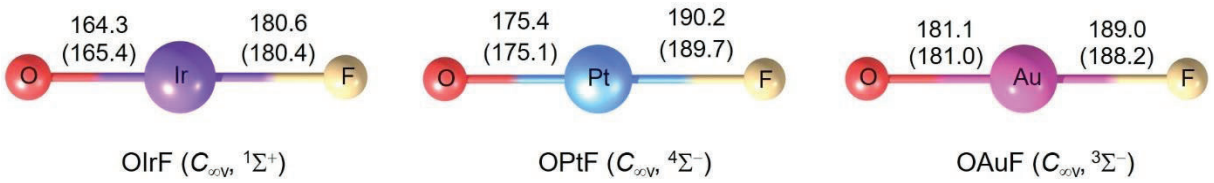

Figure S2. Optimized structures of OIrF, OPtF and OAuF in their ground states at B3LYP/aug-cc-pVTZ-PP level. Bond lengths in pm are shown. The CCSD(T) values are given in parentheses.

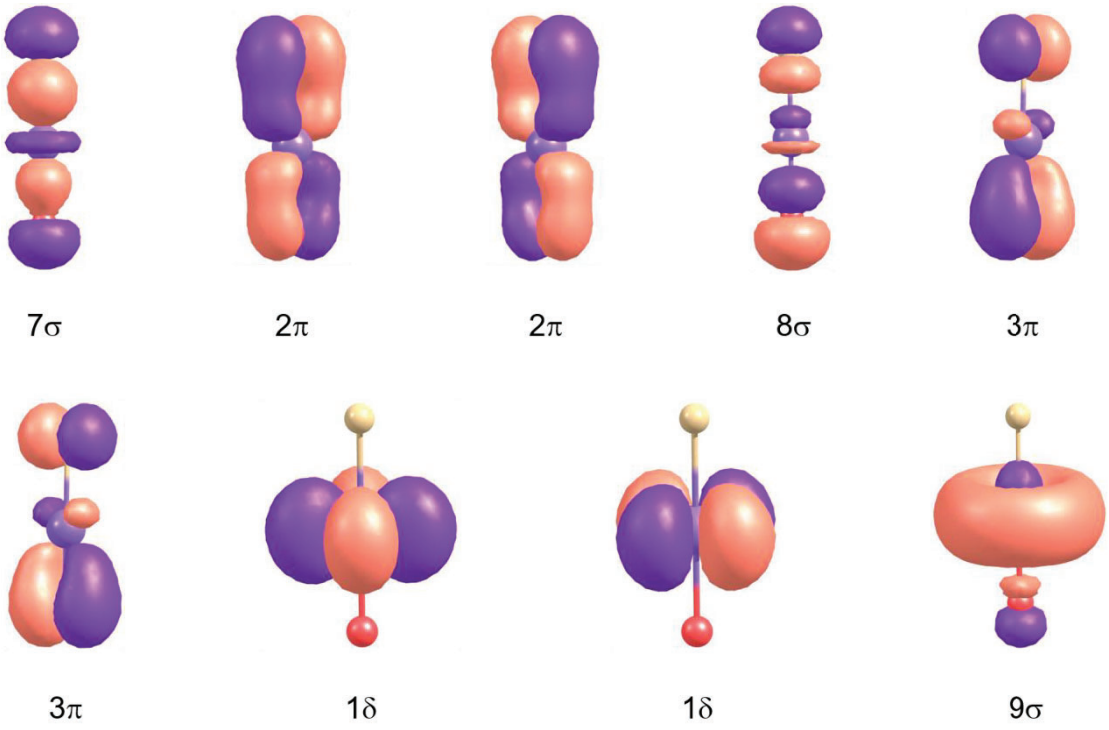

Figure S3. Molecular orbitals of OIrF computed at B3LYP/aug-cc-pVTZ-PP level.

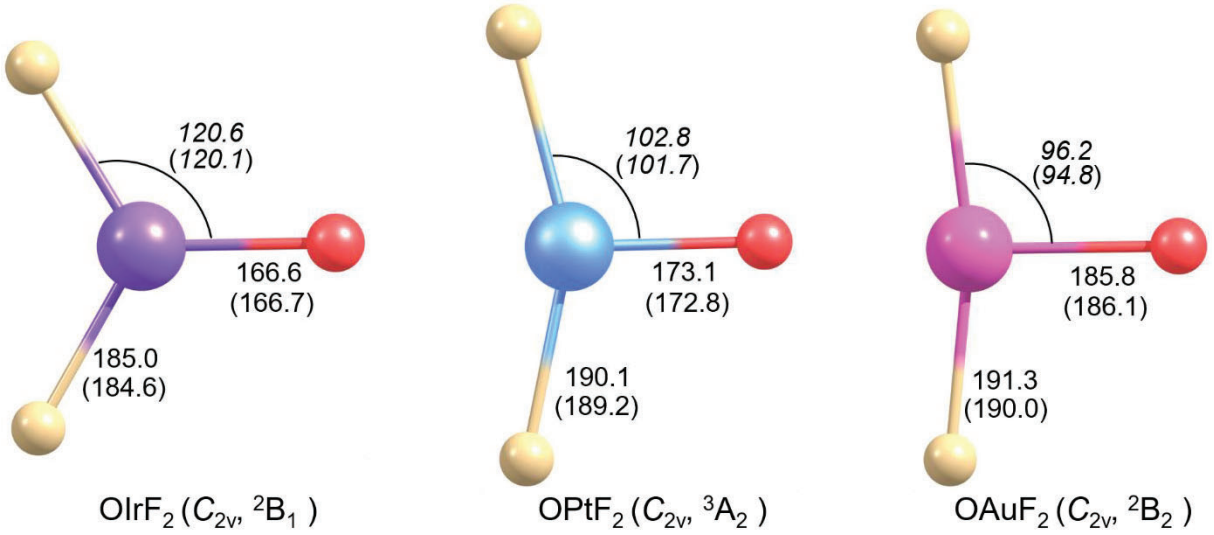

Figure S4. Optimized structures of $OIrF_2$, $OPtF_2$ and $OAuF_2$ in their ground states at B3LYP/aug-cc-pVTZ-PP level. Selected bond lengths in pm and angles in deg (in italics) are shown. The CCSD(T) values are given in parentheses.

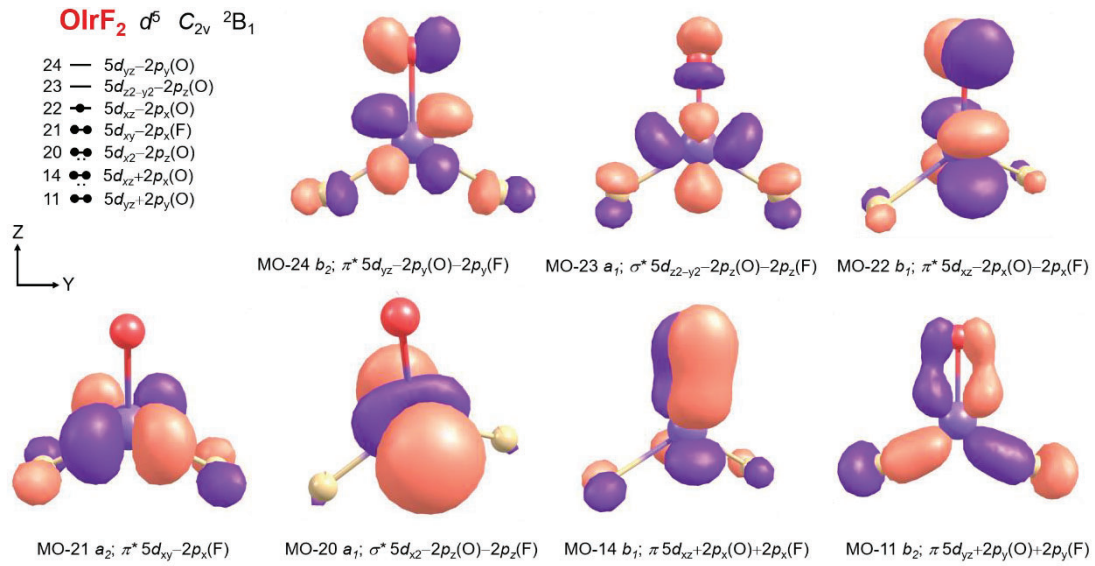

Figure S5. Selected molecular orbitals of $OIrF_2$ ($^2B_1$, C_{2v}). (B3LYP/AVTZ(-PP), Kohn-Sham orbitals with α spin; iso-surface = 0.09 electron a.u.$^{-3}$)

Table S1. Electronic states and electronic energy differences (kJ mol^{-1}) of $OIrF_2$ at scalar-relativistic pseudopotential levels.

Electronic state (Sym.)	CCSD(T)[a] $\Delta E + \Delta ZPE$	B3LYP[a] $\Delta E + \Delta ZPE$
$^2B_1$ (C_{2v})	0	0
$^4B_2$ (C_{2v})	97.4	81.9

[a]aug-cc-pVTZ-PP basis sets.

Table S2. Comparison of observed and computed vibrational frequencies (cm^{-1}) for $OIrF_2$.

	Ground state (Sym.)	Exp. Ne matrix	Ar matrix	Calc. (Int)[a] B3LYP	CCSD(T)	Modes
		984.1/980.7	976.0/973.6	1042.6 (64)	1033.1	ν(Ir–^{16}O)
$^{16}OIrF_2$	$^2B_1$ (C_{2v})	672.6	663.6	671.7 (115)	684.1	ν_{as}(Ir–F_2)
		666.8	657.5	670.5 (57)	682.8	ν_s(Ir–F_2)
		933.7/929.6	925.8/922.6	987.37 (58)	978.6	ν(Ir–^{18}O)
$^{18}OIrF_2$	$^2B_1$ (C_{2v})	672.6	663.6	671.7 (115)	684.1	ν_{as}(Ir–F_2)
		666.8	657.5	670.5 (57)	682.8	ν_s(Ir–F_2)

[a]aug-cc-pVTZ-PP basis sets. Intensities are shown in parentheses in km mol^{-1}. For the CCSD(T) calculations no intensities are available.

Table S3. Electronic states and electronic energy differences (kJ mol^{-1}) of FOIrF at scalar-relativistic pseudopotential levels.

Electronic state (Sym.)	CCSD(T)[a] $\Delta E + \Delta$ZPE	B3LYP[a] $\Delta E + \Delta$ZPE
$^2A''$ (C_s)	16.5	–
$^4A'$ (C_s)	1.2	4.9
$^4A''$ (C_s)	0	0

[a]aug-cc-pVTZ-PP basis sets.

Table S4. Comparison of observed and computed vibrational frequencies (cm^{-1}) for FOIrF.

	Electronic state (Sym.)	Calc. (Int)[a] B3LYP	CCSD(T)	Exp. Ne matrix
		–	938.5	889.3
$F^{16}OIrF$	$^2A''$ (C_s)	–	698.1	685.1
		–	464.4	–
		–	890.6	842.9
$F^{18}OIrF$	$^2A''$ (C_s)	–	697.9	684.1
		–	446.1	–
		735.8 (65)	713.6	
$F^{16}OIrF$	$^4A'$ (C_s)	621.4 (150)	625.9	
		489.6 (57)	524.2	
		704.5 (63)	741.7	
$F^{16}OIrF$	$^4A''$ (C_s)	619.8 (162)	639.8	
		494.2 (98)	741.7	

[a]aug-cc-pVTZ-PP basis sets. Intensities are shown in parentheses in km mol^{-1}. For the CCSD(T) calculations no intensities are available.

Table S5. Electronic states, structural parameters (pm, deg), electronic energy differences (kJ mol^{-1}) of selected states of OIrF at scalar-relativistic pseudopotential levels.

Electronic state (Sym.)	CCSD(T)[a] Bond lengths [pm] O–Ir/Ir–F	Angle [°] O–Ir–F	ΔE + ΔZPE	B3LYP[a] Bond lengths [pm] O–Ir/Ir–F	Angle [°] O–Ir–F	ΔE + ΔZPE
$^1\Sigma^+$ ($C_{\infty v}$)	165.4/180.4	180.0	0	164.3/180.6	180.0	0
$^3\Sigma^-$ ($C_{\infty v}$)	173.9/193.9	180.0	190.3	–	–	–
$^3\Pi$ ($C_{\infty v}$)	169.8/186.6	180.0	72.6	169.0/186.9	180.0	54.7
$^5\Delta$ ($C_{\infty v}$)	175.8/192.9	180.0	134.4	176.3/193.3	180.0	111.9

[a]aug-cc-pVTZ-PP basis sets.

Table S6. Comparison of observed and computed vibrational frequencies (cm^{-1}) for OIrF.

	Ground state (Sym.)	Exp. Ne matrix	Calc. (Int)[a] B3LYP	CCSD(T)	Modes
^{16}OIrF	$^1\Sigma^+$ ($C_{\infty v}$)	–	1106.0 (76)	1053.4	ν(Ir–^{16}O)
		732.2	735.4 (95)	741.7	ν(Ir–F)
^{18}OIrF	$^1\Sigma^+$ ($C_{\infty v}$)	–	1047.5 (71)	998.0	ν(Ir–^{18}O)
		732.2	735.1 (94)	741.4	ν(Ir–F)

[a]aug-cc-pVTZ-PP basis sets. Intensities are shown in parentheses in km mol^{-1}. For the CCSD(T) calculations no intensities are available.

Table S7. Comparison of observed vibrational frequencies (in cm^{-1}) for OIrF, OPtF and OAuF.

Species	CCSD(T)[a] Calc.	Exp. Ne matrix	Modes
OIrF ($C_{\infty v}$, $^1\Sigma^+$)	1053.4	–	ν(Ir–O)
	741.7	732.2	ν(Ir–F)
OPtF ($C_{\infty v}$, $^4\Sigma^-$)[1]	848.3	–	ν(Pt–O)
	640.3	611.8	ν(Pt–F)
OAuF ($C_{\infty v}$, $^3\Sigma^-$)[2]	767.9	–	ν(Au–O)
	642.6	629.4	ν(Au–F)

[a]aug-cc-pVTZ-PP basis sets.

Table S8. Comparison of observed vibrational frequencies (in cm^{-1}) for $OIrF_2$, $OPtF_2$ and $OAuF_2$.

Species	CCSD(T)[a] Calc.	Exp. Ne matrix	Ar matrix	Modes
$OIrF_2$ (C_{2v}, $^2B_1$)	682.2	666.8	657.5	ν_s(Ir–F_2)
	684.1	672.6	663.6	ν_{as}(Ir–F_2)
	1033.1	980.7	973.6	ν(Ir–O)
$OPtF_2$ (C_{2v}, $^3A_2$)[1]	627.0	–	–	ν_s(Pt–F_2)
	652.2	650.2	635.2	ν_{as}(Pt–F_2)
	870.8	–	–	ν(Pt–O)
$OAuF_2$ (C_{2v}, $^2B_2$)[2]	616.0	–	–	ν(Au–O)
	621.4	–	–	ν_s(Au–F_2)
	659.2	655.3	634.6	ν_{as}(Au–F_2)

[a]aug-cc-pVTZ-PP basis sets. For the CCSD(T) calculations no intensities are available.

Table S9. Computed thermochemical stability of iridium oxyfluorides (298.15 K, kJ mol^{-1}) at B3LYP and CCSD(T) level.

Reaction	B3LYP[a]		CCSD(T)[a]	
	$\Delta E + \Delta$ZPE	$\Delta_r H$	$\Delta E + \Delta$ZPE	$\Delta_r H^b$
$Ir + OF \rightarrow OIrF$	–744.6	–746.8	–778.3	–780.8
$OIrF + F \rightarrow OIrF_2$	–332.6	–336.3	–307.7	–311.7
$Ir + OF_2 \rightarrow OIrF_2$	–924.5	–926.3	–929.7	–932.4
$FOIrF \rightarrow OIrF_2$	–	–	–389.0	–
$Ir + OF_2 \rightarrow FOIrF$	–	–	–540.7	–

[a]aug-cc-pVTZ-PP basis sets. [b]The enthalpies at CCSD(T) level were calculated by adding the enthalpy corrections (B3LYP) to electronic energy changes.

Calculated atomic coordinates (in Å) of species for optimized structures at B3LYP/aug-cc-pVTZ-PP level.

OIrF $^1\Sigma^+$ ($C_{\infty v}$):

Ir	0.00000000	0.00000000	0.03303700
O	0.00000000	0.00000000	1.67632500
F	0.00000000	0.00000000	-1.77271300

OIrF $^3\Pi$ ($C_{\infty v}$):

Ir	0.00000000	0.00000000	0.03518100
O	0.00000000	0.00000000	1.72473200
F	0.00000000	0.00000000	-1.83408400

OIrF $^5\Delta$ ($C_{\infty v}$):

Ir	0.00000000	0.00000000	0.03503900
O	0.00000000	0.00000000	1.79780500
F	0.00000000	0.00000000	-1.89782500

$OIrF_2$ $^2B_1$ (C_{2v}):

Ir	0.00000000	0.00000000	0.03532600
O	0.00000000	0.00000000	1.70111100
F	0.00000000	1.59208700	-0.90716600
F	0.00000000	-1.59208700	-0.90716600

$OIrF_2$ $^4B_2$ (C_{2v}):

Ir	0.00000000	0.00000000	0.09759100
O	0.00000000	0.00000000	1.81420900
F	0.00000000	1.33096300	-1.22379000
F	0.00000000	-1.33096300	-1.22379000

FOIrF $^4A''$ (C_s):

Ir	0.00000000	0.20313300	0.00000000
O	0.81361000	-1.44114500	0.00000000
F	-0.27832700	-2.49285500	0.00000000
F	-0.44488200	2.03596000	0.00000000

FOIrF $^4A'$ (C_s):

Ir	0.00000000	0.19608700	0.00000000
O	0.82568600	-1.46042700	0.00000000
F	-0.34059900	-2.42340800	0.00000000
F	-0.39334400	2.04393600	0.00000000

Calculated atomic coordinates (in Å) of species for optimized structures at CCSD(T)/aug-cc-pVTZ-PP level.

OIrF $^{1}\Sigma^{+}$ ($C_{\infty v}$):

Ir	0.0000000000	0.0000000000	0.0288126011
O	0.0000000000	0.0000000000	1.6830588551
F	0.0000000000	0.0000000000	-1.7752224562

OIrF $^{3}\Sigma^{-}$ ($C_{\infty v}$):

Ir	0.0000000000	0.0000000000	0.0454514358
O	0.0000000000	0.0000000000	1.7844925815
F	0.0000000000	0.0000000000	-1.8932950173

OIrF $^{3}\Pi$ ($C_{\infty v}$):

Ir	0.0000000000	0.0000000000	0.0348429644
O	0.0000000000	0.0000000000	1.7328641011
F	0.0000000000	0.0000000000	-1.8310580654

OIrF $^{5}\Delta$ ($C_{\infty v}$):

Ir	0.000000000	0.000000000	0.035492183
O	0.000000000	0.000000000	1.793250147
F	0.000000000	0.000000000	-1.893723380

OIrF$_2$ $^{2}B_1$ (C_{2v}):

Ir	0.0000000000	0.0000000000	0.0274677603
O	0.0000000000	0.0000000000	1.6944354444
F	0.0000000000	1.5967376484	-0.8998991024
F	0.0000000000	-1.5967376484	-0.8998991024

OIrF$_2$ $^{4}B_2$ (C_{2v}):

Ir	0.000000000	0.000000000	0.093466085
O	0.000000000	0.000000000	1.809982368

F	0.000000000	1.330190455	-1.219614246
F	0.000000000	-1.330190455	-1.219614246

FOIrF $^{2}A''$ (C_s):

Ir	-0.2413869467	-0.1209942502	0.0000000000
O	1.3923426250	-0.6448803225	0.0000000000
F	2.5960277687	0.6042594348	0.0000000000
F	-2.0510181670	0.2495297479	0.0000000000

FOIrF $^{4}A'$ (C_s):

Ir	0.0331075569	0.1872999277	0.0000000000
O	0.8600944827	-1.4832103073	0.0000000000
F	-0.3750426727	-2.3611201206	0.0000000000
F	-0.4264163669	2.0132185002	0.0000000000

FOIrF $^{4}A''$ (C_s):

Ir	0.033226368	0.186144793	0.000000000
O	0.858337570	-1.452030730	0.000000000
F	-0.323797835	-2.430704887	0.000000000
F	-0.477365103	2.001683823	0.000000000

References

1 L. Li, H. Beckers, T. Stüker, T. Lindič, T. Schlöder, D. Andrae and S. Riedel, *Inorg. Chem. Front.*, 2021, **8**, 1215.

2 L. Li, T. Stüker, S. Kieninger, D. Andrae, T. Schlöder, Y. Gong, L. Andrews, H. Beckers and S. Riedel, *Nat. Commun.*, 2018, **9**, 1267.

3 (*a*) R. Wei, Z. T. Fang, M. Vasiliu, D. A. Dixon, L. Andrews and Y. Gong, *Inorg. Chem.*, 2019, **58**, 9796; b) L. Andrews, X. Wang, Y. Gong, T. Schlöder, S. Riedel and M. J. Franger, *Angew. Chem. Int. Ed.*, 2012, **51**, 8235.

4 A. H. Borning and K. E. Pullen, *Inorg. Chem.*, 1969, **8**, 1791.

5 M. J. Frisch, G. W. Trucks, H. B. Schlegel, G. E. Scuseria, M. A. Robb, J. R. Cheeseman, G. Scalmani, V. Barone, G. A. Petersson, H. Nakatsuji, X. Li, M. Caricato, A. V. Marenich, J. Bloino, B. G. Janesko, R. Gomperts, B. Mennucci, H. P. Hratchian, J. V. Ortiz, A. F. Izmaylov, J. L. Sonnenberg, D. Williams-Young, F. Ding, F. Lipparini, F. Egidi, J. Goings, B. Peng, A. Petrone, T. Henderson, D. Ranasinghe, V. G. Zakrzewski, J. Gao, N. Rega, G. Zheng, W. Liang, M. Hada, M. Ehara, K. Toyota, R. Fukuda, J. Hasegawa, M. Ishida, T. Nakajima, Y. Honda, O. Kitao, H. Nakai, T. Vreven, K. Throssell, J. A. Montgomery, Jr., J. E. Peralta, F. Ogliaro, M. J. Bearpark, J. J. Heyd, E. N. Brothers, K. N. Kudin, V. N. Staroverov, T. A. Keith, R. Kobayashi, J. Normand, K. Raghavachari, A. P. Rendell, J. C. Burant, S. S. Iyengar, J. Tomasi, M. Cossi, J. M. Millam, M. Klene, C. Adamo, R. Cammi, J. W. Ochterski, R. L. Martin, K. Morokuma, O. Farkas, J. B. Foresman, and D. J. Fox, *Gaussian 16*, Gaussian, Inc., Wallingford CT, 2016.

6 (*a*) P. J. Stephens, F. J. Devlin, C. F. Chabalowski and M. J. Frisch, *J. Phys. Chem.*, 1994, **98**, 11623; (*b*) A. D. Becke, *J. Chem. Phys.*, 1993, **98**, 5648; (*c*) C. Lee, W. Yang and R. G. Parr, *Phys. Rev. B*, 1988, **37**, 785; (*d*) S. H. Vosko, L. Wilk and M. Nusair, *Can. J. Phys.*, 1980, **58**, 1200.

7 R. A. Kendall, T. H. Dunning and R. J. Harrison, *J. Chem. Phys.*, 1992, **96**, 6796.

8 (*a*) D. Figgen, K. A. Peterson, M. Dolg and H. Stoll, *J. Chem. Phys.*, 2009, **130**, 164108; (*b*) K. A. Peterson, D. Figgen, M. Dolg and H. Stoll, *J. Chem. Phys.*, 2007, **126**, 124101.

9 (*a*) K. Raghavachari, G. W. Trucks, J. A. Pople and M. Head-Gordon, *Chem. Phys. Lett.*, 1989, **157**, 479; (*b*) G. D. Purvis and R. J. Bartlett, *J. Chem. Phys.*, 1982, **76**, 1910.

10 H. -J. Werner, P. J. Knowles, G. Knizia, F. R. Manby, M. Schütz, P. Celani, W. Györffy, D. Kats, T. Korona, R. Lindh, A. Mitrushenkov, G. Rauhut, K. R. Shamasundar, T. B. Adler, R. D. Amos, S. J. Bennie, A. Bernhardsson, A. Berning, D. L. Cooper, M. J. O. Deegan, A. J. Dobbyn, F. Eckert, E. Goll, C. Hampel, A. Hesselmann, G. Hetzer, T. Hrenar, G. Jansen, C. Köppl, S. J. R. Lee, Y. Liu, A. W. Lloyd, Q. Ma, R. A. Mata, A. J. May, S. J. McNicholas, W. Meyer, T. F. Miller III, M. E. Mura, A. Nicklass, D. P. O'Neill, P. Palmieri, D. Peng, K. Pflüger, R. Pitzer, M. Reiher, T. Shiozaki, H. Stoll, A. J. Stone, R. Tarroni, T. Thorsteinsson, M. Wang, M. Welborn, *MOLPRO, version 2019.2, a package of ab initio programs*.

10.2 Investigation of Molecular Iridium Fluorides IrF_n (n = 1–6): A Combined Matrix-Isolation and Quantum-Chemical Study

Chemistry—A European Journal

Supporting Information

Investigation of Molecular Iridium Fluorides IrF_n ($n = 1$–6): A Combined Matrix-Isolation and Quantum-Chemical Study

Yan Lu, Yetsedaw A. Tsegaw, Artur Wodyński, Lin Li, Helmut Beckers, Martin Kaupp, and Sebastian Riedel*

Contents

Table S1a. Electronic states, structural parameters (pm, deg), electronic energy differences (kJ mol^{-1}) of selected states of IrF_4 at scalar-relativistic pseudopotential levels.

	CCSD(T)[a]				B3LYP/aT-PP		
Electronic state (Sym.)	Bond lengths [pm] Ir–F/Ir–F'	Angle [°] F–Ir–F	ΔE	ΔE + ΔZPE	Bond lengths [pm] Ir–F/Ir–F'	Angle [°] F–Ir–F	ΔE + ΔZPE
$^2B_2$ (D_{2d})	185.3	124.1	154.6	149.5	186.3	124.3	144.5
$^2B_{1g}$ (D_{2h})	–	–	–	–	180.7/186.0	90.0	102.2
$^2B_{3g}$ (D_{2h})	179.9/185.1	90.0	109.3	108.9	–	–	–
$^4B_{2g}$ (D_{4h})	183.4	90.0	0.0	0.0	184.4	90.0	0.0
$^6A_1$ (T_d)	–	–	–	–	193.3	109.5	241.1

[a]aug-cc-pVTZ-PP basis sets.

Table S1b. Electronic states and structural parameters (pm, deg) of selected states of IrF_4 at one- and two-component all-electron X2C levels.

	1c-X2C-B3LYP all-electron		2c-X2C-B3LYP all-electron	
Electronic state (Sym.)	Bond lengths [pm] Ir–F	Angle [°] F–Ir–F	Bond lengths [pm] Ir–F	Angle [°] F–Ir–F
$^4B_{2g}$ (D_{4h})	184.5	90	184.8	90

Table S2a. Electronic states, structural parameters (pm, deg), electronic energy differences (kJ mol^{-1}) of selected states of IrF_5 at scalar-relativistic pseudopotential levels.

Electronic state (Sym.)	Parameter	CCSD(T)[a]	B3LYP/aT-PP	$\Delta E_{CCSD(T)}$	$\Delta E_{CCSD(T)}$ + ΔZPE	ΔE_{B3LYP} + ΔZPE
$^1A_1'$ (D_{3h})	$d_{Ir\text{-}F(ax)}$	192.6	194.3	41.9	42.2	61.1
	$d_{Ir\text{-}F(eq)}$	178.6	179.6			
$^1A_1$ (C_{4v})	$d_{Ir\text{-}F(ax)}$	186.8	188.0	47.0	47.3	53.3
	$d_{Ir\text{-}F(eq)}$	184.0	185.1			
	$\sphericalangle_{F(ax)\text{-}Ir\text{-}F(eq)}$	91.3	91.5			
	$\sphericalangle_{F(eq)\text{-}Ir\text{-}F(eq)}$	90.0	90.0			
$^3B_1$ (C_{2v})	$d_{Ir\text{-}F(1)}$	182.6	183.5	0.0	0.0	0.0
	$d_{Ir\text{-}F(2)}$	188.0	189.2			
	$d_{Ir\text{-}F(3)}$	182.7	184.1			
	$\sphericalangle_{F(1)\text{-}Ir\text{-}F(2)}$	91.2	91.5			
	$\sphericalangle_{F(2)\text{-}Ir\text{-}F(3)}$	89.8	89.8			
	$\sphericalangle_{F(1)\text{-}Ir\text{-}F(3)}$	98.2	98.5			
$^5B_1$ (C_{4v})	$d_{Ir\text{-}F(ax)}$	195.3	197.8	24.0	24.2	14.9
	$d_{Ir\text{-}F(eq)}$	183.8	185.0			
	$\sphericalangle_{F(ax)\text{-}Ir\text{-}F(eq)}$	96.0	95.6			
	$\sphericalangle_{F(eq)\text{-}Ir\text{-}F(eq)}$	89.4	89.4			

[a]aug-cc-pVTZ-PP basis sets.

Table S2b. Electronic states, structural parameters (pm, deg), electronic energy differences (kJ mol^{-1}) of selected states of IrF_5 at one- and two-component all-electron X2C levels.

Level	Sym.	Multiplicity	Functional[a]	E_{B3LYP} + ΔZPE	$d_{Ir\text{-}F(ax)}$ [pm]	$d_{Ir\text{-}F(eq1)}$ [pm]	$d_{Ir\text{-}F(eq2)}$ [pm]	$\sphericalangle_1$ [deg]	$\sphericalangle_2$ [deg]
1c-X2C	C_{4v}	5	B3LYP	15.4	197.8	185.0	–	95.7	–
1c-X2C	C_{2v}	3	B3LYP	0	183.5	184.1	189.2	91.5	98.5
2c-X2C	C_{4v}	(3)	B3LYP	-[b]	185.9	186.4	–	94.3	–

[a]x2c-TZVPall-2c all-electron basis sets.

[b]2c-X2C computations did not converge for quintet 1c-X2C guess. Comparison of quintet and triplet configurations is not possible.

Table S3a. Electronic states, structural parameters (pm, deg), electronic energy differences (kJ mol^{-1}) of selected states of IrF_3 at scalar-relativistic pseudopotential levels.

	CCSD(T)[a]				B3LYP/aT-PP		
Electronic state (Sym.)	Bond lengths [pm] Ir–F/Ir–F'	Angle [°] F–Ir–F	ΔE	ΔE + ΔZPE	Bond lengths [pm] Ir–F/Ir–F'	Angle [°] F–Ir–F	ΔE + ΔZPE
$^1A_1'$ (D_{3h})	181.1	120.0	37.0	37.1	181.8	120.0	44.2
$^3B_1$ (C_{2v})	183.6/185.1	164.7	0.0	0.0	184.4/185.9	164.3	0.0

[a]aug-cc-pVTZ-PP basis sets.

Table S3b. Electronic states and structural parameters (pm, deg) of selected states of IrF_3 at one- and two-component all-electron X2C levels.

	1c-X2C-B3LYP all-electron		2c-X2C-B3LYP all-electron	
Electronic state (Sym.)	Bond lengths [pm] Ir–F/Ir–F'	Angle [°] F–Ir–F	Bond lengths [pm] Ir–F/Ir–F'	Angle [°] F–Ir–F
$^3B_1$ (C_{2v})	184.4/185.9	164.3	185.9/186.4	165.2

Table S4a. Electronic states, structural parameters (pm, deg), electronic energy differences (kJ mol^{-1}) of selected states of IrF_2 at scalar-relativistic pseudopotential levels.

	CCSD(T)[a]				B3LYP/aT-PP		
Electronic state (Sym.)	Bond lengths [pm] Ir–F	Angle [°] F–Ir–F	ΔE	ΔE + ΔZPE	Bond lengths [pm]	Angle [°] F–Ir–F	ΔE + ΔZPE
$^2A_2$ (C_{2v})	–	–	–	–	179.8	166.2	62.7
$^4\Delta_g$ ($D_{\infty h}$)	184.9	180.0	0.0	0.0	185.4	180.0	0.0
$^4\Sigma_g^-$ ($D_{\infty h}$)	184.7	180.0	6.1	6.1	–	–	–
$^4\Phi_g$ ($D_{\infty h}$)	190.4	180.0	71.5	70.9	–	–	–

[a]aug-cc-pVTZ-PP basis sets.

Table S4b. Electronic states and structural parameters (pm, deg) of selected states of IrF_2 at one- and two-component all-electron X2C levels.

	1c-X2C-B3LYP all-electron		2c-X2C-B3LYP all-electron	
Electronic state (Sym.)	Bond lengths [pm] Ir–F	Angle [°] F–Ir–F	Bond lengths [pm] Ir–F	Angle [°] F–Ir–F
$^4\Delta_g$ ($D_{\infty h}$)	185.3	180.0	186.0	180.0

Table S5a. Electronic states, structural parameters (pm), electronic energy differences (kJ mol^{-1}) and predicted frequencies (cm^{-1}) of selected states of IrF at scalar-relativistic pseudopotential levels.

	CCSD(T)[a]				B3LYP/aT-PP		
Electronic state (Sym.)	Bond lengths [pm] Ir–F	Freq.	ΔE	ΔE + ΔZPE	Bond lengths [pm] Ir–F	Freq.	ΔE + ΔZPE
$^1\Sigma^+$ ($C_{\infty v}$)	181.7	638.0	123.1	123.2	180.9	656.4	152.8
$^3\Sigma^-$ ($C_{\infty v}$)	182.9	614.8	0.4	0.3	182.2	618.4	17.1
$^3\Phi$ ($C_{\infty v}$)	186.1	632.6	0.0	0.0	186.4	628.5	0.0
$^3\Delta$ ($C_{\infty v}$)	190.7	615.7	8.4	8.3	–	–	–

[a]aug-cc-pVTZ-PP basis sets.

Table S5b. Electronic states, structural parameters (pm) and predicted frequencies (cm^{-1}) of selected states of IrF at one- and two-component all-electron X2C levels.

	1c-X2C-B3LYP all-electron		2c-X2C-B3LYP all-electron	
Electronic state (Sym.)	Bond lengths [pm] Ir–F	Freq.	Bond lengths [pm] Ir–F	Freq.
$^3\Phi$ ($C_{\infty v}$)	186.1	639	186.2	652

Table S6. Calculated IR frequencies of IrF_6 and IrF_7.

Molecule	Electronic state (Sym.)	mode	B3LYP/aT-PP	1c-X2C-B3LYP	2c-X2C-B3LYP	Ref.[1]
IrF_6	$^4A_{1g}$ (O_h)	T_{1u}	711.6 (177)	715 (174)	716 (149)[a]	
		T_{1u}	711.6 (177)	715 (174)	716 (153)[a]	
		T_{1u}	711.6 (177)	715 (174)	715 (149)[a]	
		A_{1g}	706.8 (0)	709 (0)	707 (1)	
		E_g	647.1 (0)	648 (0)	656 (0)	
		E_g	647.1 (0)	648 (0)	654 (0)	
		T_{1u}	278.5 (14)	278 (15)	302 (7)[a]	
		T_{1u}	278.5 (14)	278 (15)	299 (8)[a]	
		T_{1u}	278.5 (14)	278 (15)	299 (10)[a]	
		T_{2g}	262.1 (0)	267 (0)	278 (0)	
		T_{2g}	262.1 (0)	267 (0)	276 (0)	
		T_{2g}	262.1 (0)	267 (0)	274 (0)	
		T_{2u}	204.3 (0)	207 (0)	238 (0)	
		T_{2u}	204.3 (0)	207 (0)	235 (0)	
		T_{2u}	204.3 (0)	207 (0)	235 (0)	
IrF_7	$^3A_1'$ (D_{5h})	A_2''	714.4 (153)	718 (149)	718 (122)	691.0
		A_1'	681.4 (0)	683 (0)	681 (1)	657.4
		E_1'	661.9 (113)	662 (110)	665 (88)[a]	635.4
		E_1'	661.9 (113)	662 (110)	659 (94)[a]	
		A_1'	628.2 (0)	628 (0)	636 (0)	606.7
		E_2'	562.5 (0)	560 (0)	564 (0)[a]	542.6
		E_2'	562.5 (0)	560 (0)	563 (0)[a]	
		E_2'	472.8 (0)	471 (0)	479 (0)[a]	456.1
		E_2'	472.8 (0)	471 (0)	477 (0)[a]	
		E_1'	335.3 (14)	331 (13)	347 (5)[a]	319.2
		E_1'	335.3 (14)	331 (13)	346 (5)[a]	
		A_2''	302.7 (13)	300 (13)	325 (7)	292.8
		E_1''	260.3 (0)	262 (0)	276 (0)[a]	255.2
		E_1''	260.3 (0)	262 (0)	273 (0)[a]	
		E_1'	237.3 (3)	237 (4)	262 (1)[a]	227.8
		E_1'	237.3 (3)	237 (4)	260 (2)[a]	
		E_2''	94.8 (0)	102 (0)	154 (0)[a]	91.3
		E_2''	94.8 (0)	102 (0)	152 (0)[a]	

[a]Observed splitting for the degenerate modes in the 2c-calculation is due to numerical errors resulting from the use of C_1 symmetry. Frequencies in cm^{-1}, intensities are shown in parentheses in km mol^{-1}.

Table S7. Calculated IR frequencies of IrF_5.

Electronic state (Sym.)	mode	B3LYP/aT-PP	1c-X2C-B3LYP	2c-X2C-B3LYP	CCSD(T)[a]	Ref.[2]
$^3B_1$ (C_{2v})	A_1	716.8 (16)	720 (16)	–	725.8	–
	B_2	702.4 (177)	706 (177)	–	724.4	–
	A_1	692.2 (15)	695 (15)	–	710.4	–
	B_1	662.3 (194)	667 (190)	–	682.5	–
	A_1	633.6 (0)	637 (0)	–	652.5	–
	B_1	261.8 (8)	276 (8)	–	263.5	–
	A_1	247.1 (12)	247 (12)	–	254.1	–
	B_2	219.5 (13)	240 (13)	–	229.8	–
	A_2	215.3 (0)	257 (0)	–	223.1	–
	A_1	162.4 (1)	164 (1)	–	168.0	–
	B_2	112.8 (1)	130 (1)	–	125.0	–
	B_1	67.5 (3)	84 (3)	–	90.2	–
$^5B_1$ (C_{4v})	E	704.4 (174)	708 (173)	–	724.1	702 (173)
	E	704.4 (174)	708 (173)	–	724.1	702 (173)
	A_1	693.4 (3)	697 (3)	–	710.7	693 (1)
	B_2	630.0 (0)	633 (0)	–	647.6	628 (0)
	A_1	524.4 (51)	524 (48)	–	566.2	526 (21)
	B_1	273.9 (0)	278 (0)	–	280.0	267 (0)
	E	247.1 (9)	248 (9)	–	250.5	239 (9)
	E	247.1 (9)	248 (9)	–	250.5	239 (9)
	A_1	215.1 (10)	214 (10)	–	219.2	218 (10)
	E	173.2 (1)	173 (1)	–	179.3	172 (1)
	E	173.2 (1)	173 (1)	–	179.2	172 (1)
	B_2	135.0 (0)	144 (0)	–	137.2	139 (0)
Spin-orbit (C_{4v})	A_1	–	–	690 (186)	–	702 (173)
	A_1	–	–	690 (187)	–	702 (173)
	A_1	–	–	696 (1)	–	693 (1)
	A_1	–	–	638 (37)	–	628 (0)
	A_1	–	–	608 (0)	–	526 (21)
	A_1	–	–	266 (0)	–	267 (0)
	A_1	–	–	245 (10)	–	239 (9)
	A_1	–	–	244 (10)	–	239 (9)
	A_1	–	–	233 (14)	–	218 (10)
	A_1	–	–	163 (0)	–	172 (1)
	A_1	–	–	152 (2)	–	172 (1)
	A_1	–	–	150 (1)	–	139 (0)

[a]aug-cc-pVTZ-PP basis sets. Frequencies in cm^{-1}, intensities are shown in parentheses in km mol^{-1}.

Table S8. Calculated IR frequencies of IrF_4.

Electronic state (Sym.)	mode	B3LYP/aT-PP	1c-X2C-B3LYP	2c-X2C-B3LYP	CCSD(T)[a]
$^2B_2$ (D_{2d})	B_2	680.3 (141)	–	–	696.4
	A_1	677.3 (0)	–	–	690.6
	E	603.4 (80)	–	–	621.1
	E	603.4 (80)	–	–	620.6
	A_1	261.3 (0)	–	–	261.7
	B_2	215.6 (17)	–	–	208.7
	E	73.3 (14)	–	–	49.6
	E	73.3 (14)	–	–	45.7
	B_1	28.1 (0)	–	–	37.2
$^2B_{1g}$ (D_{2h})	B_{2u}	739.9 (191)	–	–	–
	A_g	723.0 (0)	–	–	–
	B_{1u}	683.9 (0)	–	–	–
	A_g	636.7(0)	–	–	–
	B_{3u}	270.5(5)	–	–	–
	B_{3g}	224.5(0)	–	–	–
	B_{1u}	217.9(16)	–	–	–
	B_{3u}	182.3(1)	–	–	–
	B_{2u}	168.9(19)	–	–	–
$^4B_{2g}$ (D_{4h})	E_u	710.6 (185)	716 (183)	715 (161)[b]	727.9
	E_u	710.6 (185)	716 (183)	713 (168)[b]	727.9
	A_{1g}	706.1 (0)	710 (0)	704 (1)	722.0
	B_{1g}	652.8 (0)	655 (0)	657 (0)	669.8
	B_{2g}	264.3 (0)	268 (0)	277 (0)	270.2
	E_u	244.7 (8)	245 (8)	263 (5)[b]	247.6
	E_u	244.7 (8)	245 (8)	261 (6)[b]	247.6
	A_{2u}	200.4 (11)	198 (11)	224 (10)	203.2
	B_{2u}	131.5 (0)	129 (0)	165 (0)	132.1
$^2B_{3g}$ (D_{2h})	B_{2u}	–	–	–	753.6
	A_g	–	–	–	733.1
	B_{1u}	–	–	–	699.8
	A_g	–	–	–	644.9
	B_{3u}	–	–	–	272.6
	B_{3g}	–	–	–	221.1
	B_{1u}	–	–	–	210.8
	B_{3u}	–	–	–	182.8
	B_{2u}	–	–	–	164.1

[a]aug-cc-pVTZ-PP basis sets. [b]Observed splitting for the degenerate modes in the 2c-calculation is due to numerical errors resulting from the use of C_1 symmetry. Frequencies in cm^{-1}, intensities are shown in parentheses in km mol^{-1}.

Table S9. Calculated IR frequencies of IrF_3.

Electronic state (Sym.)	mode	B3LYP/aT-PP	1c-X2C-B3LYP	2c-X2C-B3LYP	CCSD(T)[a]
$^1A_1'$ (D_{3h})	A_1'	718.0 (0)	–	–	726.8
	E'	699.8 (126)	–	–	712.4
	E'	699.8 (126)	–	–	712.3
	E'	170.8 (3)	–	–	169.1
	E'	170.8 (3)	–	–	165.6
	A_2''	92.9 (4)	–	–	165.0
$^3B_1$ (C_{2v})	A_1	694.4 (1)	700 (0)	680 (9)	710.6
	B_2	691.4 (202)	699 (200)	689 (181)	708.3
	A_1	650.4 (61)	655 (62)	651 (42)	663.9
	B_1	194.4 (5)	196 (5)	198 (7)	197.5
	A_1	187.3 (8)	188 (8)	197 (7)	194.7
	B_2	119.2 (5)	122 (5)	167 (5)	169.5

[a]aug-cc-pVTZ-PP basis sets. Frequencies in cm^{-1}, intensities are shown in parentheses in km mol^{-1}.

Table S10. Calculated IR frequencies of IrF_2.

Electronic state (Sym.)	mode	B3LYP/aT-PP	1c-X2C-B3LYP	2c-X2C-B3LYP	CCSD(T)[a]
$^4\Delta_g$ ($D_{\infty h}$)	Σ_u^+	700.5 (178)	709 (176)	701 (158)	709.8
	Σ_g^+	666.1 (0)	673 (0)	665 (0)	671.2
	Π_u	156.6 (5)	158 (5)	182 (4)[b]	159.0
	Π_u	156.6 (5)	158 (5)	179 (4)[b]	159.0
$^4\Phi_g$ ($D_{\infty h}$)	Σ_u^+	–	–	–	643.0
	Σ_g^+	–	–	–	634.4
	Π_u	–	–	–	208.4
	Π_u	–	–	–	109.3
$^4\Sigma_g^-$ ($D_{\infty h}$)	Σ_u^+	–	–	–	687.5
	Σ_g^+	–	–	–	676.5
	Π_u	–	–	–	173.0
	Π_u	–	–	–	173.0
$^2A_2$ (C_{2v})	B_2	746.2 (176)	–	–	–
	A_1	712.8 (3)	–	–	–
	A_1	64.6 (2)	–	–	–

[a]aug-cc-pVTZ-PP basis sets. [b]Observed splitting for the degenerate modes in the 2c-calculation is due to numerical errors resulting from the use of C_1 symmetry. Frequencies in cm^{-1}, intensities are shown in parentheses in km mol^{-1}.

Table S11. Calculated IR frequencies of difluorine complex $IrF_4 \cdot F_2$.[a]

		ΔE_{B3LYP} + ΔZPE [kJ mol^{-1}]	Freq.		ΔE_{B3LYP} + ΔZPE [kJ mol^{-1}]	Freq.
			1051.9 (0)			1050.9 (0)
			740.0 (183)			710.6 (182)
			722.8 (0)			710.3 (178)
			682.2 (180)			706.1 (0)
			635.3 (0)			652.6 (0)
			270.7 (5)			264.4 (0)
			218.2 (0)			244.8 (7)
side-on	doublet	102.5	217.7 (16)	quartet	0.0	244.7 (7)
			182.2 (1)			200.5 (12)
			169.6 (18)			131.4 (0)
			36.0 (0)			38.8 (0)
			35.0 (0)			29.9 (0)
			13.0 (0)			13.8 (0)
			11.0 (0)			8.6 (0)
			4.8 (0)			8.4 (0)
			967.1 (66)			1016.9 (14)
			742.2 (185)			712.1 (181)
			724.0 (1)			712.1 (181)
			684.7 (178)			707.1 (1)
			637.8 (0)			654.3 (0)
			270.8 (3)			264.9 (0)
			245.0 (0)			245.0 (7)
end-on	doublet	102.6	218.4 (16)	quartet	1.5	245.0 (7)
			182.2 (0)			199.9 (10)
			169.6 (19)			131.5 (0)
			70.0 (0)			34.9 (0)
			59.4 (0)			30.3 (0)
			41.7 (1)			30.3 (0)
			21.8 (0)			14.3 (0)
			20.3 (0)			14.3 (0)

[a]B3LYP/aug-cc-pVTZ-PP-D3 level. Frequencies in cm^{-1}, intensities are shown in parentheses in km mol^{-1}.

Table S12. Computed thermochemical stability of iridium fluorides in kJ mol^{-1} at different levels of theory.

Reaction	B3LYP/aT-PP		1c-X2C-B3LYP[a]		2c-X2C-B3LYP[a]		CCSD(T)[b]	
	ΔE + ΔZPE	ΔH	ΔE + ΔZPE	ΔH	ΔE + ΔZPE	ΔH	ΔE + ΔZPE (B3LYP)[c]	ΔH[d]
$IrF_6 \rightarrow IrF_4 + F_2$	336.4	339.9	321.9	325.5	312.7	316.6	308.9	312.5
$IrF_6 \rightarrow IrF_5 + F$	329.6	334.8	302.7	305.2	256.0	260.5	310.1	315.4
$IrF_5 \rightarrow IrF_3 + F_2$	394.3	396.3	397.1	402.0	421.3	424.6	374.4	376.5
$IrF_5 \rightarrow IrF_4 + F$	155.8	157.8	166.3	171.1	204.0	207.0	145.0	146.9
$IrF_4 \rightarrow IrF_2 + F_2$	544.6	547.8	528.1	531.2	507.2	510.6	526.2	529.4
$IrF_4 \rightarrow IrF_3 + F$	387.5	391.2	378.0	381.7	364.6	368.5	375.7	379.4
$IrF_3 \rightarrow IrF + F_2$	654.2	656.3	638.4	640.5	607.2	609.5	654.1	656.2
$IrF_3 \rightarrow IrF_2 + F$	306.2	309.3	297.2	300.3	289.9	293.1	296.8	299.8
$IrF_2 \rightarrow Ir + F_2$	730.8	733.1	701.9	704.3	681.7	684.3	716.9	719.2
$IrF_2 \rightarrow IrF + F$	497.1	499.7	488.3	490.9	464.5	467.3	503.6	506.2
$IrF \rightarrow Ir + F$	382.7	386.0	360.8	364.1	364.5	367.9	359.6	362.9

[a]x2c-TZVPall-2c basis sets. [b]aug-cc-pVTZ-PP basis sets. [c]Using B3LYP zero point energy corrections for the electronic energies at CCSD(T) level. [d]The enthalpies at CCSD(T) level were calculated by adding the enthalpy corrections (B3LYP) to electronic energy changes.

Table S13. T1 and D1 diagnostics values of IrF_n (n = 1–6) calculated at the CCSD(T)/aug-cc-pVTZ-PP level of theory. These values are smaller than the T ≥ 0.05 and D ≥ 0.15 limits proposed in the literature for transition metal compounds,[3] so no multiconfiguration calculations were employed for these species.

Species	**T1**	**D1**
IrF_6	0.03425218	0.12759613
IrF_5	0.03238256	0.12958705
IrF_4	0.03527559	0.11454362
IrF_3	0.03148315	0.09254815
IrF_2	0.02993183	0.08749521
IrF	0.02846659	0.08275391

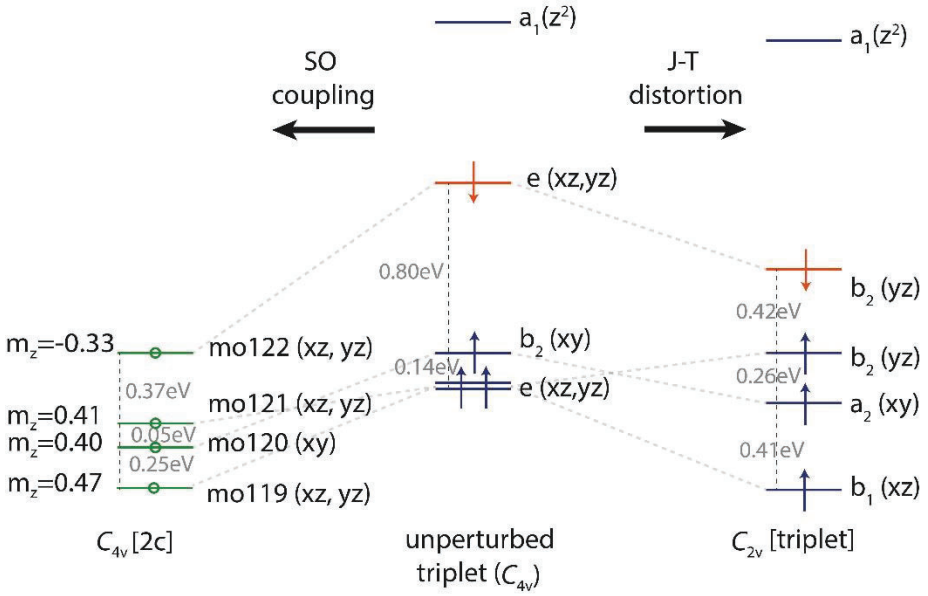

Figure S1. Simplified scheme of Jahn-Teller (JT) distortion and spin-orbit coupling (SOC) on the iridium 5d orbital splitting of triplet pyramidal IrF_5. The energy levels for the unperturbed C_{4v} triplet state were modeled from an unrestricted calculation by spatial averaging of the b_1 and b_2 levels of a C_{2v}-symmetrical wave function to the e-level that is shown.

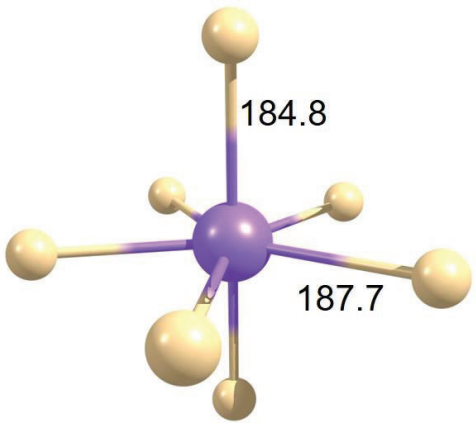

Figure S2. Computed structures of molecular IrF_7 at the B3LYP/aug-cc-pVTZ-PP level. Selected bond lengths (pm) are shown.

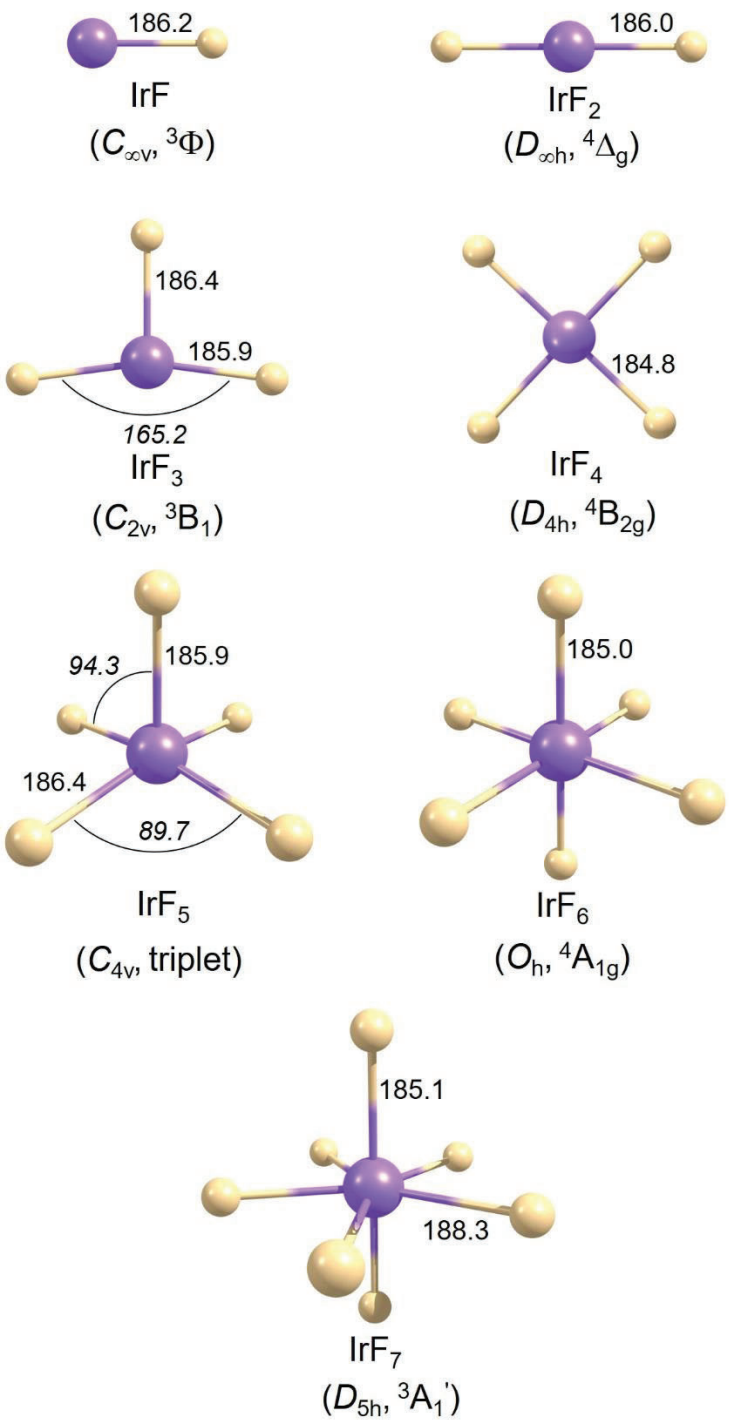

Figure S3. Computed structures of molecular iridium fluorides IrF_n (n = 1–7) at 2c-X2C-B3LYP/x2c-TZVPall-2c level. Selected bond lengths (pm) and angles (º, in *italics*) are shown.

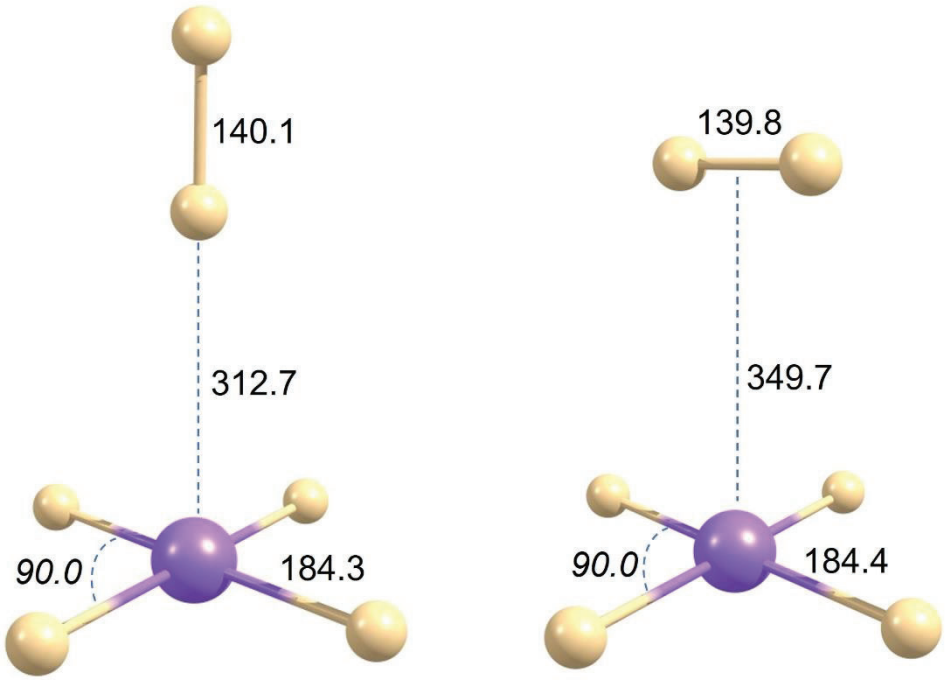

Figure S4. Computed structures of end-on and side-on structures of the quartet difluorine complex $IrF_4 \cdot F_2$ at the B3LYP/aug-cc-pVTZ-PP-D3 level. Bond lengths [pm] and angles [º, in *italics*] are shown.

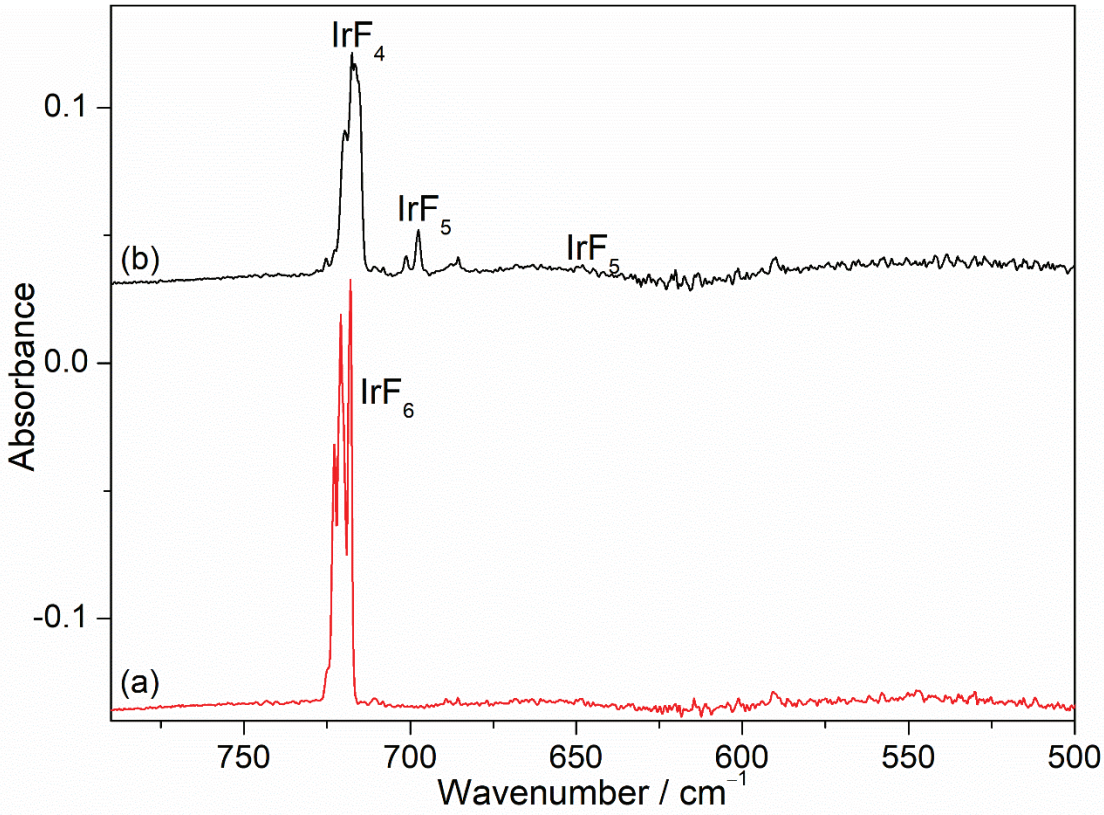

Figure S5. IR spectra in neon matrix at 6 K showing the photochemistry of IrF_6. (a) Spectrum of IrF_6 obtained after deposition for 15 min, (b) IR spectrum obtained after $\lambda = 278$ nm irradiation for 90 min.

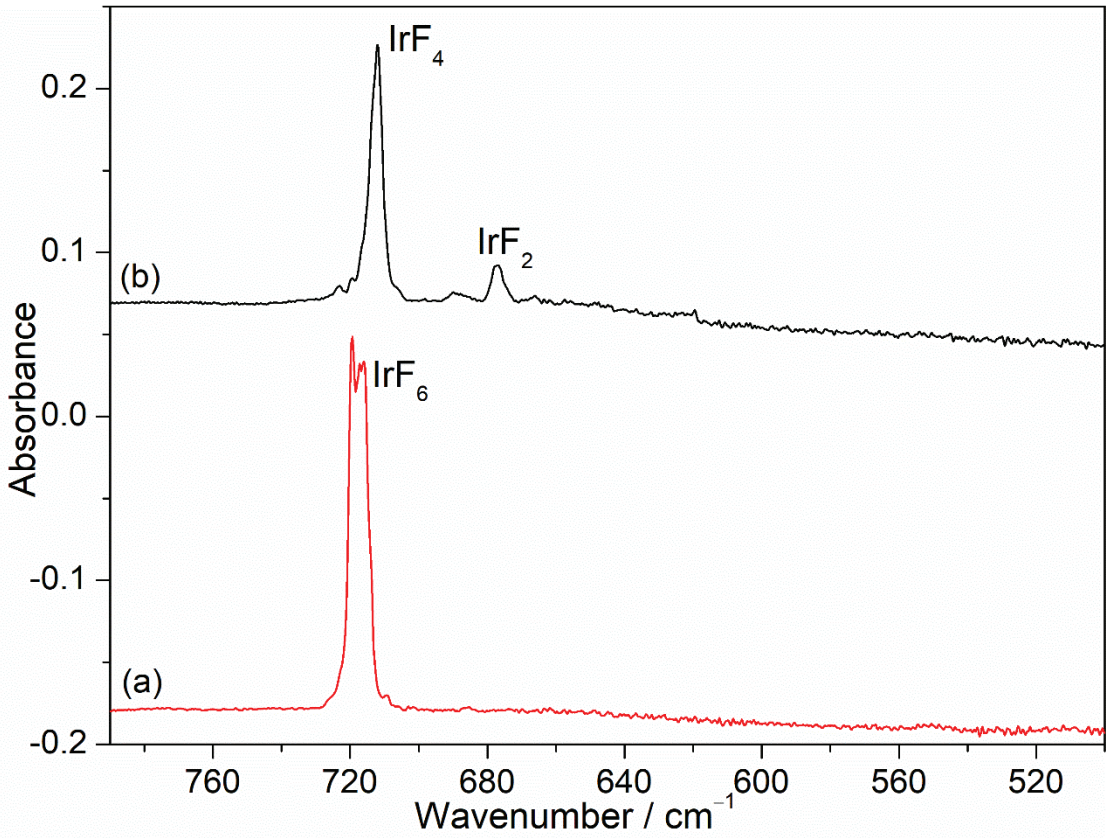

Figure S6. IR spectra in argon matrix at 6 K showing the photochemistry of IrF_6. (a) Spectrum of IrF_6 obtained after deposition for 25 min, (b) IR spectrum obtained after λ = 278 nm irradiation for 110 min.

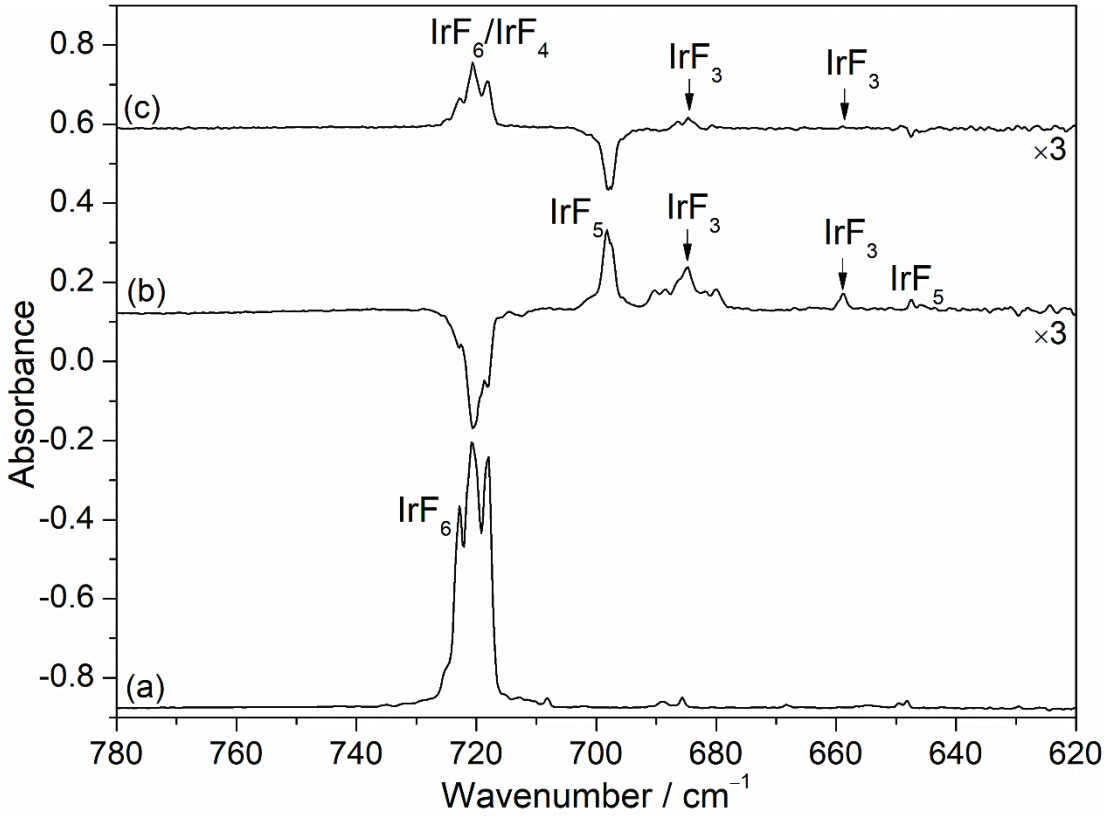

Figure S7. IR spectra in neon matrix at 6 K showing the photochemistry of IrF_6. (a) Spectrum of IrF_6 obtained after deposition for 30 min, (b) difference IR spectrum obtained after λ = 365 nm irradiation for 40 min, and (c) subsequent irradiation of the same matrix at λ = 470 nm irradiation for 15 min.

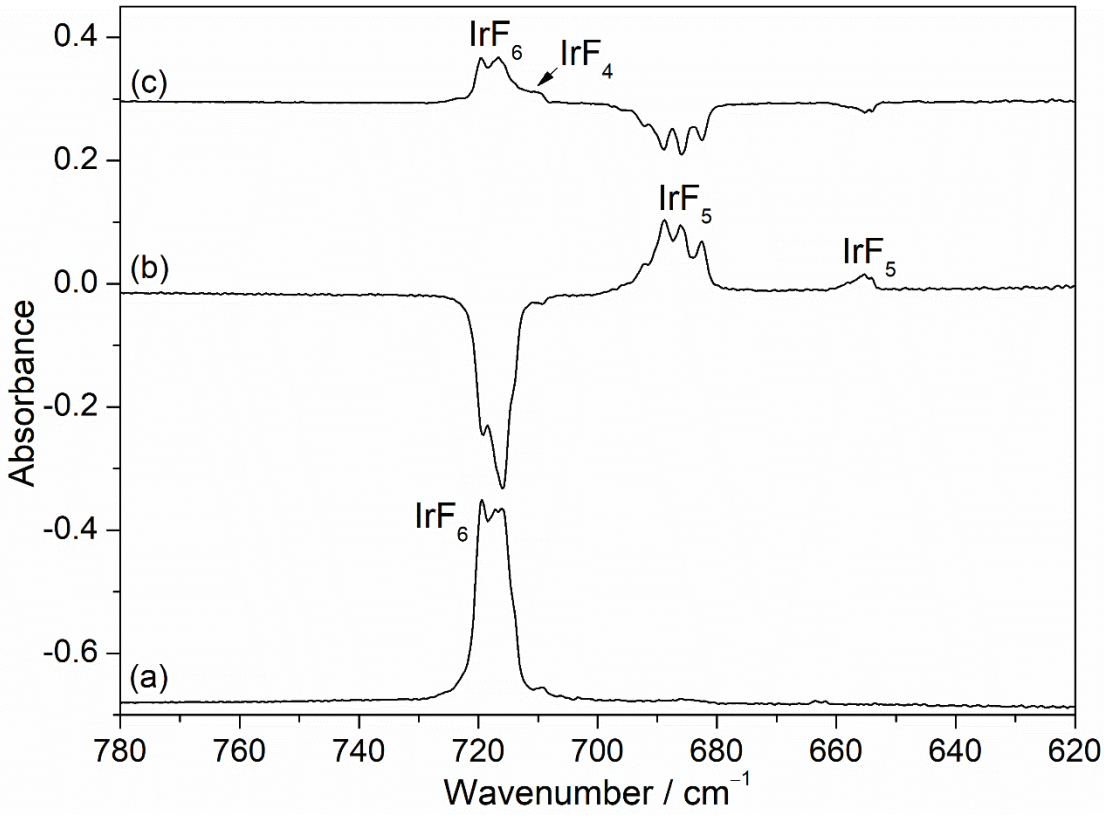

Figure S8. IR spectra in argon matrix at 6 K showing the photochemistry of IrF_6. (a) Spectrum of IrF_6 obtained after deposition for 30 min, (b) difference IR spectrum obtained after λ = 365 nm irradiation for 60 min, and (c) subsequent irradiation of the same matrix at λ = 470 nm for 45 min.

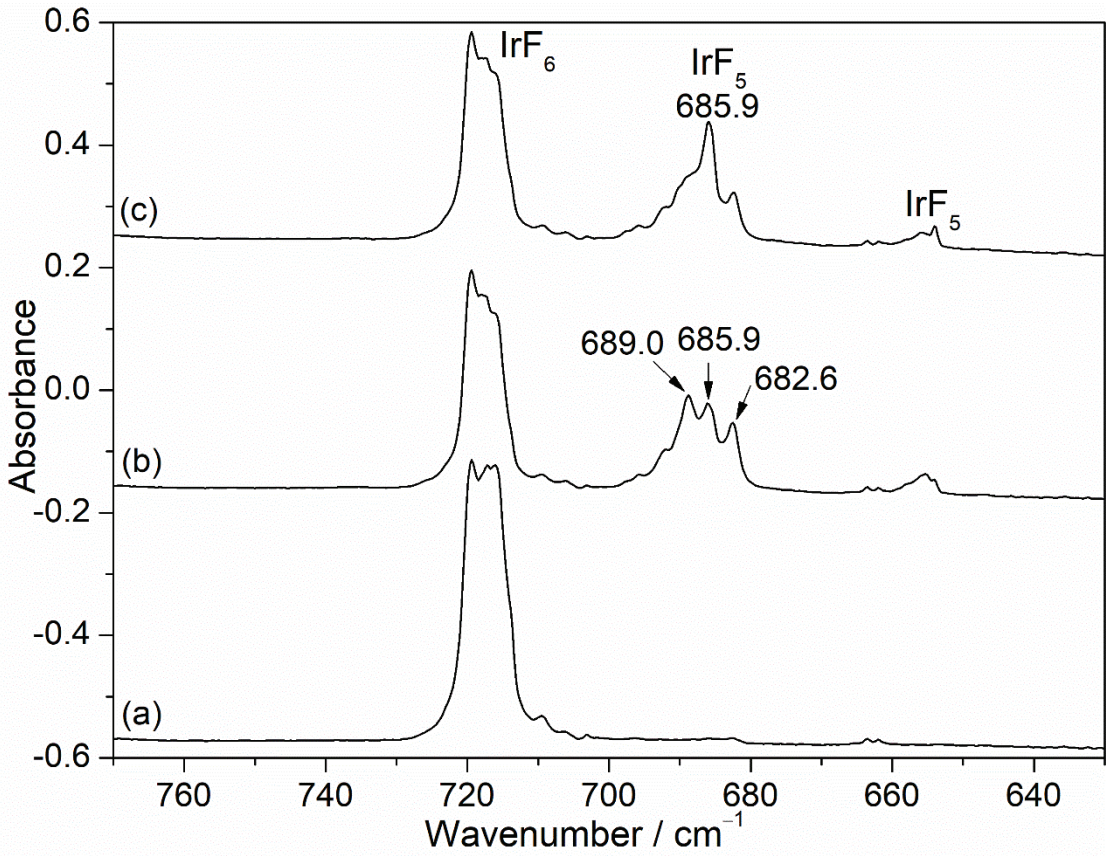

Figure S9. IR spectra in argon matrix at 6 K showing the photochemistry of IrF_6. (a) Spectrum of IrF_6 obtained after deposition for 20 min, (b) IR spectrum obtained after λ = 365 nm irradiation for 90 min, and (c) subsequent annealing to 15 K.

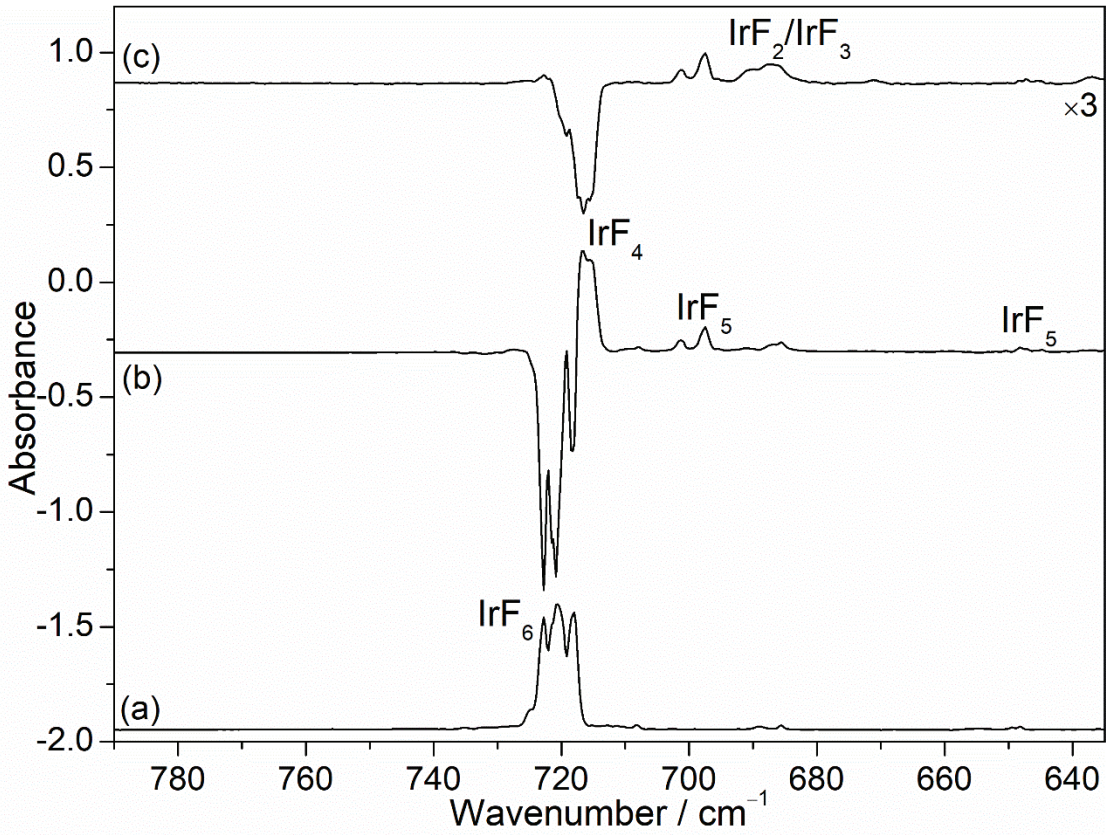

Figure S10. IR spectra in neon matrix at 6 K showing the photochemistry of IrF_6. (a) Spectrum of IrF_6 obtained after deposition for 20 min, (b) difference IR spectrum obtained after λ = 278 nm irradiation for 180 min, and (c) subsequent irradiation of the same matrix at λ = 266 nm irradiation for 25 min.

Calculated atomic coordinates (in Å) of species for optimized structures at B3LYP/aug-cc-pVTZ-PP level.

IrF_7 $^3A_1'$ (D_{5h})

Ir	0.000000000	0.000000000	0.000000000
F	0.000000000	0.000000000	1.848213000
F	0.000000000	1.876680000	0.000000000
F	-1.784829000	0.579926000	0.000000000
F	0.000000000	0.000000000	-1.848213000
F	-1.103085000	-1.518266000	0.000000000
F	1.103085000	-1.518266000	0.000000000
F	1.784829000	0.579926000	0.000000000

IrF_6 $^4A_{1g}$ (O_h)

Ir	0.00000000	0.00000000	0.00000000
F	0.00000000	0.00000000	1.84598900
F	0.00000000	1.84598900	0.00000000
F	-1.84598900	0.00000000	0.00000000
F	0.00000000	0.00000000	-1.84598900
F	0.00000000	-1.84598900	0.00000000
F	1.84598900	0.00000000	0.00000000

IrF_5 $^1A_1'$ (D_{3h})

Ir	0.00000000	0.00000000	0.00000000
F	0.00000000	1.79587400	0.00000000
F	0.00000000	0.00000000	1.94339800
F	-1.55527200	-0.89793700	0.00000000
F	1.55527200	-0.89793700	0.00000000
F	0.00000000	0.00000000	-1.94339800

IrF_5 $^1A_1$ (C_{4v})

Ir	0.00000000	0.00000000	0.12427700

F	0.00000000	0.00000000	-1.75525400
F	0.00000000	1.85073600	0.17299900
F	-1.85073600	0.00000000	0.17299900
F	0.00000000	-1.85073600	0.17299900
F	1.85073600	0.00000000	0.17299900

IrF_5 $^3B_1$ (C_{2v})

Ir	0.00000000	0.00000000	0.08782400
F	0.00000000	0.00000000	-1.74758300
F	0.00000000	1.82014900	0.36097100
F	-1.89125800	0.00000000	0.13713100
F	0.00000000	-1.82014900	0.36097100
F	1.89125800	0.00000000	0.13713100

IrF_5 $^5B_1$ (C_{4v})

Ir	0.00000000	0.00000000	0.09091000
F	0.00000000	0.00000000	-1.88715500
F	0.00000000	1.84025600	0.27734200
F	-1.84025600	0.00000000	0.27734200
F	0.00000000	-1.84025600	0.27734200
F	1.84025600	0.00000000	0.27734200

IrF_4 $^2B_2$ (D_{2d})

Ir	0.00000000	0.00000000	0.00000000
F	0.00000000	1.23104200	1.39804300
F	1.23104200	0.00000000	-1.39804300
F	0.00000000	-1.23104200	1.39804300
F	-1.23104200	0.00000000	-1.39804300

IrF_4 $^2B_{1g}$ (D_{2h})

Ir	0.00000000	0.00000000	0.00000000
F	0.00000000	1.80716000	0.00000000

F	0.00000000	0.00000000	1.86041500
F	0.00000000	-1.80716000	0.00000000
F	0.00000000	0.00000000	-1.86041500

IrF_4 $^4B_{2g}$ (D_{4h})

Ir	0.00000000	0.00000000	0.00000000
F	0.00000000	1.84418000	0.00000000
F	1.84418000	0.00000000	0.00000000
F	0.00000000	-1.84418000	0.00000000
F	-1.84418000	0.00000000	0.00000000

IrF_4 $^6A_1$ (T_d)

Ir	0.00000000	0.00000000	0.00000000
F	1.11573600	1.11573600	1.11573600
F	-1.11573600	-1.11573600	1.11573600
F	-1.11573600	1.11573600	-1.11573600
F	1.11573600	-1.11573600	-1.11573600

IrF_3 $^1A_1'$ (D_{3h})

Ir	0.00000000	0.00000000	0.00000000
F	0.00000000	1.81795400	0.00000000
F	1.57439400	-0.90897700	0.00000000
F	-1.57439400	-0.90897700	0.00000000

IrF_3 $^3B_1$ (C_{2v})

Ir	0.00000000	0.00000000	0.11738300
F	0.00000000	1.82650300	0.36867300
F	0.00000000	0.00000000	-1.74162400
F	0.00000000	-1.82650300	0.36867300

IrF_3 $^5A_1$ (C_{2v})

Ir	0.00000000	0.00000000	0.12136700
F	0.00000000	1.84407800	0.39689600
F	0.00000000	0.00000000	-1.83215500
F	0.00000000	-1.84407800	0.39689600

IrF_2 $^2A_2$ (C_{2v})

Ir	0.00000000	0.00000000	0.04081900
F	0.00000000	1.78454400	-0.17461400
F	0.00000000	-1.78454400	-0.17461400

IrF_2 $^4\Delta_g$ ($D_{\infty h}$)

Ir	0.00000000	0.00000000	0.00000000
F	0.00000000	0.00000000	1.85380700
F	0.00000000	0.00000000	-1.85380700

IrF $^1\Sigma^+$ ($C_{\infty v}$)

Ir	0.00000000	0.00000000	0.18931600
F	0.00000000	0.00000000	-1.61970800

IrF $^3\Sigma^-$ ($C_{\infty v}$)

Ir	0.00000000	0.00000000	0.19071800
F	0.00000000	0.00000000	-1.63169900

IrF $^3\Phi$ ($C_{\infty v}$)

Ir	0.00000000	0.00000000	0.19506000
F	0.00000000	0.00000000	-1.66884500

Calculated atomic coordinates (in Å) of species for optimized structures at CCSD(T)/aug-cc-pVTZ-PP level.

IrF_5 $^1A_1'$ (D_{3h})

Ir	0.0000000000	-0.0000021894	0.0000000000
F	0.0000000000	1.7858844439	0.0000000000
F	0.0000000000	-0.0000107211	1.9255839565
F	-1.5465875916	-0.8929304062	0.0000000000
F	1.5465875916	-0.8929304062	0.0000000000
F	0.0000000000	-0.0000107211	-1.9255839565

IrF_5 $^1A_1$ (C_{4v})

Ir	0.0000000000	0.0000000000	-0.1136207475
F	0.0000000000	0.0000000000	1.7546770550
F	1.8395213628	0.0000000000	-0.1562561180
F	0.0000000000	-1.8395213628	-0.1562561179
F	-1.8395213628	0.0000000000	-0.1562561180
F	0.0000000000	1.8395213628	-0.1562561179

IrF_5 $^3B_1$ (C_{2v})

Ir	0.0000000000	0.0000000000	-0.0841215721
F	0.0000000000	0.0000000000	1.7418697652
F	-1.8787702202	0.0000000000	-0.1237788603
F	0.0000000000	1.8076245988	-0.3460919093
F	1.8787702202	0.0000000000	-0.1237788603
F	0.0000000000	-1.8076245988	-0.3460919093

IrF_5 $^5B_1$ (C_{4v})

Ir	0.0000000000	0.0000000000	0.0833796243
F	0.0000000000	0.0000000000	-1.8691161046
F	0.0000000000	1.8281909117	0.2747148701
F	-1.8281909117	0.0000000000	0.2747148701

F	0.0000000000	-1.8281909117	0.2747148701
F	1.8281909117	0.0000000000	0.2747148701

IrF_4 $^2B_2$ (D_{2d})

Ir	0.0000000000	0.0000000000	-0.0000000000
F	0.0000000000	1.2270071678	1.3884295643
F	1.2270071678	0.0000000000	-1.3884295643
F	0.0000000000	-1.2270071678	1.3884295643
F	-1.2270071678	0.0000000000	-1.3884295643

IrF_4 $^2B_{3g}$ (D_{2h})

Ir	0.0000000000	0.0000000000	0.0000000000
F	0.0000000000	-1.7987451494	0.0000000000
F	0.0000000000	0.0000000000	1.8508826315
F	0.0000000000	1.7987451494	0.0000000000
F	0.0000000000	0.0000000000	-1.8508826315

IrF_4 $^4B_{2g}$ (D_{4h})

Ir	0.0000000000	0.0000000000	0.0000000000
F	1.8338159512	0.0000000000	0.0000000000
F	0.0000000000	-1.8338159512	0.0000000000
F	-1.8338159512	0.0000000000	0.0000000000
F	0.0000000000	1.8338159512	0.0000000000

IrF_3 $^1A_1'$ (D_{3h})

Ir	0.0000000000	0.0000000000	0.0000000000
F	1.8114360398	0.0000000000	0.0000000000
F	-0.9057180199	-1.5687496278	0.0000000000
F	-0.9057180199	1.5687496278	0.0000000000

IrF_3 $^3B_1$ (C_{2v})

Ir	0.0000000000	0.0000000000	-0.1044083496
F	0.0000000000	1.8198888966	-0.3485354800
F	0.0000000000	0.0000000000	1.7466478094
F	0.0000000000	-1.8198888966	-0.3485354800

IrF_2 $^4\Delta_g$ ($D_{\infty h}$)

Ir	0.0000000000	0.0000000000	0.0000000000
F	0.0000000000	0.0000000000	1.8494035118
F	0.0000000000	0.0000000000	-1.8494035118

IrF_2 $^4\Sigma_g^-$ ($D_{\infty h}$)

Ir	0.0000000000	0.0000000000	0.0000000000
F	0.0000000000	0.0000000000	1.8469905399
F	0.0000000000	0.0000000000	-1.8469905399

IrF_2 $^4\Phi_g$ ($D_{\infty h}$)

Ir	0.0000000000	0.0000000000	0.0000000000
F	0.0000000000	0.0000000000	1.9037004685
F	0.0000000000	0.0000000000	-1.9037004685

IrF $^1\Sigma^+$ ($C_{\infty v}$)

Ir	0.0000000000	0.0000000000	-0.1634695662
F	0.0000000000	0.0000000000	1.6539348080

IrF $^3\Sigma^-$ ($C_{\infty v}$)

Ir	0.0000000000	0.0000000000	-0.1645219864
F	0.0000000000	0.0000000000	1.6645828721

IrF $^3\Phi$ ($C_{\infty v}$)

Ir	0.0000000000	0.0000000000	-0.1673994752
F	0.0000000000	0.0000000000	1.6936964188

IrF $^3\Delta$ ($C_{\infty v}$)

Ir	0.0000000000	0.0000000000	-0.1715145870
F	0.0000000000	0.0000000000	1.7353318550

Calculated atomic coordinates (in Å) of $IrF_4 \cdot F_2$ complex for optimized structures at B3LYP/aug-cc-pVTZ-PP-D3 level.

$IrF_4 \cdot F_2$ complex (doublet, side-on)

Ir	0.00000000	0.00000000	0.48672000
F	1.86125900	0.00000000	0.48641700
F	0.00000000	1.80697400	0.48461000
F	0.00000000	-1.80697400	0.48461000
F	-1.86125900	0.00000000	0.48641700
F	0.00000000	-0.69855000	-3.05310700
F	0.00000000	0.69855000	-3.05310700

$IrF_4 \cdot F_2$ complex (quartet, side-on)

Ir	0.00000000	0.00000000	0.48079400
F	1.84415400	0.00000000	0.48021500
F	0.00000000	1.84424100	0.47955100
F	0.00000000	-1.84424100	0.47955100
F	-1.84415400	0.00000000	0.48021500
F	0.00000000	-0.69879500	-3.01649700
F	0.00000000	0.69879500	-3.01649700

$IrF_4 \cdot F_2$ complex (doublet, end-on)

Ir	-0.50296600	0.00000000	0.00000000
F	-0.50656800	0.00000100	-1.80617700
F	-0.50494300	-1.86010500	-0.00000100
F	-0.50494500	1.86010500	-0.00000100
F	-0.50656900	0.00000100	1.80617700
F	2.45907600	0.00000000	0.00000000
F	3.86710600	0.00000100	0.00000000

$IrF_4 \cdot F_2$ complex (quartet, end-on)

Ir	0.00000000	0.00000000	0.52515300
F	0.00000000	1.84345300	0.52810400
F	-1.84345300	0.00000000	0.52810400
F	1.84345300	0.00000000	0.52810400
F	0.00000000	-1.84345300	0.52810400
F	0.00000000	0.00000000	-2.60232400
F	0.00000000	0.00000000	-4.00307000

Calculated atomic coordinates (in Å) for optimized structures at X2C-B3LYP level of theory.

IrF $^3\Phi$ ($C_{\infty v}$):

1c-X2C:

Ir	0.0000000	0.0000000	-0.9306234
F	0.0000000	0.0000000	0.9306234

2c-X2C:

Ir	0.0000000	0.0000000	-0.9309340
F	0.0000000	0.0000000	0.9309340

IrF_2 $^4\Delta_g$ ($D_{\infty h}$)

1c-X2C:

Ir	0.0000000	0.0000000	0.0000000
F	0.0000000	0.0000000	1.8529207
F	0.0000000	0.0000000	-1.8529207

2c-X2C:

Ir	0.0000000	0.0000000	-0.0000003
F	-0.0000000	-0.0000000	1.8595828
F	-0.0000000	-0.0000000	-1.8595825

IrF_3 $^3B_1$ (C_{2v})

1c-X2C:

Ir	-0.0000000	0.0000000	0.3390455
F	-1.8265789	0.0000000	0.5904084
F	1.8265789	0.0000000	0.5904084
F	0.0000000	0.0000000	-1.5198623

2c-X2C:

Ir	0.0000076	-0.0000000	0.3461477
F	-1.8432062	0.0000000	0.5856082
F	1.8432140	0.0000000	0.5856248
F	-0.0000154	0.0000000	-1.5173807

IrF_4 $^4B_{2g}$ (D_{4h})

1c-X2C:

Ir	-0.0000000	0.0000000	0.0000000
F	1.3049003	-1.3049003	-0.0000000
F	1.3049003	1.3049003	0.0000000
F	-1.3049003	-1.3049003	0.0000000
F	-1.3049003	1.3049003	0.0000000

2c-X2C:

Ir	0.0000001	0.0000000	0.0000000
F	1.3073090	-1.3072893	-0.0000000
F	1.3073090	1.3072893	0.0000000
F	-1.3073091	-1.3072890	0.0000000
F	-1.3073090	1.3072890	-0.0000000

IrF_5

1c-X2C: $^3B_1$ (C_{2v})

Ir	0.0000000	0.0000000	-0.0692357
F	-0.0000000	1.8912404	-0.1177466
F	1.8208254	0.0000000	-0.3398580
F	-1.8208254	0.0000000	-0.3398580
F	0.0000000	-1.8912404	-0.1177466
F	-0.0000000	0.0000000	1.7658462

2c-X2C: triplet (C_{4v})

Ir	0.0000002	-0.0000001	-0.0858969
F	1.8586769	-0.0000001	-0.2252280
F	0.0000007	-1.8586862	-0.2252225
F	0.0000006	1.8586860	-0.2252219
F	-1.8586764	-0.0000001	-0.2252259
F	-0.0000020	0.0000005	1.7733872

IrF_6 $^4A_{1g}$ (O_h)

1c-X2C:

Ir	-0.0000000	-0.0000000	0.0000000
F	-1.8491586	-0.0000000	-0.0000000
F	0.0000000	-0.0000000	-1.8491586
F	-0.0000000	1.8491586	0.0000000
F	-0.0000000	-0.0000000	1.8491586
F	0.0000000	-1.8491586	-0.0000000
F	1.8491586	0.0000000	-0.0000000

2c-X2C:

Ir	-0.0000006	0.0000003	-0.0000000
F	-1.8505831	-0.0000005	0.0000001
F	0.0000005	0.0000001	-1.8490661
F	0.0000005	1.8505900	0.0000000
F	0.0000004	0.0000001	1.8490659
F	0.0000006	-1.8505893	0.0000000
F	1.8505817	-0.0000006	0.0000001

IrF_7 $^3A_1'$ (D_{5h})

1c-X2C:

Ir	0.0000000	0.0000000	0.0000000
F	0.0000000	0.0000000	-1.8507642
F	1.8810853	0.0000000	0.0000000
F	0.5812873	-1.7890184	0.0000000
F	0.0000000	0.0000000	1.8507642
F	-1.5218300	-1.1056742	0.0000000
F	-1.5218300	1.1056742	0.0000000
F	0.5812873	1.7890184	0.0000000

2c-X2C:

Ir	-0.0001633	0.0000003	-0.0000001
F	-0.0000806	-0.0000001	-1.8515630

F	1.8830669	-0.0000001	0.0000000
F	0.5819599	-1.7904372	0.0000000
F	-0.0000806	-0.0000001	1.8515629
F	-1.5233310	-1.1068413	0.0000001
F	-1.5233312	1.1068412	0.0000000
F	0.5819600	1.7904374	0.0000001

References

[1] S. Riedel, M. Kaupp, *Angew. Chem. Int. Ed.* **2006**, *45*, 3708–3711.

[2] R. Craciun, D. Picone, R. T. Long, S. Li, D. A. Dixon, K. A. Peterson, K. O. Christe, *Inorg. Chem.* **2010**, *49*, 1056–1070.

[3] W. Jiang, N. J. DeYonker, A. K. Wilson, *J. Chem. Theory Comput.* **2012**, 8, 2, 460–468.

10.3 Investigation of Isolated IrF_5^-, IrF_6^- Anions and $M[IrF_6]$ (M = Na, K, Rb, Cs) Ion Pairs by Matrix-Isolation Spectroscopy and Relativistic Quantum-Chemical Calculations

Supporting Information

Investigation of Isolated IrF_5^-, IrF_6^- Anions and $M[IrF_6]$ (M = Na, K, Rb, Cs) Ion Pairs by Matrix-Isolation Spectroscopy and Relativistic Quantum-Chemical Calculations

Yan Lu,[a] Artur Wodyński,[b] Marc Reimann,[b] Robert Medel,[a] Martin Kaupp,*[b] Sebastian Riedel*[a]

[a] M. Sc. Yan Lu, Dr. Robert Medel, Prof. Dr. Sebastian Riedel, Freie Universität Berlin, Institut für Chemie und Biochemie, Anorganische Chemie, Fabeckstrasse 34/36, 14195 Berlin, Germany. E-mail: s.riedel@fu-berlin.de.

[b] Dr. Artur Wodyński, Dr. Marc Reimann, Prof. Dr. Martin Kaupp, Technische Universität Berlin, Institut für Chemie Theoretische Chemie/Quantenchemie, Sekr. C7, Strasse des 17. Juni 135, 10623 Berlin, Germany. E-mail: martin.kaupp@tu-berlin.de.

Contents

Comment S1. Spin-Orbit Coupling and Spin Magnetization Directions in IrF_6^-: Implications for Electronic Configuration and Symmetry in 2c DFT[1]

In single-determinant, two-component density functional theory and for the case of IrF_6^-, spin-orbit coupling (SOC) in the presence of symmetry leads to the splitting of scalar relativistic orbitals with t_{2g} symmetry (threefold degenerate) into a fourfold degenerate spinor ($f_{(3/2)g}$) and a higher-lying twofold degenerate spinor ($e_{(5/2)g}$). This results in the stabilization of a Kramers-restricted pseudo-closed-shell solution, as the four d-electrons can occupy the $f_{(3/2)g}$ spinor. However, in the context of Kramers-unrestricted solution (pseudo-triplet), the question remains on how to position the two unpaired electrons. One possibility is to place two unpaired electrons into $f_{(3/2)g}$ and the remaining two into $e_{(5/2)g}$. This could lead to a situation akin to single-component occupation where the Aufbau principle is violated but symmetry is preserved. As another possibility, three electrons can be placed into $f_{(3/2)g}$ and the last electron into $e_{(5/2)g}$. However, this scenario leads to an occupation that can be identified as having broken symmetry. The energies of both configurations calculated using 2c-X2C are summarized in Table S3. Interestingly, the $(f_{(3/2)g})^2(e_{(5/2)g})^2$ configuration is about 22–27 kJ/mol above the Kramers-restricted $(f_{(3/2)g})^4$, while $(f_{(3/2)g})^3$ $(e_{(5/2)g})^1$ is around 7 kJ/mol below $(f_{(3/2)g})^4$. However, due to the broken-symmetry character of this state, we cannot consider it a physically acceptable solution. Similar observations were noted earlier for PtF_6.[2]

Typically, in the case of pseudo-triplets (for variational inclusion of SOC in 2c-DFT computations), we test various directions of the spin magnetization (directly related to the projection of spin on a chosen axis), as the energy may depend on the direction of this projection (for 1c scalar-relativistic calculations, the energies of all projections are degenerate). Interestingly, in this case, the rotation of spin magnetization leads to a significant energy reduction and a spin magnetization oriented along one of the C_2 axes (in a plane bisecting the angle between two PtF bonds) in D_{4h} symmetry (in our case, we used the x and y coordinate axes) results in an energy below the Kramers-restricted closed-shell configuration. However, upon closer analysis of properties of the solutions in specific cases, we concluded that solutions obtained through the rotation of spin magnetization can exhibit broken-symmetry character and thus will not be considered in the further discussion.

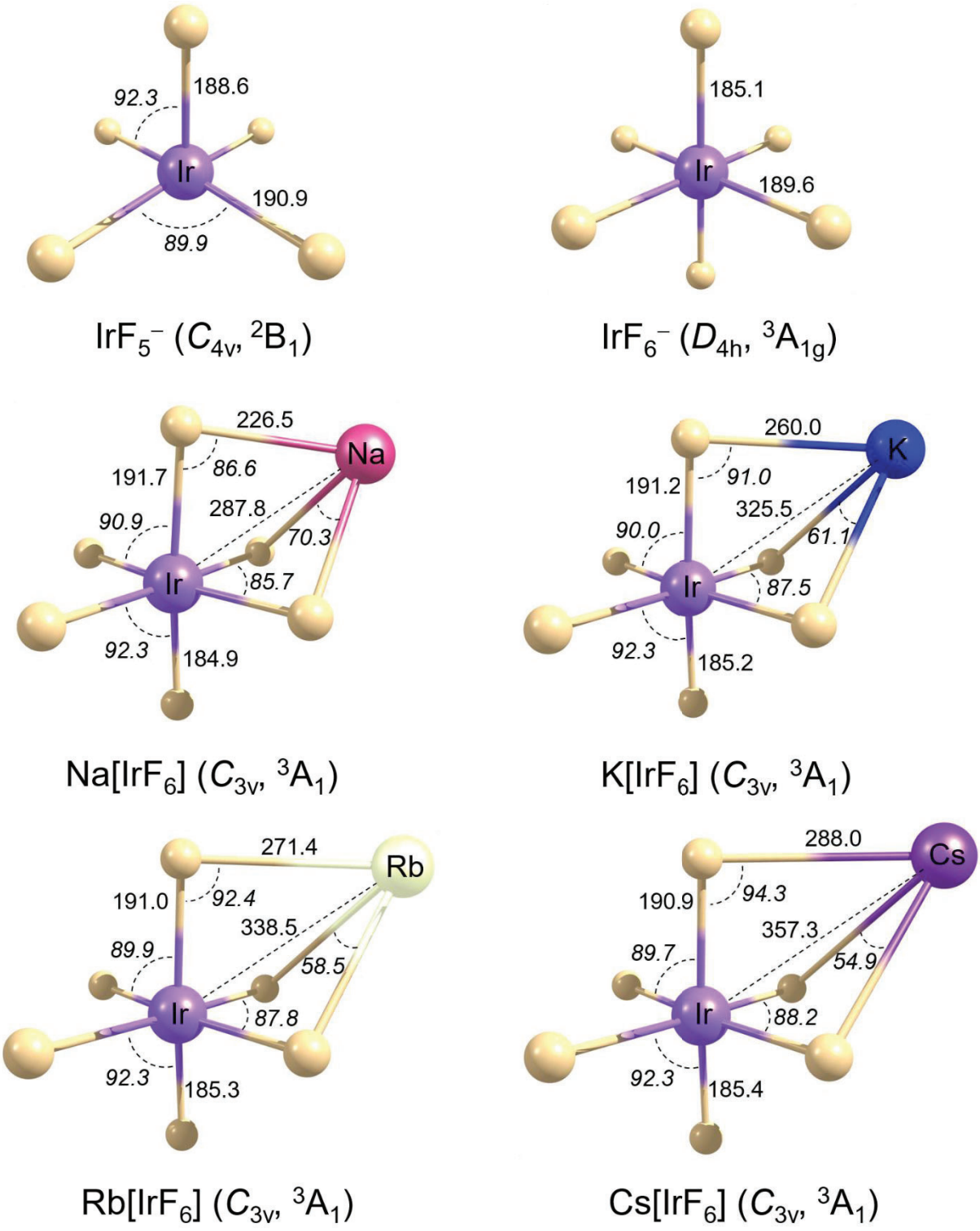

Figure S1. Structures of the M[IrF_6] ion pairs (M = Na, K, Rb, Cs) in C_{3v} symmetry and the free anions IrF_6^- and IrF_5^- in their ground states obtained at the 1c-X2C-PBE0-D3(BJ)/x2c-TZVPall-2c (M[IrF_6]) and 1c-X2C-PBE0/x2c-TZVPall-2c (free anions) levels. Selected bond lengths (pm) and angles (°, in *italics*) are shown.

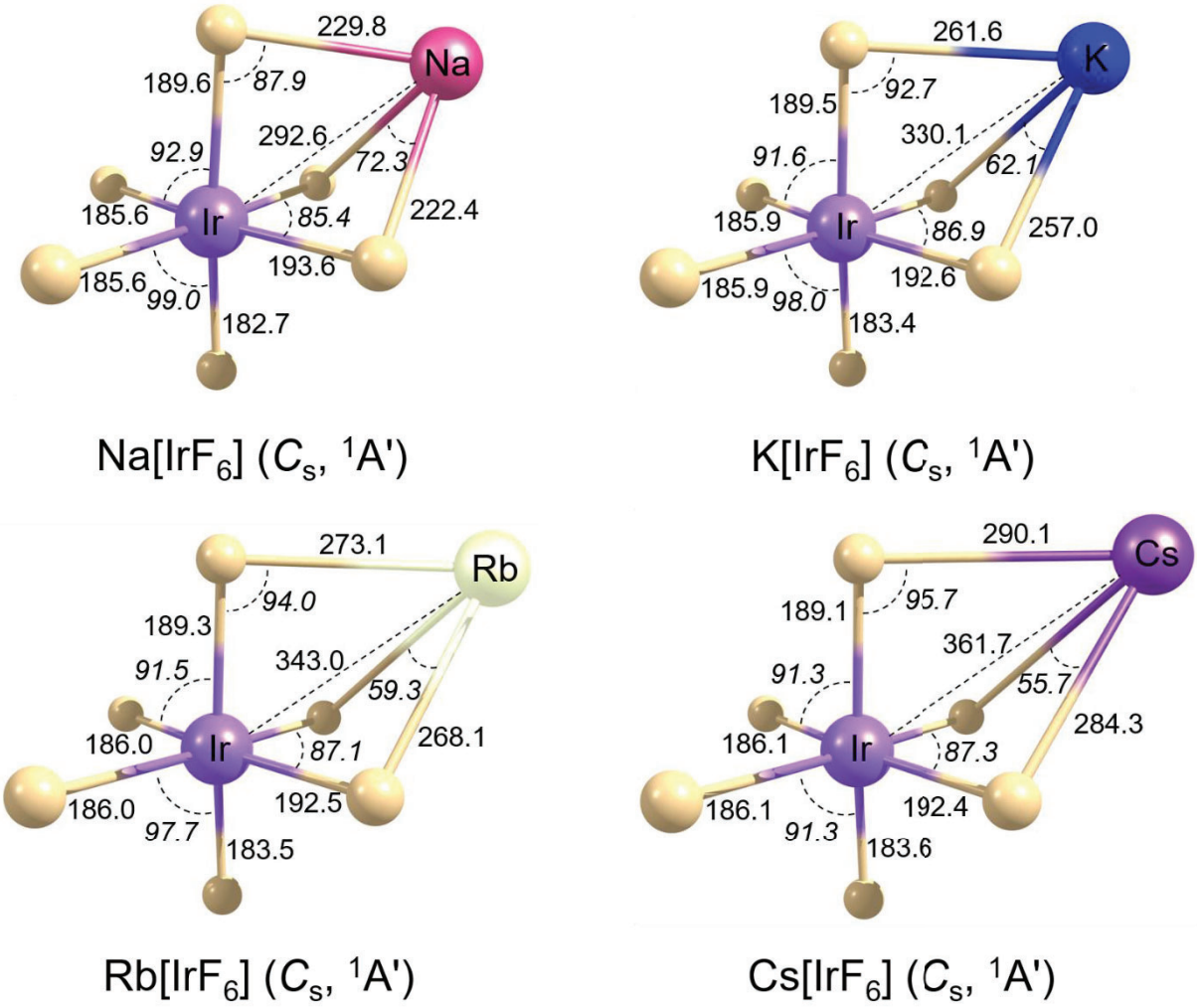

Figure S2. Structures of the M[IrF_6] ion pairs (M = Na, K, Rb, Cs) in the lowest singlet states obtained at the 1c-X2C-PBE0-D3(BJ)/x2c-TZVPall-2c level. Selected bond lengths (pm) and angles (°, in *italics*) are shown.

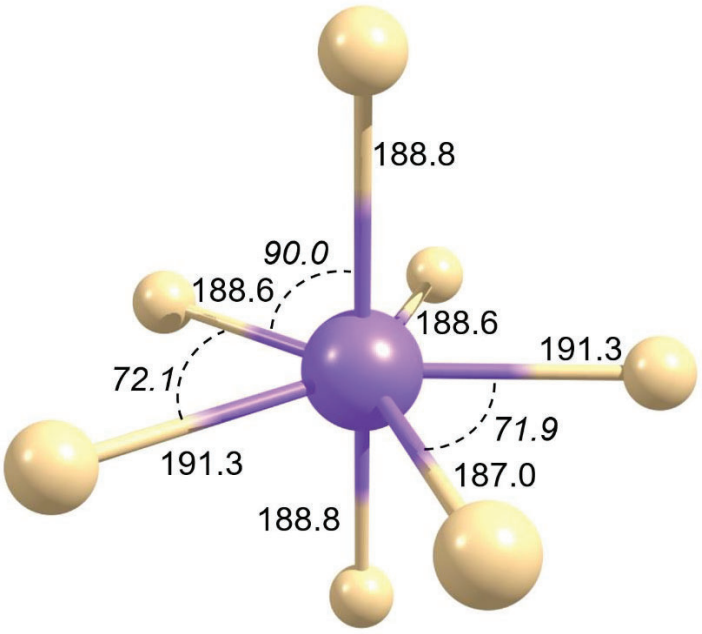

IrF_7^- (C_{2v}, $^2B_1$)

Figure S3. Structure of the IrF_7^- anion obtained at the 1c-X2C-PBE0/x2c-TZVPall-2c level. Selected bond lengths (pm) and angles (°, in *italics*) are shown.

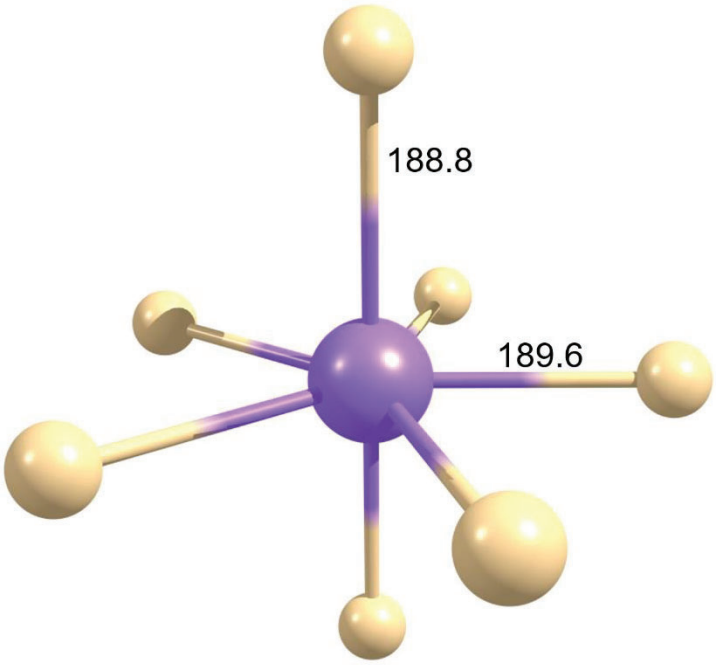

IrF_7^- (D_{5h}, pseudo-$^2E_1$")

Figure S4. Structure of the IrF_7^- anion obtained at the 2c-X2C-PBE0/x2c-TZVPall-2c level. Selected bond lengths (pm) and angles (°, in *italics*) are shown.

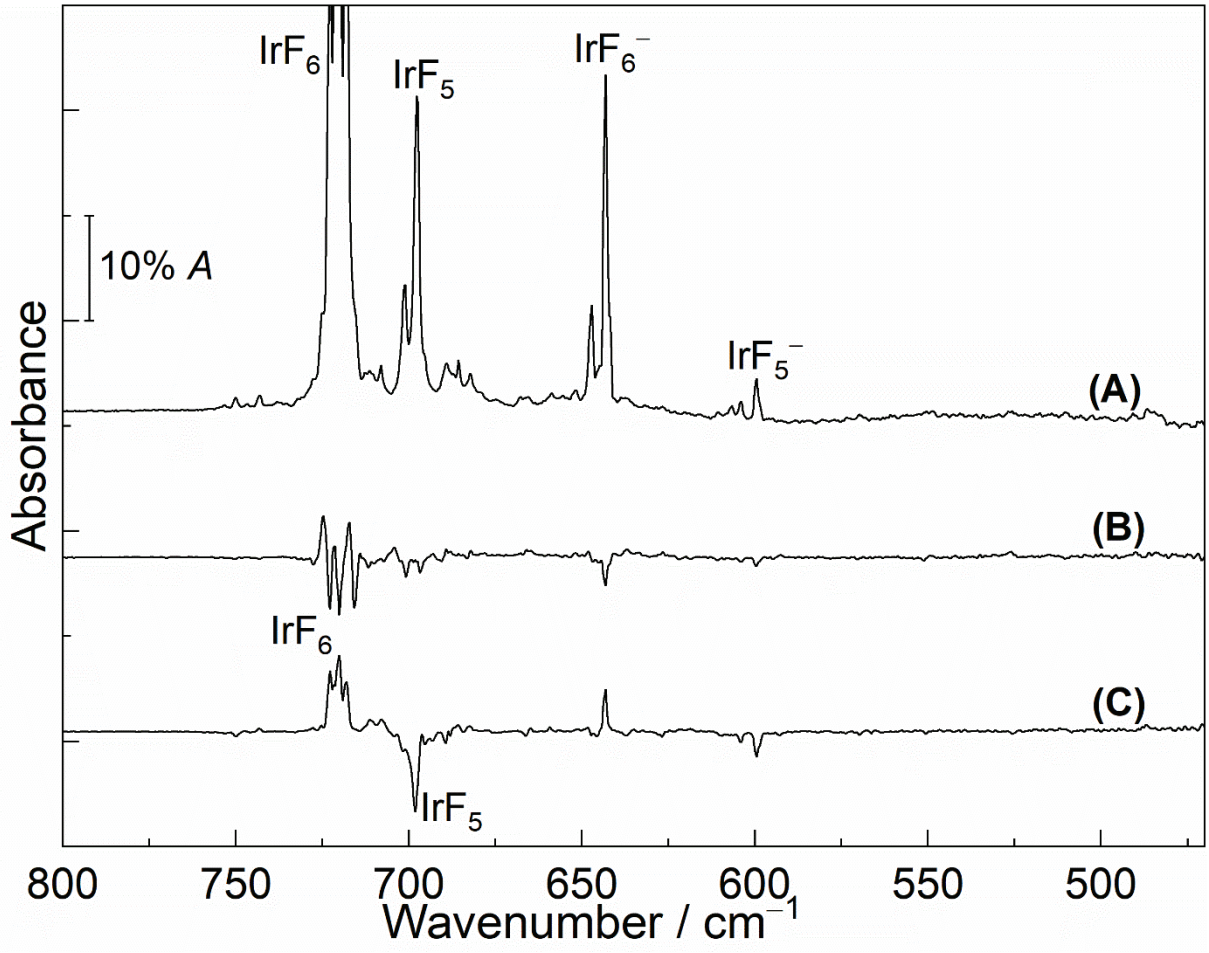

Figure S5. IR spectra of neon matrices at 5 K. (A) Spectrum of the reaction products from laser ablation of Pt with IrF_6. (B) Difference IR spectrum obtained after annealing to 9 K and (C) subsequent LED irradiation (λ = 656 nm) for 20 min.

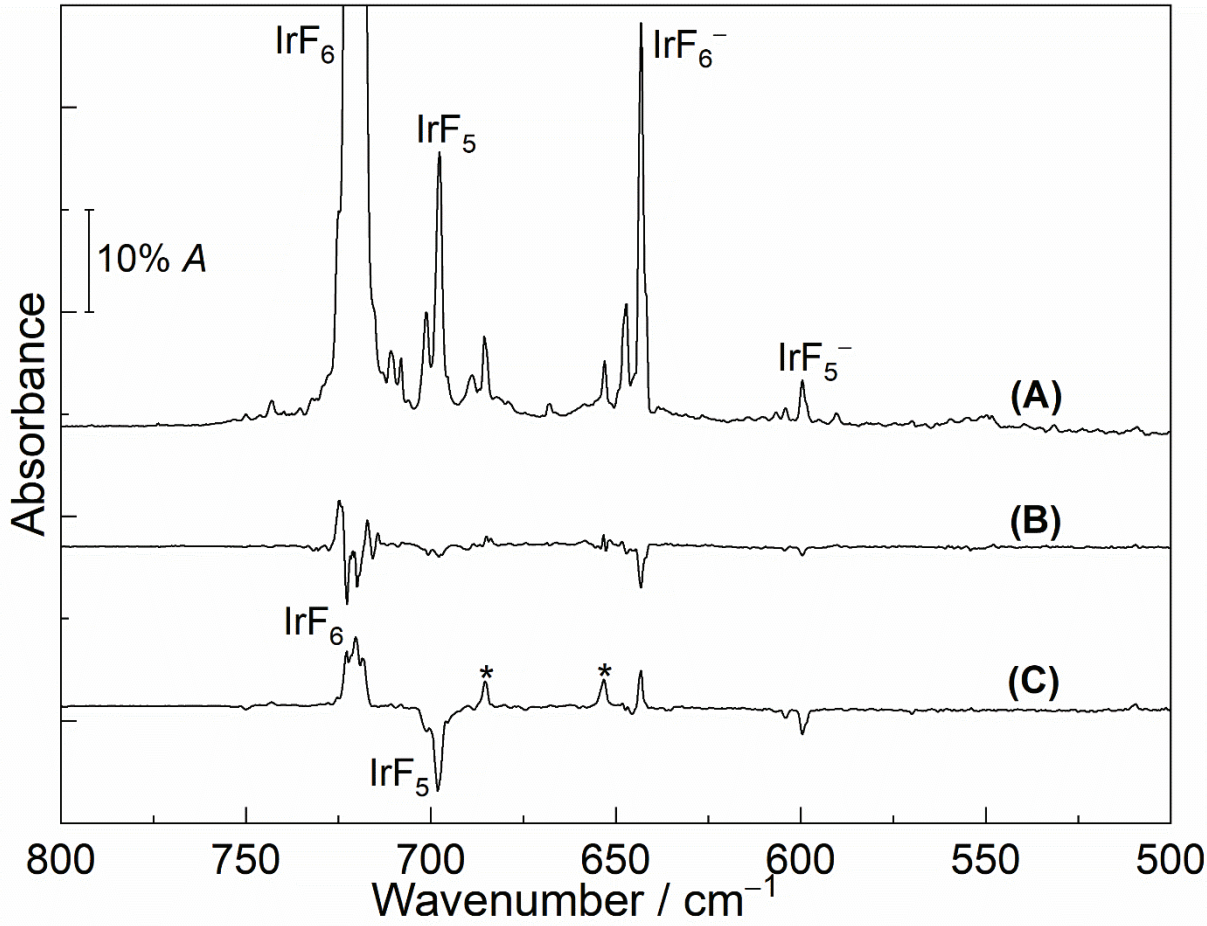

Figure S6. IR spectra of neon matrices at 5 K. (A) IR spectrum of the reaction products from laser ablation of Ir with IrF_6. (B) Difference IR spectrum obtained after annealing to 9 K and (C) subsequent LED irradiation (λ = 656 nm) for 20 min. The bands marked with asterisks are assigned to unknown impurities.

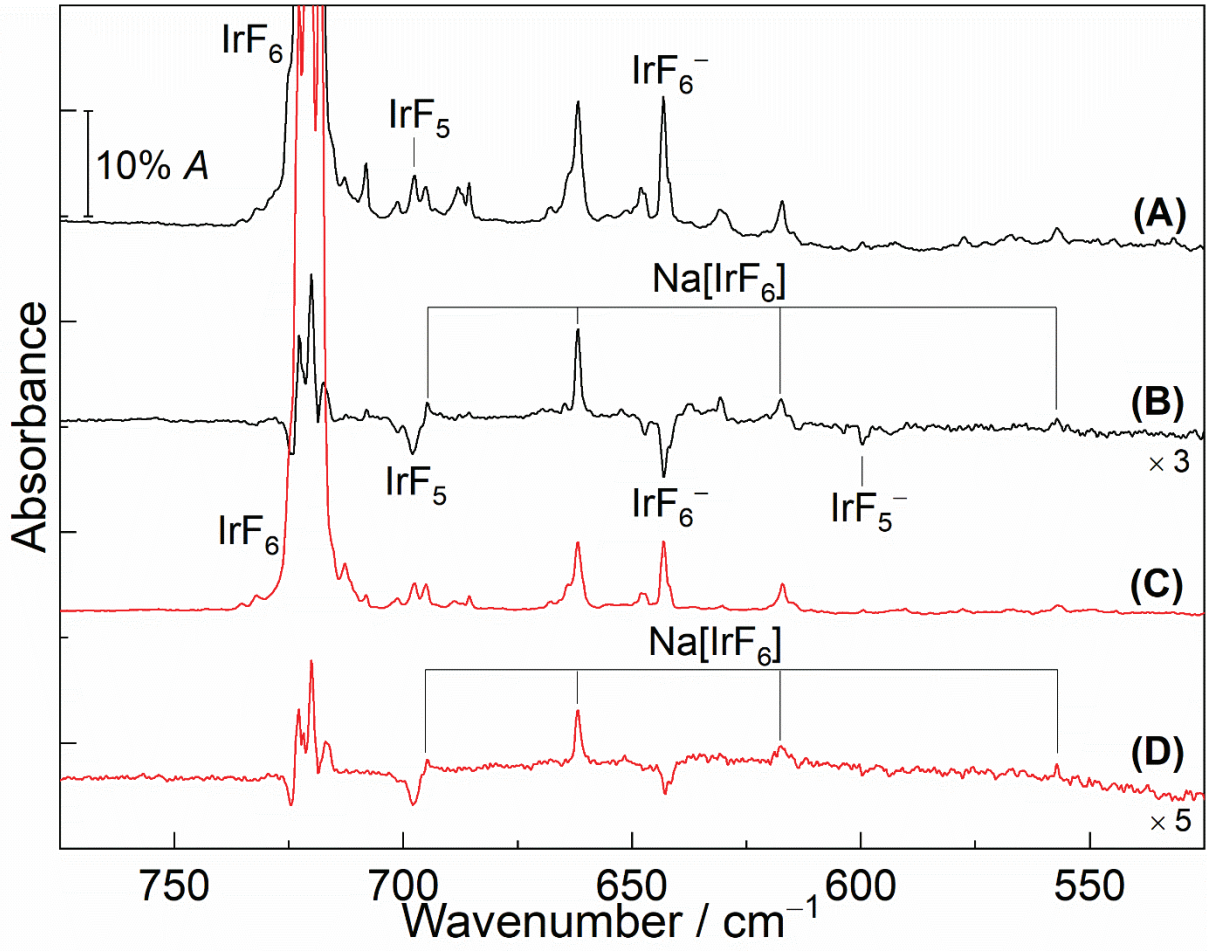

Figure S7. IR spectra of neon matrices at 5 K. (A) IR spectrum of reaction products of laser-ablated NaF with IrF_6. (B) Difference IR spectrum obtained after LED irradiation ($\lambda = 656$ nm) for 30 min. (C) IR spectrum of reaction products of laser-ablated NaCl with IrF_6. (D) Difference IR spectrum obtained after LED irradiation ($\lambda = 656$ nm) for 30 min.

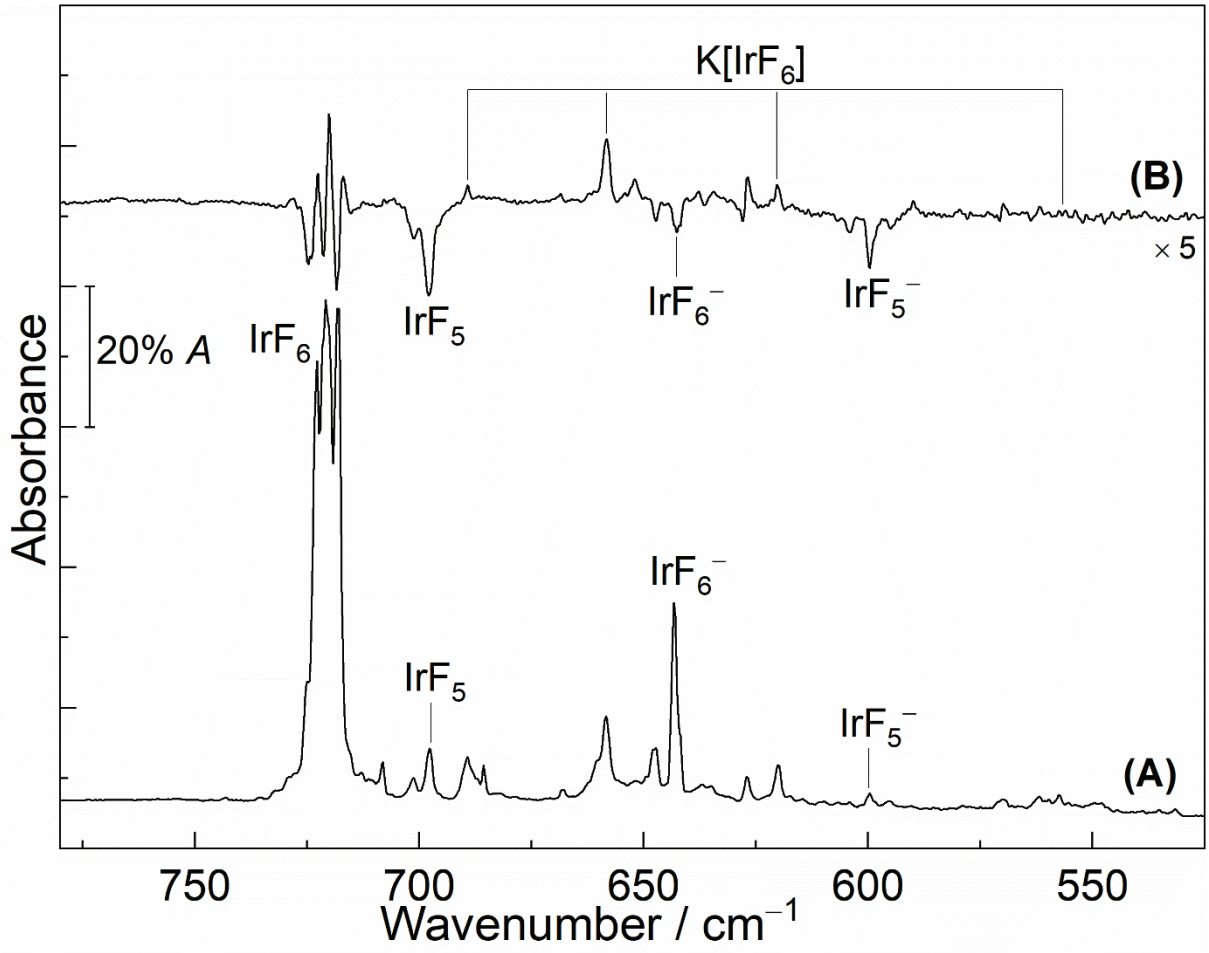

Figure S8. IR spectra of neon matrices at 5 K. (A) Spectrum of reaction products of laser-ablated KF with IrF_6. (B) Difference IR spectrum obtained after LED irradiation (λ = 656 nm) for 35 min.

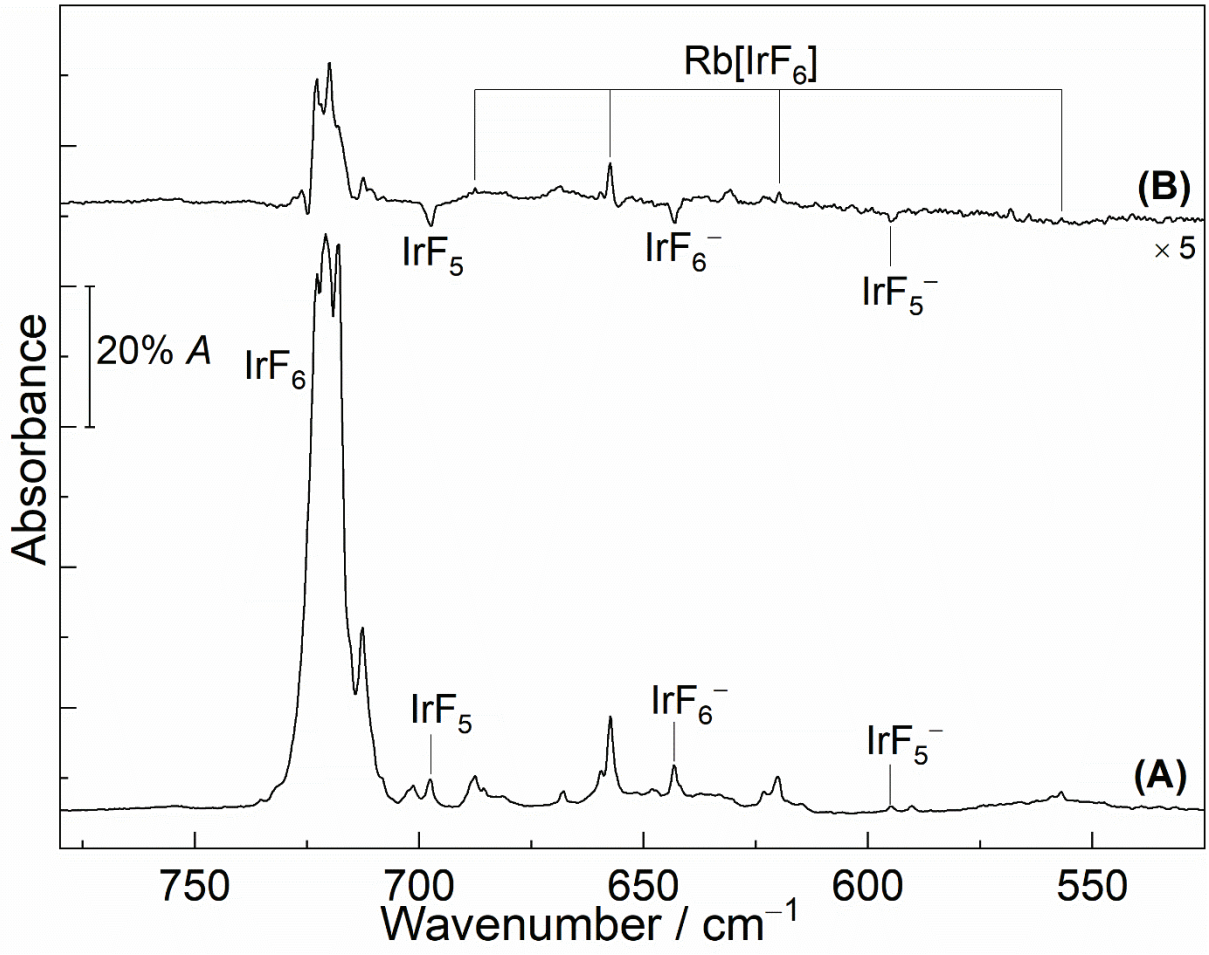

Figure S9. IR spectra of neon matrices at 5 K. (A) Spectrum of reaction products of laser-ablated RbF with IrF_6. (B) Difference IR spectrum obtained after LED irradiation (λ = 656 nm) for 35 min.

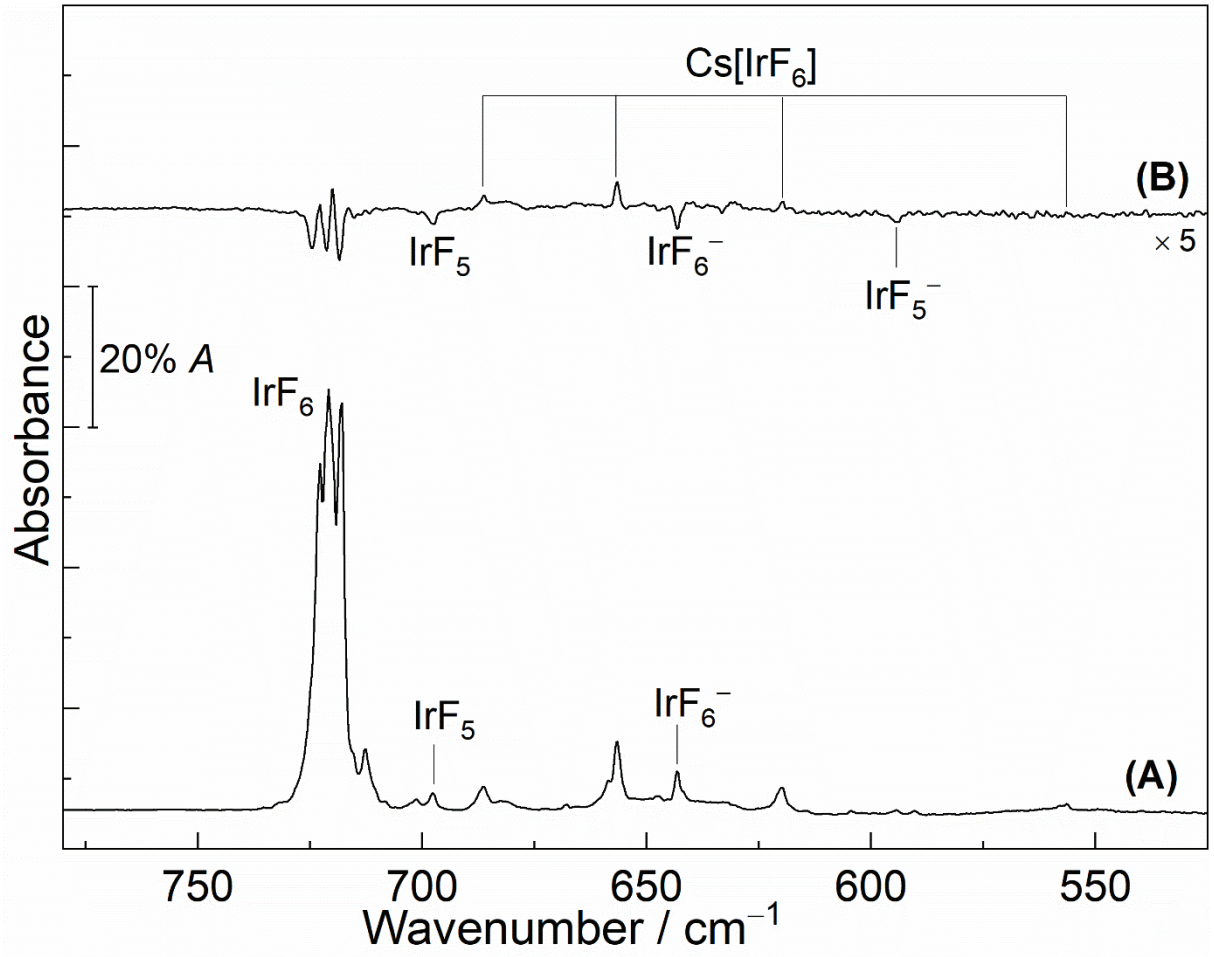

Figure S10. IR spectra of neon matrices at 5 K. (A) Spectrum of reaction products of laser-ablated CsF with IrF_6. (B) Difference IR spectrum obtained after LED irradiation (λ = 656 nm) for 25 min.

Table S1. Electronic energy differences ($\Delta E + \Delta$ZPE, kJ mol^{-1}) of doublet and quartet states of IrF_5^- at one- and two-component all-electron X2C levels.

	Electronic states (Sym.)	1c-X2C[a] B3LYP	PBE0	2c-X2C[a] B3LYP	PBE0
IrF_5^-	$^2B_1$ (C_{4v})	0.0	0.0	–[b]	–[b]
	$^4B_1$ (C_{2v})	26.1	24.3	–[b]	–[b]

[a] x2c-TZVPall-2c basis sets. [b] 2c-X2C computations did not converge for a quartet 1c-X2C guess. Comparison of doublet and quartet configurations is not possible.

Table S2. Electronic energy differences ($\Delta E + \Delta$ZPE, kJ mol^{-1}) of singlet and triplet states of IrF_6^- at one-component all-electron X2C levels.

	Electronic states (Sym.)	1c-X2C[a] B3LYP	PBE0
IrF_6^-	$^1A_{1g}$ (D_{4h})	99.4	107.0
	$^3A_{1g}$ (D_{4h})	0.0	0.0

[a] x2c-TZVPall-2c basis sets.

Table S3. Electronic energy differences ($\Delta E + \Delta$ZPE, kJ mol^{-1}) of singlet and triplet states of IrF_6^- at two-component all-electron X2C levels.

	Electronic states	symmetry	Spin magn.	2c-X2C[a] B3LYP	PBE0
IrF_6^-	pseudo-$^1A_{1g}$	O_h		0.0	0.0
	Pseudo-triplet	D_{2h}	X (BS)	–4.5	–7.3
		D_{2h}	Y (BS)	–4.5	–7.4
		D_{4h}	Z	26.8	22.0
		D_{4h}	Z (BS)	–4.6	–7.4

[a] x2c-TZVPall-2c basis sets.

Table S4. Calculated IR frequencies of IrF_5^- at 1c- and 2c-X2C levels.[a]

Species	Sym.[b]	1c-X2C[c] (C_{4v}, $^2B_1$)		2c-X2C[c] (C_{4v}, pseudo-$^2B_1$)	
		B3LYP	PBE0	B3LYP	PBE0
	a_1	644.6 (23)	671.9 (26)	560.9 (47)	589.1 (46)
	a_1	616.5 (8)	639.7 (8)	619.2 (6)	644.8 (8)
	e	588.5 (249)	606.5 (261)	585.8 (238)	604.1 (250)
	e	588.5 (249)	606.5 (261)	584.8 (239)	603.2 (251)
	b_2	563.5 (0)	584.4 (0)	544.6 (0)	565.0 (1)
IrF_5^-	a_1	246.8 (15)	255.1 (16)	231.5 (8)	238.6 (8)
	b_1	228.6 (0)	232.5 (0)	229.2 (9)	236.2 (9)
	e	219.2 (13)	224.3 (13)	218.1 (21)	228.5 (20)
	e	219.2 (13)	224.3 (13)	214.3 (1)	220.0 (0)
	b_2	194.8 (0)	203.4 (0)	166.5 (0)	175.2 (0)
	e	66.9 (4)	78.9 (4)	97.3 (4)	106.8 (4)
	e	66.9 (4)	78.9 (4)	91.1 (5)	100.3 (4)

[a] Frequencies in cm^{-1}, intensities are shown in parentheses in km mol^{-1}. [b] Symmetry species for the C_{4v} symmetry. [c] x2c-TZVPall-2c basis sets.

Table S5. Calculated IR frequencies of IrF_6^- anion in triplet ground state at 1c-X2C level.[a]

Species	Sym.	1c-X2C	
		B3LYP[b]	PBE0[b]
IrF_6^- (D_{4h},$^3A_{1g}$)	a_{1g}	656.7 (0)	683.0 (0)
	a_{2u}	657.6 (240)	677.7 (256)
	e_u	620.6 (216)	641.0 (229)
	e_u	620.6 (216)	641.0 (229)
	b_{1g}	596.6 (0)	620.6 (0)
	a_{1g}	584.5 (0)	606.7 (0)
	e_u	279.2 (7)	286.7 (7)
	e_u	279.2 (7)	286.7 (7)
	a_{2u}	243.3 (21)	249.0 (21)
	e_g	239.1 (0)	243.6 (0)
	e_g	239.1 (0)	243.6 (0)
	e_u	222.4 (2)	228.8 (2)
	e_u	222.4 (2)	228.8 (2)
	b_{2u}	186.8(0)	192.2 (0)
	b_{2g}	187.4 (0)	190.8 (0)

[a] Frequencies in cm^{-1}, intensities are shown in parentheses in km mol^{-1}. [b] x2c-TZVPall-2c basis sets.

Table S6. Calculated IR frequencies of IrF_6^- anion in Kramers-restricted nondegenerate ground state at 2c-X2C level.[a]

Species	2c-X2C[b]	
	B3LYP	PBE0
IrF_6^- (O_h, pseudo-$^1A_{1g}$)	645.5 (0)	672.0 (0)
	632.0 (217)	653.5 (228)
	631.2 (219)	652.1 (233)
	630.8 (220)	651.5 (233)
	565.8 (0)	589.6 (0)
	562.1 (0)	585.3 (0)
	267.8 (10)	273.9 (10)
	265.9 (10)	272.9 (10)
	262.8 (11)	270.0 (11)
	233.2 (0)	239.0 (0)
	232.4 (0)	238.1 (0)
	230.9 (0)	236.6 (0)
	217.3 (0)	225.7 (0)
	216.0 (0)	223.6 (0)
	214.4 (0)	222.1 (0)

[a] Frequencies in cm^{-1}, intensities are shown in parentheses in km mol^{-1}. [b] x2c-TZVPall-2c basis sets.

Table S7. Calculated IR frequencies of IrF_7^- anion at 1c-X2C level.[a]

Species	Sym.	1c-X2C[b]	
		B3LYP	PBE0
	b_1	637.2 (195)	659.6 (211)
	a_1	634.8 (1)	662.7 (1)
	a_1	626.6 (159)	650.2 (171)
	b_2	604.2 (144)	626.6 (155)
	a_1	594.9 (0)	619.5 (0)
	a_1	522.0 (0)	543.1 (0)
	b_2	505.2 (0)	520.6 (0)
	a_1	438.2 (0)	453.6 (0)
IrF_7^-	b_2	428.5 (0)	442.8 (0)
(C_{2v}, $^2B_1$)	a_1	323.9 (15)	334.8 (15)
	b_2	321.9 (12)	337.0 (11)
	b_1	300.8 (6)	309.4 (6)
	b_2	251.5 (0)	265.7 (0)
	b_1	232.8 (0)	238.1 (0)
	a_1	212.5 (4)	218.6 (5)
	a_2	204.6 (0)	214.8 (0)
	a_2	95.4 (0)	100.9 (0)
	b_1	90.7 (1)	96.1 (1)

[a] Frequencies in cm^{-1}, intensities are shown in parentheses in km mol^{-1}. [b] x2c-TZVPall-2c basis sets.

Table S8. Calculated IR frequencies of IrF_7^- anion at 2c-X2C level.[a]

Species	2c-X2C[b]	
	B3LYP	PBE0
	635.6 (198)	658.1 (188)
	629.2 (1)	656.6 (26)
	606.8 (153)	632.1 (163)
	605.6 (153)	630.7 (163)
	584.6 (0)	610.6 (0)
	504.7 (0)	524.0 (0)
	503.0 (0)	523.6 (0)
	428.3 (0)	446.1 (0)
IrF_7^-	427.1 (0)	445.0 (0)
(D_{5h}, pseudo-$^2E_1$")	320.0 (16)	332.9 (14)
	318.9 (16)	331.4(14)
	297.7 (6)	306.5 (6)
	232.3 (1)	239.3 (1)
	231.0 (1)	238.7 (1)
	218.5 (0)	222.6 (0)
	217.7 (0)	222.2 (0)
	103.7 (0)	108.5 (0)
	100.8 (0)	106.7 (0)

[a] Frequencies in cm^{-1}, intensities are shown in parentheses in km mol^{-1}. [b] x2c-TZVPall-2c basis sets.

Table S9. Calculated IR frequencies of Na[IrF_6] in singlet state at 1c- and 2c-X2C levels.[a]

Species	1c-X2C-PBE0-D3(BJ)[b] (^{1}A', C_s)		2c-X2C-PBE0-D3(BJ)[b] (pseudo-$^1A_{1g}$, C_{3v})	
	Sym.	Freq. (Int.)	Sym.	Freq. (Int.)
Na[IrF_6]	a'	710.8 (72)	a_1	713.4 (76)
	a'	700.6 (147)	a_1	683.2 (156)
	a"	631.0 (207)	a_1	682.1(154)
	a'	620.6 (137)	a_1	619.9 (148)
	a'	525.6 (47)	a_1	567.6 (54)
	a"	499.8 (3)	a_1	566.4 (53)
	a'	349.0 (48)	a_1	338.2 (58)
	a"	302.4 (0)	a_1	273.3 (9)
	a'	291.3 (0)	a_1	271.1 (10)
	a"	274.7 (8)	a_1	265.1 (3)
	a'	260.0 (20)	a_1	264.2 (2)
	a"	249.8 (4)	a_1	263.0 (5)
	a'	243.1 (10)	a_1	226.9 (0)
	a'	207.0 (2)	a_1	224.7 (0)
	a'	178.7 (18)	a_1	217.2 (23)
	a"	154.8 (12)	a_1	207.1 (0)
	a"	131.3 (9)	a_1	131.4 (9)
	a'	90.8 (7)	a_1	128.5 (9)

[a] Frequencies in cm^{-1}, intensities are shown in parentheses in km mol^{-1}. [b] x2c-TZVPall-2c basis sets.

Table S10. Calculated IR frequencies of K[IrF_6] in singlet state at 1c- and 2c-X2C levels.[a]

Species	1c-X2C-PBE0-D3(BJ)[b] (^{1}A', C_s)		2c-X2C-PBE0-D3(BJ)[b] (pseudo-$^1A_{1g}$, C_{3v})	
	Sym.	Freq. (Int.)	Sym.	Freq. (Int.)
K[IrF_6]	a'	704.2 (67)	a_1	707.4 (78)
	a'	690.1 (166)	a_1	675.3 (168)
	a"	634.4 (204)	a_1	673.6 (169)
	a'	623.7 (157)	a_1	622.5 (167)
	a'	524.0 (34)	a_1	564.0 (41)
	a"	492.7 (1)	a_1	561.9 (38)
	a'	322.9 (28)	a_1	311.2 (43)
	a"	295.2 (3)	a_1	267.3 (11)
	a"	281.8 (3)	a_1	266.0 (11)
	a'	279.1(10)	a_1	255.9 (0)
	a'	247.6 (12)	a_1	255.1 (1)
	a"	246.8 (3)	a_1	250.6 (1)
	a'	235.4 (12)	a_1	225.6 (0)
	a'	182.3 (1)	a_1	224.6 (0)
	a'	157.3 (26)	a_1	209.8 (0)
	a"	143.8 (3)	a_1	166.8 (28)
	a"	112.2 (9)	a_1	103.3 (5)
	a'	78.2 (5)	a_1	100.5 (5)

[a] Frequencies in cm^{-1}, intensities are shown in parentheses in km mol^{-1}. [b] x2c-TZVPall-2c basis sets.

Table S11. Calculated IR frequencies of Rb[IrF_6] in singlet state at 1c- and 2c-X2C levels.[a]

Species	1c-X2C-PBE0-D3(BJ)[b] (^{1}A', C_s)		2c-X2C-PBE0-D3(BJ)[b] (pseudo-$^1A_{1g}$, C_{3v})	
	Sym.	Freq. (Int.)	Sym.	Freq. (Int.)
Rb[IrF_6]	a'	703.4 (71)	a_1	706.4 (81)
	a'	689.0 (164)	a_1	674.3 (167)
	a"	634.2 (200)	a_1	672.7 (167)
	a'	624.8 (165)	a_1	623.2 (175)
	a'	523.7 (31)	a_1	563.8 (38)
	a"	491.3 (1)	a_1	562.6 (35)
	a'	315.2 (23)	a_1	303.5 (39)
	a"	289.8 (2)	a_1	267.4 (10)
	a'	275.9 (10)	a_1	266.2 (11)
	a"	268.7 (4)	a_1	252.0 (0)
	a"	245.7 (3)	a_1	251.0 (0)
	a'	244.0 (8)	a_1	247.3 (0)
	a'	227.9 (11)	a_1	225.6 (0)
	a'	177.1 (6)	a_1	224.5 (0)
	a"	145.9 (4)	a_1	209.7 (0)
	a'	117.4 (18)	a_1	121.1 (18)
	a"	90.7 (4)	a_1	90.3 (2)
	a'	65.5 (2)	a_1	86.2 (2)

[a] Frequencies in cm^{-1}, intensities are shown in parentheses in km mol^{-1}. [b] x2c-TZVPall-2c basis sets.

Table S12. Calculated IR frequencies of Cs[IrF_6] in singlet state at 1c- and 2c-X2C levels.[a]

Species	1c-X2C-PBE0-D3(BJ)[b] (^{1}A', C_s)		2c-X2C-PBE0-D3(BJ)[b] (pseudo-$^1A_{1g}$, C_{3v})	
	Sym.	Freq. (Int.)	Sym.	Freq. (Int.)
Cs[IrF_6]	a'	702.1 (74)	a_1	704.8 (84)
	a'	687.1 (162)	a_1	672.7 (164)
	a"	633.7 (194)	a_1	671.2 (164)
	a'	625.7 (177)	a_1	624.1 (186)
	a'	523.6 (26)	a_1	563.0 (32)
	a"	485.7 (0)	a_1	562.9 (31)
	a'	311.1 (23)	a_1	296.7 (42)
	a"	287.8 (4)	a_1	267.2 (10)
	a'	274.9 (10)	a_1	266.0 (11)
	a"	268.7 (3)	a_1	248.1 (0)
	a"	245.1 (2)	a_1	247.7 (0)
	a'	242.2 (7)	a_1	246.2 (0)
	a'	222.9 (13)	a_1	226.1 (0)
	a'	173.5 (7)	a_1	225.0 (0)
	a"	148.7 (4)	a_1	210.7 (0)
	a'	98.3 (16)	a_1	99.9 (16)
	a"	78.0 (3)	a_1	81.0 (1)
	a'	58.4 (1)	a_1	77.6 (1)

[a] Frequencies in cm^{-1}, intensities are shown in parentheses in km mol^{-1}. [b] x2c-TZVPall-2c basis sets.

Table S13. Calculated electron affinities (EAs) and fluoride ion affinities (FIAs) of IrF_5 ground state and IrF_6 at the 1c-X2C-B3LYP/x2c-TZVPall-2c level.

Species	Calculated	
	EA [eV]	FIA [kJ mol^{-1}][a]
IrF_5	5.84	502.0[b]
IrF_6	6.38[b]	233.3

[a] 2c-X2C-B3LYP/x2c-TZVPall-2c level with additional diffuse basis functions for fluorine. [b] For a triplet ground state of IrF_6^-.

Calculated atomic coordinates (in Å) of species for optimized structures

IrF_5^-

1c-X2C-B3LYP/x2c-TZVPall-2c level

(C_{4v}, $^2B_1$)

Ir	-0.0000000	-0.0000000	0.2618393
F	0.0000000	0.0000000	-1.6448137
F	-1.3610785	1.3610785	0.3457436
F	-1.3610785	-1.3610785	0.3457436
F	1.3610785	-1.3610785	0.3457436
F	1.3610785	1.3610785	0.3457436

(C_{2v}, $^4B_1$)

Ir	0.0000000	0.0000000	0.2624918
F	0.0000000	0.0000000	-1.8082283
F	0.0000000	1.8684298	0.4544026
F	-1.9319942	0.0000000	0.3184656
F	-0.0000000	-1.8684298	0.4544026
F	1.9319942	0.0000000	0.3184656

2c-X2C-B3LYP/x2c-TZVPall-2c level

(C_{4v}, pseudo-$^2B_1$)

Ir	0.0000352	0.0000418	0.2379920
F	-0.0001823	-0.0002322	-1.6763813
F	-1.3629873	1.3649346	0.3596157
F	-1.3630094	-1.3648393	0.3594437
F	1.3630829	-1.3648296	0.3595797
F	1.3630609	1.3649248	0.3597503

1c-X2C-PBE0/x2c-TZVPall-2c level

(C_{4v}, $^2B_1$)

Ir	-0.0000000	0.0000000	0.2627861
F	0.0000000	0.0000000	-1.6234149
F	-1.3486823	1.3486823	0.3401572
F	-1.3486823	-1.3486823	0.3401572
F	1.3486823	-1.3486823	0.3401572
F	1.3486823	1.3486823	0.3401572

(C_{2v}, $^4B_1$)

Ir	0.0000000	0.0000000	0.2624052
F	0.0000000	0.0000000	-1.7827228
F	0.0000000	1.8522520	0.4447711
F	-1.9142289	-0.0000000	0.3153877
F	0.0000000	-1.8522520	0.4447711
F	1.9142289	0.0000000	0.3153877

2c-X2C-PBE0/x2c-TZVPall-2c level

(C_{4v}, pseudo-$^2B_1$)

Ir	-0.0000544	0.0000000	0.2416413
F	0.0003265	-0.0000004	-1.6511726
F	-1.3506578	1.3525413	0.3525039
F	-1.3506587	-1.3525411	0.3525032
F	1.3505227	-1.3525933	0.3522622
F	1.3505218	1.3525935	0.3522620

IrF_6^-

1c-X2C-B3LYP/x2c-TZVPall-2c level

(D_{4h}, $^1A_{1g}$)

Ir	-0.0000000	0.0000000	-0.0000000
F	-1.3195560	1.3195560	0.0000000
F	-0.0000000	0.0000000	-1.9698100
F	-1.3195560	-1.3195560	0.0000000
F	-0.0000000	0.0000000	1.9698100
F	1.3195560	1.3195560	-0.0000000
F	1.3195560	-1.3195560	0.0000000

(D_{4h}, $^3A_{1g}$)

Ir	-0.0000000	-0.0000000	0.0000000
F	-1.3537400	1.3537400	0.0000000
F	-1.3537400	-1.3537400	0.0000000
F	-0.0000000	-0.0000000	1.8684415
F	1.3537400	1.3537400	0.0000000
F	-0.0000000	0.0000000	-1.8684415
F	1.3537400	-1.3537400	0.0000000

1c-X2C-PBE0/x2c-TZVPall-2c level

(D_{4h}, $^1A_{1g}$)

Ir	-0.0000000	-0.0000000	0.0000000
F	-1.3074659	1.3074659	-0.0000000
F	-0.0000000	-0.0000000	-1.9494038
F	-1.3074659	-1.3074659	-0.0000000
F	-0.0000000	-0.0000000	1.9494038
F	1.3074659	1.3074659	-0.0000000
F	1.3074659	-1.3074659	-0.0000000

(D_{4h}, $^3A_{1g}$)

Ir	0.0000000	0.0000000	0.0000000
F	-1.3408118	1.3408118	0.0000000
F	-1.3408118	-1.3408118	0.0000000
F	0.0000000	0.0000000	1.8510469
F	1.3408118	1.3408118	0.0000000
F	0.0000000	0.0000000	-1.8510469
F	1.3408118	-1.3408118	0.0000000

2c-X2C-B3LYP/x2c-TZVPall-2c level

(O_h, pseudo-$^1A_{1g}$)

Ir	-0.0000014	0.0000006	-0.0000006
F	-1.3438468	1.3438238	0.0000006
F	0.0000009	-0.0000005	-1.9004613
F	-1.3438456	-1.3438237	0.0000002
F	0.0000009	-0.0000003	1.9004602
F	1.3438465	1.3438210	0.0000004
F	1.3438454	-1.3438209	0.0000005

(D_{2h}, pseudo-triplet) Spin magnetization direction along X axis (broken symmetry)

Ir	-0.0000009	0.0000004	0.0000005
F	-1.3503474	1.3395761	-0.0000005
F	-1.3503465	-1.3395760	-0.0000002
F	0.0000006	-0.0000003	1.8966982
F	1.3503471	1.3395743	-0.0000002
F	0.0000007	-0.0000003	-1.8966972
F	1.3503463	-1.3395743	-0.0000006

(D_{2h}, pseudo-triplet) Spin magnetization direction along Y axis (broken symmetry)

Ir	-0.0000010	0.0000004	0.0000005
F	-1.3395956	1.3503242	-0.0000005
F	-1.3395949	-1.3503240	-0.0000002
F	0.0000004	-0.0000003	1.8967037
F	1.3395956	1.3503222	-0.0000002
F	0.0000006	-0.0000004	-1.8967026
F	1.3395949	-1.3503220	-0.0000006

(D_{4h}, pseudo-triplet) Spin magnetization direction along Z axis (broken symmetry)

Ir	-0.000000851975	0.000000354549	0.000000428634
F	-1.341630332483	1.341580817372	-0.000000444509
F	-1.341629565176	-1.341580690369	-0.000000153461
F	0.000000502718	-0.000000254005	1.906577874679
F	1.341630173730	1.341578997002	-0.000000190504
F	0.000000597970	-0.000000291047	-1.906576985661
F	1.341629469924	-1.341578933501	-0.0000005344

(D_{4h}, pseudo-triplet) Spin magnetization direction along Z axis

Ir	0.0000004	0.0000001	-0.0000005
F	-1.9117322	0.0000001	0.0000000
F	0.0000001	-1.9117399	0.0000002
F	-0.0000005	-0.0000002	1.8790067
F	0.0000002	1.9117398	0.0000002
F	-0.0000005	-0.0000002	-1.8790065
F	1.9117324	0.0000002	0.0000000

2c-X2C-PBE0/x2c-TZVPall-2c level

(O_h, pseudo-$^1A_{1g}$)

Ir	-0.0000015	0.0000005	-0.0000006

F -1.3310089 1.3309865 0.0000005

F 0.0000009 -0.0000004 -1.8824080

F -1.3310079 -1.3309864 0.0000003

F 0.0000009 -0.0000004 1.8824069

F 1.3310087 1.3309835 0.0000003

F 1.3310078 -1.3309834 0.0000005

(*D_{2h}*, pseudo-triplet) Spin magnetization direction along X axis (broken symmetry)

Ir -0.0000008 0.0000004 0.0000005

F -1.3393361 1.3255852 -0.0000005

F -1.3393353 -1.3255851 -0.0000002

F 0.0000005 -0.0000002 1.8776854

F 1.3393359 1.3255835 -0.0000002

F 0.0000006 -0.0000002 -1.8776844

F 1.3393351 -1.3255835 -0.0000006

(*D_{2h}*, pseudo-triplet) Spin magnetization direction along Y axis (broken symmetry)

Ir -0.0000009 0.0000003 0.0000005

F -1.3256110 1.3393113 -0.0000005

F -1.3256103 -1.3393111 -0.0000002

F 0.0000004 -0.0000003 1.8776846

F 1.3256109 1.3393094 -0.0000002

F 0.0000005 -0.0000004 -1.8776836

F 1.3256103 -1.3393092 -0.0000006

(*D_{4h}*, pseudo-triplet) Spin magnetization direction along Z axis (broken symmetry)

Ir -0.000000752971 0.000000306530 0.000000391806

F -1.328267499439 1.328491260895 -0.000000401102

F -1.328266827393 -1.328491144248 -0.000000152524

F	0.000000468643	-0.000000227017	1.889767926263
F	1.328267340116	1.328489654431	-0.000000185801
F	0.000000544859	-0.000000254518	-1.889767106802
F	1.328266726184	-1.328489596073	-0.00000047183

(D_{4h}, pseudo-triplet) Spin magnetization direction along Z axis

Ir	0.0000004	0.0000001	-0.0000003
F	-1.8937638	0.0000001	0.0000001
F	0.0000000	-1.8937715	0.0000002
F	-0.0000004	-0.0000002	1.8601826
F	0.0000001	1.8937715	0.0000002
F	-0.0000004	-0.0000001	-1.8601830
F	1.8937640	0.0000001	0.0000001

IrF_7^-

1c-X2C-B3LYP/x2c-TZVPall-2c level

(C_{2v}, $^2B_1$)

Ir	0.000000000	0.000000000	0.000167500
F	0.000000000	-1.907310700	-0.001037900
F	0.000000000	0.000000000	1.889682200
F	-1.837419400	0.000000000	0.599251100
F	0.000000000	1.907310700	-0.001037900
F	-1.118250400	0.000000000	-1.543138100
F	1.118250400	0.000000000	-1.543138100
F	1.837419400	0.000000000	0.599251100

1c-X2C-PBE0/x2c-TZVPall-2c level

(C_{2v}, $^2B_1$)

Ir	0.000000000	0.000000000	0.000335000

F	0.000000000	-1.888221800	-0.001155400
F	0.000000000	0.000000000	1.870127500
F	-1.819066700	0.000000000	0.593166800
F	0.000000000	1.888221800	-0.001155400
F	-1.106982800	0.000000000	-1.527242600
F	1.106982800	0.000000000	-1.527242600
F	1.819066700	0.000000000	0.593166800

2c-X2C-B3LYP/x2c-TZVPall-2c level

(D_{5h}, pseudo-$^2E_1$")

Ir	0.000000200	0.000001100	-0.000132700
F	-0.000000300	-1.907205300	-0.000185000
F	0.000000100	-0.000189300	1.916253500
F	-1.821875100	0.000179300	0.592184300
F	0.000000100	1.907201700	-0.000183200
F	-1.126320600	-0.000099000	-1.550060800
F	1.126320300	-0.000018600	-1.550060500
F	1.821875300	0.000130000	0.592184500

2c-X2C-PBE0/x2c-TZVPall-2c level

(D_{5h}, pseudo-$^2E_1$")

Ir	-0.035374100	-0.086976000	0.054842400
F	-0.025020100	-1.975026400	0.061239000
F	0.143051300	-0.080034100	1.942708400
F	-1.775483200	-0.093659800	0.807686500
F	-0.045701500	1.801076000	0.048520300
F	-1.289026600	-0.098417400	-1.367835000
F	0.930137100	-0.087671200	-1.577041000

F 1.815088900 -0.075090400 0.468648600

Na[IrF_6]

1c-X2C-PBE0-D3(BJ)/x2c-TZVPall-2c level

(^{1}A', C_s)

Ir -0.2414221 -0.3892585 0.0000000

F 1.6414987 -0.1701502 0.0000000

F -0.1470691 1.0298492 1.3128967

F -0.1470691 1.0298492 -1.3128967

F -2.0435539 -0.0869870 0.0000000

F -0.1780641 -1.7574738 -1.2529844

F -0.1780641 -1.7574738 1.2529844

Na 1.2937437 2.1016448 0.0000000

($^3A_1$, C_{3v})

Ir 0.0000000 0.0000000 0.4203707

F -0.7527746 1.3038438 -0.7655899

F -0.7527746 -1.3038438 -0.7655899

F 1.5055491 0.0000000 -0.7655899

F 0.7694213 -1.3326768 1.4446623

F 0.7694213 1.3326768 1.4446623

F -1.5388426 0.0000000 1.4446623

Na -0.0000000 0.0000000 -2.4575880

2c-X2C-PBE0-D3(BJ)/x2c-TZVPall-2c level

(C_{3v}, pseudo-$^1A_1$)

Ir -0.2451885 -0.3534009 -0.0000026

F 1.6671150 -0.2008689 -0.0000037

F -0.1651485 1.0672567 1.2864605

F -0.1651561 1.0672649 -1.2864605

F -2.0956133 -0.3379298 0.0000035

F -0.2072782 -1.6443011 -1.3253879

F -0.2072970 -1.6442987 1.3253915

Na 1.4185667 2.0462778 -0.0000010

K[IrF_6]

1c-X2C-PBE0-D3(BJ)/x2c-TZVPall-2c level

(^{1}A', C_s)

Ir -0.2639040 -0.4090722 0.0000000

F 1.6233371 -0.2393000 0.0000000

F -0.2008833 0.9877577 1.3248955

F -0.2008833 0.9877577 -1.3248955

F -2.0805437 -0.1565688 0.0000000

F -0.1938985 -1.7722348 -1.2622981

F -0.1938985 -1.7722348 1.2622981

K 1.5106744 2.3738952 0.0000000

(^{3}A_1, C_{3v})

Ir 0.0000000 0.0000000 0.4537784

F -0.7632903 1.3220576 -0.6966088

F -0.7632903 -1.3220576 -0.6966088

F 1.5265806 0.0000000 -0.6966088

F 0.7710896 -1.3355664 1.4792347

F 0.7710896 1.3355664 1.4792347

F -1.5421792 0.0000000 1.4792347

K 0.0000000 0.0000000 -2.8016562

2c-X2C-PBE0-D3(BJ)/x2c-TZVPall-2c level

(C_{3v}, pseudo-$^1A_1$)

Ir -0.2627727 -0.3823916 -0.0000004

F 1.6459655 -0.2614255 -0.0000000

F -0.2128132 1.0172601 1.3026463

F -0.2128137 1.0172609 -1.3026463

F -2.1168390 -0.3744303 0.0000003

F -0.2232084 -1.6770103 -1.3267031

F -0.2232095 -1.6770099 1.3267033

K 1.6056910 2.3377466 -0.0000001

Rb[IrF_6]

1c-X2C-PBE0-D3(BJ)/x2c-TZVPall-2c level

($^1A'$, C_s)

Ir -0.2732991 -0.4186764 0.0000000

F 1.6137825 -0.2681602 0.0000000

F -0.2060525 0.9752047 1.3265191

F -0.2060525 0.9752047 -1.3265191

F -2.0899413 -0.1623650 0.0000000

F -0.2129221 -1.7818240 -1.2639404

F -0.2129221 -1.7818240 1.2639404

Rb 1.5874070 2.4624402 0.0000000

($^3A_1$, C_{3v})

Ir 0.0000000 0.0000000 0.4673718

F -0.7651412 1.3252635 -0.6763934

F -0.7651412 -1.3252635 -0.6763934

F 1.5302824 0.0000000 -0.6763934

F 0.7713716 -1.3360547 1.4931046

F 0.7713716 1.3360547 1.4931046

F -1.5427431 0.0000000 1.4931046

Rb -0.0000000 0.0000000 -2.9175053

2c-X2C-PBE0-D3(BJ)/x2c-TZVPall-2c level

(C_{3v}, pseudo-$^1A_1$)

Ir -0.2722950 -0.3922681 -0.0000002

F 1.6362402 -0.2865363 0.0000003

F -0.2206163 1.0031890 1.3054733

F -0.2206164 1.0031898 -1.3054731

F -2.1269503 -0.3766177 0.0000002

F -0.2390391 -1.6877992 -1.3268849

F -0.2390398 -1.6877991 1.3268848

Rb 1.6823166 2.4246415 -0.0000005

Cs[IrF_6]

1c-X2C-PBE0-D3(BJ)/x2c-TZVPall-2c level

($^1A'$, C_s)

Ir -0.2824064 -0.4360132 0.0000000

F 1.6035616 -0.2927170 0.0000000

F -0.2238577 0.9551309 1.3278023

F -0.2238577 0.9551309 -1.3278023

F -2.1020936 -0.1929688 0.0000000

F -0.2209955 -1.7982690 -1.2662137

F -0.2209955 -1.7982690 1.2662137

Cs 1.6706448 2.6079751 0.0000000

($^3A_1$, C_{3v})

Ir 0.0000000 0.0000000 0.4879580

F -0.7671990 1.3288277 -0.6483187

F -0.7671990 -1.3288277 -0.6483187

F 1.5343981 0.0000000 -0.6483187

F 0.7717706 -1.3367458 1.5141283

F 0.7717706 1.3367458 1.5141283

F -1.5435411 0.0000000 1.5141283

Cs -0.0000000 0.0000000 -3.0853867

2c-X2C-PBE0-D3(BJ)/x2c-TZVPall-2c level

(C_{3v}, pseudo-$^1A_1$)

Ir -0.2822015 -0.4099546 -0.0000003

F 1.6250503 -0.3038387 0.0000002

F -0.2422103 0.9809798 1.3088604

F -0.2422106 0.9809805 -1.3088603

F -2.1378006 -0.4035794 0.0000002

F -0.2436375 -1.7064135 -1.3270721

F -0.2436382 -1.7064133 1.3270721

Cs 1.7666484 2.5682394 -0.0000003

References

[1] L. Alvarez-Thon, J. David, R. Arratia-Pérez, K. Seppelt, *Phys. Rev. A* **2008**, *77*, 34502.

[2] G. Senges, L. Li, A. Wodyński, H. Beckers, R. Müller, M. Kaupp, S. Riedel, *Chem. Eur. J.* **2021**, *27*, 13642.